České vysoké učení technické v Praze
Fakulta elektrotechnická

Habilitační práce

2013 Pavel PAČES

České vysoké učení technické v Praze
Fakulta elektrotechnická

Netradiční metody měření polohových úhlů v letectví

Habilitační práce

2013 Pavel PAČES

Poděkování

Na tomto místě bych chtěl poděkovat rodině za jejich pomoc a podporu. Další poděkování patří lidem, kteří mi s touto prací pomohli a v její realizaci motivovali a podporovali.

Obsah

1. Úvod

Tato práce se zaměřuje na problémy s přesností elektronického měřicího a navigačního systému, který se používá pro určení polohy a orientace letadel hlavně v oblasti rekreačního létání. Jedná se o návrh měřicího systému, který určuje polohové úhly letadla (podélný sklon a příčný náklon) netradičním způsobem na základě měření malých rozdílů tlaku v atmosféře.

Rekreační létání tvoří v současné době majoritní část veškerého leteckého provozu a to jak v České republice (1) (2), tak i v zahraničí (3). V leteckém provozu se pohybují piloti s různým stupněm zkušeností a tím dochází ke vzniku velkého množství nehod zaviněných tzv. lidským činitelem (4), (5). Typickým příkladem je série špatných rozhodnutí pilota při řízení letadla, která následně končí havárií. Jedná se např. o špatné řešení situace vzniklé po výpadku pohonné jednotky (6), (7). Mnoho z těchto situací je možné řešit pomocí systému, který pilota upozorní na možný vznikající problém (8). Pro realizaci popisovaného systému varování je jednou z nejdůležitějších informací údaj o aktuální poloze a orientaci (tzv. polohových úhlech) letadla. Polohu a polohové úhly je možné měřit za pomoci jednotky inerciální navigace využívající triády akcelerometrů a senzorů úhlových rychlostí spolu s výpočetním algoritmem, který implementuje dvojitý číslicový integrál změřených zrychlení, a využívá i senzorů úhlových rychlostí za účelem získání polohových úhlů a polohy (9). Pro spolehlivé řešení této úlohy je ovšem nutné, aby použité senzory úhlových rychlostí a zrychlení splňovaly alespoň minimální požadavky na přesnost (10). Použití velmi přesných senzorů ovšem znamená, že výsledná cena navigačního systému převyšuje cenu letadel, které se běžně pro rekreační létání používají. Z důvodu ceny je snaha pro snímání zrychlení a úhlových rychlostí využívat mikro-mechanické elementy MEMS. Přesnost těchto systémů je ovšem nedostatečná, což se řeší slučováním jejich informace se zdroji, které využívají absolutní způsob měření informace. Jedná se například o algoritmy kombinující výstup ze senzorů úhlových rychlostí, akcelerometrů a senzorů magnetického pole. K těmto údajům se ještě přidává informace o poloze poskytované systémem GPS a v letecké technice také informace o výšce, případně vertikální rychlosti a rychlosti letu. Tato kombinace systémů je poté označována jako AHRS (10). Systém sběru dat je možné dále rozšířit o měření úhlu náběhu a vybočení, který je používaný pro získání přesnější informace ohledně možnosti ztráty vztlaku na křídle, nebo síle a vektoru větru. I přes veškerou snahu výrobců levných AHRS jednotek a aplikaci různých kalibračních metod (11), (12) řešených na různých úrovních, je použití levných MEMS senzorů stále problematické a výstupní údaj je dlouhodobě nepřesný z důvodu přítomnosti vnějších vlivů působících na letadlo. Mezi rušivé vlivy patří změny teploty ovlivňující výstupy senzorů (13), (14), vibrace pohonné jednotky a různá zrychlení generovaná pohybem letadla např. odstředivé zrychlení při provádění zatáčky.

Obsahem této práce je postupná analýza problémů levných MEMS inerciálních senzorů, metody fúze jejich dat s dalšími zdroji informace a nakonec návrh nového systému pro měření polohových úhlů. Jeho výstupní údaj je použitý pro zlepšení dlouhodobé přesnosti levného systému pro určení polohy a orientace letadel.

2. Příčiny nehod malých letadel

První část práce si klade za cíl zmapovat nejčastější příčiny nehod malých letadel a navrhnout metody, jak těmto nehodám předcházet. Z obr. 1 publikace (4) plyne, že rostoucí oblibu rekreačního létání doprovází i rostoucí nehodovost. Dělení příčin nehod je zobrazeno na obr. 2. Tento rostoucí trend nehodovosti je možné zvrátit, je žádoucí na palubu letadla instalovat zařízení, které pilotovi poradí v případě výskytu nestandardní situace.

V článku (4) je představen koncept zvaný Integrovaná modulární avionika (IMA), který díky technologickému pokroku postupně proniká i do oblasti malých letadel. Jedná se o postupnou změnu principu realizace avionických systémů, kde jsou místo klasického měřicího řetězce (viz obr. 1, (15)) použity softwarové funkce. Důvodem je dostupnost výpočetně výkonné elektroniky, která je potřebná pro realizaci elektronických zobrazovačů zvaných EFIS (15). Tyto systémy mají v současné době část nevyužitého výkonu procesoru, který je možné použít i jiným způsobem. V článku (4) je navrženo použití volného výkonu procesoru pro bezpečnostní doplňkové funkce, které na základě měřených dat ohodnotí aktuální stav letounu. Na základě této informace a dalších zdrojů (např. terénní databáze, databáze překážek) systém vyhodnotí možnosti letounu – dolet a počet možných zatáček, viz obr. 11, publikace (4). Jedním příkladem je SW modul pro průběžné vyhledávání vhodné plochy na přistání v případě výskytu mimořádných situací, jehož princip je zobrazen na obr. 14. Z provedených testů bylo zjištěno, že implementace těchto podpůrných prostředků je reálná, a celkové ohodnocení scény zobrazené na obr. 15, trvá na moderním osobním počítači přibližně 2 s (překreslení situace, ohodnocení binárního terénu, zahrnutí překážek). Informace ohledně navržených řešení může být pilotovi poskytovaná v různých formách, např. jako zvukové, nebo jako vizuální hlášení. Zatímco vhodnost zvukových pokynů je v současné době podrobována dalším výzkumům, tak vizuální pokyny je možné umístit na displej elektronického systému EFIS (viz obr. 16, (4)), nebo na tzv. head-up display (viz obr. 18, (4)).

Zatímco uvedené doplňkové SW funkce využívají dostupného výkonu moderního počítače, tak přetrvávajícím problémem zůstává přesnost senzorového vybavení měřicího systému letadla, na němž tyto nadstavbové funkce závisí. Jedná se o potřebu měřit aktuální polohové úhly letadla, které jsou nutné pro udržení vodorovného letu, a také jeho polohu, která je nutná pro výpočet trajektorie vhodné pro dosažení zvoleného cíle. V textu (4) je uveden příklad realizace systému (viz obr. 4), který je používán pro průběžné sledování letadel ve vzdušném prostoru. Systém byl testován v reálném provozu až na vzdálenost 100 km a jeho realizace byla oceněna cenou v soutěži o nejlepší diplomovou práci o oboru IT v roce 2009. Tento sledovací systém je v současné době nasazován při soutěžích v bezmotorovém létání. Sledovací systém poskytuje data o poloze a chování letadla, které je možné použít pro vyhodnocení aktuálního pořadí v soutěžích bezmotorového létání. Tyto informace jsou vhodné i pro realizaci dalších SW funkcí (16), např. bezpečnostní SW modul vyhodnocující ohrožení letadly v okolí na kolizním kurzu (4).

Detailní informace jsou dostupné v:

Pačes, P. - Levora, T. - Bruna, O. - Popelka, J. - Mlejnek, J.: Integrated Modular Avionics Onboard of Small Airplanes - Fiction or Reality?. In 30th DASC Digital Avionics Systems Conference [CD-ROM]. Piscataway: IEEE, 2011, p. 7A1-1-7A1-12. ISBN 978-1-61284-796-2.

Rozšířená varianta článku je v recenzním řízení v časopise AIAA Journal of Aircrafts.

3. Elektronické měřicí systémy využívané v malém letectví

Z předcházejícího textu plyne, že z hlediska realizace systému ohodnocení stavu letadla (4) a generování nápovědy pro řešení potenciálně nebezpečných situací, je nejobtížnější realizace měřicího systému. Tato kapitola představuje senzory a systémy, které jsou využívané v letecké technice. Dále se zaměřujeme na problémy související se zpracováním měřených informací do formátu, který je pilotovi srozumitelný (15). Postupně jsou představeny principy vývoje elektronických zobrazovacích systémů (17), požadavky na senzory pro měření rychlosti, výšky a také vlastnosti senzorů používaných pro určení orientace v prostoru (10). Z uvedených rozborů vyplývá, že v současné době používané mikro-mechanické senzorové systémy nemají dostatečnou přesnost pro realizaci dlouhodobě spolehlivého systému, který bude poskytovat informaci o polohových úhlech letadla (18). Budoucí vývoj spíše směřuje k realizaci výpočetního systému integrujícího data různých měřicích modulů, a který bude data zpracovávat v souboru několika navzájem izolovaných funkcí (4). Tento trend odpovídá konceptu Integrované modulární avioniky, který byl představen v předchozí kapitole.

3.1. Elektronické zobrazovací systémy

Elektronické zobrazovače se s postupujícím rozvojem elektroniky stávají nedílnou součástí i avioniky používané na palubách malých letadel. V současné době již pro kategorii malého letectví snad ani není efektivní vyvíjet nový zobrazovací systém, protože je jednodušší takový systém koupit od zavedeného výrobce. Problém, který ovšem ani zavedení výrobci (např. Honeywell) v současné době nejsou schopni uspokojivě levně řešit, je získávání spolehlivé informace ohledně orientace letadla z levných inerciálních senzorů (18). Pro vývoj zobrazovacích aplikací a také vývoj funkcí používaných v rámci integrované modulární avioniky (16), představené v (4), se jako nejvhodnější jeví navrhnout HW nezávislou vývojovou platformu, která umožní komfortní testování zobrazovacích a dalších funkcí, např. bezpečnostní funkce představené v (4). Článek (15) představuje právě takovou vývojovou platformu, která je v současné době využívána jak pro testování bezpečnostních funkcí, tak i pro výuku. Studentské skupiny na této platformě vyvíjí zobrazovací moduly (např. obr. 8, (15) a obr. 16, (4)), které představují jednotlivé části zobrazovače EFIS. Skupiny vývojářů mají na konci semestru za úkol složit různé části jednoho systému do jednoho modulu (viz obr. 8, (15)) a tím integrovat jednotlivé funkce na jednu výpočetní platformu podobně, jako při vývoji IMA funkcí (4). Názor studentů na obsah předmětu je shrnut na obr. 6, (15).

Detailní informace jsou dostupné v:

Pačes, P. - Šipoš, M.: Introducing Students to Aerospace Board Information Systems Using an Embedded Graphics System Simulator. In ICALT 2010 - Proceedings of 10th IEEE International Conference on Advanced Learning Technologies [CD-ROM]. Los Alamitos: IEEE Computer Society, 2010, p. 397-399. ISBN 978-0-7695-4055-9.

3.2.Senzory a systémy

Zatímco v oblasti HW elektronických zobrazovacích systémů určených k zabudování na palubní desku letadla již pravděpodobně není prostor pro přílišné inovace, tak v oblasti senzorového vybavení a integrace jednotlivých údajů poskytovaných různými senzorovými systémy tento prostor stále nacházíme. V článku (10) jsou představeny senzorové systémy používané v letecké technice. Dále jsou uvedeny požadavky na systémy používané pro měření rychlosti (viz obr. 5) a výšky letu (viz obr. 4). Tyto systémy, přestože je využívána MEMS technologie senzorů, je poměrně jednoduché realizovat (19) a i přes náchylnost senzorového vybavení na změny okolního prostředí kalibrovat, viz (13) a (14). Obecnou výhodou, oproti inerciálním měřením, obou uvedených typů měření (výška a rychlost) je to, že se jedná o absolutní měření, tj. i v případě výskytu náhodné chyby měření, se tato chyba dlouhodobě neprojeví do přesnosti výstupní informace. To bohužel neplatí pro senzory zrychlení a úhlových rychlostí letadla, protože pro získání polohových úhlů a případně pozice v tří-dimensionálním prostoru, je potřeba provést numerickou integraci jejich výstupů a také korekce na další působící vlivy (17). Nejjednodušším a v současnosti hojně využívaným systémem pro měření polohových úhlů je systém založený na principu AHRS (viz obr. 1, (10)), který poskytuje údaje o pozici na základě příjmu signálu poskytovaného systémem GPS a inerciální senzory slouží pouze pro měření orientace. Systém AHRS využívá různých zdrojů informace (viz obr. 10, (10)) k průběžnému zjišťování aktuálních chyb ofsetu a zesílení, jak u senzorů zrychlení, tak i úhlových rychlostí, a na základě toho umožňuje průběžně aktualizovat chybové modely senzorů. V tomto případě (AHRS) ovšem není řešena celá navigační úloha, ale údaje senzorů jsou použity pouze pro zjišťování polohových úhlů. Jedná se tedy o jednu numerickou integraci výstupu senzoru pro měření úlových rychlostí, která je transformována z měřicí do navigační soustavy letadla (viz obr. 5, (20)). V důsledku toho, že na letadlo, a tím i na senzory, působí i další vnější vlivy způsobené vibrujícím motorem, pojížděním, startem, přistáním a také prováděním zatáček v průběhu letu (21), tak ani v případě využití zjednodušení AHRS systému, tj. pouze jedna integrace, není měřicí systém založený na MEMS senzorech dlouhodobě použitelný jako zdroj informace pro realizaci umělého horizontu (18) a tím i pro realizaci dalších podpůrných funkcí, které byly navrženy dříve (4). Jako zdroj korekční informace k údaji integrovanému ze senzorů úhlových rychlostí se v současné době používá údaj z magnetometru (20) a GPS. V případě, že na letadlo nepůsobí žádné další zrychlení mimo gravitačního pole Země, tak je možné použít pro korekce vektor gravitačního pole, který je vypočítaný z údajů senzorů zrychlení (20).

V článku (10) je navržen nový měřicí systém, který umožňuje měřit polohové úhly podobným způsobem, jako zmíněné moduly měření výšky a rychlosti, tj. absolutním způsobem, kde se neprojevují krátkodobé rušivé vlivy na jeho vstupech. Předpokládá se, že tento systém rozšíří množinu vstupů jednotky AHRS (viz obr. 11, (20)) a bude použit pro dlouhodobé korekce inerciálních senzorů. Metoda pracuje na principu měření malých tlakových rozdílů ve vertikálním směru (viz obr. 12 a 15, (10)), kde vznikají rozdíly do velikosti 12 Pa (viz tab. 1, (10)). Po formulaci teoretického základu bylo provedeno první ověřovací měření pomocí systému, který je zobrazený na obr. 17, (10). Měření bylo prováděno ve dvou bodech jedné osy (viz obr. 16, (10)). Výsledky měření (obr. 18, (10)) bohužel ne zcela odpovídají předpokladům (viz tab. 1, (10)) a na základě toho byl základní princip měřicí metody přepracován a publikován v (22).

Detailní informace jsou dostupné v:

Pačes, P. - Popelka, J. - Levora, T.: Advanced Display and Position Angles Measurement Systems. In ICAS 2012 - 28th Congress of the International Council of the Aeronautical Sciences - Proceedings [CD-ROM]. Brisbane: ICAS - the International Council of the Aeronautical Sciences, 2012, vol. 1, p. P6.3.1-P6.3.14. ISBN 978-0-9565333-1-9.

3.3.Vliv okolního prostředí na senzory

Okolní prostředí velmi výrazným způsobem ovlivňuje výstupní údaj senzorů, které jsou založené na MEMS technologii. Důvodem je použitý materiál snímače, jeho uložení, uložení elementů převádějících měřenou veličinu na elektrický signál atd. Ve většině případů má největší vliv teplota.

Mimo vlivu teploty na senzor se může jednat i o změnu měřeného signálu podobně, jak je to běžné u senzorů magnetického pole. Magnetické pole Země je výrazně ovlivňováno feromagnetickými materiály, které mění jeho vektor a intenzitu. Z tohoto důvodu je potřeba provádět po instalaci AHRS systému do letadla jeho kalibraci, která odsraní vliv vnějších polí na senzor (viz obr. 9, (20)). V článku (10), je navrženo uspořádání levných senzorů magnetického pole do kruhu tak, aby toto uspořádání bylo schopné změřit kalibrační kružnici magnetometru v jednom odměru (viz obr. 11, (10)).

Problematika měření teplotní závislosti několika MEMS senzorů tlaku a metody, jak se s problémem vyrovnat je prezentována v (13). Měření prokázalo velmi výrazné změny výstupního signálu v závislosti na změnách teploty v rozsahu od -40°C do 60°C u devíti senzorů. V praxi se teplotní závislost odstraňuje buď pomocí kalibrační tabulky, nebo kalibračního polynomu, které kalibrují chyby ofsetu a zesílení senzoru (viz rovnice 1, (10), obr. 1, (13)). Tyto metody kompenzace chyb byly použity u senzorů zobrazených na obr. 2, 3, 9, 10, (13). Tento způsob kalibrace funguje po určitou omezenou dobu, ale z důvodu stárnutí snímacího elementu výstupní údaj postupně ztrácí na přesnosti. Jako další možné řešení se nabízí temperování celého měřicího systému, nebo pouze senzorového elementu, čímž výsledná přesnost měření výrazně narůstá, viz porovnání obrázků obr. 11 a obr. 12, (13).

Perspektivní se do budoucna u senzorů tlaku jeví možnost využití dvou stejných senzorů tlaku, přičemž jeden z nich je použitý pouze jako senzor teploty (14) a druhý pro vlastní měření. Metoda využívá vlastností izochorického děje u zaslepeného senzoru. Matematický popis slouží pro korekce změn v uzavřené vstupní části senzoru, který je využívaný jako teplotní senzor, pro korekci výstupu měřicího senzoru, viz rovnice 3, (14).

Detailní informace jsou dostupné v:

Pačes, P. - Šipoš, M. - Reinštein, M. - Roháč, J.: Sensors of Air Data Computers - Usability and Environmental Effects. In ICMT'09 - Proceedings of the International Conference on Military Technologies. Brno: Univerzita obrany, 2009, p. 401-409. ISBN 978-80-7231-649-6.

Pačes, P. - Šipoš, M. - Draxler, K.: Temperature Effects and Non-linearity Corrections of Pressure Sensors. In ICMT'11 International Conference on Miltary Technologies 2011 [CD-ROM]. Brno: Univerzita obrany, 2011, p. 651-656. ISBN 978-80-7231-788-2.

3.4. Kalibrace senzorů

Podobné problémy, jako u tlakových senzorů, jsou měřitelné i na dalších senzorech používaných v letecké technice, např. inerciálních senzorech zrychlení a úhlových rychlostí. Problematika se v tomto případě ještě komplikuje faktem, že inerciální senzory jsou většinou uspořádány po třech v ortogonální soustavě. Uložení inerciálních senzorů, a opět jejich závislosti na vlivu okolního prostředí, hraje ve výsledné přesnosti měřicího systému velkou roli. Kalibrace senzorů je možná za pomoci několika algoritmů, jejichž porovnání z hlediska časové náročnosti a nákladů na laboratorní vybavení je publikováno v (12). V článku jsou analyzovány tři triády inerciálních senzorů s tím, že provedená kalibrace mnohonásobně zlepšila jejich výsledné vlastnosti.

Na trhu jsou dostupné různé typy senzorů s rozdílnou přesností, viz obr. 7, (10), přičemž malá změna výstupního údaje senzoru může výrazným způsobem ovlivnit celé měření. Zatímco u tlakových měření, prováděných za účelem získání výšky a rychlosti, se jedná o konstantní chybu, která se přičítá k výstupní hodnotě, tak při zpracování výstupu inerciálních senzorů chyba lineárně (jedna numerická integrace) nebo nelineárně narůstá (dvojitá numerická integrace, viz obr. 9, (10)). Přesnost měřicího systému a vliv chyby na výstupní údaje je závislá na kvalitě senzorů. Obr. 7, (10) zobrazuje porovnání dvou senzorů úhlové rychlosti, které jsou používané v měřících jednotkách IMU (viz obr. 1, (10)). V prvním případě se jedná o MEMS senzor a ve druhém případě o laserový RLG (9) senzor nasazený v letectví využívané AHRS jednotce (23). Tyto parametry byly měřeny v rámci stáže u firmy Honeywell, v rámci programu Honeywell Innovator. Z provedených měření je zřejmé, že kvalita výstupu laserového gyroskopu pětinásobně předčí MEMS senzor. Na základě tohoto porovnání je možné formulovat závěr, že pro realizaci AHRS jednotky s levnými MEMS senzory a přesností potřebnou pro realizaci bezpečnostních funkcí (4) je nutné používat další zdroje informace.

Detailní informace jsou dostupné v:

Šipoš, M. - Pačes, P. - Roháč, J. - Nováček, P.: Analyses of Triaxial Accelerometer Calibration Algorithms. IEEE Sensors Journal. 2012, vol. 12, no. 5, p. 1157-1165. ISSN 1530-437X.

3.5.Další zdroje informace

Pro realizaci bezpečnostních funkcí navržených v (4) a pro zlepšení přesnosti měření výšky a rychlosti letu letadla, je vhodné opravovat výstup Pitot-statické sondy o změny způsobené nabíhajícím proudem vzduchu. Úhel nabíhajícího proudu vzduchu je možné měřit několika způsoby, přičemž jednotlivé varianty jsou shrnuté v (24). Článek shrnuje kompletní vývoj zařízení pro měření úhlu náběhu a vybočení, které je založeno na měření tlakové diference na dvou vstupech umístěných na půlkulové hlavě. K tomuto tvaru bylo přistoupeno po pokusech s různým uspořádáním vstupů senzoru, tak jak je to zobrazeno na obr. 2, 3, 4, (24). Předpokládá se, že senzor bude umístěný na křídle podobně, jako je to naznačeno na obr. 1, (24). V článku je představeno unikátní uspořádání senzorů, které zdvojnásobuje amplitudu výstupního údaje senzorového systému (viz obr. 5, (24)). V rámci vývoje byl realizován funkční vzorek měřicího systému (obr. 6) s jehož pomocí byly změřeny parametry několika typů sond. Jednotlivá měření byla také porovnána s výpočty proudění provedenými v prostředí Ansys a to za účelem ověření možnosti využití tohoto typu výpočtů pro analýzu návrhu nového systému měření polohových úhlů. Z porovnání numerických výsledků a reálných měření, vyplynuly malé rozdíly dané reálnou hladkostí vyrobené sondy a také přesností provedených měření. Na základě tohoto porovnání jsme dospěli k závěru, že numerické výpočty je možné s opatrností použít. Z uvedených měření a rozborů vyplynulo, že kulová hlava poskytuje výstup s nejlepší linearitou (viz obr. 8, 9, 12, (24)) a také, že pro výpočet je možné použít poměr měřeného k dynamickému tlaku (viz rovnice 5), který výrazně usnadňuje vyhodnocení úhlu. V článku jsou na závěr shrnuty důležité poznatky ohledně konstrukce sondy, umístění vstupů tlaku a měřicího systému, které byly následně aplikovány v (25).

Údaj poskytovaný systémem pro měření úhlu náběhu a vybočení je možné využít pro zpřesnění výpočtu dokluzu letadla v IMA funkcích (4), pro výpočet vlivu ovlivnění statických vstupů používaných pro měření výšky barometrickou metodou (jsou použity také v novém systému pro měření polohových úhlů) a také pro zjišťování okamžiku, kdy letadlo vlivem přetažení začíná ztrácet vztlak na křídlech potřebný k udržení letu.

Detailní informace jsou dostupné v:

Pačes, P. - Čenský, T. - Hanzal, V. - Draxler, K. - Vaško, O.: A Combined Angle of Attack and Angle of Sideslip Smart Probe with Twin Differential Sensor Modules and Doubled Output Signal. In IEEE Sensors 2010 - Proceedings [CD-ROM]. Stoughton, Wisconsin: IEEE Sensors Council, 2010, p. 284-289. ISBN 978-1-4244-8168-2.

4. Nový systém měření polohových úhlů

Následující část pojednává o výsledcích testování a integrace nového systému pro měření polohových úhlů (22) do existujícího konceptu AHRS jednotky (10). Pro zpracování informací poskytovaných jednotlivými senzory se využívá Kalmanova filtrace.

V článku (11) je proveden rozbor nástrojů, které umožňují integrovat principy kalibrace, filtrování dat a digitální komunikace přímo do senzoru, případně akčního členu. Problematika je v článku ilustrována na digitálním servomechanismu, který je využívaný pro řízení bezpilotního prostředku Mamok Manta (viz obr. 1). Servomechanismus obsahuje senzor i akční člen, které jsou využívané ve zpětnovazební smyčce, která řídí polohu páky servomechanismu. Vývoj byl proveden za účelem zvýšení robustnosti servomechanismu následujícími způsoby:

- Servomechanismus je vybaven elektronickým technickým listem, který popisuje jak senzor, tak i akční člen. Popis byl realizován implementací standardu IEEE1451.
- Senzorová část umožňuje detekovat několik chybových stavů (viz obr. 7).
- V případě výskytu poruchy na senzorové části je použito principu odhadu budoucích stavů (polohy) servomechanismu pomocí Kalmanova filtru.

Implementací uvedených bodů do řídicího systému servomechanismu jsme si vyzkoušeli práci s odhadem budoucích stavů pomocí Kalmanova filtru. Z obrázků uvedených v publikaci jsou patrné dva závěry. Prvním závěrem je, že odhady budoucích stavů po výpadku informace ze senzoru fungují velmi dobře v případě, že nedochází k velkým změnám odhadovaného signálu (viz obr. 14). Druhým závěrem je, že odhady sledují referenční signál pouze po určitou dobu s následným kumulováním chyby (viz obr. 15). Kalmanova filtrace je jedním z nástrojů, který se používá pro zpracování dat z různých senzorů a také ze senzorů s různou periodou vzorkování. Tato metoda bude použita také v dalších kapitolách, kde jsou zpracovávány data z MEMS senzorů zrychlení, úhlových rychlostí a magnetometru. V dalším článku je představena metoda zpracování výstupů z akcelerometrů pomocí dvojí integrace a dále je uvedena její modifikace pro využití v AHRS systému.

Detailní informace jsou dostupné v:

Pačes, P. - Reinštein, M. - Draxler, K.: Fusion of Smart Sensor Standards and Sensors with Self-Validating Abilities. Journal of Aircraft. 2010, vol. 47, no. 3, p. 1041-1046. ISSN 0021-8669.

4.1. Zpracování dat z inerciálních senzorů

Zkušenosti získané v předcházejících pracích byly použity pro implementaci inerciální měřicí jednotky s výstupy v podobě Eulerových úhlů a quaternionů (20). Data ze senzorů byla zpracována pomocí Kalmanova filtru, který na základě odhadu budoucí stavů systému průběžně upravuje chybové modely senzorů. Jednotka byla otestována (20), přičemž senzory byly před provedeným testem kalibrovány pro kompenzaci chyb posunu nuly (offset).

Jako testovací systém byl použit model, který ilustruje princip stabilizace kosmických prostředků ve vesmíru (viz obr. 1, (20)). Model využívá AHRS jednotku poskytovanou ve formě vývojového modulu iNemo firmou ST microelectronics. Schéma vnitřního zapojení modelu a připojení inerciální měřicí jednotky k systému s bezdrátovým přenosem dat je zobrazeno na obr. 2, (20). Software AHRS jednotky využívá Kalmanův filtr, jehož principiální schéma funkce je zobrazeno na obr. 8, (20). S modelem byla v rámci testu provedena jedna otáčka v horizontální rovině o 360°, přičemž byla z modelu průběžně přenášena měřená a vypočtená data s frekvencí 50 Hz. Průběhy vybraných signálů z jednotlivých senzorů jsou vyneseny v grafech na obr. 9, (20). Zejména na výstupu magnetometru je vidět, že jednotlivé senzory byly kalibrovány na posun ofsetu. Pro změření offsetu bylo u senzorů zrychlení použito ke kalibraci gravitační pole Země, offset senzorů úhlové rychlosti byl měřen v okamžiku, kdy byla jednotka v klidu, a offsety vektorového magnetometru byly zjištěny změřením tzv. kalibračního kruhu, viz obr. 11, (10).

Algoritmus integrace dat z různých senzorů byl otestován v průběhu jedné otáčky systému v horizontální rovině o 360° s tím výsledkem, že systém po dokončení pohybu měří stejné hodnoty jako na jeho počátku. Toto platí pouze v případě kalibrovaných senzorů. V případě nekalibrovaných senzorů je výstupní hodnota velmi ovlivněna parametry magnetometru (viz obr. 6, (20)).

Bez použití filtračního algoritmu, který do výpočtu polohových úhlů zavádí absolutně změřené hodnoty z dalších senzorů (viz obr. 6, (20)), dochází k tzv. driftu výstupu, přičemž se výstupní hodnota stává nepoužitelnou za přibližně 2s (10), (18), (22).

Princip nového systému pro měření polohových úhlů je navržený v (10) přičemž způsob využití jeho výstupu je navržen na obr. 11, (20). Detailní způsob implementace výstupu nového systému měření polohových úhlů je popsán v (22). Do budoucna se pro integraci magnetometru s inerciálními senzory jeví jako výhodné použít novou senzorovou hlavu, viz obr. 11, (10), která je schopná v jednom odměru zjistit ofsety jednotlivých senzorů bez nutnosti otáčet s celým systémem trojosého magnetometru o 360°.

Detailní informace jsou dostupné v:

Pačes, P. - Popelka, J. - Marchitto, Emidio - Levora, T.: Smart Sensor Data Processing for Aerospace Applications in Education Illustrated by a Small Satellite Platform Demonstrator. In DASC 2012 - 31th Digital Avionics System Conference - Proceedings [CD-ROM]. Piscataway: IEEE Operations Center, 2012, vol. 1, p. 1-8. ISBN 978-1-4673-1698-9.

Rozšířená varianta článku je v recenzním řízení v časopise AIAA Journal of Aircrafts.

4.2.Integrace nového systému měření polohových úhlů s AHRS

Využití levných MEMS senzorů inerciálních veličin se jeví z hlediska dlouhodobé přesnosti určení polohových úhlů jako nevhodné (18). Dlouhodobou přesnost je možné dosáhnout s pomocí dalších senzorů, které měří požadovanou veličinu dalším, většinou absolutním způsobem. Jedná se například o určení kurzu, který je možné získat jako jeden z výstupů algoritmu zpracování dat z inerciálních senzorů, nebo pomocí vektorového magnetometru, viz např. (10). Zatímco v případě kurzu je možné pro jeho určování použít vektorový magnetometr, tak u polohových úhlů je možné využít senzorů zrychlení a rozkladu vektoru gravitačního pole v závislosti na natočení letadla a měřicího systému. Tato metoda je účinná v případě, že na letadlo nepůsobí žádná další zrychlení způsobená např. prolétanou zatáčkou. Detekce tohoto stavu je poměrně jednoduchá, viz rovnice 8, (20), ale rozlišení zrychlení způsobených zatáčkou a gravitačním polem již není triviální. Z tohoto důvodu se jako perspektivní jeví využití nějakého dalšího způsobu měření polohových úhlů, např. systému, který je navržený v (10).

Článek (22) shrnuje výsledky testů tří navržených realizací nového systému měření polohových úhlů (10) a hlavně, prezentuje data naměřená s druhou, vylepšenou variantou systému, viz obr. 3, (10). Z výsledků měření uvedených na obr. 4, (22), je vidět, že systém poskytuje mnohem průkaznější výsledky než předchozí varianta, viz obr. 18, (10). Prozatím nejlepšího výsledku měření bylo dosaženo pomocí třetí varianty zobrazené na obr. 2, (22). Na základě změřených výsledků bylo formulováno několik závěrů a předpokladů. Jako jeden z nejdůležitějších se jeví předpoklad, že nový systém měření polohových úhlů je schopný detekovat průchod dvou jeho měřicích bodů referenční rovinou, viz kapitola Metody, bod 1a, (22). Tuto informaci je možné následně použít jako vstup do algoritmu zpracování dat z jednotlivých senzorů, viz obr. 11, (20). Z analýzy provedené v (22) plyne, že pro zvýšení dlouhodobé přesnosti měření polohového úhlu je dostačující opakovaně nulovat chybu numerické integrace údajů ze senzorů úhlových rychlostí, tj. využít údaj z detektoru průchodu referenční rovinou, kterou nový systém pro měření polohových úhlů poskytuje (22). Tato funkce byla s úspěchem otestována pomocí modelu nového systému pro měření polohových úhlů a senzoru úhlových rychlostí s reálnými chybovými parametry (viz obr. 15, (22)). Zatímco přímé použití integrace údaje senzoru úhlové rychlosti vede k okamžitému nárůstu chyby určení polohového úhlu, tak v případě využití informace poskytované novým systémem měření polohových úhlů dochází k zastavení růstu chyby (viz obr. 18) a v případě využití dalších předpokladů (22) dokonce k jejímu potlačování (viz obr. 21).

Detailní informace jsou dostupné v:

Pačes, P. - Popelka, J.: IMU Aiding Using Two AHRS Units. In DASC 2012 - 31th Digital Avionics System Conference - Proceedings [CD-ROM]. Piscataway: IEEE Operations Center, 2012, vol. 1, p. 1-12. ISBN 978-1-4673-1698-9.

Rozšířená varianta článku je v recenzním řízení v časopise AIAA Journal of Aircrafts.

4.3.Praktická realizace sondy pro nový systém měření polohových úhlů

Funkce nového systému měření polohových úhlů (10) byla úspěšně otestována v laboratorních podmínkách (22). Pro využití tohoto systému na letadle tak, jak je naznačeno na obr. 16, (10), je nutné zkonstruovat sondu, vstupní bod, který bude podobný montáži zobrazené na obr. 1, (24). Z důvodu možného natáčení sondy v proudění je vhodné měřit také úhel náběhu a vybočení, které mohou ovlivňovat měření výšky. Na základě uvedených zkušeností byla zkonstruována sonda, jejíž popis je možné nalézt v (25).

Sonda je určena pro dva způsoby montáže. V prvním případě je možné její zavěšení pod letadlo na závěsné lano a v druhém případě je možné sondu přímo montovat na křídlo letadla (viz porovnání obr. 1, (24) a 11, (25)). Při konstrukci sondy byly využity zkušenosti získané při práci na systému měření úhlu náběhu a vybočení (24). Výsledkem je modulární konstrukce sondy zobrazená na obr. 5, (25), přičemž blokové schéma vnitřní elektroniky je zobrazeno na obr. 13, (25). Pro měření statického tlaku je v sondě umístěný senzor Memscap SP82, který po provedení kalibrace měří statický tlak s přesností +/- 6 Pa (viz obr. 22, (25)). Tato sonda je připravena pro otestování třetí varianty implementace nového systému měření polohových úhlů, která je zobrazena na obr. 2 (22).

Detailní informace jsou dostupné v:

Pačes, P. - Popelka, J. - Auersvald, J.: Standalone Trailing Probe for Aero metrical Measurements. In DASC 2012 - 31th Digital Avionics System Conference - Proceedings. Piscataway: IEEE Operations Center, 2012, vol. 1, p. 1-12. ISBN 978-1-4673-1698-9.

Rozšířená varianta článku je v recenzním řízení v časopise AIAA Journal of Aircrafts.

5. Závěr

V této práci je prezentován návrh a laboratorní otestování nového systému pro měření polohových úhlů, který je určený pro zlepšení dlouhodobé přesnosti systému pro měření polohy a polohových úhlů AHRS, který využívá MEMS senzory inerciálních veličin. Navržená metoda byla otestována v laboratorních podmínkách, kde se potvrdilo, že navržený princip je funkční. Do budoucna je otázkou, zda navržená metoda bude fungovat i za reálného letu, kdy budou jednotlivé sondy namontované na letadle. Do současné doby byly všechny testy provedeny v laboratorních podmínkách v situaci, kdy byla okolní atmosféra v klidu – statická. V reálném provozu se do přesnosti systému promítnou dynamické jevy způsobené letem. Pro reálnou zástavbu na letadlo byl navržen fyzický tvar sondy, kterou je možné přišroubovat na křídlo letadla. Dále byla pro sondu navržena měřicí elektronika s bezdrátovým přenosem měřené informace do nadřazeného systému.

V průběhu práce na tématu netradičních metod pro měření polohových úhlů bylo realizováno několik funkčních vzorků. Za zmínku stojí hlavně „Small Satellite Platform“, která obsahuje kompletní inerciální měřicí jednotku a Kalmanův filtr pro zpracování dat z jednotlivých senzorů za účelem získání Eulerových úhlů a quaternionů. Tato platforma, mimo použití v této práci, slouží rovněž jako laboratorní pomůcka v průběhu kurzu Palubní informační a řídicí systémy vyučovaného na ČVUT v Praze a byla použita i na několika kurzech v zahraničí.

Nový způsob měření polohových úhlů využívá ke své funkci rozložení tlaku v atmosféře Země, který nelineárně klesá s výškou. Jedná se o přesné měření malých tlakových diferencí na různých částech letadla. Metoda umožňuje detekci nulového náklonu, což umožňuje průběžné nulování integrační chyby ve výpočtech aplikovaných na inerciální senzory. To má velmi pozitivní vliv na dlouhodobou přesnost určování polohových úhlů. V práci je navržený způsob integrace nového systému měření polohových úhlů s existujícími algoritmy zpracování dat z inerciálních senzorů a vektorového magnetometru. Magnetometr je velmi náchylný na umístění a přítomnost materiálů, které ovlivňují okolní magnetické pole. Potlačení vlivu rušivých polí umožňuje nově navržené uspořádání magnetometrické hlavy, které poskytuje možnost změřit kalibrační kruh (a získání korekčních parametrů) senzoru v jednom odměru.

Citovaná literatura

1. **Černohorský, Jiří.** Český letecký průmysl na počátku roku 2010. *Technický týdeník.* 2009, Sv. 1, 1.

2. **CzechInvest.** Aerospace Industry in the Czech Republic - Investment Opportunities. *CzechInvest - Agentura pro podporu podnikání a investic.* [Online] 2008. [Citace: 17. 9 2010.] www.czechinvest.org/data/files/aerospace-99-en.pdf.

3. **Aircraft Owners and Pilots Association.** AOPA Online. *AOPA Organization homepage.* [Online] AOPA, 2010. [Citace: 4. 4 2010.] www.aopa.org.

4. **Pačes, Pavel, a další, a další.** *Integrated Modular Avionics Onboard of Small Airplanes - Fiction or Reality?* Piscataway : IEEE, 2011. ISBN 978-1-61284-796-2.

5. **Kenny, David Jack.** *Nall Report -2009 Accident Trends and Factors for 2008.* Frederick, Maryland, Uniíted States : AOPA Air Safety Foundation, 2010.

6. **LAA.** Školení pro sportovní a rekreační piloty. *Bezpečnostní kampaň 2010 – PŘEMÝŠLEJ,…DOLETÍŠ.* [Online] Letecká amatérská asociace, 2010. http://www.skolenipilotu.cz.

7. Rozbor mimořádných událostí v provozu SLZ za rok 2010. *Letecká amatérská asociace ČR.* [Online] [Citace: 11. Prosinec 2012.] http://www.laa.cz/index.php?Action=View&ARTICLE_ID=1943.

8. **Pačes, Pavel.** *Zvýšení bezpečnosti letu letadel UL kategorie podporou avionického systému.* Praha : České vysoké učení technické v Praze, 2010.

9. **King, A. D.** Inertial Navigation - Forty Years of Evolution. *GEC REVIEW.* 13, 1998, Sv. 3, 1.

10. **Pačes, Pavel, Popelka, Jan a Levora, Tomáš.** *Advanced Display and Position Angles Measurement Systems.* Brisbane : ICAS - the International Council of the Aeronautical Sciences, 2012. ISBN 978-0-9565333-1-9.

11. **Pačes, Pavel, Reinštein, Michal and Draxler, Karel.** Fusion of Smart-Sensor Standards and Sensors with Self-Validating Abilities. [ed.] Thomas M. Weeks. *Journal of Aircrafts 2010.* AIAA, 2010, Vol. 57, no.3, pp. 1041-1046.

12. **Šipoš, Martin, a další, a další.** Analyses of Triaxial Accelerometer Calibration Algorithms. *IEEE Sensors Journal.* 12, 2012, Sv. 5, ISSN 1530-437X.

13. **Pačes, Pavel a et_al.** *Sensors of Air Data Computers - Usability and Environmental Effects.* Brno : Univerzita obrany, 2009. stránky 401-409, ICMT'09 - Proceedings of the International Conference on Military Technologies. ISBN 978-80-7231-649-6.

14. **Pačes, Pavel, Šipoš, Martin a Draxler, Karel.** *Temperature Effects and Non-linearity Corrections of Pressure Sensors.* Brno : Univerzita obrany, 2011. ISBN 978-80-7231-788-2.

15. **Pačes, Pavel a Šipoš, Martin.** *Introducing Students to Aerospace Board Information Systems Using an Embedded Graphics System Simulator.* Tunis : IEEE, 2010. ISBN 978-0-7695-4055-9.

16. **Rierson, Leanna K.** Best Practices for Certifying IMA Systems in Civil Aircraft. *IEEE A&E Systems Magazine.* Aerospace and Electronics, 2010, Sv. 25, 1.

17. **Stovall, Sherryl H.** *Basic Inertial Navigation.* California : Naval Air Warfare Center, Weapons Division, 1997. NAWCWPNS TM 8128.

18. **Crittenden, Jordan a Evans, Parker.** *MEMS Inertial Navigation System.* ECE : Cornell University, 2008.

19. **Nedvěd, Jan.** Aerometrický systém pro malá letadla. *Diplomová práce, vedoucí práce Ing. Pavel Pačes.* Praha : České vysoké učení technické v Praze, 2009. Sv. 1, 1.

20. **Pačes, Pavel, a další, a další.** *Smart Sensor Data Processing for Aerospace Applications in Education Illustrated by a Small Satellite Platform Demonstrator.* Piscataway : IEEE , 2012. ISBN 978-1-4673-1698-9.

21. **MGL Avionics.** *SP-2 Magnetometer, SP-4 AHRS User and installation manual.* [Dokument] Somerset West : MGL Avionics, 2010. SP2-SP4.

22. **Pačes, Pavel a Popelka, Jan.** *IMU Aiding Using Two AHRS Units.* Piscataway : IEEE, 2012. ISBN 978-1-4673-1698-9.

23. **Honeywell.** Micro Inertial Reference System SM µIRS. *Inertial Navigation Products - Product Description.* [Online] March 2004. [Citace: 27. 6 2010.] http://www51.honeywell.com/aero/common/documents/Laseref_V_Micro_IRS_SM.pdf.

24. **Pačes, Pavel, a další, a další.** *A Combined Angle of Attack and Angle of Sideslip Smart Probe with Twin Differential Sensor Modules and Doubled Output Signal.* Waikoloa : IEEE, Přijato k publikaci na konferenci IEEE Sensors 2010, 2010.

25. **Paces, Pavel, Popelka, Jan a Auersvald, Jan.** *Standalone Trailing Probe for Aero Metrical Measurements.* Piscataway : IEEE, 2012. ISBN 978-1-4673-1698-9.

Přílohy

Jednotlivé kapitoly této práce jsou tvořeny následujícími články:

1. Pačes, P. - Levora, T. - Bruna, O. - Popelka, J. - Mlejnek, J.: Integrated Modular Avionics Onboard of Small Airplanes - Fiction or Reality?. In 30th DASC Digital Avionics Systems Conference [CD-ROM]. Piscataway: IEEE, 2011, p. 7A1-1-7A1-12. ISBN 978-1-61284-796-2.
2. Pačes, P. - Šipoš, M.: Introducing Students to Aerospace Board Information Systems Using an Embedded Graphics System Simulator. In ICALT 2010 - Proceedings of 10th IEEE International Conference on Advanced Learning Technologies [CD-ROM]. Los Alamitos: IEEE Computer Society, 2010, p. 397-399. ISBN 978-0-7695-4055-9.
3. Pačes, P. - Popelka, J. - Levora, T.: Advanced Display and Position Angles Measurement Systems. In ICAS 2012 - 28th Congress of the International Council of the Aeronautical Sciences - Proceedings [CD-ROM]. Brisbane: ICAS - the International Council of the Aeronautical Science, 2012, vol. 1, p. P6.3.1-P6.3.14. ISBN 978-0-9565333-1-9.
4. Pačes, P. - Šipoš, M. - Reinštein, M. - Roháč, J.: Sensors of Air Data Computers - Usability and Environmental Effects. In ICMT'09 - Proceedings of the International Conference on Military Technologies. Brno: Univerzita obrany, 2009, p. 401-409. ISBN 978-80-7231-649-6.
5. Pačes, P. - Šipoš, M. - Draxler, K.: Temperature Effects and Non-linearity Corrections of Pressure Sensors. In ICMT'11 International Conference on Miltary Technologies 2011 [CD-ROM]. Brno: Univerzita obrany, 2011, p. 651-656. ISBN 978-80-7231-788-2.
6. Šipoš, M. - Pačes, P. - Roháč, J. - Nováček, P.: Analyses of Triaxial Accelerometer Calibration Algorithms. IEEE Sensors Journal. 2012, vol. 12, no. 5, p. 1157-1165. ISSN 1530-437X.
7. Pačes, P. - Čenský, T. - Hanzal, V. - Draxler, K. - Vaško, O.: A Combined Angle of Attack and Angle of Sideslip Smart Probe with Twin Differential Sensor Modules and Doubled Output Signal. In IEEE Sensors 2010 - Proceedings [CD-ROM]. Stoughton, Wisconsin: IEEE Sensors Council, 2010, p. 284-289. ISBN 978-1-4244-8168-2.
8. Pačes, P. - Reinštein, M. - Draxler, K.: Fusion of Smart Sensor Standards and Sensors with Self-Validating Abilities. Journal of Aircraft. 2010, vol. 47, no. 3, p. 1041-1046. ISSN 0021-8669.
9. Pačes, P. - Popelka, J. - Marchitto, Emidio - Levora, T.: Smart Sensor Data Processing for Aerospace Applications in Education Illustrated by a Small Satellite Platform Demonstrator. In DASC 2012 - 31th Digital Avionics System Conference - Proceedings [CD-ROM]. Piscataway: IEEE Operations Center, 2012, vol. 1, p. 1-8. ISBN 978-1-4673-1698-9.
10. Pačes, P. - Popelka, J.: IMU Aiding Using Two AHRS Units. In DASC 2012 - 31th Digital Avionics System Conference - Proceedings [CD-ROM]. Piscataway: IEEE Operations Center, 2012, vol. 1, p. 1-12. ISBN 978-1-4673-1698-9.
11. Pačes, P. - Popelka, J. - Auersvald, J.: Standalone Trailing Probe for Aero metrical Measurements. In DASC 2012 - 31th Digital Avionics System Conference - Proceedings. Piscataway: IEEE Operations Center, 2012, vol. 1, p. 1-12. ISBN 978-1-4673-1698-9.

INTEGRATED MODULAR AVIONICS ONBOARD OF SMALL AIRPLANES – FICTION OR REALITY?

Pavel Paces, Tomas Levora, Ondrej Bruna, Jan Popelka, Jiri Mlejnek

Czech Technical University in Prague, Department of Measurement, Prague, Czech Republic

Abstract

Integrated Modular Avionics begins a core part of aircraft electronic installations on military airplanes. Based on more available and powerful electronics this concept is introduced also in to the area of civil aviation despite of more demanding certification process. Modern electronics penetrate also into ultra-light class of airplanes that are more accessible to flying public. Accidents of small and ultra-light airplanes were analyzed in order to identify ways to improve flight safety of this category of airplanes. Proposed solutions and the main findings are introduced here together with the development, evaluation and various test results. This paper presents a set of tools that allow rapid development of IMA functions and of Synthetic Vision Information System displays. System evaluation is illustrated on an IMA function performing online search for the most suitable place for landing under emergency situations. This function is also used during standard approaches to cope with high accident rate occurring during landings. It is called Safe Landing Advisory function. The function provides guidance to a pilot and navigates him to the selected safe landing place, which is evaluated by data from different sources but the final decision to use or not use the advisory service still lays on pilot. The function was evaluated with help of our custom Ground Proximity Warning System, an airplane online tracking system and a Traffic Collision and Avoidance System. Evaluation was performed with help of a free flight full-motion simulator and during a glider contest in the Czech Republic.

Introduction

The FAA estimates that non-commercial flying made up 87% of total fixed-wing time and 58% of total helicopter flight time. With total of 1310 accidents in the year 2009, the accidents of amateur-build aircrafts represents 21% of all non-commercial fixed-wing accident aircraft, a proportion that has increased steadily for more than ten years [1], see Figure 1, where there was 248 accidents in 2009.

- Previous paragraph means more and more people fly for fun – flying is more available to general public – but their pilot's experience is not enough to manage complexity of the flight under all conditions. The increasing accident rate has to be solved and one solution is better flight guidance, e.g by an electronic system that controls pilots' behavior.

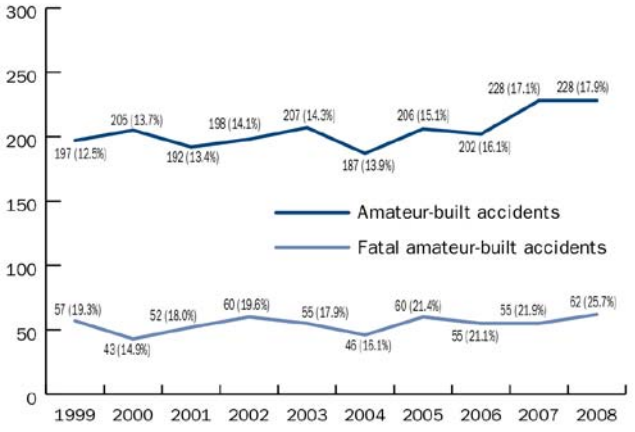

Figure 1. Accident Trend for Amateur-Built Aircraft [1]

The higher accident rate among amateur-built aircraft is not surprising. Both their physical characteristics and the way they're used expose them to greater risk and make accidents less survivable. Even by GA standards, the amateur-built fleet is exceptionally diverse, ranging from open-framework designs with no cabin structure to pressurized cross-country machines. However, the majority are small, simple craft used primarily for short pleasure flights, meaning more frequent takeoffs and landings – which together account for almost half of all fixed-wing GA accidents. Another major source of problems for pilots is unexplained loss of engine power. This is because the owners are free to experiment with

978-1-61284-798-6/11/$26.00 ©2011 IEEE

untested systems, including engines. Detailed division of accident types is depicted in Figure 2.

The experience of pilots also varies with regards of the availability of useful transition training and flying frequency [1]. Acrobatic maneuvers are prohibited in this category of airplanes but some accidents in "mechanical" and "other" categories presented in Figure 2 counts for cases where pilots took their airplanes behind the allowed flight envelope – flying low, low speed for better photographing, aerobatics, etc.

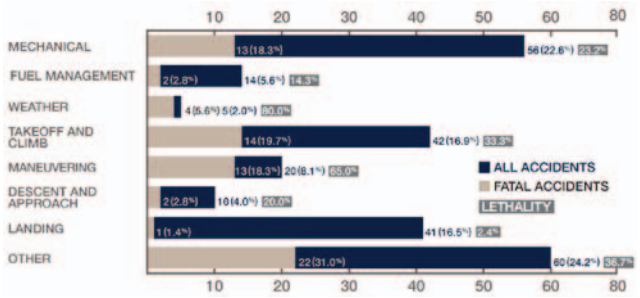

Figure 2. Types of Fixed-Wing Amateur-Built Aircraft Accidents [1]

Figure 1 and Figure 2 represent actual state in USA, but similar trend can be found worldwide and it reflects situation in the Czech Republic. Also the presented home-built airplanes accidents occur within all fleet of small airplanes that includes: homebuilts, FAR103, CS-VLA, LSA, ELA, ELSA, etc. All these categories are linked into the term "ultra-light airplane" (ULL) and this expression is used in the further text.

In order to cope with the rising accident rate in these categories of airplanes we prepared and evaluated low-cost concept of an avionic system extension that aim to advise pilots what to do in difficult phases of the flight. The proposed avionic system will deal with:

- Detection of flying behind allowed envelope;
- Future state prediction, e.g. stalled turn maneuver in low altitude, terrain collision;
- Safe landing-path advisory service for:
    - common landing and
    - unexpected engine power loss with safe landing strip detection.

The proposed system consists of:

- Position and position angles measurement system;
- Display system with advisory services – head-up, or head down;
- Data transmission channel for flight parameters broadcast.
- Computing core running IMA functions;
    - Custom Ground Proximity Warning System (GPWS);
    - Custom Traffic collision and Avoidance System (TCAS)
    - Safe Landing Advisory (SLA) function

While GPWS and TCAS are well known technologies used in aeronautics, the SLA is not and all of them forms Avionics Aided Flight Advisory System. In this article we have implemented the SLA as an Integrated Modular Avionics [2] (IMA) function to the existing Electronics Flight Instrument System (EFIS). This EFIS is intended to show mainly flight data but part of its unused computational power is used for SLA or other functions. The situation is illustrated in the Figure 3 which shows primarily flight data where part of the unused computational power is used for other (e.g. SLA) functions.

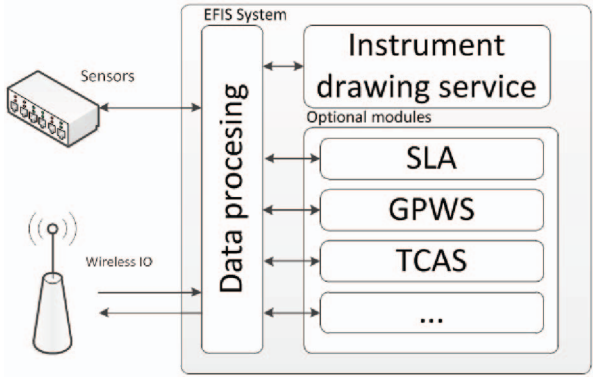

Figure 3. EFIS Module

Safe Landing Advisory System

To fulfill points defined in the previous chapter we need to develop a set of modules intended to measure and show data used for SLA implementation. First module measures position of

the airplane that is compared with actual terrain database. The final approach safe landing area detection can be performed by a special sensors [3] or data processing [4] by a digital communication system [6]. Airplane position is broadcasted outside of the airplane and received by other airplanes and also by the airfield ground station [5]. The onboard avionics system can be composed from modules connected to a CAN bus network with onboard data processing [7].

All the flight and engine parameters measurement modules are easy to develop, manufacture and certify except for Inertial Navigation System (INS) and precise position measurement system. The Global Positioning System (GPS) is used for airplane position measurement in our SLA system. We need to be independent on the ground antennas of the Instrument Landing System (ILS) [8] and GPS data provide basics for a glide path and a glide slope to be generated by a computer to guide the pilot to the detected safe landing strip. Precision of the GPS is enhanced by two means: by the data stream provided from the airfield ground station and the new system for position angles measurement that improves precision of the INS [9].

The low-cost INS systems still suffer by inaccuracies of small micro-mechanical sensors (MEMS) but its precision can be increased by new measurement devices [9]. The precision of GPS data can be also increased by other sources of information – correction receiver. The communication transceiver, which was developed for aircraft tracking system and is described in this paper, allows us to transfer data in both directions between airplanes or an airplane and a ground station.

Aircraft Tracking System

There are systems that allow tracking of airplanes in specific area. The oldest is the ground radar which was extended by Secondary Surveillance Radar and now, the latest, Automatic Dependent Surveillance, variant B (ADSB), is being introduced into general practice [10]. Commercially available modules of these systems are expensive for use within ULL category of airplanes and so we developed an ADSB transceiver variant. Our transceiver takes following parameters into account: multiple stations (tenths), small dimensions, simple installation, low consumption, minimal maintenance costs and long range (at least 60km). Technologies listed in Table 1 were considered for selection. GSM (GPRS data) network is not usable for altitude above 300 meters in some areas and satellite data transmission (THURAYA [11], IRIDIUM) is expensive.

Table 1. Solutions Available for Data Transfer

Technology	Range	Antenna size	Consumption	Operational Costs
GSM	☹	☺ integrated	☺ 0,5 W	☺
Satellite	☺ global	😐 integrated	😐 1,5 W	☹
Radio	😐 up to 90 km	😐 extern	☺ 1 W	☺

According to the given requirements, a new transceiver module was developed [5]; see Figure 4; with following components:

- uBlox GPS receiver uBlox Lea-5H;
- Radiometrix BiM1T radio module, Tx. 155,725 MHz;
- NBEK-000 data modem – 1200 bd;
- Time mark generator for TDMA synchronization;
- VF amplifier, 500 mW;
- Mikro-processor PIC18F458 with ISP debugging interface; and
- Support electronics (timing circuits, power, etc.).

Figure 4. Transceiver Developed for Aircraft Tracking

The module allows connection of a dipole antenna mounted on airplanes fuselage (see Figure 5) or a mast antenna (Figure 6) that makes installation even simpler but it is exchanged by lower communication range. The transceiver depicted in Figure 4 allows just data transmission. The receiver module is depicted in Figure 7. It is based on Radiometrix BiM1R receiver, NBEK-000 modem and it allows direct connection to a PC through the RS232.

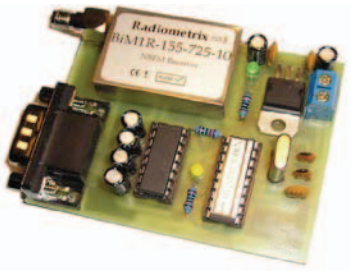

Figure 5. Receiver Module

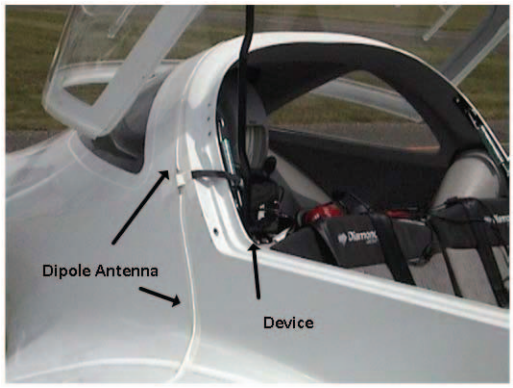

Figure 6. The Transponder and a Dipole Antenna on HK36 Dimona Test Aircraft

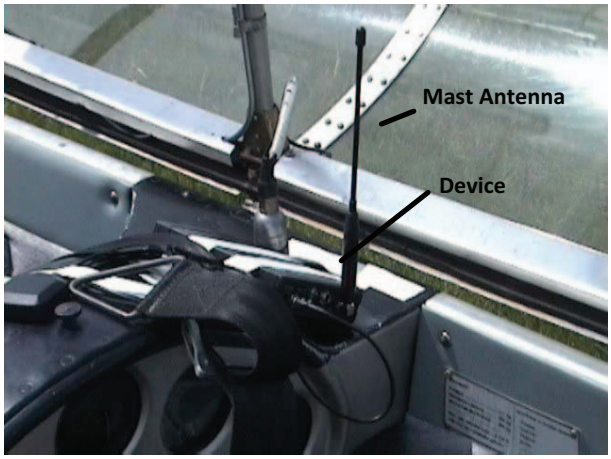

Figure 7. The Developed Transponder and a Mast Antenna on L13 Blanik

Data synchronization is based on GPS time-mark signal worldwide available with 1 micro second precision. Data can be received by a ground station and saved within a database for further processing which was used for online tracking of airplanes during glider contests. The result of the aircraft tracking is depicted in Figure 8 that shows results of airplane tracking with help of Google Earth Map. Concept of the tracking system usage during a glider contest is depicted in Figure 9. It shows airplanes transmitting their position to the ground station (the airfield, receiver and antenna installation is depicted in Figure 10). Received data are online processed by Naviter SeeYou software package and actual result of the contest is calculated. Actual performance of a selected contestant can be displayed to the public on the airfield and the data are also available from the internet for general use. It means that people with gliding simulator can compete with real contestants.

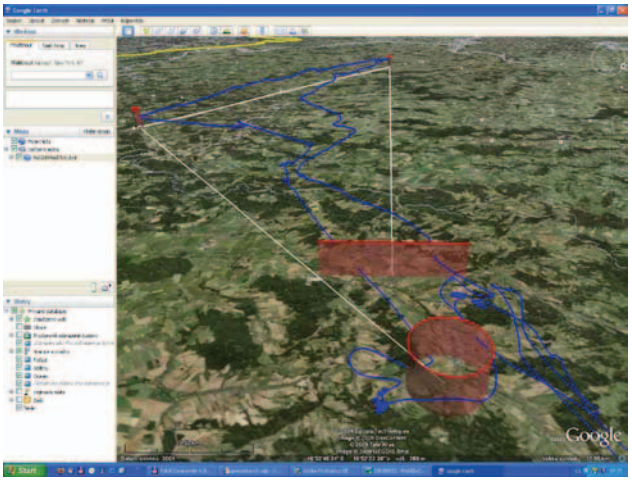

Figure 8. Flight Path Visualisation Using Google Earth

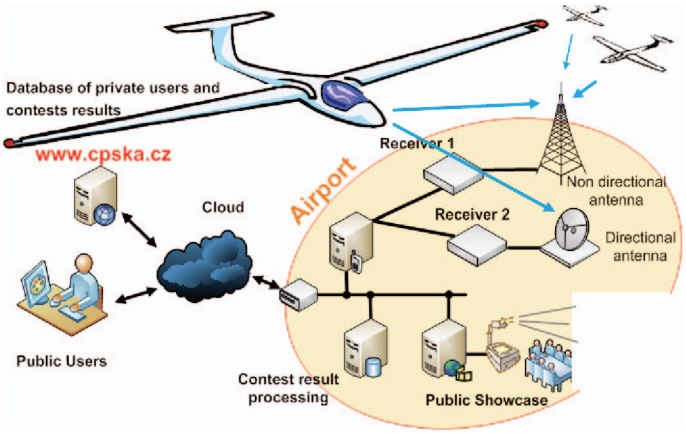

Figure 9. Aircraft Tracking System Concept Used During Glider Contest

Figure 10. Receiver Antena and Receiver Module at LKMB Airport

System Parameters

The online tracking system was used multiple times and its operational range is 80 km. The system works within speed range from 0 to 300 km/h and works within altitude up to 5 km. The improved variant can reach 120 km and it is now commercially used for airplane tracking [12].

Safe Landing Advisory Function with Real-Time Terrain Evaluation

Different statistics shows one-third of all accidents happen during landing. The SLA function is supposed to cope with accidents caused mainly by low pilot's experience by advising him most promising solution of the situation. Figure 11 shows the basic dataflow of consequent actions forming the SLA function. It continuously in a loop compares aircraft performance with airplanes current position and its state from which it is able to determine airplanes actual operational range with, or without its engine. The function compares the calculated range with terrain characteristics, near airfield database and obstacle database to determine a safe landing site. First of all, based on the actual operation range reachable airfields are identified and considered for pilot's guidance. If no fixed airfield is available the pilot is notified and direction to the nearest suitable

emergency landing site is presented on the SLA function display. The emergency landing site determination is performed by terrain evaluation.

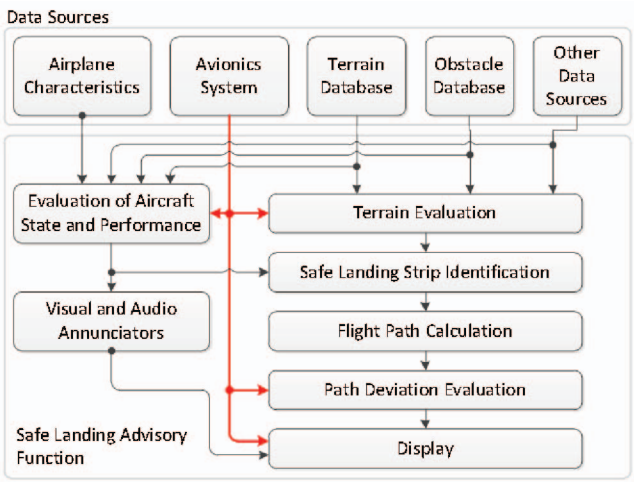

Figure 11. Data Flow Diagram in the Safe Landing Advisory Function

It is intended mainly for emergency situations like engine failure which happens often in the homebuilt category of airplanes. Obstacles are taken into account during the emergency site evaluation and the safe path generated in the computer memory avoids them. Currently, there are up to three turns of the airplane allowed to avoid dangerous obstacles. Actual number of turns that will be advised to the pilot depends on the actual airplane altitude, its characteristics (gliding ratio) and radius of the turn. After the destination safe landing strip is determined and the flight path is constructed, the system starts providing the guidance along the path. The guidance service visualization was implemented as ILS guidance beams. The ILS display instruments can be used or this visualization can be easily implemented into all display systems (e.g. [13], or [14]). We proposed extension of an EFIS display screen and also a low-cost head-up system that was developed specially for this application.

Flight States Evaluation

Actual stage of the normal flight means taxiing, engine test, take-off, hold, climb, cruise, landing, hold, touch-down, etc [15]. Other extra stages are detected when the flight envelope is overpassed. All the states are used in three subroutines of the SLA function:

- Emergency situation detection that triggers immediate search for safe landing strip;
- Continuous comparison of the actual flight stage with airplanes flight envelope that provides immediate warning to the pilot and post flight report for the airplane owner; and
- Prediction of future airplane position (up to 30 seconds) with controlled-flight-into-terrain (CFIT) detection for GPWS function.

Actual airplane position is recorded by the GPS tracking system presented in the previous chapter. Figure 12 shows actual approach landing maneuver with evaluated flight stages that are distinguished by different colors. The situation is also depicted in 2D in Figure 13 that shows top view on the recorded approach. Single stages depicted in Figure 12 and 13 are evaluated by a state machine with defined transition conditions. In our case no fuzzy logic approach [16] was used and the state machine is able to detect 20 flight stages that describe the whole flight from an engine start at the stand, over take-off, cruise, landing and return back to hangar. Flight evaluation is based on data provided by the avionics system, see Figure 11. It uses an air-data computer extended with a smart probe measuring angle-of-attack [17] of the airplane for its lift (c_x) and resistance (c_y) coefficients evaluation. Angle-of-attack measured by the system matches a point on the polar line that is combined with a table value describing glide ratio for the actual flight range calculation. The calculated operational range determines the area where the terrain is evaluated.

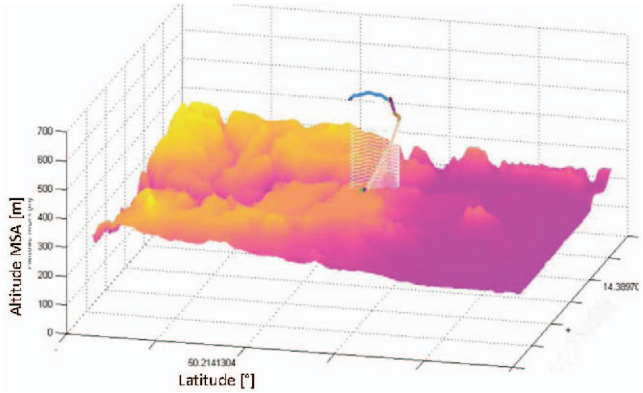

Figure 12. 3D Ilustration of Recorded Landing Maneuver with Evaluated Flight Stages

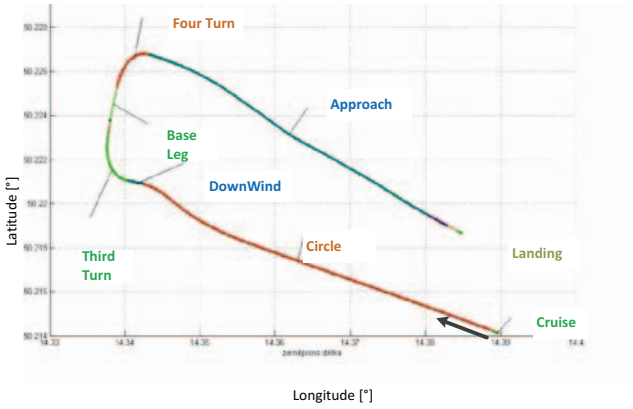

Figure 13. Top View on the Recorded Landing Maneuver with Evaluated Flight Stages

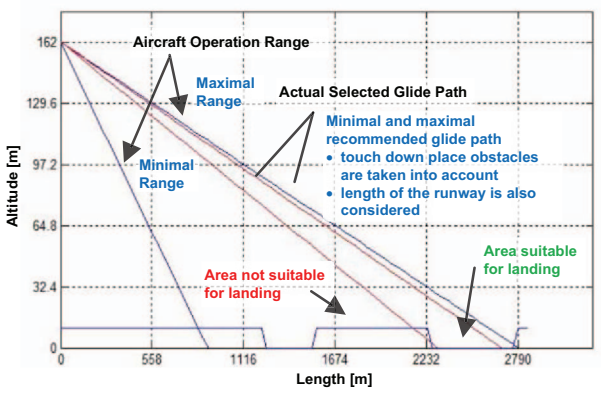

Figure 14. Vertical Situation Evaluated by SLA Function

Terrain and Landing Site Evaluation

Terrain evaluation is performed in the square area under the airplane with one side equal the double of the operational range detected in the previous step. Landing is possible just in the area with low (or zero) gradient of the slope without any obstacle, like buildings, high-voltage transmission lines, holes, streams, etc [18]. SRTM project data are used as basis for the terrain evaluation with other data sources: like custom databases and OpenStreetMap project for urban areas identification.

The ICAO standards prescribes the airfield slope has to be 2° maximum. Our algorithm detects fixed airfields and it is able to guide the pilot to them. Other landing sites are detected for emergency purposes and there our algorithm uses 5° limit for the emergency landing strip detection. This detection threshold leads to the binary terrain evaluation. The evaluation map contains two values: suitable for landing or not. The result of the terrain evaluation for emergency landing is depicted in the bottom part of the Figure 14. This figure also depicts the minimal and maximal detected approach angle that is based on the airplane performance, its actual position, speed, altitude and angle-of-attack.

Within the detected operational range of the airplane, the recommended approach glide path to the selected landing strip is offered to the pilot. The selection considers runway length necessary for the safe landing of the plane and it also try to avoid obstacles near to the touch-down point. While Figure 14 depicts the vertical situation then Figure 15 illustrates horizontal situation of a maneuver including one turn point. This scenario illustrates engine failure followed by safe landing site detection. Flight path was proposed and the pilot decided to follow the recommended trajectory. Real flight trajectory follows the recommended one with delay caused by all the data processing from sensor to the computation algorithm. The measured delay was caused mainly by the GPS sensor (~1 sec), the algorithm (~3 sec) and the reaction times of the pilot.

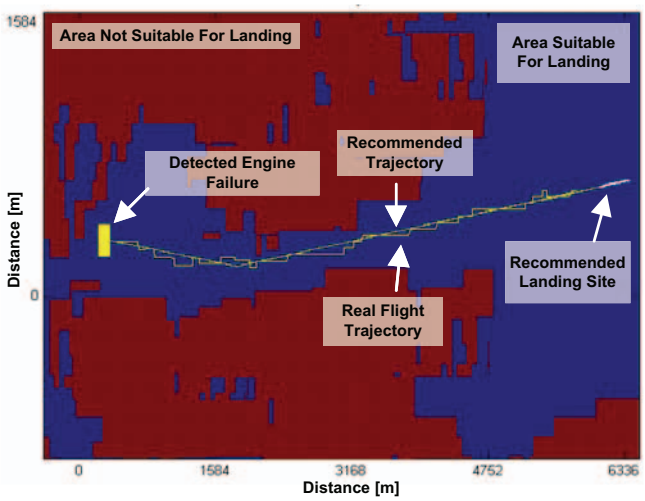

Figure 15. Horizontal Situation with Recommended and Real Flight Trajectory

The algorithm determining the recommended flight path starts in the actual direction (heading ψ) of the airplane as depicted in the Figure 14 in a vertical cut. If algorithm does not find any suitable landing site in this direction it starts the detection again with heading $\psi+n*k$ [°], where k represents one detection step, e.g. difference in heading (k=0.5°). The k is incremented by n, where n belongs to 0, +1, -1, +2, -2, etc. The algorithm ends when it finds suitable landing strip or when it finishes detection around the airplane without any result.

Flight Path Guidance and Display Devices

The result of the previously described algorithms is the optimal flight path. Flight guidance shows the horizontal and vertical distance of the airplane from the calculated flight path. The most common way of the displacement depiction is the beams currently used by the ILS system. Our SLA function is a GPS based approach guidance system that automatically construct the glideslope and the localizer wherever it is suitable - it is not fixed on the specific place as the ILS system. The glideslope and localizer displacement is aimed to be displayed at standard head-down displays or with help of a head-up display. The head-down display of ILS beams was developed with help of an IMA function development framework described in [19]. It allows common development of an EFIS screen on a standard PC and the design then also works on an embedded target platform. Our proposal of the EFIS display with SLA advisory beams is depicted in Figure 16. The actual deviation from the calculated landing path is depicted by red lines over the displacement dots drawn in the black color. The recommended airplane angle-of-attack is also given by a red line over the angle-of-attack indicator.

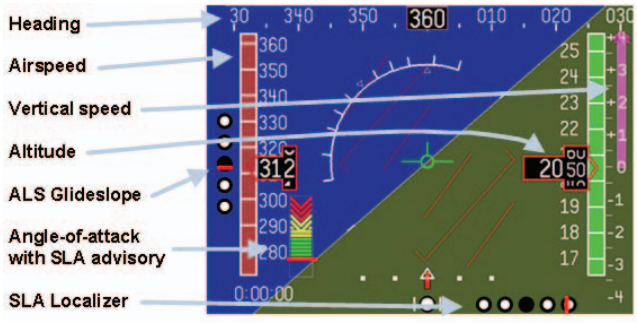

Figure 16. HeadDown Display with SLA Advisory Beams

Because the head-down displays are going to be obsolete in near future we also aim on low-cost head-up technology. Our first prototype of a head-up display is depicted in Figure 17. The device is designed mainly for the SLA guidance function based on ILS like beams. High resolution of the display is not required but simple and readable information is desirable. Head-down displays suffer from the poor visibility under bright ambient light conditions. The head-ups have to cope with even worse conditions. The image generator of our display is based on the 24x16 matrix of LED diodes with brightness ≈1cd. Their footprint is 0603 SMD package which means 1.6x0.8 mm. The image generator and optical system of the device provide symbology depicted in Figure 18. The display supports three display modes: a number representing selected quantity, artificial horizon and ILS like beams. The beams show actual displacement from the path calculated by SLA function. Figure 18c illustrates situation where the airplane is aligned with suggested flight path.

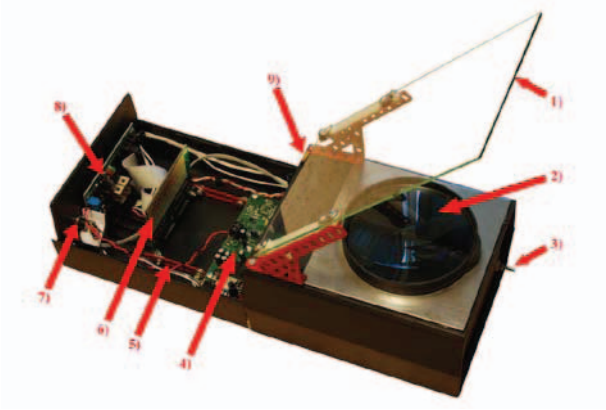

Figure 17. Headup Display Showing SLA Advisory Information

a) **b)** **c)**

Figure 18. Headup System Display Modes: Numbers, Artificial Horizon, and Advisory Beams

The head-up display (Figure 17) is a refraction head-up type with semi-transparent glass (1), collimation lens (2) that hides 45° mirror, mode selection switch (3), control and communication electronics (4. 7, 8), adjustable rails and LED matrix of the image generator (6). Currently, the display needs to improve its resolution, brightness and size. The head-up length can be shortened by adding other refractive components, which, however, results in more complex optical system that needs to be calculated correctly, e.g. a Fresnel lens with a short focus can be used instead of a classic lens (Figure 17, 2). Its resolution can be upgraded by smaller LED diodes in 0402 SMD package (1.0 x 0.5mm) but its brightness will depend on the LED diode type. The basic parameters of our head-up display compared to the commercial unit are described in Table 2 [20].

Table 2. Comparison of the Developed Headup and Its Commercial Counterpart

Parameter	Unit Under Development	Commercial Unit
View angles (TFOV)	14° x 6°	20-25°
View distance	0.3-0.5m	0.6m
Resolution	24 x 16	640 x 480

SLA Function Performance and Requirements

The main performance indicator is the time the algorithm consume for its proper operation. The time consumption presented here was measured on a 32 bit system with CPU speed 1.6 GHz and 256 MB RAM, e.g. eBOX510-820-FL, by time marks-placed in the code. The SLA function can be divided on:

- The airplane state evaluation; and
- The terrain evaluation and landing path calculation.

Evaluation of the airplane states takes 0,3 sec with main load caused by all the data acquisition from the avionics system (see Figure 11). The second biggest load is caused by CFIT algorithm of the GPWS function.

Terrain evaluation and landing path calculation results are depicted in Table 3. It shows the maximum time delay caused by the algorithm is 3 seconds. A typical situation is represented by an airplane flying at low altitude where no turns are necessary for safe landing. The maximal time was measured for scenario with an airplane flying at 1 km altitude where one turn was imposed on the pilot.

Table 3. SLA function time consumption

Task	Typ. Time [s]	Max. Time [s]
To get result about terrain evaluation	0.7	1.3
Recalculate actual position and flight path deviation evaluation	0.2	0.2
Perform all calculations	1.1	1.6
Perform all calculations and draw all the graphs online (Figure 14 and 15)	1.6	2.4

The precision of the landing was not evaluated because the SLA function just intents to guide the pilot to the specific area and then the final landing is up to him. It is a guidance algorithm and its precision depends on the precision of the GPS system which can be improved by its D-GPS variant described within the aircraft online tracking system in the previous chapter. Other precision improvements can be reached with new measurement modules [21] included into the avionic system, see Figure 11.

Practical Application

Both main parts presented in this article are going to get practical application. The airplane tracking system based on GPS satellite network and data transmission line is now online tracking system, which started as a school project, being commercially used for glider contests [5, 12] with open access database of flight tracks available at no cost.

The commercialization of the SLA function is planned as an optional part of existing EFIS system Integra (see Figure 19) offered by TL electronic company [22]. It will extend existing functionality of the EFIS for pilots who are interested in SLA function.

Figure 19. EFIS Integra for SLA function [22]

Conclusion

This article describes a function that aims to increase safety of flight by interrupting the chain of events resulting in unrecoverable pilot failure. The described function guides pilot to a safe landing strip under normal or emergency situation. The emergency situation often relates to an engine failure or maneuvering at low altitude. Under these situations pilot often overestimate his capabilities and does not evaluate his surrounding environment correctly. The guidance function reads data provided by avionics system: from a GPS sensor, an AirData computer, a terrain database and other special devices. Data are processed and recommended solution is presented to the pilot in form of an EFIS extended head-down screen or by beams showed on a low-cost head-up display that was developed directly for this application.

Our approach supposes that the guidance function remains the aid for a pilot who is the highest responsible decision maker in the airplane. He can follow the guidance or he can choose another way for the safe landing. The advisory function will follow pilot's decision and it will find a safe landing strip in the direction that was chosen by the pilot.

The guidance function is implemented as an independent module, sold separately, that will extend functionality of an existing EFIS system. Its system integration matches IMA function integration which was up to this time used mainly for military or big commercial airplanes. In our case we are an IMA function provider for the instrument integrator but the integration is often performed by the pilot in the field.

The GPS tracking system extended with local correction exchange data channel which is the integral part of the presented function is now being regularly sold as a service for an online airplane tracking during contests or for rental companies. A general GPS receiver can be used for the airplane tracking and the guidance function implementation but the extended system presented in this article brings an advantage of an independent data channel for GPS correction exchange that increases precision of the position measurement. Current system disadvantage is in time synchronized messaging.

All the modules developed, tested and presented here are standard parts that are widely available. The precision of the system is provided by new ways of measurement, e.g. the new position angles measurement system. The commercial use of both products in ultra-light category of airplanes will allow collecting pilots experience about usefulness of the presented functions in the category of airplanes not demanding so expensive certification process.

References

[1] AOPA, 2010, Joseph T. Nall Report, Aircraft Owners and Pilots Association, AOPA Air Safety Foundation home page [Online], http://www.aopa.org/asf/publications/nall.html

[2] Rierson, L.K.; 2010, "Best Practices for Certifying IMA Systems in Civil Aircraft," Aerospace and Electronic Systems Magazine, IEEE , vol.25, no.1, pp.4-8, Jan. 2010, doi: 10.1109/MAES.2010.5442147
URL: http://ieeexplore.ieee.org/stamp/stamp.jsp?tp=&arnumber=5442147&isnumber=5442141

[3] Bosch, S., Lacroix, S. & Caballero, F., 2006. Autonomous Detection of Safe Landing Areas for an UAV from Monocular Images. Proceedings of the IEEE/RSJ International Conference on Intelligent Robots and Systems (2006), p. 5522-5527. Available at: http://ieeexplore.ieee.org/lpdocs/epic03/wrapper.htm?arnumber=4059308.

[4] Takahashi, M.D., Abershitz, A., Rubinets, R., Whalley, M., 2011, Evaluation of Safe Landing Area Determination Algorithms for Autonomous Rotorcraft Using Site Benchmarking, American Helicopter Society 67th Annual Forum, Virginia Beach, VA, May 3-5.

[5] Mlejnek, J., Paces, P., 2009, Online Aircraft Tracking System, CTU in Prague thesis, In Czech, Prague, 2010.

[6] Makula, Petr; Andrle, Milos. 2009, Conception of the Digital Communication System for Small UAVs, Proceedings of the International Conference on Military Technologies, ICMT 2009, May 5-6, Brno, Czech Republic, University of Defence, pp. 235-239, ISBN 978-80-7231-649-6.

[7] Dub, Michal; Jalovecky, Rudolf; 2009, Possibilities of Flight Data Online Processing, Proceedings of 13th International Conference Transport Means, October 22-23, 2009, Kaunas, Lithuania, Kaunas University of Technology, pp. 91-94, ISSN 1822-296.

[8] Bojda, Petr; Bloudicek, Radim; 2010, Multiple Source Navigation Signal Receiver, Proceedings of 29th Digital Avionics Systems Conference, NY USA, IEEE, ISSN 2155-7209. ISBN 978-1-4244-6617-7.

[9] Paces, Pavel, 2011, Apparatus for Inertial Navigation Systems Inaccuracies Correction, Industrial Property Office of the Czech Republic, Patent No. 302336.

[10] Whalen, D.; Rathinam, S.; Bagge, C.; 2003, "Advanced Developments in Airport Surface and Terminal Area Traffic Surveillance Applications," Digital Avionics Systems Conference, 2003. DASC '03. The 22nd , vol.2, no., pp. 9.B.3- 9.1-9 vol.2, 12-16 Oct. 2003, doi: 10.1109/DASC.2003.1245908 URL: http://ieeexplore.ieee.org/stamp/stamp.jsp?tp=&arnumber=1245908&isnumber=27920

[11] Navisat Stadler, Thuraya – satellite communication network, [online 23.8.2011], URL: http://www.thuraya.cz

[12] Mlejnek, J.: FT100 product page, http://www.fid-avionics.eu/public_fid/index.php?option=com_content&view=article&id=50&Itemid=59

[13] Bojda, P.; Frantis, P.; , "Multipurpose Visualization System," Aerospace and Electronic Systems Magazine, IEEE , vol.24, no.4, pp.4-8, April 2009, doi: 10.1109/MAES.2009.4839270, URL: http://ieeexplore.ieee.org/stamp/stamp.jsp?tp=&arnumber=4839270&isnumber=4839120

[14] Chudy, Peter; Rydlo, Karol; 2011, Intuitive Flight Displays for Light Aircraft, AIAA Modeling and Simulation Technologies Conference, AIAA, Portland, OR, 2011, pp. 1-10.

[15] Hruska, M., Paces, P., 2011, Flight Parameterization with Avionics System Support, CTU in Prague thesis, In Czech, Prague, 2011.

[16] Kelly, W.E., Painter, J.H., Flight Segment Identification as a Basis for Pilot Advisory Systems, 2006, Journal of Aircraft, Vol.: 43, Issue: 6, pp. 1628-1635, doi: 10.2514/1.20484, 2006, ISSN: 0021-8669

[17] Pačes, P.; Draxler, K.; Hanzal, V.; Čenský, T.; Vaško, O.; 2010, "A Combined Angle of Attack and Angle of Sideslip Smart Probe with Twin Differential Sensor Modules and Doubled Output Signal," Sensors, 2010 IEEE , vol., no., pp.284-289, 1-4 Nov. 2010, doi: 10.1109/ICSENS.2010.5689866, URL: http://ieeexplore.ieee.org/stamp/stamp.jsp?tp=&arnumber=5689866&isnumber=5689839

[18] Nekvasil, V., Paces, P., 2010, Algorithm For Safe Landing Guidance, CTU in Prague Thesis, In Czech, Prague, 2010.

[19] Pavel, P.; Martin, S.; 2010, "Introducing Students to Aerospace Board Information Systems Using an Embedded Graphics System Simulator," Advanced Learning Technologies (ICALT), 2010 IEEE 10th International Conference on , vol., no., pp.397-399, 5-7 July 2010, doi: 10.1109/ICALT.2010.114, URL: http://ieeexplore.ieee.org/stamp/stamp.jsp?tp=&arnumber=5571408&isnumber=5571093

[20] Paces, P., Hajny, J., Popelka, J., 20111, Advanced Display Methods for Small Airplanes, Proceedings of MDS PSL, Brno, Czech Republic

[21] Sotak, M.; Labun, J., 2011, The New Approach of Evaluating Differential Signal of Airborne FMCW Radar-Altimeter. In: Aerospace Science and Technology, Elsevier, Article in Press, doi: 10.1016/j.ast.2011.02.007, ISSN: 1270-9638

[22] TL Elektronic,2011, Online: www.tl-elektronic.com/

Acknowledgements

This work was supported by the research program No. MSM6840770015 "Research of Methods and Systems for Measurement of Physical Quantities and Measured Data Processing " of the CTU in Prague sponsored by the Ministry of Education, Youth and Sports of the Czech Republic. Some parts of the work were supported by the research program no. TA01030651 "Safety Improvement of Flight, Crew and Other Participants of Flight Transport in Normal and Emergency Situations by Assistive Technologies" of the Czech Technical University in Prague, sponsored by the Technological Agency of the Czech Republic.

Email Addresses

Authors can be contacted at these email addresses:

Pavel Pačes: pacesp@feld.cvut.cz,

Tomas Levora: levortom@feld.cvut.cz,

Ondrej Bruna: brunao1@feld.cvut.cz,

Jan Popelka: popelj3@fel.cvut.cz, and

Jiri Mlejnek: mlejnek@fid-avionics.eu.

30th Digital Avionics Systems Conference
October 16-20, 2011

Introducing Students to Aerospace Board Information Systems

Using an Embedded Graphics System Simulator

PAČES Pavel, ŠIPOŠ Martin
Department of Measurement
Czech Technical University in Prague
Technicka 2, 166 27, Prague, Czech Republic
e-mail: pacesp@feld.cvut.cz, siposmar@feld.cvut.cz

***Abstract*—A graduate-level engineering course in airborne sensor and control systems taught at the Czech Technical University in Prague under the title Board Information Systems takes a novel systematic and comprehensive approach to teaching airborne digital avionics systems, together with system certification and life-cycle operations. The course brings together materials from various sources to cover practical aspects of avionics systems ranging from design, prototyping, testing, certification and production through to maintenance. It prepares students to deal with a wide range of the type of real-world problems that they will meet in their professional careers. This is a required course offered in 10th semester as a part of the study programme in Airborne Information and Control Instrumentation (AICI) by the Department of Measurement. The course was redesigned with new lecture content, practical exercises and field trips. The course evaluation survey results from 2008 and 2009 show that recent students have considered the course a valuable part of their curriculum, and that it has made them feel more competent in the field of digital avionics systems.**

The course syllabus and other data are available online at http://www.pacespavel.net/PRS/.

Computer Aided Education; Airplanes; Avionics; Systems; Synthetic Vision Systems

I. INTRODUCTION

This paper provides an overview of a course in Board Instruments Systems (BIS) [1] that is taught in compliance with European Aviation Safety Agency (EASA) aerospace standards. The BIS curriculum develops students' knowledge of electrical engineering, computer engineering and information technologies. Computer simulation, which has become increasingly available [2] even for industrial environments [3], is used to attract students' attention. Students develop their own avionics instruments, which are later connected into a network with modeled flight data. During the classes, teams of students work with standards, and teachers act as a delegated certification authority for student products that are finally approved (or rejected) and used as a part of student's final assessment (it represents an analogy to the real instrument certification process). The whole content of the course in BIS is based on the authors' personal experience acquired during their work in the aerospace industry.

Current avionics installations consist of a sensor that converts a magnitude into electrical signals measured by a signal converter. This converter transforms the measurement into digital values that are sent through an avionic network to a display instrument placed in the cockpit of the aircraft. The scenario is displayed in Fig. 1, which shows a retrofitted installation of the avionics system on a Mil Mi 171 military transport helicopter [4] that is the most used for civil and military airplanes [5].

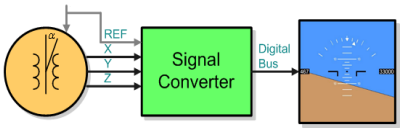

Figure 1. Basic Measurement Chain of an Aerospace Systems.

Figure 2. Dynon D-10A EFIS System.

The first two blocks (a sensor and a converter) can be joined into a single system called a "smart" sensor, which is characterized by its ability to transmit digital values. Smart sensors usually utilize a built-in-test (BITE) capability for monitoring accuracy of provided data through fusion of values from multiple sources. An example of this approach is presented in a patented technology for airspeed error monitoring [6] submitted by Airbus after an unexplained A330 crash during a flight from Brazil on 1 June 2009.

The state-of-the-art of avionics systems is influenced by smart sensors and Liquid Crystal Display (LCD) technology that leads to reductions in weight, size, energy consumption, and brings a huge advantage in the variability of displayed information (see Fig. 2 for an example).

II. BOARD INFORMATION SYSTEMS

CTU students take a master's study programme in Cybernetics and Robotics. After general courses the students choose a specialization, e.g. Airborne Information and Control Instrumentation (AICI) in which BIS is a required course.

A. *Course content, course aims and style of teaching*

The BIS courses start with an introductory lecture about the course content followed by lectures in quantity measurements, smart sensors, signal processing and on ways of transferring the available data into the pilot's cabin and displaying it in the clearest and richest possible format. There are practical exercises, home assignments and field trips to external companies.

1) *Lectures*

The BIS lectures introduce the life-cycle of an aircraft instrument, followed by a description of specific problems related to:

- Legal aspects of airborne system certification.
- Special issues in digital avionics systems.
- Training devices and flight simulators.
- Redundant systems and safety assurance.
- Special issues in digital avionics systems: Full Authority Digital Engine Control, Ground Proximity Warning Systems, and the Traffic Collision and Avoidance System.

Emphasis is placed on systems integration, aerospace standards and future trends. The lectures are supported by experiments and games to aid students' understand and memory of the presented topics. The subject is supplemented by professional visits to companies producing aircraft parts and appliances, e.g. GE Aviation Prague (M601 turboprop engines), Microtechna Modrany (flight instruments), to companies providing maintenance and training services, e.g. the CA Training Centre [13] (A320 full-motion simulators).

2) *Exercises*

The exercises place emphasis on student collaboration, project presentation skills, and working with standards. Students develop their ability to debug visualization software composed from multiple libraries and prepared by various teams. The course is divided into:

- Measurement exercises, and
- Development of a cockpit display instrument phase.

The measurement exercises work on instrument testing during its certification phase. This part of the exercises involves performing measurements of selected quantities of aircraft systems, e.g. accelerometers, the engine monitoring system and the influence of temperature on sensing elements.

The development of a cockpit display instrument forms a key part of the exercises. The students are divided into teams and receive prepared pieces of software representing a smart sensor (Magnitude Generator (MG)) and a display instrument (Magnitude Instrument (MI) [7]). These programs communicate with each other over a Universal Datagram Protocol (UDP) but with the CANaerospace [8] protocol layer. The MG sends simulated sensor data to an MI, which receives a data stream and depicts the data on the prepared graphics interface. These programs, depicted in Fig. 3, are analogous with the previously described interconnection of avionics systems (see Fig. 1). The students' home assignment involves gathering information about their systems. This data and the proposed assignment solution plan are presented after the measurement exercises.

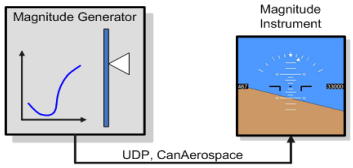

Figure 3. Software blocks used during BIS exercises

The final students' evaluation requires successful completion of all parts of the instrument development process, followed by a test of the display system in a network with flight data provided by the Flight Gear [9] simulator.

All the software was developed with support of the Microsoft Development Network Academic Alliance [10] program (MSDN AA), which makes available products such as Microsoft Visual Studio (MSVS). MSVS was used for developing a graphical embedded system simulator [7] that is internally composed of the four pieces (libraries) depicted in Fig. 4 that are in direct relation to an embedded system (Fig. 5). The MI API is compatible with the Ingenia [11] Duet embedded system. Students work on the Gauge project (Fig. 5B) with comfortable debugging tools (Fig. 5D). The MI provides them all resources as a real computer with an LCD display (Fig. 5A, C).

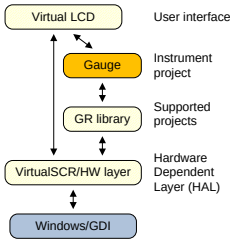

Figure 4. Magnitude Instrument internal structure

Figure 5. MI relation to an embedded system

III. Results and Student Survey

The results of the students' work at the end of the 2009 winter term are depicted in Fig. 7, which displays real data collected from the Flight Gear simulator flying a Cessna Citation-X jet aircraft over the Golden Gate Bridge in San Francisco. The picture shows an Electronic Flight Instrument System that can be compared with the real D10 instrument available from Dynon (see Fig. 2).

A. *Course Evaluation*

The results presented here cover years 2008 and 2009. The main difference between the two years is the introduction of the FlightGear simulator as the data source for students' projects. The usage of this simulator was appreciated by 100% of the 2009 participants. There were 35 course participants in 2008 and 23 participants in 2009. In both years, about 93% of the students evaluated their own attitude toward aeronautics as positive. Fig. 6 shows positive changes in students' opinion on the course. However, students showed very little interest in the lectures that were offered, more than 90% of which were attended just by 6% of students in 2008. However, the percentage of attendance

rose to 46% in 2009. In both years, there was 80% participation in the practical exercises. At CTU in Prague, attendance at lectures is optional, but satisfactory attendance of practical seminars is required.

According to responses to a questionnaire, students were given the option to do instrument development at home, on their own computers [12] supported by consultancy with teachers. None of the students considered that more difficult exercises were needed.

Important results for the course in BIS are displayed in Fig. 7, which presents students' opinions about usefulness of the presentations made by each team in the middle of the semester, where they present their plan for carrying out their assignment, the instrument functionality, the shape that they will draw in MI, and the communication packets that they need. The expected answer about the usefulness of this presentation would have been 100% Yes in both years. However, the results are considerably uncertain, and it is necessary to investigate ways of raising the approval rating.

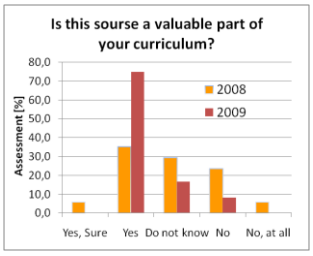

Figure 6. Changes in students' opinion about the course.

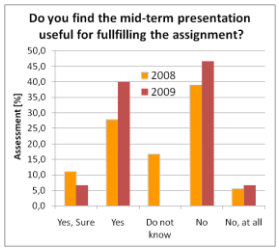

Figure 7. Students' opinion about the mid-term presentation.

IV. Conclusion and Lessons Learned

The presented simulator of a graphical development environment makes significant savings in education in such expensive area as aircraft systems are. This paper briefly introduces the course in Board Information Systems that is being taught at CTU in Prague. Students learn how to design and certify their products in procedures similar to the real ones required by EASA. Students' products are software blocks running on a prepared embedded system simulator that enables a simple and rapid development process for graphical applications. The aim of the course is to prepare avionics systems professionals who, after graduation, will work in development, maintenance or civil aviation authority organizations.

This paper has presented the application of a free flight simulator in classes dealing with instrument development and certification problems for aircraft, trains and other systems. It provides a very cheap and available configuration that has been very much appreciated by all students together with field trips to companies working in the field of aviation products and services, especially the full motion simulators.

The course was first offered in 2008 and questionnaires filled in by students show the growing reputation of the course. However, the course is still developing and will continue to develop, because BIS is a dynamically developing field. The survey also gives valuable suggestions for future improvements of the course. The aim is to achieve as near as possible 100% student approval for the course, and to reduce drop-out and failure rates as far as is compatible with the university's high standards. Higher attendance at lectures is also desirable, though many of the questions that this raises are beyond the control of the authors of this paper.

Figure 8. Final Instrument Developed by Students and Connected to the Flight Gear Simulator (comparable with Fig. 2).

Acknowledgment

This acknowledgment thanks all students who filled in the questionnaires. We also express our gratitude for the project under which the embedded simulator used during the BIS lectures and classes was developed (MSM6840770015).

References

[1] Pačes, P., "Curriculum of Board Information Systems. Board Information Systems - Information for students," [Online] 1.0, 2009. [Cited: 01 12, 2010.] http://www.pacespavel.net/PRS.

[2] Sopata, M., Soták, M. and Bréda, R., "Missile Systems Education using Simulation Environment," Prague: Simulation Almanac 2005, Praha: Czech and Slovak Simulation Society and Department of Computer Science and Engineering FEE CTU, 2005. pp. 119-124. ISBN 80-01-03322-8.

[3] Conn, R., "Developing software engineers at the C-130J Software Factory," IEEE Software, 2002 , Vol. 5, pp. 25–29, ISSN: 0740-7459.

[4] Pačes, P., Jelínek, L. and Jaroš, R., "LUN 1794 Converter - Special Functions," Brno: University of Defense, Faculty of Military Technologies, 2008. pp. 55-66. ISBN 978-80-7231-555-0.

[5] Pařízek, J., "Overview of JAS-39C GRIPEN Avionics Systems," Proceedings of the International Conference on Measuremnt, Diagnostics, Reliability of Avionics Systems 2008. Brno: UNOB, Faculty of Military Technologies, 2008. ISBN 978-80-7231-555-0.

[6] Freissinet, S., "Method and Device for Monitoring the Speed of an Aircraft," Patent 20090299554, USA, 12 03, 2009.

[7] Pačes, P., "Development Platform for Avionics Instrumentation". Prague: Czech Technical University, 2008 PEGASUS-AIAA Conference.

[8] Stock Flight Systems, "CAN Aerospace Interface specification for airborne CAN applications V 1.7," Berg/Farchach, Germany.

[9] The FlightGear flight simulator project. [Online] http://www.flightgear.org/.

[10] Microsoft Corporation, "MSDNAA Overview - Microsoft MSDN Academic Alliance Program,". [Online] [Cited: 01 12, 2010.] http://msdn.microsoft.com/en-us/academic/default.aspx.

[11] DevCom Ltd., "MPC 880 Ingenia . Single-board computers," [Online] DevCom, 2009. [Cited: 01 12, 2010.] http://www.devcom.cz/en/industrial-systems/products/mpc880-ingenia.

[12] M. Khalifa and R. Lam, "Web-based learning: Effects on learning process and outcome," IEEE Trans. Educ., vol. 45, pp. 350–356, Nov. 2002.

[13] Czech Airlines, "Introducing the Czech Airlines Training Centre," [Online] [Cited: 01 12, 2010.] http://www.csa.cz/en/stredisko/index_stredisko.htm?userLanguage=en.

ADVANCED DISPLAY AND POSITION ANGLES MEASUREMENT SYSTEMS

Paces Pavel*, Popelka Jan*, Levora Tomas*
***Czech Technical University in Prague**
pacesp@fel.cvut.cz; popelj3@ fel.cvut.cz; levortom@ fel.cvut.cz

Keywords: *head-up, avionics, navigation, position angles, data fusion*

Abstract

In this article we introduce a patented and a completely new concept of airplane orientation angles measurement system which is furthermore referred as a pressure reference system. The authors also propose an arrangement of a magnetometer unit with multiple sensors that perform online calibration of hard iron and soft iron distortions. These systems are mutually connected to a WiFi network with other modules, head-down and head-up displays. There is also description of common avionics system units and sensors and their relation to the new proposed system.

General aviation accounts for about 77 percent of the total flight hours while the rest are routinely scheduled flights. General aviation operations range from short-distance flights in single engine light aircraft to long-distance international flights in private jets, aero-medical operations and flying for fun. Electronics onboard of the airplane nowadays costs around one third of the airplane total price which vary with the precision and capabilities of the electronics system. Demand for the more precise but low-cost navigation which could improve some safety issues is being solved by data fusion of different sets of low-cost micro-mechanical sensors. Mainly signals provided by global position system and triads of inertial measurement sensors are being investigated and tightly coupled. This combination is capable to provide position of the airplane and its orientation angles. This article presents a new system that provides new information about orientation angles which can be used within data fusion algorithms to increase precision of the displayed information.

1 Avionics System

General aviation airplanes [1] include wide variety of types whose mechanical and electronic systems (avionics) [2][3] are designed according to their intended use with regard to ambient conditions [4]. The systems are divided according to visual meteorological conditions (VMC) and instruments meteorological conditions (IMC) capable avionics which differs mainly in presence of an attitude indicator that provides information about horizon. The simplest avionics system is composed from mechanical instruments that are old, hard to interface with other systems, but reliable. The amount of electronics that is incorporated in the instrument allows us to divide instruments into the following maturity types:

- Type 1: mechanical or simple electromechanical instruments, e.g. rotating gyroscope based attitude indicator or a volt meter used to indicate exhaust gas temperatures.
- Type 2: simple electronic instruments with a digital information display, e.g. an altimeter with numerical output.
- Type 3: advanced display system with embedded graphic computer

Because type 1 instruments are long time available on the market they are also reliable, but difficult to manufacture and calibrate. Type 2 instruments provide just simple numerical information which is not ergonomically optimized, e.g. it takes time to interpret the displayed value and its changes [5]. The disadvantage of type 3 is the difficulty of their

certification process but manufacturers and mainly users like the possibility to extend functionality of the system.

General aviation airplanes use all the three instrument maturity types. In modern installations, types 1 and 2 are used as a backup instruments and type 3 as the main source of information that combines engine, flight and navigation data. The latest development effort is aimed to add a smart guidance or a virtual assistant to these systems in order to improve flight safety [6][7][8][9][10].

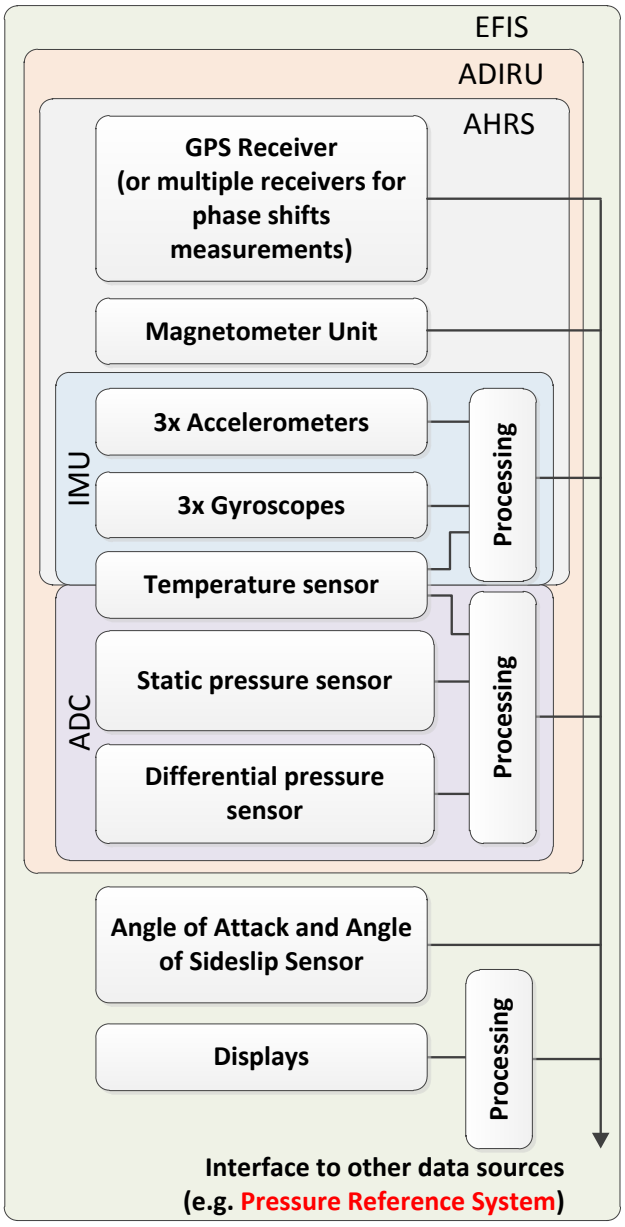

Fig. 1. Avionics System Sensors with Possibility to Interface Other Data Sources

1.1 Sensors and Systems

Reliable information [11] is necessary for safe airplane guidance during flight time and also during taxiing [12]. There are different principles being used that measures ambient environment around the airplane, its motion changes [13] and receives signals from different sources [14]. Pilots interact with dashboard gauges and control items. The past systems used independent data sources and display instruments. With electronics advancements the independent systems became replaceable electronic blocks that are able to distribute data [15] to other systems [16]. This concept is known as federated avionics and the blocks are called Line Replaceable Units (LRU).

The latest development of the modern avionic systems integrates all the sensors and processing modules into a network that allows data sharing [17]. Task of the LRUs, which contains electronics and software, has changed. In the new concept software functions performs tasks which were intended for single LRUs before. This approach is called Integrated Modular Avionics which is used mainly on brand new airliners. With rapidly increasing infrastructure available onboard of the airplane there arise new problems with safety [18][19] which were not present before and for which there are no certification guidelines.

The certification process [4][18] also changes with changing approaches for avionics development [20]. In the area of flying for fun airplanes, the development of avionics system is the most progressive because there is no demand for time consuming and costly certification. The avionics development for these airplanes is driven mainly by customer demand.

There are multiple systems commercially available for very low prices. The low price often means also low precision of the measurement system that is based on Micro-mechanical System (MEMS) sensors. Accelerometers, angular rate sensors, pressure sensors and temperature sensors are often used. In order to improve performance of the overall system different data fusion algorithms are used [21] within an electronic unit that contains all

the necessary sensors which is called an Electronic Flight Instrument System (EFIS) [6] (see the block diagram in Fig. 1). These EFIS systems include a powerful processor and all the necessary sensors that are usually used with Air Data and Inertial Reference Units (ADIRU) [22].

As it was mentioned the sensors used within these systems requires calibration before it is possible to use them for different data fusion algorithms. It is possible to update calibration data during the flight which is usually based on a signal from a sensor that provides, in a specific state of the flight [6], more precise information [21][23]. The sources of information and sensors used for data acquisition are described in the following chapters where we describe single modules used in an airplane that are depicted in Fig. 1 within one EFIS instrument.

1.1.1 MEMS Challenges

Nowadays there is demand for systems based on low-cost micro-mechanical (MEMS) sensors [24]. These systems are not precise [25] because their precision depends on characteristics of used sensors that are in case of MEMS sensors highly dependent on the ambient environment. Despite continuous improvement of the material characteristics [26], the environment still influences linearity, scale factor, offset and hysteresis of the sensor, long term stability, their response on overloading, output value change caused by exposition to boundary temperature, etc. It is possible to correct all the long term changes with help of a polynomial function or a table whose coefficients were acquired from a set of demanding and often repeated measurements of all the sensor's characteristics. Another approach is to employ natural characteristics of redundant sensors.

Natural characteristics of sensors can be used to remove their dependence on the ambient environment [27]. First approach is to use multiple sensors of the required quantity and use them to improve precision of the output value, e.g. sensors with different measurement ranges and sensors that are used just to determine outside influences effecting on the sensor. To use a sensor just to measure ambient environment influences requires isolating it from the measured media. In case of pressure sensors, a blinded one can be used to measure outside temperature effects and also aging of the sensing element. In case of blinded sensor the isochoric process behavior can be used to extract sensors temperature dependences. What will rest after isochoric process subtraction is the temperature influence and aging effects. Another approach is to use a feedback system which in a loop periodically adjusts the correction coefficients of the sensors based on external information [25]. For example, the external information for an accelerometer sensor can be provided by the absolute pressure sensor which measures constant output value which means there is no vertical acceleration and so the actual offset of the acceleration sensor can be measured and stored for future use.

When MEMS sensors are used for precise measurements they are no longer low-cost. For example Air Data Computer uses sensors measuring absolute and relative pressures, see Fig. 3, where the required precision of the measurement is given by safety standards. For this special application it is possible to use sensors which were specially and carefully manufactured, tested, pre-selected, provided with a polynomial expression [28] describing its behavior with regard to temperature and fulfilled procedures required by Civil Aviation Authorities (CAA).

1.1.2 Sensor Calibration

Sensors used within Air Data Computer [29] provide one dimensional pressure data that depends on the quality of the sensor. According to the equation (1) calibration of the sensor reading x is usually performed whit regards to temperature t where both offset b and scale factor a parameters are function of temperature. These parameters can be either functions or tables or a different method of temperature corrections can be used, e.g. as described in [27].

$$y = a(t, \dots)x + b(t, \dots) \qquad (1)$$

One dimensional example can be extended for vector quantities as angular rate, acceleration and magnetic field sensors. These values are usually used to compute position of the vehicle [30]. The 3D sensor error model is usually denoted as (2):

$$\begin{bmatrix} x \\ y \\ z \end{bmatrix} = \boldsymbol{M} \cdot \boldsymbol{S} \cdot \begin{bmatrix} x_m & o_x \\ y_m - o_x \\ z_m & o_z \end{bmatrix} \qquad (2)$$

Where x_m, y_m and z_m are data provided by the sensor; o_x, o_y and o_z are offsets of single axes; $\boldsymbol{S}$ is a 3x3 matrix of scale factors; $\boldsymbol{M}$ is a 3x3 matrix describing misalignment of the orthogonal sensor arrangement; and x, y and z are calibrated output values. Comparison of different calibration methods is described in [31]. While it is quite simple to use described sensor calibration with angular rate or acceleration sensors the airplane heading is determined by a three dimensional magnetometer whose output depends on the position of the sensor and also on the presence of any ferrous material in the surrounding of the measurement unit. Fig. 2 depicts output of a magnetometer sensor with offsets in all three axes that are caused by hard iron distortions.

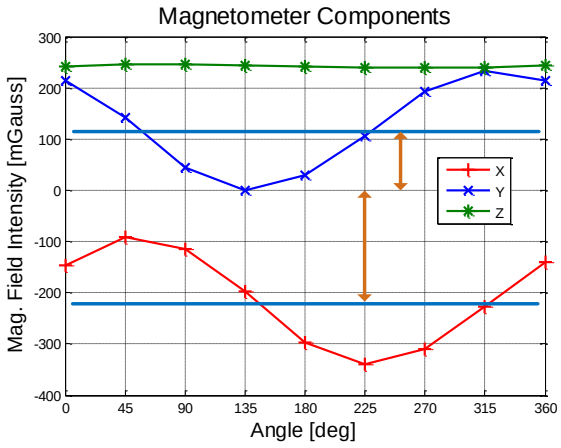

Fig. 2. Outputs of a Magnetometer Sensor before Calibration

The sensor calibration described in equation (2) will work properly just until the composition of the items disturbing the Earth magnetic field keeps stable. Any change of the field caused by surrounding material will change offsets of the measured components and resulting heading computation (3)

$$\psi = arctg(Y/X) \qquad (3)$$

will provide unexpected results. This magnetometer behavior causes problem during magnetometer usage for indoor navigation. One possible solution that removes described problems with hard iron distortions is proposed below in this article.

1.1.3 Air Data Computer

The safety of aviation depends on the precision of pressure measurements performed onboard of an airplane. An altitude measured by the atmospheric pressure is called barometric altitude where the pressure measurement conversion into altitude is calculated according to the International Standard Atmosphere (ISA) and the derived barometric formula. The important part of the barometric formula is the reference pressure level that defines origin for the calculation. The mostly used reference pressure level is a pressure at 0 m above ground level (AGL) defined according to ISA. When all the measurements on all airplanes are related to one reference level and all planes fly at different altitudes, with a safety margin, then there is no chance the airplanes could crash each other because pressure changes are smooth (continuous). This expectation is one condition for the successful operation of a concept of a new system for position angles measurement.

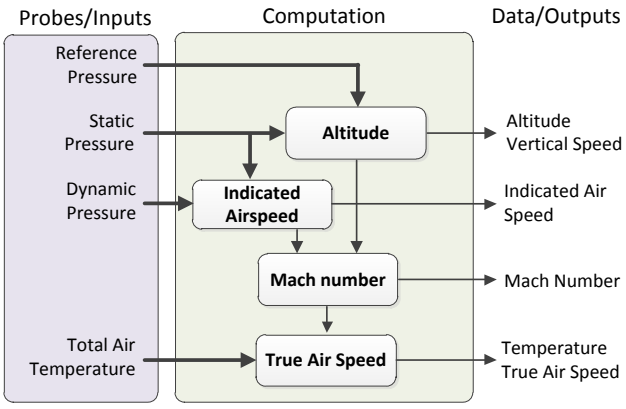

Fig. 3. Air Data Computer, Its Inputs and Outputs

The movement of the airplane in air mas generates a pressure that is related to the speed of flight. This pressure is called dynamic pressure and it is measured to get indicated air speed which is related to the wing-lift that allows the airplane to maintain altitude.

While the new system for position angles measurement uses pressure readings in principle multiple Pitot-static probes will be used. Generally the movement of the airplane and dynamic pressure will cause problems.

A combined device that measures static and dynamic pressure is called Air Data Computer. This device performs measurements, calibration of sensors, altitude calculations, calculations of different air speeds [32] and it also provides other data (see Fig. 3). Pressure sensors are highly dependent on the ambient environment [29]. Precision of the static pressure measurement is the most demanding at the 0 m AGL (6 meters or 75 Pascal) as it is depicted in meters and related pressure in Fig. 4. There are similar requirements on the differential air speed sensor which are depicted in Fig. 5. The highest requirements on the precision of the air speed measurement are around the stall speed which is usually under 100 km/h and the required precission is 8 km/h or 60 Pa.

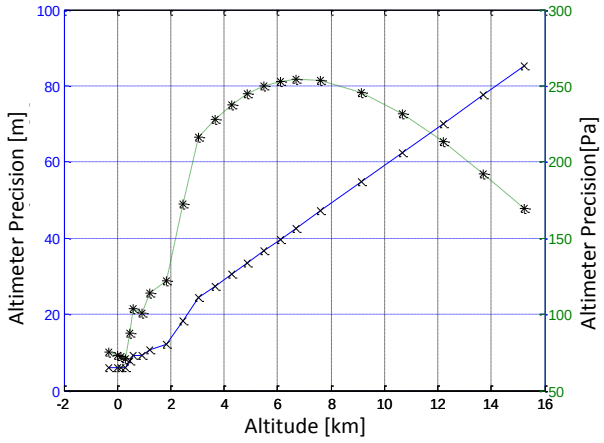

Fig. 4. Requirement for Altimeter Precision in km and Pa Related to Altitude

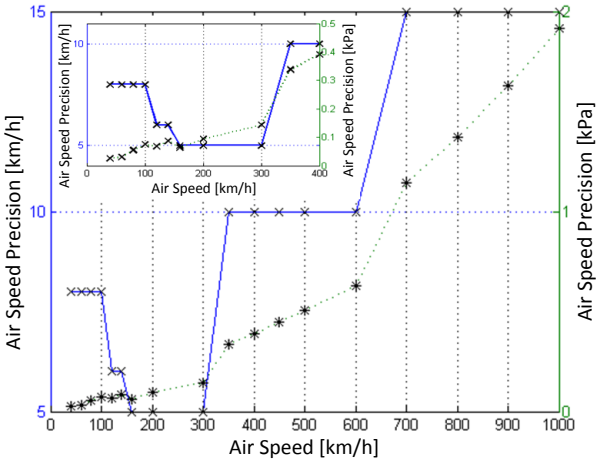

Fig. 5. Requirement for Air Speed Measurement System Precision in km/h and kPa Related to the Actual Speed

1.1.4 Inertial Measurement Unit and Global Positioning System

An Inertial Measurement Unit [13] is a device that contains a triad of accelerometers and a triad of angular speed sensors. These sensors are used to calculate orientation angles of an airplane and sometimes, also, they are used as the information source for the whole navigation solution. An IMU is a part of an Attitude Heading and Reference System (AHRS) or an Inertial Measurement System (INS). The sensors used in these systems differ in precision which is connected with their price. An INS [33], which is based on very precise and expensive sensors ~ 75 000 USD is able to maintain required navigation performance, which is a change of calculated position lower then ± 500 m, for about one hour in a mode that is based solely on the inertial sensors (pure inertial mode). Because of the price and precision, the low-cost and low precision sensors are used just for orientation angles determination. These sensors are complemented by a GPS receiver that is used as a source of navigation data. This combination is usually referred as an AHRS unit whose precision is then based mainly on the GPS and this mode is called hybrid mode. During the whole operation time, this mode keeps constant precision of 25 meters which is often supported by data fusion algorithms [34]. The INS unit referred here uses Honeywell Ring Laser Gyroscopes and

Honeywell Q-FLEX QA-950 accelerometers which provide parameters several orders better than we can get from MEMS sensors.

Qualitative comparison between a group of sensors can be performed based on Allan Variance method of moving average which plots averaging products based on averaging time. This is an official method [35] for angular rate sensors comparison. In this article we compare Allan Variance deviation for an output of Honeywell LaseRef V RLG angular rate sensor and STmicroelectronics iNemo MEMS based AHRS unit. The data were simultaneously measured from LaseRef V unit and iNemo AHRS for about one day. The output of Honeywell system is depicted in Fig. 6 from which we selected night part of the measurement with no noise caused by the people walking and closing doors in the surrounding. The Allan Variance plots comparison is depicted in figure Fig. 7. From the graphs we can read sampling frequencies of both signals which were 100 Hz for LaseRef label 327 and 50 Hz for iNemo LY330 angular rate sensor. The vertical difference clearly shows superior performance of the laser gyroscope over its MEMS alternative. We can also get impression about the best possible output provided by both sensors at the lowest point of the depicted curves. Angular rate sensor of iNemo AHRS reaches the minimum around 10^3 s which is also presented by the sensor's manufacturer. There is no minimum for the RLG gyroscope because the selected data acquisition time is too short.

The key problem with navigation solution computation and therefore conversion of the sensor inertial data to position is influenced mainly by the double integration algorithm that highlights all the sensor errors and ambient environment problems. The simplest flat Earth navigator [36] which does not take into account changes in gravitational and magnetic field, Earth coordinates and Earth rotation is depicted in Fig. 8. The accelerometer output is double integrated to provide position and velocity but before the integration the signals are usually transposed from the body frame of the strap-down measurement unit into the navigation frame where the vehicle performs its navigation. The figure clearly shows that the angular rate sensors are used to provide transformation matrix between body and navigation frame with help of single integration or fusion from different sources, e.g. accelerometers in rest, magnetometer, etc.

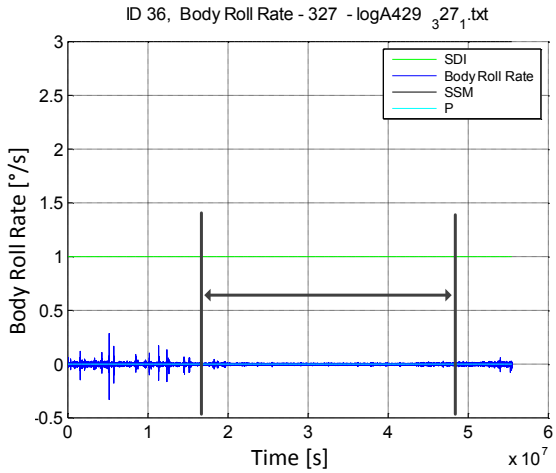

Fig. 6. Illustration of Acquired Data Set (Honeywell LaseRef V) and an Interval Used for Evaluation by Allan Variance method

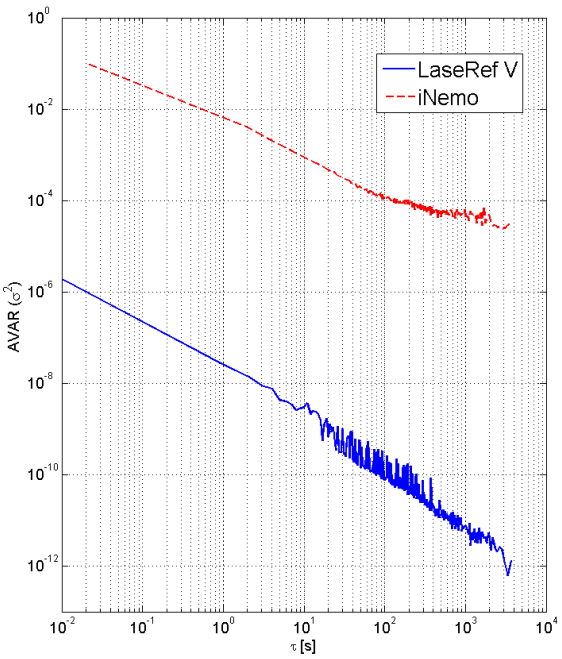

Fig. 7. Allan Variance Plot for a RLG sensor and a MEMS based device

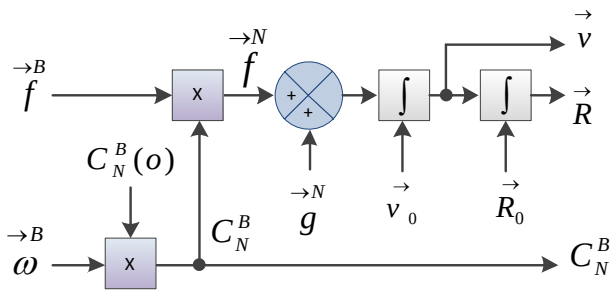

Fig. 8. Flat Earth Navigator [36]

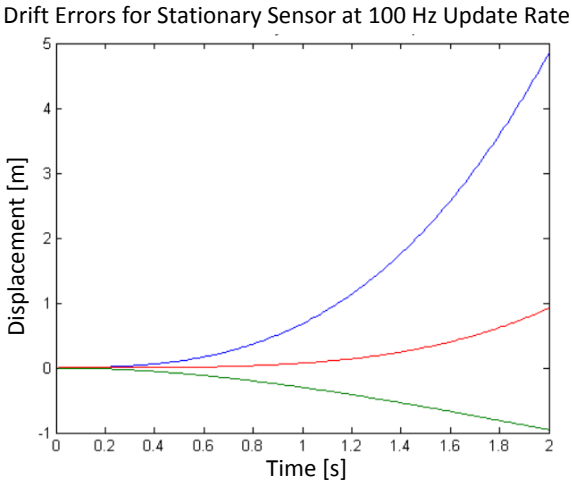

Fig. 9. Typical Output of a Flat Earth Navigator – Sensor Drift Errors [37]

To compute navigation solution with flat Earth navigator will not provide required output not even in case of better sensors (LRG). Due to the drift at the output of the sensors which is processed by the double integration algorithm the computed position of the navigation system will move for a system which is in fact stationary. The typical output [37] of a flat Earth navigator using MEMS sensors is depicted in Fig. 9 which depicts displacement after two seconds in each axe (x, y, z). The maximal displacement which is reached after two seconds is five meters in one axe. Fig. 9 shows exponential shape of the displacement drift which can be caused by the double integrated constant offset at the sensor output. It can show the calibration of the sensor was not well done or the parameters of the sensor changed based on the ambient environment and some sensor error correction mechanism has to be used.

Sensor output calibration can be performed by a set of measurements as described above but it is not usually enough because output of a sensor changes with change of the ambient environment. This problem is usually solved by fusion of multiple sensor sources as depicted in Fig. 10 where the result computed from Inertial Data is supported by Air Data Computer and GPS data [38]. The other sources of information can be compared with actual output of the inertial sensors or their computational products and the error parameters of the sensors can be estimated by a filtering.

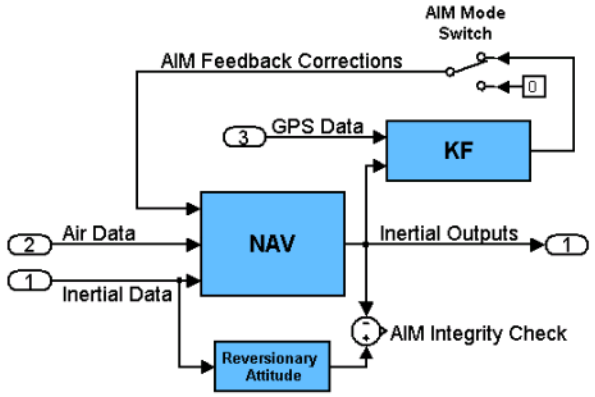

Fig. 10. LaseRefV Inertial Navigation System Dataflow, Inputs and Outputs [38]

Inertial sensors and their precision are crucial for the precision of the navigation solution. Their error models can be estimated online with help of other sources of information which usually performs more precise and in time stable measurements. The new system for position angles measurement could provide angles for body to navigational frame transformation (see Fig. 8) and also it could provide information based on which the double integration algorithm and integrated error could be reset.

1.1.5 Other Sources of Information, Magnetometer Unit and Pressure Reference System

To increase precision of the navigation solution other sources of information can be used. In the area of inertial navigation sensor an odometer, which e.g. provides information about vehicle movement based on the wheel speed sensor, is

often used. For airplanes and to display safety instructions related to the actual situation engine parameters are usually measured [39] and the engine health is evaluated during the engine operation and also for emergency landing assistants [7]. This electronic assistant needs information about angle of attack and angle of sideslip which are related to the distance for which the plane can glide without properly working engine. All the data [40] are often stored in a data recorder [41] and used for more precise post flight analysis. An example of the landing assistant system is described in [42].

A magnetometer measuring Earth magnetic field is often used as another data source of the airplane heading. There is a three axes sensor which provides data about the sensor orientation with regards to the magnetic flux sensor. This is stable information that changes with Earth's latitude and longitude but the actual vector orientation can be calculated from a model or from a table. The problem with magnetometer is caused by its calibration which is valid for one location and composition of the surrounding that contains sources of hard iron and soft iron distortions. The magnetometer calibration procedure usually provides a calibration ellipse whose deformation and position of the center allows us to get the distortion parameters (Fig. 11A). But these parameters are valid just for the single calibration and at the calibration place. While the modern MEMS sensors are small and cheap enough it allows us to design a magnetic field measurement unit that contains multiple magnetic field sensors arranged in a circle which provide possibility to measure all calibration data in one sample for the actual magnetic field distribution. This method expects that all the sensors were calibrated by a known magnetic field and their behavior is similar. In that case we can get the hard and soft iron distortions as depicted in Fig. 11A. The proposed sensor head with six sensors is depicted in Fig. 11B. Three pieces of this head rotated for 20 and 40 degrees compose a Magnetometer Automatic Calibration Sensor which is depicted in Fig. 11C. This calibration head will provide calibration data as depicted in Fig. 2 by one reading with step of 20 degrees. The precision of the sensor head depends just on the number of sensors used. The data allows us to determine X and Y offsets of the ellipse (Fig. 11A) which represent hard iron distortions and shape of the ellipse represented by q and r diameters and angle of rotation of the ellipse α that are caused by soft iron distortions. The advantage of this arrangement is independence of the magnetometer output on its actual position and magnetic field fluctuations.

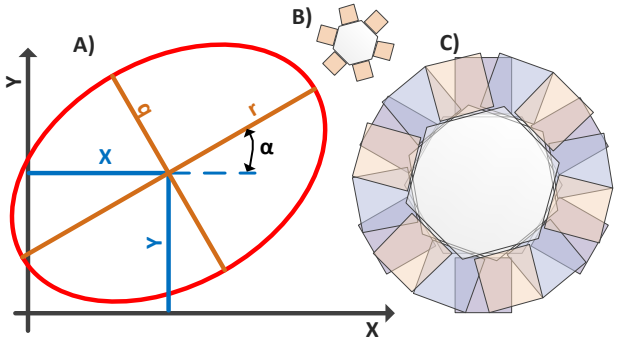

Fig. 11. A magnetometer Calibration Ellipse and Proposal of the Automatic Calibration Sensor Head

Instrument flying requires information about position angles which means pitch and roll angles to keep stable orientation of the plane which is not possible with human body sensors. Because the MEMS sensor precision is not enough and the more precise sensors are very expensive a new source of information about orientation angles is required. In aerospace the international standard atmosphere is used to maintain flight altitude and vertical distance between airplanes from 50's. It is internationally used and recognized. Because the behavior of the atmospheric pressure is very well described we propose a position angles measurement system which is based on precise measurements of small pressure differences in the vertical direction in the atmosphere. The pressure behavior with relation to altitude is depicted in Fig. 12 where we can see a pressure change related to an altitude change. This system will be furthermore referred as Pressure Reference System.

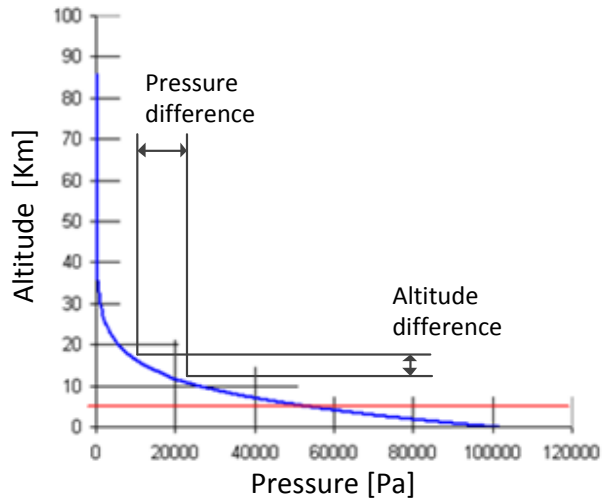

Fig. 12. Behavior of Standard Atmosphere Pressure and Principle of Pressure Reference System

1.2 Displays

The data acquired and processed by the above described systems and methods need to be visualized to the pilot. There are requirements for simple, informative way to display data based on the ergonomics of the cockpit [43][5]. The display units are generally divided on the head down displays mounted on the airplane dashboard and the head up displays mounted in the pilot's field of view.

1.2.1 Head-Down Displays

Dashboard instruments are still the most common way of displaying data. Small airplanes usually uses instruments type 1 and 2 (see introduction section of this article). Type 3 usually contains a custom made computer with all the sensors embedded into the device. Nowadays the current development effort in the area of dashboard instruments is focused on improvement of its advanced functionalities. There are different software functions performing checklists, data storage, evaluation which follows the approach generally recognized as Integrated Modular Avionics (IMA) [20][6]. The advanced display functions usually have form of electronic assistants [7] providing advices that increase safety of the flight. These systems are usually developed for one specific EFIS platform with some exceptions providing a universal programming interface [44][45].

The Pressure Reference System is being developed as a part of a set of independent distributed modules where all the main EFIS components (see Fig. 1) are developed as standalone units sharing data over WiFi network. Acer Iconia Tab is intended as a master module that controls single data providers. Fig. 13 shows the tablet running flight display instruments and also disassembled AHRS unit that contains GPS, 3x accelerometers, 3x angular rate sensors, 3x magnetometer, pressure and temperature sensors with 7-state extended Kalman filter providing output in form of quaternions, heading, pitch, and roll angles. The unit is based on ST microelectronics iNemo IMU whose parameters were described before.

Fig. 13. EFIS Running on Acer Iconia Tab Windows7 with Disassembled AHRS unit

1.2.2 Head-Up Displays

Pilots are requested to keep track with the situation outside of the airplane. While they look down on the airplane dashboard they do not pay attention on the surrounding situation which is considered as potentially dangerous. HeadUp displays solve this problem for aerospace and other vehicles. This type of display shows just a subset of all the measured data including artificial horizon which could be provided by Pressure Reference System.

Within the scope of this work a head up display was constructed and tested. The display uses 2D array of bright LED diodes which are externally controlled. The display unit is

depicted in Fig. 14 which clearly shows discrete steps of the image generator. The detailed description of the display unit is available in [6].

Fig. 14. Artificial Horizon Depicted by a HeadUp display using 2D array of bright LED diodes

2 Pressure Reference System

Fig. 12 shows atmospheric pressure behavior with relation to altitude which is described in International Standard Atmosphere (ISA). The pressure difference which is recalculated to one meter of the vertical distance is 12 Pa/m at the ground level and 7 Pa/m at 5 km altitude. The graph describing atmospheric pressure change on one meter with regards to altitude is depicted in Fig. 15. This graph proves that there is a small pressure difference between two vertical sampling places that can be used for orientation angle measurement. We are trying to utilize the depicted relation for vertical distance measurements. An airplane provides possibility to mount twin sensors on places that mutually changes their position with regard to the center of the airplane as it is depicted in Fig. 16.

Fig. 16 shows an airplane flying at altitude with pressure value Pref at the point of its center of mass. While the plane flies aligned with horizon the wings keeps horizontal position and the vertical difference of the both wing tips is 0 which means the pressure difference is 0 Pa. In case the plane starts turning the wing tips change their position with regards to the reference plane and the measured pressure will be $P_{ref.} - \Delta P$ and $P_{ref.} + \Delta P$ respectivelly. The total pressure difference between these two points will be $dZ = 2\Delta P$.

Pressure differences depicted in Fig. 15 disappears in resolution and errors of absolute pressure sensors used in ADCs. Because of small pressure values a differential pressure sensor has to be used. Honeywell DC001 NDC pressure sensor is proposed to evaluate measurement principle of the Pressure Reference System. Tab. 1 shows expected voltage outputs of the selected sensor with regards to maximal and minimal pressure changes.

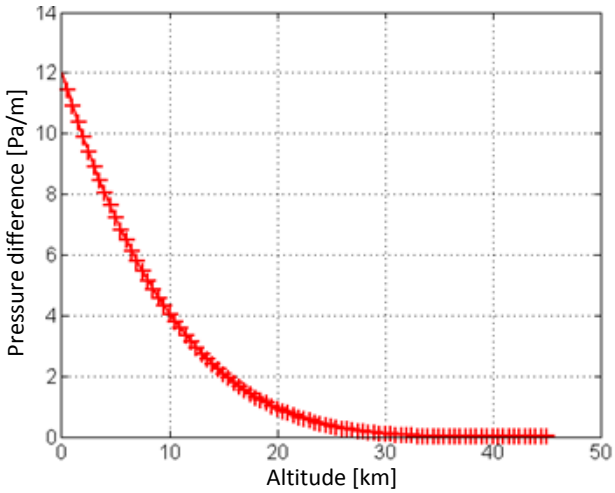

Fig. 15. One Meter Pressure Change Related to Altitude above Ground Level

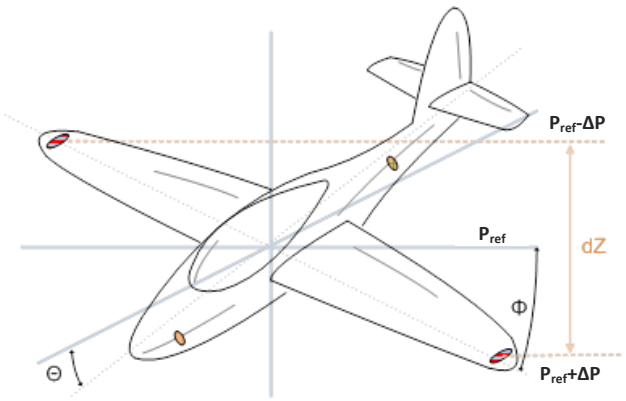

Fig. 16. Proposed Placement of Entry Points for the Pressure Reference System

Tab. 1. Differential Pressure Sensor Voltage Outputs Related to Selected Pressure Changes

Pressure [Pa]	ΔU_{out} [mV] DC001
12	96
8	64
6	48
4	32
2	16

2.1 Measurement Setup

To evaluate capability of the Pressure Reference System to measure orientation angles the measurement setup depicted in Fig. 17 was proposed and used. There were two DC001 sensors used in differential arrangement described in [42]. The sensor outputs were sampled by HP Data Acquisition Unit HP34970 together with actual power source output. DAQ unit was remotely controlled by a personal computer through Agilent 82357A GPIB to USB converter. The measurement setup also uses mechanical switch which is able to exchange measurement inputs In1 and In2 between each other. The switch is also remotely controlled by a one purpose electronic board over CAN bus. Data were acquired with help of Matlab Instrument Toolbox and a custom made toolbox used to access CAN bus.

Measurement was performed as follows: the sensor was placed at one meter above ground level; Input In1 was placed at 0 m AGL; and Input In2 at 2 m AGL. The DAQ system measured output of each sensor, their difference and power supply voltage. Mechanical switch allowed mechanically exchange pressure feeds to the sensor. A data set of fifty samples was acquired during each orientation of the inputs.

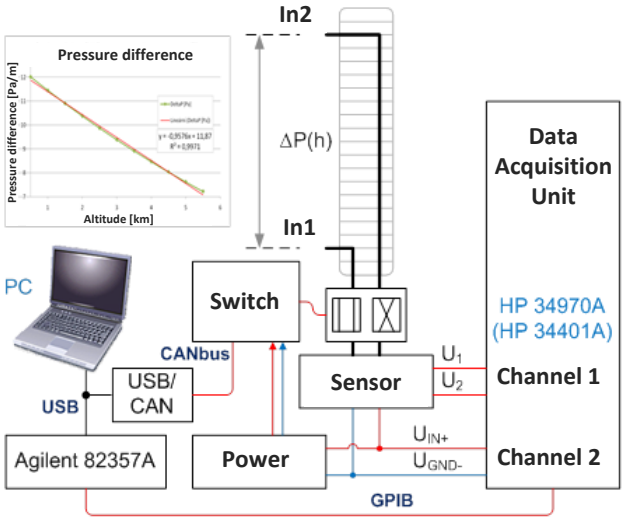

Fig. 17. Test Setup Used to Prove Capability of the Pressure Reference System

2.2 Results and Discussion

Results of the measurements acquired with help of the system depicted in Fig. 17 are depicted in Fig. 18. Every column represents average value of fifty samples for two orientations of the system inlets (in the figure the orientation is denoted as A and B). The result of the measurement can be interpreted as follows:

- In principle, the method allows vertical distance measurement.
- The amplitude for orientation A is 82 mV and for orientation B it is 88 mV which does not satisfy theoretically expected values presented in Tab. 1.
- Output signal difference is 6 mV for vertical difference of 2 m.
- The output value significantly changes with regards to the ambient pressure conditions. The maximal difference of the output signal was 20 mV and minimal was 1mV and the measured value disappears in noise.

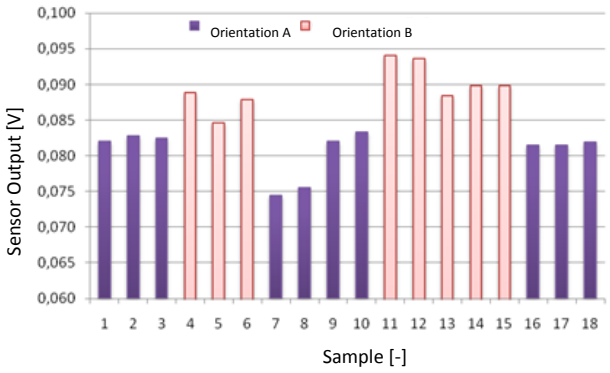

Fig. 18. Measurement Results

Unfortunately the result does not reflect expectations and a better sensor arrangement has to be prepared. Following conclusions were proposed:

- Long tubes feeding the pressure to the sensor has to be as short as possible.
- There is no time for sequential measurement. The pressure has to be measured simultaneously at different places.
- The sensitivity of the measurement module has to be increased.

3 Conclusion

This article presents a concept of a new system for position angles measurement which is based on attributes of International Standard Atmosphere and does not include double integration algorithm which is common in currently used AHRS units. The output of the Pressure Reference System should keep its precision in time regardless on short term disturbances. The article presents results of the measurements that prove capability of the proposed system for orientation angles measurement. Because the measured results do not follow theoretical expectations a closed reference volume is proposed to increase resolution of the measurement.

Next to the Pressure Reference System, a new head of a magnetometer sensor is presented that is able to measure its calibration circle in one sample and so it does not suffer by the magnetic field fluctuations.

We also summarize current situation in the area of measurement and display systems used by small airplanes. Precision of these systems is discussed, compared and disadvantages of currently used solutions are presented here. The article presents a set of modules forming distributed set of sensors of an avionics system including display units and especially a head up display unit.

References

[1] Clay C.W. Digital Electronic Flight Decks: The Outlook for Commercial Aviation. *Aerospace and Electronic Systems, IEEE Transactions on* , vol.AES-20, no.3, pp.221-226, May 1984, doi: 10.1109/TAES.1984.310503

[2] Williams F. The general aviation technology revolution. *Digital Avionics Systems Conference*, 1995., 14th DASC , vol., no., pp.207-212, 5-9 Nov 1995, doi: 10.1109/DASC.1995.482831.

[3] Ananda C.M. General aviation aircraft avionics: Integration & system tests. *Aerospace and Electronic Systems Magazine*, IEEE , vol.24, no.5, pp.19-25, May 2009, doi: 10.1109/MAES.2009.5109949

[4] Pačes P, Jelínek L, Jaroš R. LUN 1794 Converter - Special Functions. In *Proceeedings of 8. International Scientific Conference Measurement, Diagnostics and Reliability of Aerospace Systems*. Brno: University of Defense. 2008, p. 55-66. ISBN 978-80-7231-555-0.

[5] Bruna O. Usability Testing of Interface for Emergency Landing Navigation Assistant. In *POSTER 2012 - 16th International Student Conference on Electrical Engineering* [CD-ROM]. Praha: Czech Technical University in Prague, 2012, p. 1-4. ISBN 978-80-01-05043-9.

[6] Paces P, Levora T, Bruna O, Popelka J, Mlejnek J. Integrated modular avionics onboard of small airplanes — Fiction or reality? *Digital Avionics Systems Conference* (DASC), 2011 IEEE/AIAA 30th , vol., no., pp.7A1-1-7A1-12, 16-20 Oct. 2011, doi: 10.1109/DASC.2011.6096112.

[7] Frantis P.Emergency and precautionary Landign Assistant. In: *30th Digital Avionics Systems Conference*. IEEE, 2011, p. 1-6. ISBN 978-1-61284-796-2.

[8] Mahapatra P.R, Zrnic D.S. Sensors and systems to enhance aviation safety against weather hazards. *Proceedings of the IEEE* , vol.79, no.9, pp.1234-1267, Sep 1991, doi: 10.1109/5.97295.

[9] Chudy P, Rzucidlo P. Analysis of Interactions between Pilot-Operator and Advanced Flight Control System. In: *Solid State Phenomena*, vol. 1, č. 2, 2012, Dürnten, CH, s. 101-108, ISSN 1662-9779

[10] Chudy P, Rzucidlo P. Real-Time Simulations of Environmentaly Friendly Flight Control System. In: *9th IEEE international Symposium on Applied Machine Inteligence and Informatics*, Smolenice, SK, IEEE, 2011, s. 161-164, ISBN 978-1-4244-7428-8

[11] Kaparias I, Bell M.G.H. Testing a reliable in-vehicle navigation algorithm in the field. *Intelligent Transport Systems, IET* , vol.3, no.3, pp.314-324, September 2009, doi: 10.1049/iet-its.2008.0075

[12] Guilloton A, Arethens J.-P, Macabiau C, Escher A.C, Koenig D. State of the art in airport navigation. *Digital Avionics Systems Conference* (DASC), 2011 IEEE/AIAA 30th , vol., no., pp.4B3-1-4B3-11, 16-20 Oct. 2011, doi: 10.1109/DASC.2011.6096072

[13] King A.D. Inertial Navigation - Forty Years of Evolution. *GEC REVIEW*. Vol. 13, 1998

[14] Bojda P, Bloudicek R. Multiple Source Navigation Signal Receiver. *Proceedings of 29th Digital Avionics Systems Conference*, 2010, NY USA, IEEE, ISSN 2155-7209. ISBN 978-1-4244-6617-7.

[15] Jalovecky R, Bajer J, Janu P. Controller Area Network based On-board Data Acquisition System on Military Aircraft. In *Concepts and Implementation for Innovative Military Communications and Information Technologies*. Warsaw, Poland: Military University of Technology, 27.-28.9.2010. s. 589-598. ISBN 978-83-61486-70-1

[16] Dub M, Jalovecky R. Possibilities of Flight Data Online Processing. *Proceedings of 13th International Conference Transport Means*, October 22-23, 2009, Kaunas, Lithuania, Kaunas University of Technology, 2009, pp. 91-94, ISSN 1822-296

[17] Watkins C.B, Walter R, Transitioning from federated avionics architectures to Integrated Modular Avionics. *Digital Avionics Systems Conference*, 2007. DASC '07. IEEE/AIAA 26th , vol., no., pp.2.A.1-1-2.A.1-10, 21-25 Oct. 2007, doi: 10.1109/DASC.2007.4391842

[18] Rierson L.K. Best practices for certifying IMA systems in civil aircraft. *Aerospace and Electronic Systems Magazine*, IEEE , vol.25, no.1, pp.4-8, Jan. 2010, doi: 10.1109/MAES.2010.5442147

[19] Sampigethaya K, Poovendran R, Bushnell L. Secure Operation, Control, and Maintenance of Future E-Enabled Airplanes. *Proceedings of the IEEE* , vol.96, no.12, pp.1992-2007, Dec. 2008, doi: 10.1109/JPROC.2008.2006123

[20] Lewis J, Rierson L. Certification concerns with integrated modular avionics (IMA) projects. *Digital Avionics Systems Conference*, 2003. DASC '03. The 22nd , vol.1, no., pp. 1.A.3- 1.1-9 vol.1, 12-16 Oct. 2003, doi: 10.1109/DASC.2003.1245803

[21] Alouani A.T, Gray J.E, McCabe D.H. Theory of distributed estimation using multiple asynchronous sensors. *Aerospace and Electronic Systems, IEEE Transactions on*. vol.41, no.2, pp. 717- 722, April 2005, doi: 10.1109/TAES.2005.146876

[22] Sheffels M.L. A fault-tolerant air data/inertial reference unit. *Aerospace and Electronic Systems Magazine, IEEE*. vol.8, no.3, pp.48-52, March 1993, doi: 10.1109/62.199822

[23] Cizmar J, Jalovecky R. Design of an Inertial Reference Unit with the mixed gravitational and magnetic correction of gyroscopic drift. *Transport Means - Proceedings of the International Konference*, Kaunas;21 October 2010, ISSN: 1822296X

[24] Leclerc J. MEMs for Aerospace Navigation," *Aerospace and Electronic Systems Magazine, IEEE*. vol. 22, no. 10, pp. 31-36, 2007, doi: 10.1109/MAES.2007.4385708

[25] Ryan, Matthew W, Miller Geoff, MEMS based AHRS with adaptive bias estimation for high performance rate sensor replacement. *Position Location and Navigation Symposium* (PLANS), 2010 IEEE/ION , vol., no., pp.214-220, 4-6 May 2010, doi: 10.1109/ PLANS.2010.5507126

[26] Wenwen Wang, Chunzhi Li, Junying Zhang, Xungang Diao. Effects of atomic oxygen treatment on structures, morphologies and electrical properties of ZnO:Al films, *Journal of Applied Surface Science*. 2010, Elsevier, ISSN: 0169-4332.

[27] Pačes P, Šipoš M, Draxler K. Temperature Effects and Non-linearity Corrections of Pressure Sensors. In *ICMT'11 International Conference on Miltary Technologies 2011* [CD-ROM]. Brno: Univerzita obrany, 2011, p. 651-656. ISBN 978-80-7231-788-2.

[28] Memscap, The Power of a Small Word, online: http://www.memscap.com/

[29] Pačes P, Šipoš M, Reinštein M, Roháč J. Sensors of Air Data Computers - Usability and Environmental Effects. In *ICMT'09 - Proceedings of the International Conference on Military Technologies*. Brno: Univerzita obrany, 2009, p. 401-409. ISBN 978-80-7231-649-6.

[30] Šipoš M, Pačes P, Reinštein M, Roháč J. Flight Attitude Track Reconstruction Using Two AHRS Units under Laboratory Conditions. In *IEEE SENSORS 2009 - The Eighth IEEE Conference on Sensors* [CD-ROM]. Christchurch: IEEE, 2009, p. 675-678. ISBN 978-1-4244-5335-1.

[31] Šipoš M, Pačes P, Roháč J, Nováček P. Analyses of Triaxial Accelerometer Calibration Algorithms. *IEEE Sensors Journal*. 2012, vol. 12, no. 5, p. 1157-1165. ISSN 1530-437X.

[32] Hospodar P, Proks M, Golda M. Levné senzory pro identifikaci aerodynamických veličin. *Czech Aerospace Proceedings*. Aerospace, 2009.

[33] Honeywell. Micro Inertial Reference System SM μIRS. Inertial Navigation Products - Product Description. [Online] March 2004.

[34] Dittrich P, Chudy P. Application of Kalman Filter to oversampled data from Global Position System, In: *ElectroScope*, vol. 2011, 2, CZ, p. 6, ISSN 1802-4564

[35] IEEE standard specification format guide and test procedure for single-axis interferometric fiber optic gyros. IEEE Std 952-1997 (1998).

[36] Sherryl H. Stovall Basic Inertial Navigation, Naval Air Warfare Center Weapons Division, September 1997, fas.org/spp/military/program/nav/basicnav.pdf.

[37] Crittenden J, Evans P. MEMS Inertial Navigation System. 2008.

[38] Weed D, Broderic J, Love J, Ryno T, GPS Align In Motion of Civilian Strapdown INS. Honeywell Commercial Aviation Products, Honeywell International. Development, Picastaway. IEEE, 2004. p. 184- 192. ISBN 0-7803-8416-4/04.

[39] Pačes P, Mareš V, Engine Parameters Measurement and Display Unit for Small Sports and Ultra-light - aircrafts. In *Applied Electronics 2005 - International Conference*. Pilsen: University of West Bohemia, 2005, p. 257-260. ISBN 80-7043-369-8.

[40] Jalovecky R, Janu P, Bystricky R, Boril J, Bojda P, Bloudicek R. Polasek M, Bajer J. Data fusion from avionic sensors employing CANaerospace. In: *Mechatronics, Recent technological and scientific advances*. Berlin: Springer, 2011, p. 297-301. ISBN 978-3-642-23243-5.

[41] Bystricky R, Bajer J, Janu P. Proposal of low cost flight data recorder for ultralight aircraft. In: *Modern Safety Technologies In Transportation. Košice*, Slovensko: Suprema Ltd., 2011, p. 54-59. ISSN 1338-5232. ISBN 978-80-970772-0-4.

[42] Pačes P, Čenský T, Hanzal V, Draxler K, Vaško O. A Combined Angle of Attack and Angle of Sideslip Smart Probe with Twin Differential Sensor Modules and Doubled Output Signal. In *IEEE Sensors 2010 - Proceedings* [CD-ROM]. Stoughton, Wisconsin:

IEEE Sensors Council, 2010, p. 284-289. ISBN 978-1-4244-8168-2.

[43] Chudy P, Rydlo K, Intuitive flight display for light aircraft. In AIAA. Portland: 2011. p. 1-10. AIAA-2011-6348, *AIAA Modeling and Simulation Technologies Conference*, Portland, Oregon, 2011

[44] Bojda P, Frantis P, Multipurpose visualization system. *Aerospace and Electronic Systems Magazine*, IEEE, vol.24, no.4, pp.4-8, April 2009, doi: 10.1109/MAES.2009.4839270.

[45] Pačes P, Šipoš M, Introducing Students to Aerospace Board Information Systems Using an Embedded Graphics System Simulator. In *ICALT 2010 - Proceedings of 10th IEEE International Conference on Advanced Learning Technologies* [CD-ROM]. Los Alamitos: IEEE Computer Society, 2010, p. 397-399. ISBN 978-0-7695-4055-9.

[46] Mahapatra P.R, Zrnic D.S, Sensors and systems to enhance aviation safety against weather hazards. *Proceedings of the IEEE*, vol.79, no.9, pp.1234-1267, Sep 1991, doi: 10.1109/5.97295.

Acknowledgement

This work was supported by the research program No. TA01030651 "Safety Improvement of Flight, Crew and Other Participants of Flight Transport in Normal and Emergency Situations by Assistive Technologies" of the Czech Technical University in Prague, sponsored by the Technological Agency of the Czech Republic.

Copyright Statement

SENSORS OF AIR DATA COMPUTERS – USABILITY AND ENVIRONMENTAL EFFECTS

Pavel PACES[1], Martin SIPOS[2], Michal REINSTEIN[3], Jan ROHAC[4]

SUMMARY: This paper compares static pressure sensors suitable for aircraft air data systems. Characteristics of selected sensors influenced by environmental effects are compared with regards to their price. The group of sensors was chosen in order to cover a wide range of sensor samples available on the market. The article compares characteristics of sensors manufactured by Freescale, the MPX series, Memscap SP82, Intersema MS5534, and samples from SensorTechnics and Honeywell. The measurement setup is also described in the article. Digital modules connected through the CAN bus and GPIB measurement instruments were used for data acquisition. The data was sampled through Matlab Data Acquisition System extended by our own CAN Aerospace Toolbox that is being developed at CTU in Prague. The article finally compares all tested sensors and presents possible calibration methods, in which temperature effects and non-linearity were taken into consideration.

Keywords: Static pressure sensor; Calibration; ADC; Matlab Toolbox

1. INTRODUCTION

The paper compares a group of sensors with regards to their accuracy and long term stability. All used sensors belong into easily available devices. These sensors suffer by lot of problems which origins in their principles of operation, manufacturing process and ambient environment. This paper compares sensors attributes and proposes methods of dealing with their unwanted characteristics. First, the altitude measurement problems are briefly mentioned. Then, we describe sensors used in this work and also proposed methods of enhancing sensors characteristics which are later used. The measured data are compared mainly with respect to temperature and proposed methods of temperature influence remove are presented. Finally, the article compares actual results with data measured in the past.

1.1 ALTITUDE MEASUREMENT

Altitude measurement can be performed by a sensor with the high pressure limit of approximately 115 kPa. This value results from air mass pressure on the Earth. The equation (1) describes relation between altitude and actual air pressure.

$$H = \frac{T_0}{\tau} \cdot \left[\left(\frac{p(0)}{p(H)} \right)^{R.\tau} - 1 \right]. \qquad (1)$$

[1] Ing. Pavel Paces, Faculty of Electrical Engineering, Czech Technical University in Prague, Technicka 2, 166 27, Prague, Czech Republic. E-mail: pacesp@fel.cvut.cz
[2] Ing. Martin Sipos, Faculty of Electrical Engineering, Czech Technical University in Prague, Technicka 2, 166 27 Prague, Czech Republic. E-mail: siposm1@fel.cvut.cz
[3] Ing. Michal Reinstein, Faculty of Electrical Engineering, Czech Technical University in Prague, Technicka 2, 166 27 Prague, Czech Republic. E-mail: reinsm1@fel.cvut.cz
[4] Ing. Jan Rohac, Ph.D., Faculty of Electrical Engineering, Czech Technical University in Prague, Technicka 2, 166 27 Prague, Czech Republic. E-mail: xrohac@fel.cvut.cz

Where H is altitude measured from reference level $p(0)$ [m],
$p(0)$ is pressure corresponding to a reference level [kPa],
$p(H)$ is pressure corresponding to altitude H [kPa],
T_0 is absolute temperature in zero altitude of ISA [K],
τ is a temperature constant for altitude form 0 to 11 km [K m^{-1}] and
R is corrected air constant [m K^{-1}].

Equation (1) defines an atmospheric model of the Earth atmosphere, that was released by ICAO organization in 1952 as a part of International Standard Atmosphere and is still used for guidance purposes of airplanes.

2. PRESSURE SENSORS

A sensor suitable for altitude measurement is equipped by an absolute block with is filled by a reference medium (usually vacuum). The measured pressure reacts with the reference medium through a deformation element in form of a diaphragm. The mechanical deformation caused by the pressure attached at the input side of the sensor is measured by a group of variable resistors or other principle can be used (as a vibrating string). Altitude measuring accuracy is defined by European Aviation Safety Agency in Europe. EASA releases Certification Specifications which prescribes duties of manufacturers in order to keep aviation safe. The strictest prescribed value for altitude measurements is for low altitudes. Allowed tolerance is approximately 6 meters on the Earth surface which equals to the worst sensor resolution of 73 Pa [1]. The measured range and the requested resolution together with request for sensors long term stability led to definition of demands requested from aerospace sensors. Sensor's characteristics should be compliant with these requirements:

- Sensor pressure hysteresis that is difficult to correct. Recommended value should be lower than 0.005% FS.
- We will neglect diaphragm elasticity, because is difficult to measure.
- Temperature hysteresis should be lower than 0.02% FS.
- We don't care about Non-linearity error, because it is easy to correct by a table or an equation together with Temperature dependence.
- Long term stability causes problems because this sensor's behaviour is difficult ro describe and correct later. The long term stability is dependent on production technology.
- Sensor over pressure response should be lover than 0.01% FS.
- Error caused by temperature cycling should be lover than 0.05% FS.

There are also other sensor's characteristics but difficult to measure and to use them in a common application.

Table 1 shows list of pressure sensors that were used in this work for evaluation of their characteristics and algorithms which were used for their temperature dependency correction. The table shows sensor's ranges, output type, price and housing type. The Honeywell 19U sensor price was unknown but manufacturer claims it as a low cost sensor. This sensor seems to be the best choice although the MemsCap SP82 sensor holds some certificates for usage in aerospace industry. The both sensors have metal housing that adds them more confidence. It should be interesting to compare price of 19U and SP82. The MPX series is interesting due to their low price which is reflected by their plastic housing and lower accuracy. Due to digital

interfaces the Intersema MB5534BM and SensorTechnics HCA0611 are interesting sensors for comparison with others. These sensors were acquired as samples and added into this evaluation. The last data was measured by two Air Data Computers realized with MPX and SP82 sensors that should already utilize all necessary corrections for temperature and nonlinearity errors caused by sensors principles.

Tab. 1: List of measured sensors

Sensor	Range	Package Type	Price (€)	Output	Accuracy
MPX4115AP	15-115 kPa	Plastic	8	Analogue	± 1.5 % FS
MPX4100AP	20-105 kPa	Plastic	9	Analogue	± 1.8 % FS
MPXAZ6115A	15-115 kPa	Plastic	10	Analogue	± 1.5 % FS
19U	0-15 PSI	Metal	-	Analogue	± 0.03 % FS
SP82	1 bar	Metal	100	Analogue	± 0.2 % FS
HCA0611ARH	600-1100 mbar	Plastic	10	Digital	± 1.0 % FS
MS5534BM	10 - 1100 mbar	Plastic	-	Digital	0.1 mbar
ADC1 (MPX4115AP)	15-115 kPa	-	-	Digital	-
ADC2 (SP82)	1 bar	-	-	Digital	-
Reference Sensor (RPT200)	35 - 3500 bar	-	-	Digital	0,02 % FS

2.1 SENSORS' ERRORS

As was described before, diaphragm strain gauge pressure sensors suffer by problems caused by its manufacturing process. The Micro-Electro-Mechanical System (MESM) in this article takes into account just following influences:

- Linearity error.
- Pressure hysteresis.
- Temperature dependence.
- Temperature hysteresis.

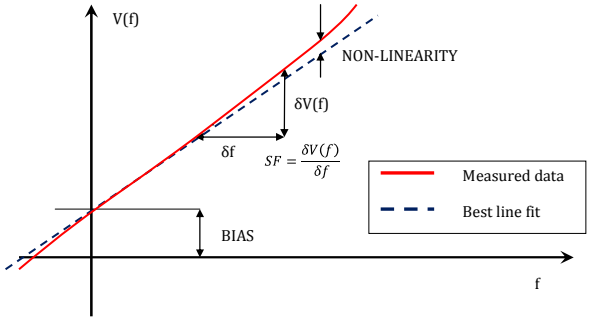

Fig. 1: Illustration of transfer characteristics non-linearity

Figure 1 describes non-linearity and bias in the 2D space however the four characteristics we take into account are better described in the 3D word. Figure 1 shows temperature dependence as a non-linearity and also shift in bias. The real measured data are depicted in Figure 2 and 3.

Figure 2 shows temperature dependency of the MPX4115 sensor in really low temperatures because the temperature range from 0 to 80 degrees of Celsius is compensated in this MEMS device. The picture shows error in altitude setting of approximately 10 meters at zero level of ISA. Figure 3 shows nonlinearity and temperature influence of the SP82 sensor.

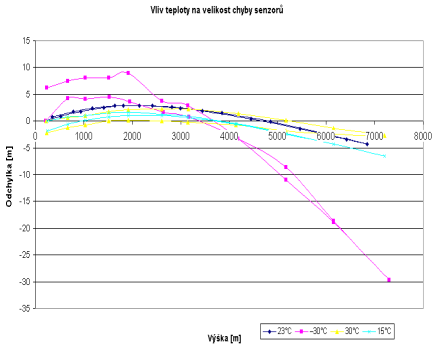

Fig. 2: Illustration of pressure hysteresis and temperature influence.

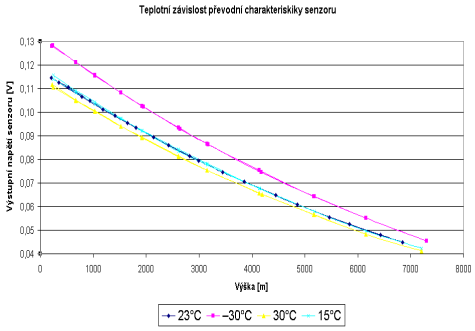

Fig. 3: SP82 transfer characteristics temperature dependences.

Sensor's errors can be reduced by these means:

- Calibration equation.
- Calibrated table.
- Sensor heating.
- Temperature measurement that is done at a reference sensor.

The first two choices defines algorithm that uses knowledge gained by previous measurement of sensor behaviour with relation to outside effects. Due to measured results, eg. Fig. 1, it can be difficult to prepare correction equation in some cases. Also the sensor characteristics over the corrected range of influences should be stable in time. In case, the sensor has good characteristics for one temperature, it is possible to equip it by a heating element that makes its environment steady. The last possibility is to use two sensors where the first one is sealed and it measures not the pressure but the environmental influences of the second sensor and its output signal is repaired respectively.

3. SENSOR EVALUATION

This article evaluates MEMS pressure sensor characteristics and mean of compensation of their output values that are described in the previous chapter. The whole test setup is described in Figure 5. The requested temperature conditions a Labio LS80 temperature chamber was used. This chamber allows stabilizing temperature in range from −30 to +70 °C. Unfortunately, the temperature varies in the chamber and the measured data are influenced by its engine switching. The measurement was done for altitudes from 240 to 5000 m and the same points were measured back. Table 1 shows measured points with respect to relating atmospheric pressure.

Altitude [m]	240	574	1000	2000	3000	4000	5000
Pressure [kPa]	98,47	94,61	89,87	79,49	70,10	61,63	54,01
Pressure [mmHg]	738,61	709,66	674,08	596,20	525,78	462,24	405,07

Tab. 1: Test curve applied to sensors

The pressure was regulated manually by the IVD regulator. The IVD consists of group of valves to control air flow into and from the system. This way of regulation allows more precise pressure setting then by an automatic system. The measured pressure was set with precision of ± 0.01inHg (±1.3Pa) during the one measurement that consists from 30 samples acquired in 3 minutes. The number of measured sensors is described in the following chapter. The slowest measuring device is the Agilent 34970A Data Acquisition Unit.

The measurement setup is based on the precision of the Druck DPI145 pressure meter that is depicted in Figure 4. This measuring instrument is equipped by the RPT 200 sensor, with measurement accuracy 0,02 %FS that means hundreds of Pascals but the laboratory environment, the real measured data shows this error lower with precision of altitude setting ±8 m.

Fig. 4: Pressure meter Druck DPI 145

3.1 TEST SETUP

A measurement test setup used in this work is depicted in the Fig. 5. The test setup consists of measured sensors and Air Data Computers (ADC), pressure regulator and vacuum pump, and personal computer which collects data using GPIB bus, RS232 and CAN bus. Matlab with Instrument Control Toolbox and CAN Aerospace Toolbox were used for data acquisition. The CAN Aerospace Matlab toolbox is being developed in the Laboratory of Aeronautical Systems. The test setup allows measuring of several sensors where part of them measures pressure connected to their inlets and the second group of sensors is sealed measuring temperature influences. The measured sensors S1a, S1b, ..., Sna, Snb (see Tab.1) are mounted on Support Platform which provides power distribution of 5V and 12V using precise voltage stabilizers, signal wiring and the output signal amplification of passive sensors. The measured sensors S1a, ..., S1n are connected to the vacuum (under pressure) distribution which is regulated by IVD Pressure Regulator. The IVD regulates pressure provided by a vacuum pump. The reference constant pressure is provided to sensors S2a, ..., S2n for measuring of temperature characteristics. The sensors with digital output were connected to a signal convertors that converts them into devices connected to a CAN bus and communicating by CAN Aerospace protocol. Also the ADC2 uses CAN bus for interconnection with other systems. All of the sensors, Air Data Computers, MB sensor (Intersema) and HCR sensor (Sensortechnics) were placed into a Temperature Chamber where temperature sensor PT100 is used as a reference.

Output data provided by sensors S1a, S1b, ..., Sna, Snb and temperature sensor PT100 are measured using Data Acquisition Unit Agilent 34970A and multi-meter Agilent 34401A. These measurement devices are connected to the computer through GPIB bus that is available through GPIB2USB converter (Agilent 82357A).

ADC1 (MPX4115AP) is connected to the computer through RS232. The ADC2 (SP82), MB5534 and HCR0611 sensors communicate with PC using CAN bus. The CAN bus is connected by USB2CAN converter with PC.

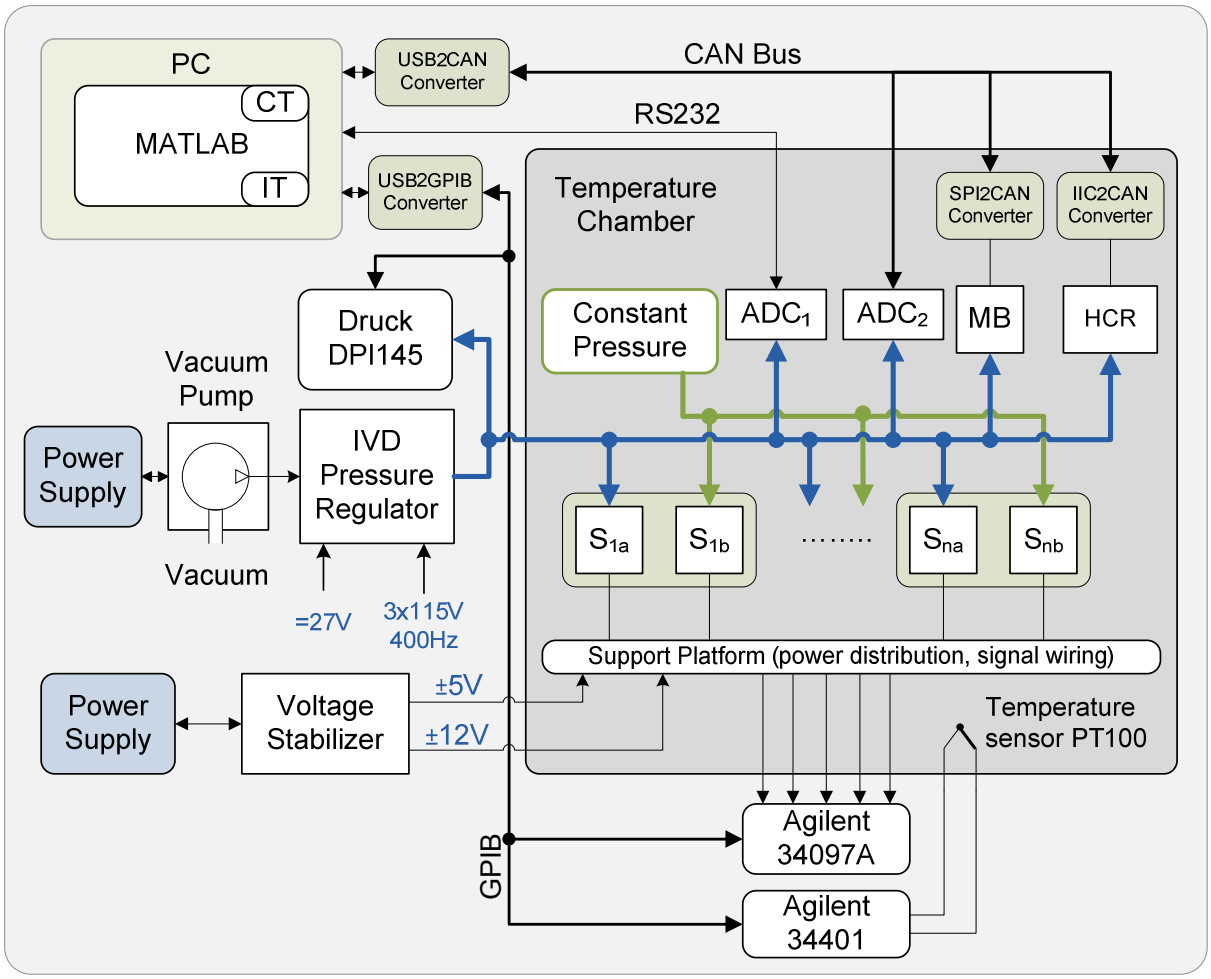

Fig. 5: Measurement Test Setup

The CAN bus communication is realized as a Matlab toolbox that is structured as showed in Figure 6. This toolbox uses USB2CAN converter with a custom DLL interface which is loaded into the Matlab environment. Also several Matlab function was defined in order to make usage of the CAN bus more comfortable. Detail about CAN aerospace protocol can be found in [2]

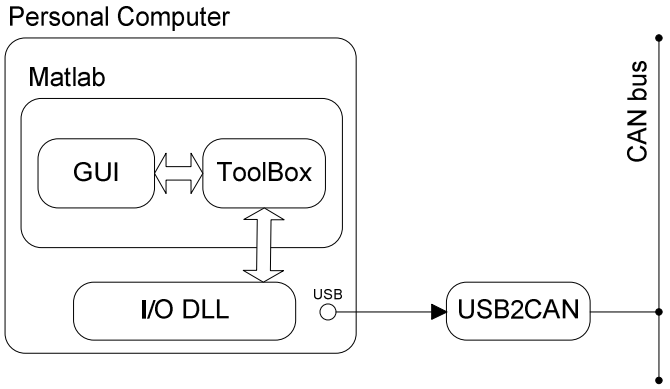

Fig. 6: Proposed Structure of the Matlab CAN Aerospace Toolbox

4. RESULTS

The measurement was designed to evaluate linearity of the output value which should be linear with no temperature influence. The 19U nonlinearity is typically ±0,1%FS (max. ±0,25%FS). The MPX4115AP type does not define nonlinearity just a total error max. ±1,5%. There is an important fact in the non-linearity error definition difference by different manufacturers. First case defines characteristics deviation from a line fitting just the characteristics end points („End point straight line fit"). This deviation is higher in number than deviation of line that fits the characteristics the best („Least square deviation"). It seems to us that the 19U sensor datasheet displays the better in number deviation which fits the sensor characteristic the best. On the other hand the Freescale sensors show deviation from a line fitting the end points of the characteristics.

The MPX4115 responses are displayed in Fig. 8. The characteristic are measured according to the test curve described earlier. The Fig. 8 shows slight differences from the ideal characteristics showed in the Fig. 7. Deviation between the sensor transfer characteristics and the ideal characteristics is depicted in the figure Fig. 9. These characteristics are comparable to the Fig. 2 that was measured about one year ago. The figure shows really high hysteresis of the measured value for temperature of -30 degrees of Celsius. Part of the difference is done bz the temperature instability, but it is obvious that the pressure value differs about 300 Pa. The figure 10 shows output values of the sealed sensor. The transfer characteristics hysteresis is not as visible as in Fig. 9 but it is still present. This values can be used for correction of the data displayed in Figure 9.

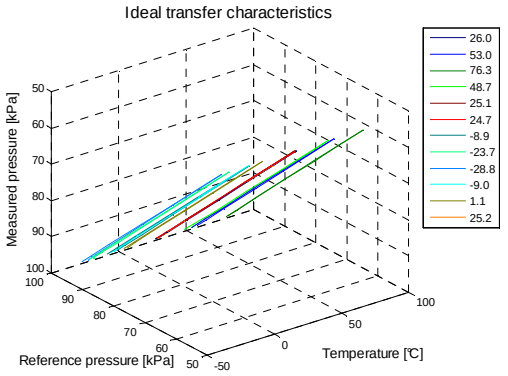

Fig. 7: The ideal transfer characteristics.

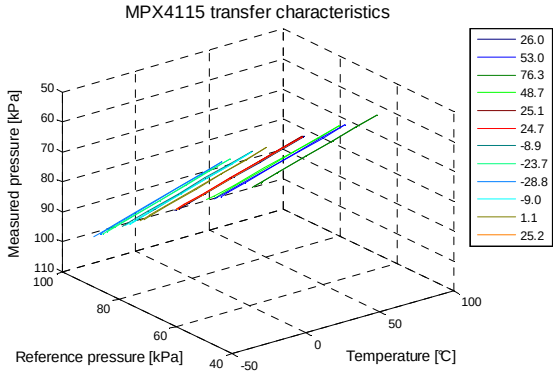

Fig. 8: MPX4115AP transfer characteristics.

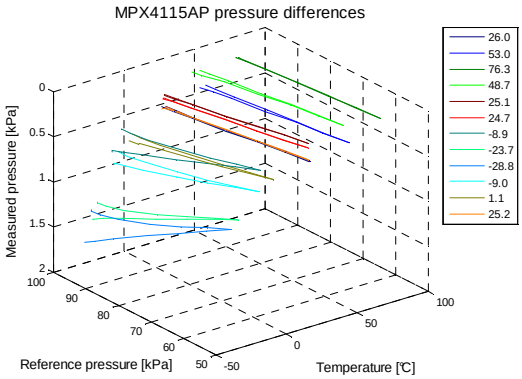

Fig. 9: MPX4115AP deviations.

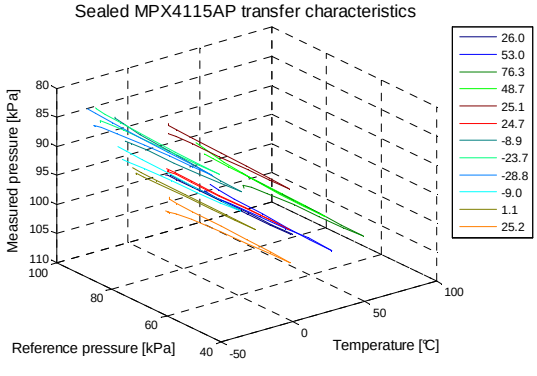

Fig. 10: Sealed MPX4115AP transfer characteristics.

The influence of the Memscap SP82 heating capability is presented in figure Fig. 11 and Fig 12. Figure Fig. 11 shows transfer characteristics measured by the ADC2 system for situation where its heating system is off. The Fig. 12 measures the same characteristic with temperature conditioning, which results in precise, temperature independent characteristics.

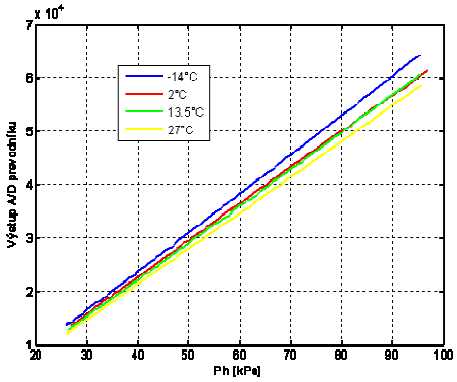

Fig. 11: The Test Setup.

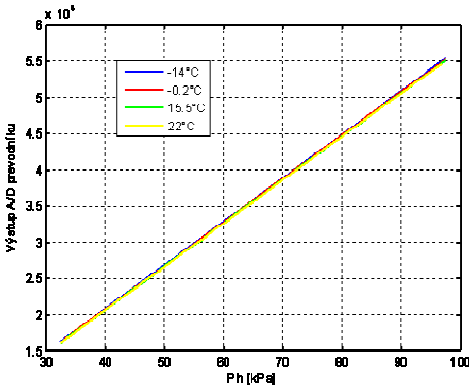

Fig. 12: Sensor to CAN Converters.

Figure 12 shows measurement setup with the temperature chamber, measurement instruments, pressure regulator and data acquisition PC. Figure 13 shows two of sensor to CAN converters and aluminum housing of 19U analogue sensors.

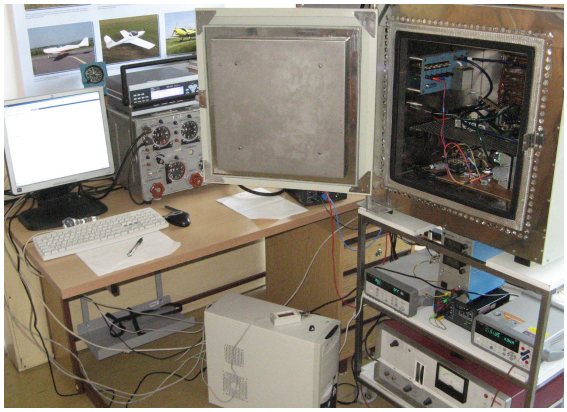

Fig. 13: The Test Setup.

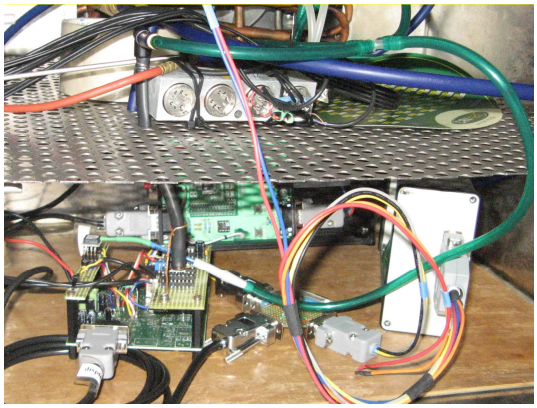

Fig. 14: Sensor to CAN Converters.

CONCLUSION

The work described in this article serves more for evaluation of the algorithm of data acquisition from number of sensors that were developed at Laboratory of Aeronautical Systems. The output values were sampled by means of different data acquisition systems. Several of used measurement systems are designed just for automated laboratory measurements and they communicate over the GPIB data bus. The Data Acquisition Unit Agilent 34097A and the multi-meter Agilent 34097A were communicated over the GPIB bus. The pressure meter DRUCK DPI 145 was placed outside of the temperature chamber and connected by RS232 to the data acquisition PC. The communication with measurement instruments was done through the VISA library and SCPI commands. These commands were called from Matlab as a part of its Instrument Control Toolbox. A measurement script was realized for data acquisition. The sensors with digital outputs unfortunately do not provide a standardized output then a unification converter had to be developed. This converter was

develop as a communication processor between the sensor and the CAN bus. Also for Matlab to CAN bus communication a CAN Toolbox had to be developed.
The article describes measurement of number of different sensors and provides first results for tested range from 0 level of ISA to 5 000 m as a set of characteristics in temperature ranges from -30 to 77 °C. The important results are provided by measurement of sealed sensors in order to correct temperature dependent value of the measuring sensor. The heating capability of the SP82 sensor is illustrated in Figures 11 and 12.
Unfortunately, the measurement was done quickly due to time constraints. The all system interconnection was evaluated and the idea of measurement over the CAN bus with Matlab interface was proved.

ACKNOWLEDGMENT

This project was partially supported by the research program No. MSM6840770015 "Research of Methods and Systems for Measurement of Physical Quantities and Measured Data Processing " of the CTU in Prague sponsored by the Ministry of Education, Youth and Sports of the Czech Republic.

REFERENCES

[1] HELFRICK, ALBERT. *Principles of Avionics* – 3rd ed. Avionics Communications Inc, 2004.

[2] Interface specification for airborne CAN applications v 1.7, CAN Aerospace, Stock Flight Systems, www.canaerospace.com

[3] NOVÁK, M. Low cost pressure sensors suitable for altitude measurement by barometric method. *Diploma Thesis*, 2006, CTU in Prague, FEE. [in Czech].

TEMPERATURE EFFECTS AND NON-LINEARITY CORRECTIONS OF PRESSURE SENSORS

Pavel PAČES[1], Martin ŠIPOŠ[2], and Karel DRAXLER[3]

SUMMARY: This paper presents a method of correction temperature effects affecting pressure sensors used mainly for dynamic and static pressure measurements within air-data systems based on low-cost sensors. The principle uses an isochoric process (or a constant-volume process) during which a thermodynamic changes cause pressure shift within the constant volume of a closed system. The closed system is presented here as a volume formed from a blinded inlet of a pressure sensor whose output is used for measurement sensor output corrections. The article presents all the equations used for the temperature effects and non-linearity corrections. The overall method of the environmental effects correction is presented on a test system and a prototype of an Air-Data Computer.

Keywords: AirData Computer, Temperature, Corrections, Isochoric, Combined Gas Laws.

Introduction

Amontons's Law of Pressure-Temperature was discovered in the late 17th century. It claims that the pressure of a fixed mass of gas kept at a constant volume is proportional to the temperature. The Amontons's work was used by Jacques Charles for formulation of Charles's law (also known as the law of volumes) that is a gas law which describes how gases expand when heated. These laws are integral part of the combined gas laws where relationship between pressure p [Pa] and temperature T [K] at points (1, 2) can be rewritten as (1):

$$\frac{p_1}{T_1} = \frac{p_2}{T_2}, \tag{1}$$

Low-cost pressure sensors are based on a set of piezoresistive Strain Gauges mounted on a diaphragm that is deformed due to applied pressure. The strain gauges are connected to form a Wheatstone bridge circuit to maximize the output of the sensor.

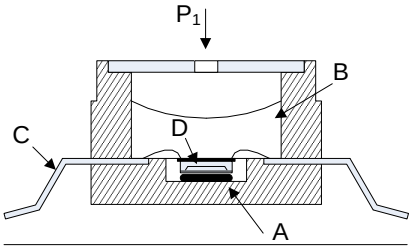

Fig. 1: Internal structure of MPX4115AP sensor

[1] Assist. Prof. Pavel Paces, Faculty of Electrical Engineering, Czech Technical University in Prague, Technicka 2, 166 27 Prague, Czech Republic. E-mail: pacesp@feld.cvut.cz

[2] Martin Šipoš, Faculty of Electrical Engineering, Czech Technical University in Prague, Technicka 2, 166 27 Prague, Czech Republic. E-mail: sipos@feld.cvut.cz

[3] Assoc. Prof. Karel Draxler, Faculty of Electrical Engineering, Czech Technical University in Prague, Technicka 2, 166 27 Prague, Czech Republic. E-mail: draxler@feld.cvut.cz

The environment surrounding the sensor affects its body (see Fig. 1) and especially the connection between the diaphragm and the Wheatstone bridge composed from Strain Gauges suffers by different expansibility.

MPX4115 family of sensors was used for the proposed method evaluation. Fig. 1 shows body of the MPX4115 family of sensors where item A, of the Fig. 1, illustrates vacuum chamber, Fig. 1D is the diaphragm with the Wheatstone bridge, Fig. 1C represents a signal output, Fig. 1B is an isolation of the sensing element and P_1 is the pressure inlet.

Temperature effects on the sensor can be calibrated by multiple ways, eg. calibration equation, look-up table, another temperature dependent element, etc. The temperature effects are then modelled and numerically eliminated [1]. In this article, we present another possibility of low-cost pressure sensor calibration based on the shift of the output signal of a sensor with known pressure at its input. Due to the temperature effects that influence also the constant volume of the blinded sensor, the Amontons's Law (sometime referred as Charles's Law) has to be applied in order to eliminate changes in the closed system. Fig. 2 shows a group of blinded sensors connected to a constant volume and another group of the same sensor types connected to a pressure intake.

Pressure sensors are essential components of AirData Computers and the safety of aviation depends on their precision [2] because the pressure and temperature decrease with the altitude [3].

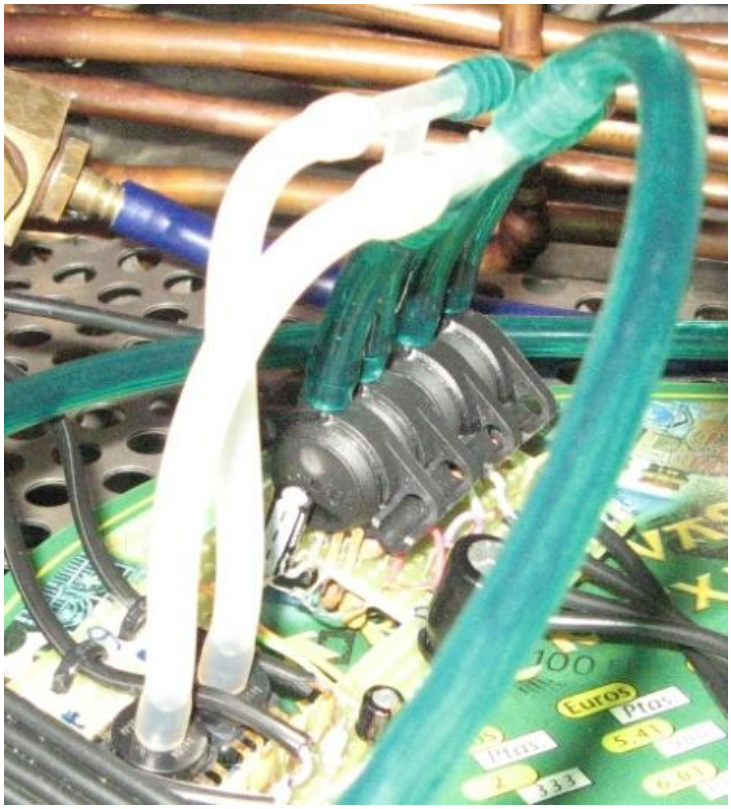

Fig. 2: Interconnection of pressure sensors – blinded group with constant volume and measurement sensors with pressure intake

Measurement System and Sensor Description

The measurement system used for data acquisition is depicted in the Fig. 3. The data was sampled simultaneously by measurement system and results are described in [4]. The data

acquisition was automatic but pressure settings were done by hand. At first, a temperature was set in the temperature chamber and then sensor characteristics were measured. The exact temperature was acquired by precise PT100 sensor and was sampled together with each pressure sample. It is necessary to mention that the temperature chamber heating and cooling system influenced all the measurements (temperature and pressure) by blowing hot or cold air inside of the chamber. This caused changes in the temperature gradient of the internal volume of the temperature chamber that also affects all sensors inside of the chamber.

Tab. 1 shows ranges, accuracy and type of the output of all sensors. The measurement setup included six pieces of MPX sensors (two of each type mentioned in Tab. 1) and one RPT200 sensor inside a Druck DPI145 pressure meter. The half of MPX sensors was blinded and the second half of the sensors was used for pressure measurements.

Tab. 1: Sensor's Parameters

Sensor	Range	Price (€)	Output	Accuracy
MPX4115AP	15-115 kPa	8	Analogue	± 1.5 % FS
MPX4100AP	20-105 kPa	9	Analogue	± 1.8 % FS
MPXAZ6115A	15-115 kPa	10	Analogue	± 1.5 % FS
Reference Sensor (RPT200)	35 - 3500 bar	-	Digital	0,02 % FS

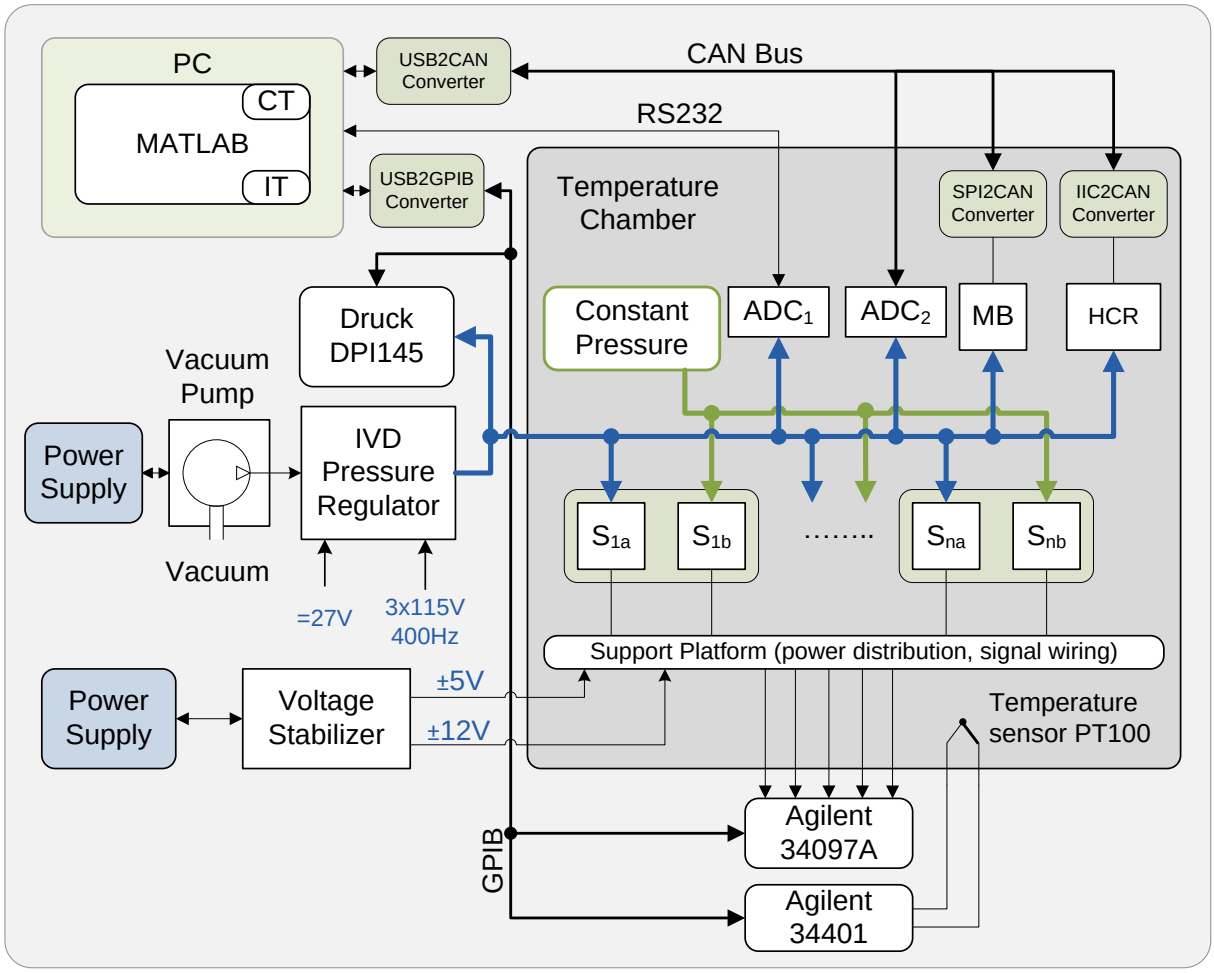

Fig. 3: Measurement System [4]

Results

The measurement should prove suitability of the blinded sensor output as a correction element of the main measurement sensor and achieve required precision and environmental effect independency (mainly on ambient temperature). The output of the blinded sensor will be used for correction of the sensor whose output is primarily intended to be used for altitude determination. Following sensors were evaluated: MPX4100A, MPX4115A and MPX6115A (two pieces each). The group of tested sensors (see Tab. 1) differs in range and in precision. The MPX4100 sensor output had deviation of 60 Pa from the ideal characteristic at zero level ISA [3], MPX4115A sensor had deviation of 200 Pa and the MPX6115A sensor had 800 Pa deviation. The first two sensors show similar temperature effects while the third sensor characteristics differ. Following pictures show data just from MPX4115A sensor because it is the oldest and the most available.

Fig. 4 shows deviations of the MPX4115AP sensor from an ideal characteristic based on data from Druck DPI145. We can see a temperature influence affecting the starting point of the characteristics and its endpoint – please note the hysteresis and change of the scale factors especially in negative temperatures. We can read hysteresis between starting point and the endpoint which is approximately 200 Pa (see characteristics at 0° C).

The deviations depicted in Fig. 4 should be calibrated by outputs provided by blinded sensors.

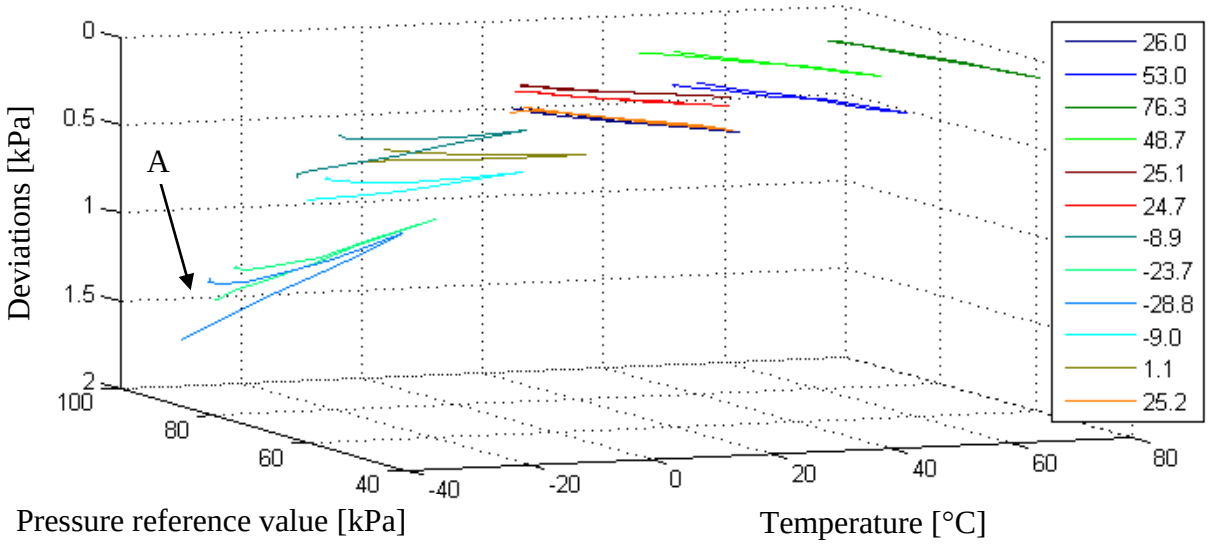

Fig. 4: MPX4115AP output signal deviations from an ideal transfer characteristics based on the data from Druck DPI145

Fig. 5 depicts outputs from the blinded MPX4115AP sensor. In this case, the output signal of the sensor is independent on the value of the applied pressure and thus the characteristics were expected as ideal straight lines. The temperature influence can be clearly observed between the starting and the end point position of the characteristics. This illustrates the problem with temperature stability in the temperature chamber – it is very intensive in cases of minimal and maximal temperature. Next effect that takes place here is the hysteresis caused by air heating and cooling during the two-day measurement (see blue and red circles). In case of the first day, the environment was heated up to 76 °C and then cooled back to 25 °C. The cooling process was so intensive that it overcooled the analogue sensors placed in front of the cooling system while the PT100 sensors measured temperature at a different place (it was mounted on an aluminum block). A similar problem can be seen during the Day 2.

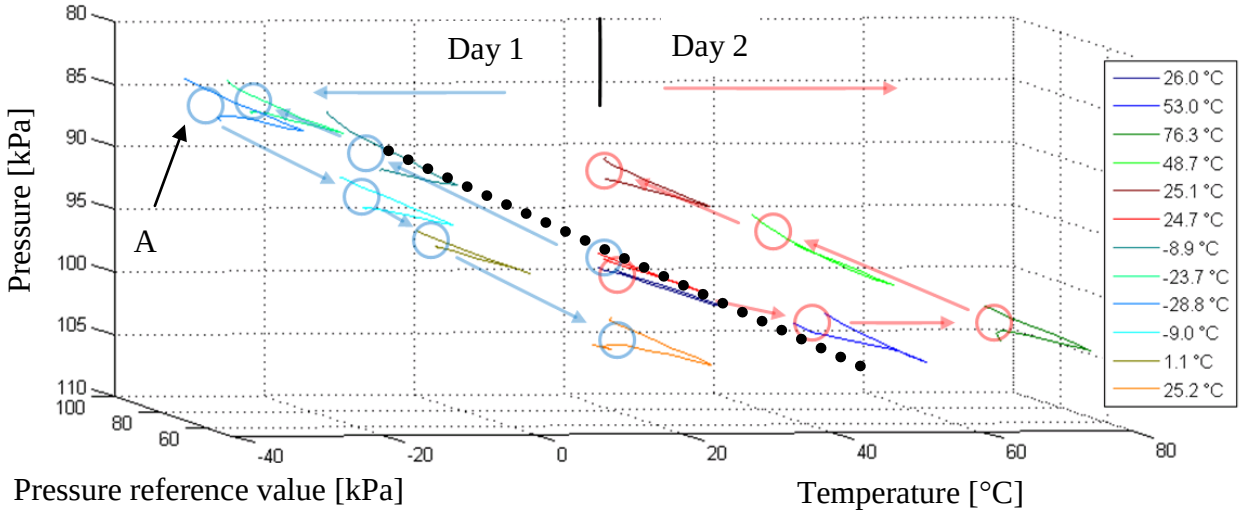

Fig. 5: Characteristics measured on the blinded MPX4115AP sensor

Fig. 5 shows dotted line illustrating Amontons's Law of Pressure-Temperature (1) that can be observed at the beginning of each measurement day. Obviously, the figure shows a hysteresis caused by fast temperature changes of the heating and cooling system. The pressure difference in the closed volume ΔP_T can be described by equation (2):

$$\Delta P_T = \frac{p_1}{T_1} T - P_{1T}\,, \tag{2}$$

Where p_1 is the pressure of the reference point [Pa],

T_1 is the temperature of the reference point [K],

P_{1T} is the pressure at the reference point [Pa] and

T is the temperature [K] measured in the closed volume.

The output of the measurement sensor calibrated by a blinded sensor will be calculated by:

$$P_{M\_S\_CORR} = P_{M\_S} + \left(P_{B\_S} - \Delta P_T\right) + c\,, \tag{3}$$

Where P_{M_S} is the measurement sensor output [Pa],

P_{B_S} is the blinded sensor output [Pa],

ΔP_T is a correction [Pa] calculated according to the (2),

c is a vertical shift of the characteristics [Pa] and

$P_{M\_S\_CORR}$ is the temperature independent pressure output [Pa].

Conclusion

We described application of Amontons's Law of Pressure-Temperature for elimination of unwanted temperature effects affecting pressure sensors in ranges from (-40 to +85) °C. One blinded sensor is used just for temperature effects measurement. Unfortunately, its output is also affected by behaviour described by Amontons's Law of Pressure-Temperature that changes pressure in the closed volume by 20 kPa in the required range (1).

We can also presume that the proposed method of temperature effect elimination will also automatically remove long term aging effects of the sensing element. It is based on the presumption that the measurement and correction elements (sensors) will age the same way because they are exposed to the same environment.

The described problems with the measurement system caused that the proposed method of temperature effects correction was derived (3) but not completely proved. The isochoric change appearing on the blinded sensor output was suppressed by too fast temperature changes in the temperature system that caused the significant hysteresis of sensor characteristics measured at different temperatures.

What was proven in the article is that the blinded sensor can be used for local temperature hysteresis elimination. The Fig. 5, point A shows behaviour of the blinded sensor that provides corrections of the data shown in Fig. 4, point A. New measurement will be performed in order to completely prove here proposed way of pressure sensor temperature calibration.

Acknowledgement

The project was supported by CTU grant no. SGS10/288/OHK3/3T/13 with help of the research program No. MSM6840770015 "Research of Methods and Systems for Measurement of Physical Quantities and Measured Data Processing " of the CTU in Prague sponsored by the Ministry of Education, Youth and Sports of the Czech Republic. The data was also used for the project program no. TA01030651 "Safety Improvement of Flight, Crew and Other Participants of Flight Transport in Normal and Emergency Situations by Assistive Technologies" of the Czech Technical University in Prague, sponsored by the Technological Agency of the Czech Republic. This research has been also partially supported by the Czech Science Foundation project 102/09/H082.

References

[1] SOPATA M., SOTAK M., BREDA R.: *Verification Mathematical Models for Aircraft Systems Development* In: Measurement, Diagnostics, Dependability of Aircraft Systems: Proceedings of the 6th conference, Brno : Univerzita obrany, 2006. - ISBN 80-7231-155-7. pp. 89-93. (in Slovak).

[2] JALOVECKÝ, R., BYSTŘICKÝ, R., JANŮ, J. *Aircraft sensors signal processing*. In Recent Advances in Mechatronics 2008-2009. Best contribution presented at the 8th International Conference "Mechatronics 2009". November 18-20, 2009, Luhačovice, Czech Republic. Berlin Heidelberg, Springer-Verlag, 2009, p.73-78, ISBN 978-3-642-05021-3.

[3] International Organization for Standardization. *Standard Atmosphere*. Geneva: ISO, 1975. ISO 2533:1975.

[4] PAČES, P.; ŠIPOŠ, M.; REINŠTEIN, M.; ROHÁČ, J.: *Sensors of Air Data Computers - Usability and Environmental Effects*, ICMT'09 - Proceedings of the International Conference on Military Technologies. Brno: University of defence, 2009, p. 401-409. ISBN 978-80-7231-649-6.

Analyses of Triaxial Accelerometer Calibration Algorithms

Martin Šipoš, Pavel Pačes, *Member, IEEE*, Jan Roháč, and Petr Nováček

***Abstract*—This paper proposes a calibration procedure in order to minimize the process time and cost. It relies on the suggestion of optimal positions, in which the calibration procedure takes place, and on position number optimization. Furthermore, this paper describes and compares three useful calibration algorithms applicable on triaxial accelerometer to determine its mathematical error model without a need to use an expensive and precise calibration means, which is commonly required. The sensor error model (SEM) of triaxial accelerometer consists of three scale-factor errors, three nonorthogonality angles, and three offsets. For purposes of calibration, two algorithms were tested—the Levenberg–Marquardt and the Thin-Shell algorithm. Both were then related to algorithm based on Matlab *fminunc* function to analyze their efficiency and results. The proposed calibration procedure and applied algorithms were experimentally verified on accelerometers available on market. We performed various analyses of proposed procedure and proved its capability to estimate the parameters of SEM without a need of precise calibration means, with minimum number of iteration, both saving time, workload, and costs.**

***Index Terms*—Accelerometers, calibration, error analysis, inertial navigation.**

I. Introduction

OVER the last decades technological progress in the precision and reliability of Micro-Electro-Mechanical-Systems (MEMS) has enabled the usage of inertial sensors based on MEMS in a wide range of military and commercial applications, e.g., in Unmanned Aircraft Systems (UASs), indoor and personal navigation, human motion tracking, and attitude-control systems [1]–[5].

The Inertial Measurement Unit (IMU), which forms a basic part of Inertial Navigation System (INS), primarily contains only inertial sensors-accelerometers and angular rate sensors or gyroscopes to provide inertial data, and additionally magnetometers. The major errors of electronically-gimbaled navigation systems with accelerometers and magnetometers are caused by sensor triplet deviations (mutual misalignment) [6], and therefore, a calibration has to take a place for their proper function. The calibration is necessary to be performed to estimate sensor errors like nonorthogonalities (misalignment) and scale factor errors for their compensation. Factory based sensor calibration is an expensive and time-consuming process, which is typically done for specific high-grade IMUs. For low-cost inertial sensors, such as MEMS based ones, manufacturers perform only basic calibration [7] which is very often insufficient, because even small uncompensated imperfections can cause position deviation growth and also inaccuracy in tilt angle evaluation [8], [9].

There are already known different sensor error models (SEMs) [10] and calibration methods based on different principles, but they have limitations such as the necessity of precise position system or a platform providing precise alignment. This requirement increases manufacturing costs, and therefore, there is a need for investigating alternatives.

One example of a commonly used calibration procedure described by Titterton and Weston in ([11] p. 238) and by Won in [8] uses six static positions, in which the sensors' axes are consecutively aligned up and down along the vertical axis of the local level frame. The calibration is capable to determine only offsets and scale factor errors, not nonorthogonalities. The calibration accuracy strongly depends on the alignment precision [7]. To increase the precision of alignment an accurate reference system is usually used, as presented in [10], [11]. In the first case a 3-D optical tracking system and nonlinear least squares algorithm were applied, the other case used an *fminunc* Matlab function as a minimizing algorithm and a robotic arm. In both cases the calibration is capable to estimate sensor' axes misalignments, offsets, and electrical gains/scale factors, which define nine-parameter-error model. The same model for a triaxial accelerometer can be estimated by an iterative calibration procedure described by Petrucha *et al.* in [12] using an automated nonmagnetic system, or the one described by Syed *et al.* in [7], in which offset and scale factor initial values are required for a modified multiposition method. Other method for an accelerometer calibration, presented by Skog and Händel in [13], is based on the cost function formulation and its minimization with respect to unknown model parameters using Newton's method. The cost function can reach several local optima, and therefore, the initial starting values have to be determined. Automatic adaptive method of a 3-D field sensor based on a linearized version of an ellipsoid fitting problem has been published in [14]. It relies on a procedure that fits an ellipsoid to data using linear regression. Based on estimated ellipsoid parameters the unknown model parameters can be evaluated. An alternative to this method using modified ellipsoidal-fitting procedure has

Manuscript received May 13, 2011; revised August 01, 2011; accepted August 24, 2011. Date of publication September 08, 2011; date of current version April 11, 2012. This work was supported in part by the Czech Science Foundation project 102/09/H082; in part by the Research Program No. MSM6840770015 "Research of Methods and Systems for Measurement of Physical Quantities and Measured Data Processing" of the CTU in Prague sponsored by the Ministry of Education, Youth, and Sports of the Czech Republic; and in part by the Grant Agency of the Czech Technical University in Prague under Grant SGS10/288/OHK3/3T/13. The associate editor coordinating the review of this paper and approving it for publication was Prof. Boris Stoeber.

The authors are with the Department of Measurement, Faculty of Electrical Engineering, Czech Technical University in Prague, Technicka 2, 166 27 Prague, Czech Republic (e-mail: siposmar@fel.cvut.cz; pacesp@fel.cvut.cz; xrohac@fel.cvut.cz; petr.novacek@fel.cvut.cz).

Digital Object Identifier 10.1109/JSEN.2011.2167319

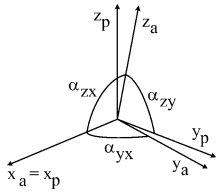

Fig. 1. Orthogonalization of sensor frame; a—nonorthogonal sensor frame; p—orthogonal sensor frame.

been described by Bonnet *et al.* in [15]. He proved that an ellipsoid fitting using either linear optimization (Merayo's algorithm) or nonlinear optimization (Quasi-Newton factorization algorithm) is robust with data sets from static positions obtained within free rotations along a vertical axis in case of accelerometers and free rotations along East-West axis in case of magnetometers.

In Section II, the SEM of triaxial accelerometer is described. We present three algorithms for its calibration in Section III; the Levenberg–Marquardt algorithm, the Thin-Shell algorithm, and an algorithm based on Matlab *fminunc* function. First two algorithms were related to third one, which was used as a reference, in order to have a means for the comparison of algorithms efficiency. In Section IV, we shortly present the most important parameters of calibrated sensors and used measurement setup. To compare a calibration effect on measured and evaluated data based on applied algorithms and SEMs we used a Rotational-Tilt Platform with precise positioning capability to provide precise tilt angles. The experiments, analyses, and result accuracy are provided in Section V.

II. Sensor Error Model

For triaxial accelerometer calibration we considered the sensor error model (SEM), which consisted of nine unknown parameters—three scale factor corrections, three angles of nonorthogonality, and three offsets. The SEM can be defined as (1). Offset forms a stochastic part of biases and can be modeled as a random constant. The time variant part of the bias is drift, which changes based on environmental and other sensor conditions. The calibration process is supposed to be performed during short-time period; therefore, drift can be considered as zero

$$\begin{aligned} a_p &= T_a^p \mathrm{SF}_a (a_m - b_a) \\ &= \begin{pmatrix} 1 & 0 & 0 \\ \alpha_{yx} & 1 & 0 \\ \alpha_{zx} & \alpha_{zy} & 1 \end{pmatrix} \begin{pmatrix} \mathrm{SF}_{ax} & 0 & 0 \\ 0 & \mathrm{SF}_{ay} & 0 \\ 0 & 0 & \mathrm{SF}_{az} \end{pmatrix} \\ &\quad \times \left(\begin{pmatrix} a_{mx} \\ a_{my} \\ a_{mz} \end{pmatrix} - \begin{pmatrix} b_{ax} \\ b_{ay} \\ b_{az} \end{pmatrix} \right) \end{aligned} \tag{1}$$

where $a_p = [a_{px}, a_{py}, a_{pz}]^T$ is the compensated vector of a measured acceleration defined in the orthogonal system (platform frame); T_a^p denotes matrix providing transformation from nonorthogonal frame to orthogonal one with nondiagonal terms $\alpha_{yx}, \alpha_{zx}, \alpha_{zy}$ that correspond to the axes misalignment (nonorthogonality angles) (Fig. 1); SF_a represents a scale factor matrix; $b_a = [b_{ax}, b_{ay}, b_{az}]^T$ is the vector of sensor offsets; $a_m = [a_{mx}, a_{my}, a_{mz}]^T$ denotes the vector of measured accelerations. The SEM and its derivation are described in more detail in [13] and [16].

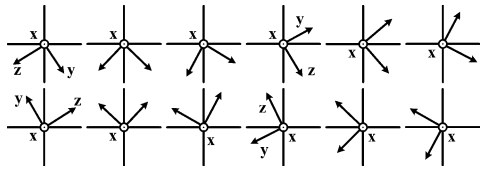

Fig. 2. Positions for calibration; rotation around x axis.

III. Calibration Algorithms

This section briefly describes the algorithms for triaxial accelerometer calibration—Levenberg–Marquardt (LM) algorithm, Thin-Shell (TS) algorithm, and algorithm based on Matlab *fminunc* function. The fundamental principle of the proposed calibration procedure is based on the fact that the magnitude of measured acceleration should be equal to the gravity magnitude, which is ensured by static conditions (2). It corresponds to "scalar field calibration" used in [17]. The proposed procedure uses only general knowledge about the applied quantity, which is in contrast to the case when precise positioning system is available, and thus, the knowledge about precise tilt angle is also provided in all steps of iteration

$$g_x^2 + g_y^2 + g_z^2 = |g|^2 \tag{2}$$

where g_i denotes sensed acceleration in direction of i axis and $|g|$ is the magnitude of gravity vector, ideally equal to $1g$.

To obtain the most accurate estimation without the need of having a precise positioning system, the sensor should be consecutively placed to positions in manner to cover the whole globe surface and the sensor should be influenced only by gravity. In practice, it is not possible to do so, because the number of measurements would be infinite. Therefore, in the proposed procedure, the number of positions is optimized and suggested their orientation, in which a high influence of all errors is expected. Only 36 positions are used, 3 times 12 positions along x, y, z axis. The positions along x axis are shown in Fig. 2. Precise knowledge of their orientations is not required, only 3 positions per quadrant are recommended.

A. Principle of Levenberg–Marquardt Algorithm

The Levenberg–Marquardt (LM) algorithm is one of the most efficient and popular algorithms. It has better convergence than the other ones for nonlinear minimization. The LM algorithm is widely utilized in software applications, neural networks, and curve-fitting problems [18]–[21]. The LM algorithm combines two algorithms: the Gradient Descent (GD) and the Gauss–Newton (GN) algorithm [22]. The LM algorithm can be described by (3)

$$S(\beta) = \sum_{i=1}^{m} [y_i - f(x_i, \beta)]^2 = \sum_{i=1}^{m} q_i(\beta)^2 \tag{3}$$

where $S(\beta)$ denotes the sum of residuals $q_i(\beta)^2$; m is the number of measurements; x_i are measured data; y_i are the reference values, and β is a vector of parameters being estimated

and forming the SEM defined in (1). The LM algorithm is iterative algorithm reducing $S(\beta)$ with respect to the parameters in vector β.

1) Gradient Descent Algorithm: The Gradient Descent (GD) algorithm is a minimization algorithm updating the estimated parameters in the direction opposite to the gradient of the cost function. The GD algorithm is highly convergent and can be used for problems with thousands of parameters forming the cost function. The h_{GD} modifies the GD algorithm step to reduce $S(\beta)$ in the direction of steepest descent and is defined by (4) [22]

$$h_{\mathrm{GD}} = \alpha J^T W(y_i - f(x_i, \beta)) \tag{4}$$

where α is a parameter corresponding to the length of step in the steepest descent direction; J is the Jacobian related to the vector β; W is the weighting diagonal matrix [22].

2) Gauss–Newton Algorithm: A main advantage of Gauss–Newton (GN) algorithm is its rapid convergence; however, it depends on the initial conditions. The GN algorithm does not require the calculation of second-order derivatives [21]. The equation for GN algorithm reducing $S(\beta)$ is given by (5)

$$\lfloor J^T W J \rfloor h_{\mathrm{GN}} = J^T W(y_i - f(x_i, \beta)) \tag{5}$$

where h_{GN} denotes the GN algorithm update of estimated parameter leading to a minimization of $S(\beta)$.

3) Levenberg–Marquardt Algorithm: As was mentioned, the Levenberg–Marquardt (LM) algorithm combines both the GD and GN algorithm. In the LM algorithm, the parameter h_{LM} is adaptively weighted with respect to h_{GD} and h_{GN} to reach optimal progress in $S(\beta)$ minimization, and thus, the LM algorithm equation is given by (6)

$$\lfloor J^T W J + \lambda \operatorname{diag}(J^T W J) \rfloor h_{\mathrm{LM}} = J^T W(y_i - f(x_i, \beta)) \tag{6}$$

where λ is a damping parameter and h_{LM} is the LM algorithm update. The parameter λ has several characteristics [23]:

- for all $\lambda > 0$, the coefficient matrix $(J^T W J + \lambda \operatorname{diag}(J^T W J))$ is positive definite, and this fact ensures that h_{LM} is descent directional;
- for large values of λ the iteration step (parameter modification) is in the steepest descent direction, which is good when the current stage is far from required solution;
- for small values of λ, the $h_{\mathrm{LM}} \cong h_{\mathrm{GN}}$ and it is good for final phases of iteration, when estimated parameters are close to required solution.

In other words, if the iteration step decreases the error, it implies that quadratic assumption $f(x_i)$ is working and λ can be reduced (usually by a factor of 10) to decrease the influence of GD. On the other hand, if $S(\beta)$ increases, λ is increased by the same factor increasing GD influence and the iteration step is repeated.

B. Thin-Shell Algorithm

The Thin-Shell (TS) algorithm is based on an estimation of Linear Minimum Mean Square Error, which is applied on SEM (1) of calibrated sensor. According to (1) nine parameters have to be estimated. The iteration is based on successive halving of intervals, in which the estimated parameter is searched for. The intervals are halved based on a standard deviation defined by (7) and if-conditions related to Fig. 3

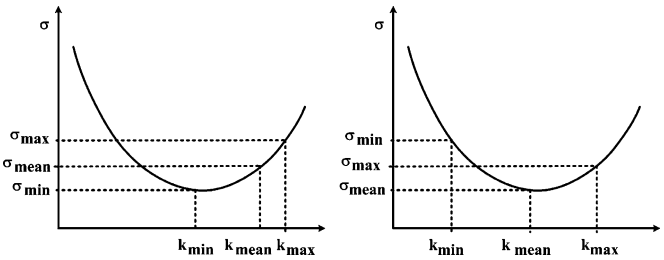

Fig. 3. Criterions for halving the interval, for which the estimated parameters are searched.

$$\sigma = \sqrt{\frac{\sum_{i=1}^{m} \left(\widehat{a}_{xi}^2 + \widehat{a}_{yi}^2 + \widehat{a}_{zi}^2 - |g|^2 \right)^2}{m-1}} \tag{7}$$

where σ is the standard deviation; m is the number of positions; $\widehat{a}_{xi}, \widehat{a}_{yi}, \widehat{a}_{zi}$ are estimations of compensated measured gravity vector components and $|g|$ is the magnitude of gravity vector corresponding to the reference value.

At the beginning of the algorithm, the minimal and maximal values of each parameter must be set (it defines the interval, in which the unknown parameter is searched for); the mean value is computed as an average of them. Each iteration cycle can be divided into three steps:

1) Min, max, and mean values of the parameter being searched for ($\mathrm{k_{min}}, \mathrm{k_{mean}}$, and $\mathrm{k_{max}}$) are used for the estimation of compensated accelerations in all positions.
2) Three corresponding standard deviations ($\sigma_{\mathrm{min}}, \sigma_{\mathrm{mean}}$, and σ_{max}) are then obtained based on (7). Other parameters are set to their mean values.
3) Based on $\sigma_{\mathrm{min}}, \sigma_{\mathrm{mean}}$, and σ_{max} the interval, in which estimated parameter should be, is halved according to Fig. 3 and following conditions:
   - if $(\sigma_{\mathrm{min}} > \sigma_{\mathrm{mean}})$ and $(\sigma_{\mathrm{max}} > \sigma_{\mathrm{mean}})$, the interval is reduced to a half around the mean value k_{mean}.
   - if $(\sigma_{\mathrm{min}} < \sigma_{\mathrm{mean}})$ and $(\sigma_{\mathrm{mean}} < \sigma_{\mathrm{max}})$ the true value of the parameter should be in the interval $(k_{\mathrm{min}}, k_{\mathrm{mean}})$; for the following iteration cycle $k_{\mathrm{max}} = k_{\mathrm{mean}}$ and k_{mean} is computed as a mean value of k_{min} and new k_{max}.
   - if $(\sigma_{\mathrm{max}} < \sigma_{\mathrm{mean}})$ and $(\sigma_{\mathrm{mean}} < \sigma_{\mathrm{min}})$ the true value of the parameter should be in the interval $(k_{\mathrm{mean}}, k_{\mathrm{max}})$; for the following iteration cycle $k_{\mathrm{min}} = k_{\mathrm{mean}}$ and k_{mean} is computed as a mean value of new k_{min} and k_{max}.

The steps described above are repeated until the computed standard deviation is less than the required value or required number of iteration cycles is reached. Consequently the rest of the parameters are estimated in the same manner. The final value of standard deviation defines the calibration algorithm accuracy. This algorithm is described in more detail in [24].

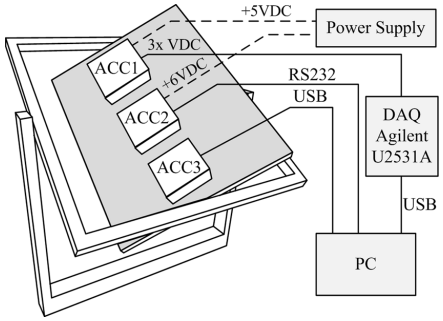

Fig. 4. Measurement setup for triaxial accelerometer calibration; ACC1—CXL02LF3; ACC2—AHRS M3; ACC3—ADIS16405.

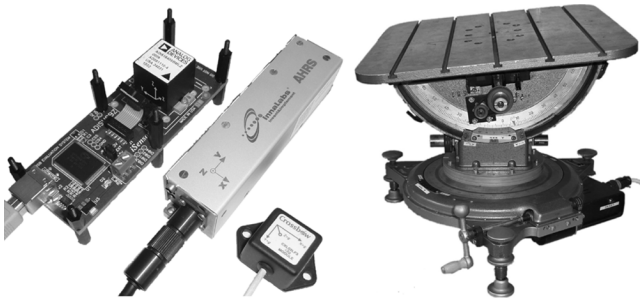

(a) (b)

Fig. 5. (a) Calibrated systems (from left): ADIS16405; AHRS M3; CXL02LF3; (b) Rotational-tilt platform.

C. Algorithm Based on Fminunc Matlab Function

To evaluate the efficiency of Levenberg–Marquardt (LM) and Thin-Shell (TS) algorithms with respect to minimum required number of iterations and reached accuracy Matlab functions *fminunc, lsqnonlin*, and *fminsearch* were tested. Based on their performances the function *fminunc* was chosen as a reference and a means for LM and TS algorithm evaluation. Function *fminunc* is based on quasi-Newton minimization with numerical gradients [25]. Its description is not the subject of this paper and can be found [26].

IV. Calibrated Sensors and Measurement Setup

In this section, we briefly present the systems used for the calibration and measurement setup (Fig. 4) which uses a simple platform enabling to measure accelerometer data in the static positions defined approximately as shown in Fig. 2. Furthermore, we used a Rotational-Tilt Platform (RoTiP), see Fig. 5(b), as a reference for analyses needed to verify the results of the proposed calibration procedure according to applied algorithms. The RoTiP parameters are shown in Table I. Although we evaluated five sensors in sum, such as AHRS M3's accelerometer (Innalabs [27]), ADIS16405's accelerometer (Analog Devices [28]), CXL02LF3 accelerometer (Crossbow [29]), 3DM-GX2's accelerometer (MicroStrain [30]), and STEVAL-MKI062V2's accelerometer (STMicroelectronics [31]), we present the results of analyses only from first three accelerometers of calibrated systems [see Fig. 5(a)]. The analyses of last two sensors were very similar.

TABLE I
Parameters of Rotational-Tilt Platform

Parameter	Range	Speed of Motion	Resolution
Pitch	±45 deg	±42 deg/s	0.00033 deg
Roll	±25 deg	±60 deg/s	0.00065 deg
Heading	0 to 360 deg	±310 deg/s	0.00074 deg

V. Calibration Analyses

Three aforementioned algorithms were used to estimate SEMs of three triaxial accelerometers described in Section IV according to measured data in suggested positions. It helped to decrease the influence of manufacturing imperfection on the sensor precision. As said in [32] other problematic errors can show up with incorrect determination of sensor error parameters; therefore, for results, a comparison Root Mean Square Error (RMSE) defined by (8) was used

$$\mathrm{RMSE}(p,g) = \sqrt{\frac{\sum_{i=1}^{n}(x_i - g)^2}{n}}$$
$$x_i = \sqrt{g_{xi}^2 + g_{yi}^2 + g_{zi}^2} \tag{8}$$

where $p = (x_1, \ldots, x_n)^T$ is n-dimensional vector; n—number of evaluated positions; g is an ideal magnitude of the gravity vector equal to $1g$; g_{xi}, g_{yi}, g_{zi} are components of the estimated gravity vector.

For the calibration purposes and consecutive analyses we measured the raw data from sensors and evaluated data in 364 positions. The number was chosen with respect to the number of suggested positions in Section III multiplied by 10 and modified to have uniformly spaced data along all axes. The analyses included the observation of estimated parameters of SEM with respect to algorithms applied, the RMSE dependence on the number of taken positions and the number of iterations, and the observation of a long-period permutation of estimated SEMs. Furthermore, the calibration effect on the precision of evaluated tilt angles and the calibration effect from the sensors' drift point of view were performed.

A. Sensor Error Models

We estimated Sensor Errors Models (SEMs) of three accelerometers. Results are listed for LM and TS algorithms in Table II. Although we estimated the SEMs using three algorithms, only LM and TS algorithms' results are listed due to the fact that the results estimated by LM algorithm were identical to the ones from algorithm based on *fminunc* function. From Table II, it can be seen that SEMs estimated by LM and TS algorithms are comparable for all tested units, which also proves the values of RMSE. The effect of SEM applying on measured data is shown in Fig. 6, where magnitude of compensated acceleration vector has approximately 100 times smaller deviation from $1g$ than the one before calibration.

B. Dependence of RMSE on Evaluated Data Positions

To prove that only 36 static positions are sufficient for the calibration purposes, we measured 364 positions uniformly spaced, and analyzed the variation of RMSE for the different number of

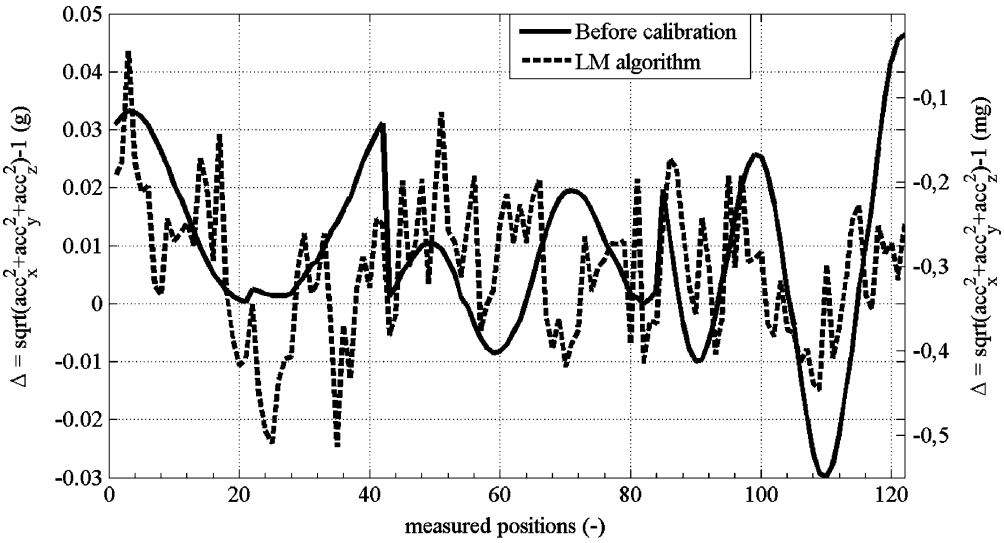

Fig. 6. Dependence of deviations of measured accelerations before (left vertical axis) and after (right vertical axis) calibration using LM algorithm applied on AHRS M3's accelerometer data in evaluated different positions.

TABLE II
SENSOR ERROR MODELS OBTAINED USING LEVENBERG–MARQUARDT (LM) AND THIN-SHELL (TS) ALGORITHM FOR ACCELEROMETERS OF AHRS M3'S (AHRS) AND ADIS16405'S (ADIS) AND CXL02LF3 (CXL) ACCELEROMETER

Par	LM AHRS	LM ADIS	LM CXL	TS AHRS	TS ADIS	TS CXL
α_{yx} (deg)	-0.8758	-0.0230	1.0237	-0.8760	-0.0227	1.0235
α_{zx} (deg)	3.0286	0.0351	-0.5217	3.0229	0.0350	-0.4476
α_{zy} (deg)	0.1765	-0.1639	-1.4939	0.1784	-0.1639	-1.4829
SF_{ax} (-)	0.99865	0.99956	1.05591	0.99866	0.99957	1.05664
SF_{ay} (-)	0.98946	1.00194	1.06517	0.98946	1.00194	1.06508
SF_{az} (-)	0.98611	0.99828	1.06144	0.98608	0.99828	1.06128
b_{ax} (g)	0.00173	-0.01354	-0.00255	0.00172	-0.01353	-0.00272
b_{ay} (g)	-0.00602	-0.00671	-0.03445	-0.00598	-0.00678	-0.03675
b_{az} (g)	0.01440	-0.00402	0.03690	0.01427	-0.00400	0.04003
RMSE [1]	0.01810	0.00948	0.06628	0.01810	0.00948	0.06628
RMSE [2]	0.00015	0.00252	0.01527	0.00017	0.00252	0.01545

Superscript 1 denotes RMSE before calibration and 2 after calibration.

positions (NoP) in intervals from 12 to 364. NoP can be seen in Table III, where N represents the relationship between Figs. 7–9 horizontal axes and the NoP used for calculation. In each static position, an average of 100 measured data samples was calculated to reduce noise. The dependence between RMSE defined in (8) and NoP is shown in Fig. 7 for AHRS M3, in Fig. 8 for ADIS16405, and in Fig. 9 for CXL02LF3. The RMSE was evaluated between an ideal magnitude of gravity vector and the magnitude of compensated measured gravity. The compensated measured gravity obtained from the measured data multiplication with SEM is further notified as a compensated result. The left vertical axes of Figs. 7–9 correspond to RMSE before calibration and right vertical axes correspond to RMSE after calibration. As a criterion for the evaluation of RMSE dependence on the number of evaluated positions we considered a maximum deviation of RMSE from RMSE in $\mathrm{N} = 1$ position to be equal or less than 1 mg, which corresponds to sensor resolutions. From Figs. 7–9 it can be seen, that 21 positions and more satisfy desired limitation no matter which algorithm was used. This means that the variation of the compensated results in the case of usage

TABLE III
RELATIONSHIP BETWEEN THE NUMBER OF EVALUATED POSITIONS (NOP) AND NOTATION OF FIGS. 7–9 HORIZONTAL AXES (N)

N	NoP	N	NoP	N	NoP	N	NoP	N	NoP
1	364	7	52	13	28	19	20	25	14
2	182	8	46	14	26	20	19	26	13
3	122	9	41	15	25	21	18	27	12
4	91	10	36	16	23	22	17		
5	73	11	34	17	22	23	16		
6	61	12	31	18	21	24	15		

21 positions or more (up to 364) differs under the required value; therefore, further differences are considered as negligible. Because having 7 positions in 360 deg and also in 4 quadrants does not have a uniform distribution with a constant number of positions per quadrant, it is suitable to increase the number to 12. This leads to having 36 positions covering all axes, which was the number we used in Section III-A. The result optimizes the number of positions needed for the calibration with respect to a workload and precision.

C. Dependence of RMSE on Number of Iterations

Based on the data measured in 36 positions as described in Section III and proven in Section V-B, we analyzed the dependency of RMSE calculated between compensated results and an ideal gravity vector on the number of iterations for LM and TS algorithms. The iteration denotes a calibration cycle, in which all measured data (in our case in 36 positions) are used for an unknown SEM parameter estimation. This analysis relied on the progress of RMSE with respect to the number of iteration. When the deviation from the steady-state value was less than 1 mg we considered the accuracy of calibration to be sufficient. Fig. 10 shows the RMSE dependency on number of iterations for TS algorithm applied on AHRS M3 accelerometer. The comparison between LM and TS algorithms from the number of iterations point of view is presented in Table IV.

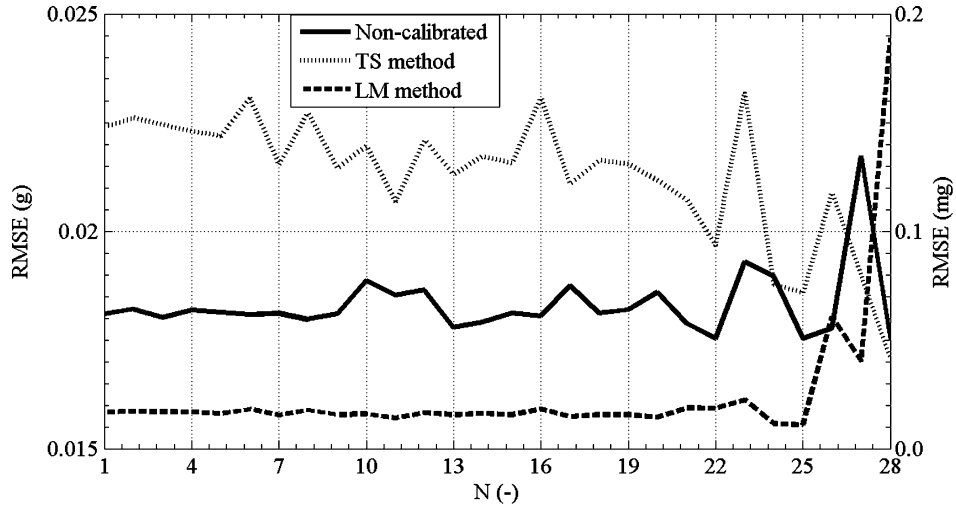

Fig. 7. Dependence of RMSE before (left axis) and after (right axis) calibration on the number of positions using AHRS M3's accelerometer.

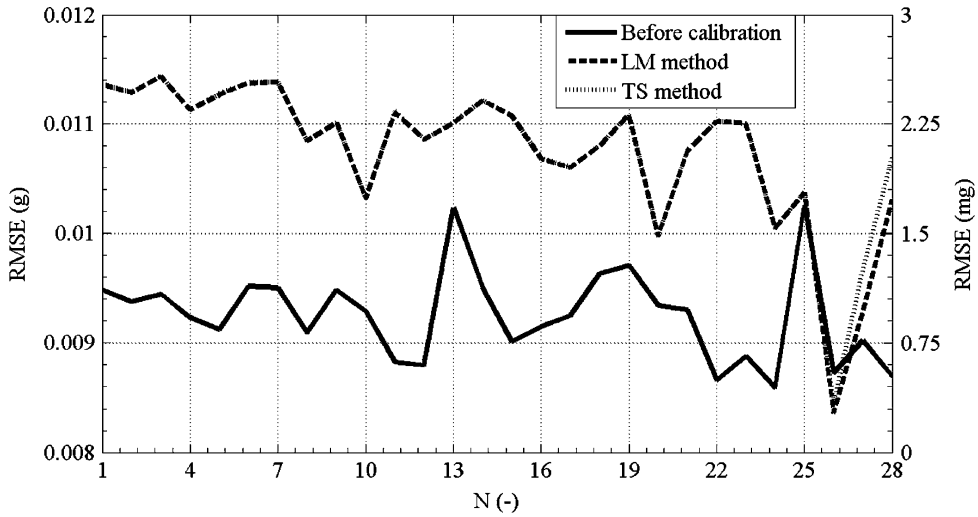

Fig. 8. Dependence of RMSE before (left axis) and after (right axis) calibration on the number of positions using ADIS16405's accelerometer.

D. Comparison of SEM During Time Period

We analyzed the variation of SEMs obtained by LM and TS algorithms during a longer time period corresponding to one and half years (the first measurement was taken in April 2009 and the second one was taken in November 2010). We measured 122 positions in both cases with different distributions as shown in Fig. 11. We analyzed the SEMs permutation and their accuracy. The SEMs evaluated based on two data sets using LM and TS calibration algorithms are presented in Table V. In each position the average of 100 data samples was used as in previous analyses.

From Table V it can be seen that parameters are slightly different, which we think was caused by reaching the resolution of the method applied. The influence of different distribution of evaluated positions shown in Fig. 11 is considered as negligible, because the number of evaluated positions was always higher than 21.

E. Comparison of Tilt Angles Before and After Calibration

To see the effect of calibration, we performed another analysis in which the tilt angles estimated based on calibration results were compared to the reference ones measured by Rotational-Tilt Platform (RoTiP).

We mounted the accelerometers on RoTiP and tilted them along two axes. A tilt corresponded to pitch (θ) and roll (ϕ) angles. Specification of RoTiP is listed in Section IV. The pitch angle calculation is defined as (9) and roll angle calculation as (10)

$$\theta = \operatorname{arctg}\left(-f_{by} \Big/ \sqrt{f_{bx}^2 + f_{bz}^2}\right) \tag{9}$$

$$\phi = \operatorname{arctg}(f_{bx}/-f_{bz}) \tag{10}$$

where θ is the pitch angle; ϕ is the roll angle; f_{bx}, f_{by}, f_{bz} are measured accelerations. For computation of *arctg* function, the Matlab function *atan2*, which returns the four-quadrant invert tangent (arctangent) of real parts x and y. [2], was used.

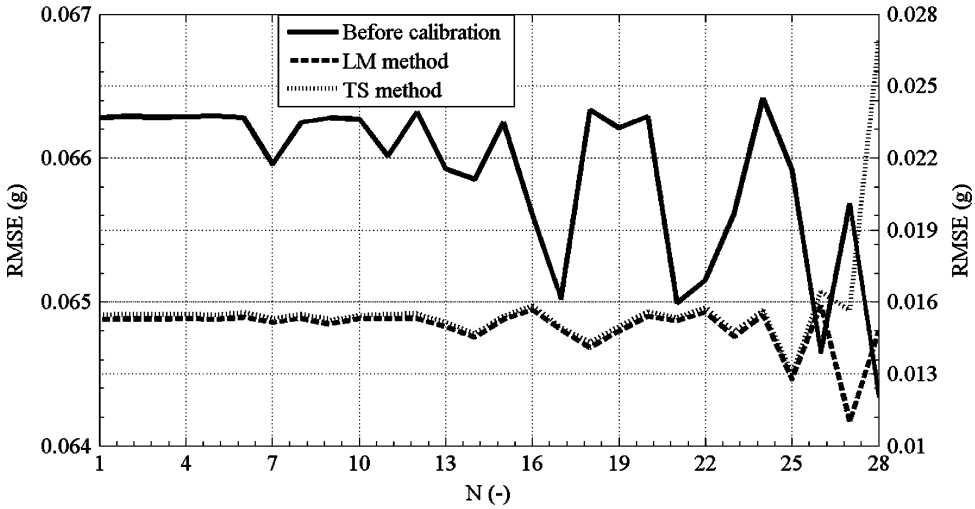

Fig. 9. Dependence of RMSE before (left axis) and after (right axis) calibration on the number of positions using CXL02LF3 accelerometer.

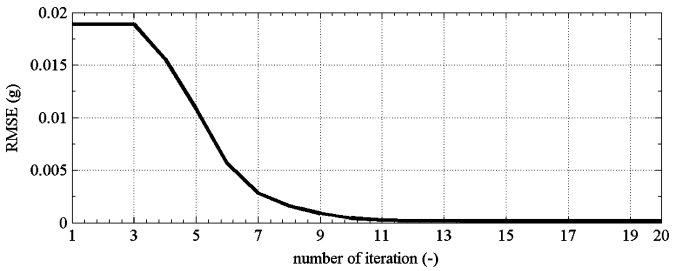

Fig. 10. Dependence of RMSE on the number of iterations for AHRS M3's accelerometer using TS calibration algorithm.

TABLE IV
NUMBER OF ITERATIONS FOR LM AND TS CALIBRATION ALGORITHMS

	AHRS M3	ADIS16405	CXL02LF3
LM Algorithm	2	1	1
TS Algorithm	9	7	6

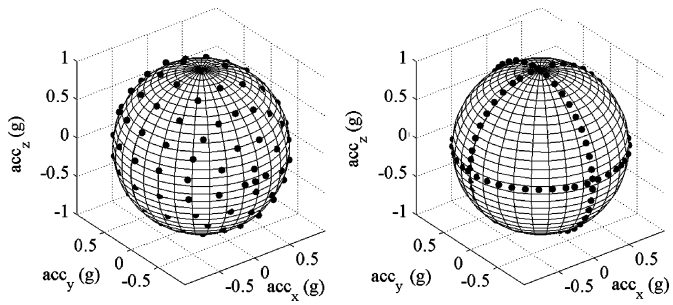

Fig. 11. Evaluated positions in April 2009 (left) and in November 2010 (right).

We analyzed the variation of results when LM and TS algorithms had been applied. The last column of Tables VI–VIII (AHRS M3, ADIS16405, CXL02LF3) describes an Error Percentage Improvement (EPI) which corresponds to the difference between particular deviations (relative errors) related to the maximum angle, i.e., 20 deg. From these tables it can be seen that due to the calibration the tilt angles are more accurate than

TABLE V
SENSOR ERROR MODELS OBTAINED USING LM ALGORITHM (LM) AND TS ALGORITHM (TS) DURING TIME INTERVAL OF ONE AND HALF YEARS FOR ACCELEROMETER CONTAINED IN AHRS M3

Parameter	LM Apr 2009	LM Nov 2010	TS Apr 2009	TS Nov 2010
α_{yx} (deg)	-0.8769	-0.8758	-0.8830	-0.8760
α_{zx} (deg)	3.0261	3.0286	3.0253	3.0229
α_{zy} (deg)	0.1794	0.1765	0.1818	0.1784
SF_{ax} (-)	0.99868	0.99865	0.99902	0.99866
SF_{ay} (-)	0.98951	0.98946	0.98828	0.98946
SF_{az} (-)	0.98609	0.98611	0.98640	0.98608
b_{ax} (g)	0.00153	0.00173	0.00156	0.00172
b_{ay} (g)	-0.00541	-0.00602	-0.00527	-0.00598
b_{az} (g)	0.01461	0.01440	0.01448	0.01427
RMSE [1]	0.01957	0.01810	0.01957	0.01810
RMSE [2]	0.00014	0.00015	0.00055	0.00017

Superscript 1 denotes RMSE before calibration and 2 after calibration.

TABLE VI
COMPARISON OF TILT ANGLES BEFORE AND AFTER CALIBRATION USING LM AND TS ALGORITHMS FOR AHRS M3; θ—PITCH, ϕ—ROLL

Reference Angle θ; ϕ (deg)	Without Calibration θ; ϕ (deg)	LM Algorithm θ; ϕ (deg)	TS Algorithm θ; ϕ (deg)	LM EPI θ; ϕ (%)
0; 0	-0.77; -0.59	-0.70; -0.30	-0.68; -0.26	0.4; 1.5
10; 0	9.18; -0.62	9.61; -0.16	9.62; -0.12	2.2; 2.3
20; 0	19.18; -0.63	20.13; 0.01	20.14; 0.05	3.4; 3.1
0; -10	-0.96; -10.83	-0.90; -10.72	-0.89; -10.69	0.3; 0.6
0; -20	-0.83; -21.10	-0.76; -21.00	-0.75; -21.06	0.4; 0.5
10; -10	9.31; -10.98	9.76; -10.82	9.77; -10.79	2.3; 0.8
20; -20	19.00; -19.62	19.98; -19.76	19.99; -19.72	4.9; 0.7

in case without calibration for all tested sensors and tilt angles.

F. Position Determination With and Without Calibration

Furthermore, we analyzed the drift influence on the accuracy of position determination when a compensated model was used. The accelerations were measured for 200 s in a static position with different tilt angles and then two times integrated to get the position. The effect of compensation applied on an

TABLE VII
COMPARISON OF TILT ANGLES BEFORE AND AFTER CALIBRATION USING LM AND TS ALGORITHMS FOR ADIS16405; θ—PITCH, ϕ—ROLL

Reference Angle θ; ϕ (deg)	Without Calibration θ; ϕ (deg)	LM Algorithm θ; ϕ (deg)	TS Algorithm θ; ϕ (deg)	LM EPI θ; ϕ (%)
0; 0	0.85; -0.29	0.07; 0.10	0.07; 0.10	3.9; 1.0
10; 0	10.80; -0.46	10.09; -0.07	10.09; -0.07	3.6; 2
20; 0	20.66; -0.36	20.04; 0.05	20.04; 0.05	3.1; 1.6
0; -10	1.11; -10.51	0.34; -10.22	0.34; -10.22	3.9; 1.5
0; -20	1.07; -20.35	0.31; -20.15	0.31; -20.15	3.8; 1.5
10; -10	10.92; -10.51	10.23; -10.20	10.23; -10.20	3.5; 1.0
20; -20	20.73; -20.21	20.16; -19.99	20.16; -19.97	2.9; 1.0

TABLE VIII
COMPARISON OF TILT ANGLES BEFORE AND AFTER CALIBRATION USING LM AND TS ALGORITHMS FOR CXL02LF3; θ—PITCH, ϕ—ROLL

Reference Angle θ; ϕ (deg)	Without Calibration θ; ϕ (deg)	LM Algorithm θ; ϕ (deg)	TS Algorithm θ; ϕ (deg)	LM EPI θ; ϕ (%)
0; 0	4.69; -3.84	-0.43; -0.92	-0.37; -0.75	21.3; 14.6
10; 0	13.48; -3.76	10.71; 0.29	10.54; 0.24	13.9; 17.4
20; 0	21.37; -3.78	20.47; 0.15	20.47; 0.09	4.6; 18.2
0; -10	4.56; -13.25	0.90; 10.37	0.71; -10.31	18.3; 9.4
0; -20	4.63; -22.52	0.94; -20.30	0.74; -20.24	18.5; 11.1
10; -10	13.67; -13.30	10.25; -10.92	10.19; -10.73	17.1; 11.9
20; -20	22.12; -22.37	18.82; -20.75	18.76; -20.54	4.9; 8.2

TABLE IX
POSITION DETERMINATION IN PLATFORM FRAME BEFORE AND AFTER CALIBRATION USING SEMS GOT FROM LM AND TS ALGORITHMS FOR AHRS M3'S ACCELEROMETER; $\delta_X, \delta_Y, \delta_Z$—DEVIATIONS IN X, Y, Z AXES

Reference Angle θ; ϕ (deg)	Without Calibration δ_X; δ_Y; δ_Z (m)	LM Algorithm δ_X, δ_Y, δ_Z (m)	TS Algorithm δ_X, δ_Y, δ_Z (m)
0; 0	-239; -56; 5867	7; 2; -160	5; 9; -160
10; 0	-1516; -36; 7224	27; 1; -116	22; 9; -117
20; 0	-3105; 51; 7987	20; -30; -50	10; -22;- 54
0; -10	-350; -1078; 6061	-121; 40; -88	-123; 44; -87
0; -20	-721; -2116; 5921	-508; 85; -67	-507; 84; -67
10; -10	-2299; -635; 7555	-674; 828; -30	-680; 832; -31
20; -20	-7555; 1618; 7981	-4553; 5026; 64	-4561; 5025; 22

TABLE X
POSITION DETERMINATION IN PLATFORM FRAME BEFORE AND AFTER CALIBRATION USING SEMS GOT FROM LM AND TS ALGORITHMS FOR ADIS16405'S ACCELEROMETER; $\delta_X, \delta_Y, \delta_Z$—DEVIATIONS IN X, Y, Z AXES

Reference Angle θ; ϕ (deg)	Without Calibration δ_X; δ_Y; δ_Z (m)	LM Algorithm δ_X, δ_Y, δ_Z (m)	TS Algorithm δ_X, δ_Y, δ_Z (m)
0; 0	-679; -107; -1825	-30; -1; 136	-27; -4; 135
10; 0	-420; 66; -2403	93; 62; 222	95; 60; 222
20; 0	-2366; 93; -6110	-1157; -70; -3050	-1156; -72; 3051
0; -10	-171; 296; 1618	-44; 156; 821	-42; 153; 821
0; -20	-693; -1492; -4065	-328; -497; -1447	-327; -501; -1423
10; -10	-1629; -548; -2659	-933; 1005; 193	-931; 1002; 194
20; -20	-8276; -1733; -2077	-7422; 6714; -1015	-7120; 6710; -1015

AHRS M3's accelerometer, ADIS16405's accelerometer, and CXL02LF3 can be seen in Tables IX–XI.

Results from Tables IX–XI show that, in most cases, the deviations in position decreased due to the calibration. The deviations in position can be partially caused by imprecise alignment of the compensated sensor frame with respect to the platform frame which lies along main axes of the moving object. Due to imprecise sensor-platform, the alignment measured acceleration deviates from the true one and causes a deviation in position as well. This can be reduced by a successive alignment procedure which was not the subject of this analysis.

TABLE XI
POSITION DETERMINATION IN PLATFORM FRAME BEFORE AND AFTER CALIBRATION USING SEMS GOT FROM LM AND TS ALGORITHMS FOR CXL02LF3 ACCELEROMETER; $\delta_X, \delta_Y, \delta_Z$—DEVIATIONS IN X, Y, Z AXES

Reference Angle θ; ϕ (deg)	Without Calibration δ_X; δ_Y; δ_Z (m)	LM Algorithm δ_X, δ_Y, δ_Z (m)	TS Algorithm δ_X, δ_Y, δ_Z (m)
0; 0	-2951; -339; -586	1668; -169; 15	1683; -190; 40
10; 0	-5867; -3609; -804	-3487; -3541; 32	-3628; -3561; 44
20; 0	-8388; -6863; -794	-6479; -6863; 162	-6534; -6824; 179
0; -10	-6187; 2908; -796	-3224; 3226; 103	-3773; 3198; 164
0; -20	-9345; 5971; 942	-6485; 5481; 210	-7059; -6455; 153
10; -10	-9140; -393; -1022	-1585; -158; 136	-1265; -184; 305
20; -20	-14242; -547; -1202	-1314; -182; 336	-1273; -205; 610

VI. CONCLUSION

The main aim of this paper was to prove the effectiveness of the calibration approach, which does not need to use precise positioning devices and thus is not expensive and time-consuming. These characteristics are the main benefits of the proposed approach. Based on Levenberg–Marquardt (LM) and Thin-Shell (TS) algorithms we evaluated sensor error models (SEMs) for accelerometers of AHRS M3, ADIS16405, CXL02LF3 units and compared them with ones obtained from a Matlab *fminunc* function, which was used as a reference. We provided various analyses to show different aspects of the calibration such as reached values of SEM when LM or TS algorithm was applied, how many taken positions had to be used and how many iterations had to be performed to reach the required precision, or how greatly SEMs changed when they were compared with long-period perspectives. In all cases, the calibration had significant effect on results, e.g., according to Fig. 6 they were approx. 100 times improved. All results proved the suitability of the proposed calibration approach.

REFERENCES

[1] D. Jurman, M. Jankovec, R. Kamnik, and M. Topic, "Calibration and data fusion solution for the miniature attitude and heading reference system," *Sens. Actuators A, Phys.*, vol. 138, no. 2, pp. 411–420, Aug. 2007.

[2] M. Soták, "Coarse alignment algorithm for ADIS16405," *Przegląd elektrotechniczny*, vol. 86, no. 9, pp. 247–251, 2010.

[3] M. Sipos, P. Paces, M. Reinstein, and J. Rohac, "Flight attitude track reconstruction using two AHRS units under laboratory conditions," in *Proc. IEEE Sensors*, Nov. 2009, vol. 1–3, pp. 630–633.

[4] M. Reinstein, J. Rohac, and M. Sipos, "Algorithms for heading determination using inertial sensors," *Przeglad Elektrotechniczny*, vol. 86, no. 9, pp. 243–246, 2010.

[5] N. Barbour and G. Schmidt, "Inertial sensor technology trends," *IEEE Sensors J.*, vol. 1, no. 4, pp. 332–339, Dec. 2001.

[6] J. Včelák, P. Ripka, J. Kubik, A. Platil, and P. Kašpar:, "AMR navigation systems and methods of their calibration," *Sens. Actuators A, Phys.*, vol. 123–124, pp. 122–128, 2005.

[7] Z. Syed, P. Aggarwal, C. Goodall, X. Niu, and N. El-Sheimy, "A new multi-position calibration method for MEMS inertial navigation systems," *Meas., Sci., Technol.*, vol. 18, no. 7, pp. 1897–1907, Jun. 2007.

[8] S. P. Won and F. Golnaraghi, "A triaxial accelerometer calibration method using a mathematical model," *IEEE Trans. Instrum. Meas.*, vol. 59, no. 8, pp. 2144–2153, Aug. 2010.
[9] S. Luczak, W. Oleksiuk, and M. Bodnicki, "Sensing tilt with MEMS accelerometers," *IEEE Sensors J.*, vol. 6, no. 6, pp. 1669–1675, Dec. 2006.
[10] A. Kim and M. F. Golnaraghi, "Initial calibration of an inertial measurement unit using optical position tracking system," in *Proc. PLANS 2004: Position Location and Navigation Symp.*, 2007, pp. 96–101.
[11] D. H. Titterton and J. L. Weston*, Strapdown Inertial Navigation Technology*. London, U.K.: Peter Peregrinis, 1997, p. 238.
[12] V. Petrucha, P. Kaspar, P. Ripka, and J. M. G. Merayo, "Automated system for the calibration of magnetometers," *J. Appl. Phys.*, vol. 105, no. 7, 2009.
[13] I. Skog and P. Händel, "Calibration of a MEMS inertial measurement unit," presented at the XVII IMEKO World Congr., Rio de Janeiro, Brazil, 2006.
[14] T. Pylvanainen, "Automatic and adaptive calibration of 3D field sensors," *Appl. Math. Model.*, vol. 32, no. 4, pp. 575–587, Apr. 2008.
[15] S. Bonnet, C. Bassompierre, C. Godin, S. Lesecq, and A. Barraud, "Calibration methods for inertial and magnetic sensors," *Sens. Actuators A, Phys.*, vol. 156, no. 2, pp. 302–311, Dec. 2009.
[16] M. Reinstein, M. Sipos, and J. Rohac, "Error analyses of attitude and heading reference systems," *Przeglad Elektrotechniczny*, vol. 85, no. 8, pp. 114–118, 2009.
[17] J. Včelák, V. Petrucha, and P. Kašpar, "Electronic compass with miniature fluxgate sensors," *Sensor Lett.*, vol. 5, no. 1, pp. 279–282, 2007.
[18] B. M. Wilamowski and H. Yu, "Improved computation for Levenberg & Marquardt training," *IEEE Trans. Neural Netw.*, vol. 21, no. 6, pp. 930–937, Jun., 2010.
[19] L. S. H. Ngia and J. Sjoberg, "Efficient training of neural nets for nonlinear adaptive filtering using a recursive Levenberg–Marquardt algorithm," *IEEE Trans. Signal Process.*, vol. 48, no. 7, pp. 1915–1927, Jul. 2000.
[20] A. Ranganathan, The Levenberg–Marquardt Algorithm. Atlanta, GA, College of Computing, Georgia Inst. Technol., 2004.
[21] L. M. Saini and M. K. Soni, "Artificial neural network based peak load forecasting using Levenberg–Marquardt and quasi-Newton methods," *Proc. IEEE Proc.*, vol. 149, no. 5, pp. 578–584, 2002, Generation, Transmission and Distribution.
[22] H. Gavin, "The Levenberg–Marquardt method for nonlinear least squares curve-fitting problems," Dept. Civil and Environmental Engineering, Duke Univ. Durham, NC, 2011.
[23] K. Madsen, H. B. Nielsen, and O. Tingleff*, Methods for Non-Linear Least Squares Problems*, 2nd ed. Lyngby, Denmark: Tech. Univ. Denmark, 2004, Informatics and Mathematical Modelling.
[24] M. Soták, M. Sopata, R. Bréda, J. Roháč, and L. Váci, Navigation System Integration, Košice: Robert Breda. Kosice, Slovak Republic, 2006.
[25] E. L. Renk, W. Collins, M. Rizzo, F. Lee, and D. S. Bernstein, "Calibrating a triaxial accelerometer-magnetometer—Using robotic actuation for sensor reorientation during data collection," *IEEE Control Syst. Mag.*, vol. 25, no. 6, pp. 86–95, Jun. 2005.
[26] Find Minimum of Unconstrained Multivariable Function—MATLAB [Online]. Available: http://www.mathworks.com/help/toolbox/optim/ug/fminunc.html [Accessed: 29-Apr-2011].
[27] Attitude and Heading Reference System, Innalabs AHRS M3, Datasheet [Online]. Available: http://www.galaxynav.com/AHRS_M3_datasheet_2008.10.08.pdf [Accessed: 29-Apr-2011].
[28] ADIS16405 | High Precision Tri-Axis Gyroscope, Accelerometer, Magnetometer | Inertial Sensors | Sensors | Analog Devices [Online]. Available: http://www.analog.com/en/sensors/inertial-sensors/adis16405/products/product.html [Accessed: 24-Apr-2011].
[29] Crossbow Accelerometers, High Sensitivity, LF Series [Online]. Available: http://www.datasheetarchive.com/cxl-datasheet.html [Accessed: 29-Apr-2011].
[30] MicroStrain: Inertial Systems—3DM-GX2® [Online]. Available: http://www.microstrain.com/3dm-gx2.aspx [Accessed: 29-Apr-2011].
[31] STEVAL-MKI062V2—STMicroelectronics [Online]. Available: http://www.st.com/internet/evalboard/product/250367.jsp [Accessed: 29-Apr-2011].
[32] J. Vcelak, P. Ripka, A. Platil, J. Kubik, and P. Kaspar, "Errors of AMR compass and methods of their compensation," *Sens. Actuators A, Phys.*, vol. 129, no. 1–2, pp. 53–57, 2006.

Martin Šipoš was born in Prague, Czech Republic, in 1983. He received the Engineering degree (M.Sc. equivalent) with a specialization in aeronautical instrumentation systems from the Department of Measurement, Faculty of Electrical Engineering, Czech Technical University, Prague, in 2008, where he is currently pursuing the Ph.D. degree in the Laboratory of Aeronautical Information Systems with a dissertation titled "Improvement of INS accuracy using alternative sensors."

His main research activity is INS, GPS, Earth's magnetic field navigation, and adaptive filtering.

Pavel Pačes (M'09) was born in Prague, Czech Republic, in 1978. He received the M.Sc. degree in aerospace engineering from the Faculty of Electrical Engineering, Czech Technical University, Prague, in 2005, and the Ph.D. degree from the air traffic control program with two patent applications in 2011.

He gained industrial experience as a programmer and tester of avionics instruments at DevCom, as an HW and SW developer for the Aircraft Research Institute of the Czech Republic, etc.

Dr. Pačes is member of the IEEE Aerospace and Electronic Systems Society and the American Institute of Aeronautics and Astronautics. Currently, he is a National Point of Contact for the Space Generation Advisory Council in support of the United Nations Program on Space Applications.

Jan Roháč received the Ing. degree (M.Sc. equivalent) and the Ph.D. degree from the Faculty of Electrical Engineering (FEE), Czech Technical University (CTU), Prague, Czech Republic, in 2000 and 2005, respectively.

He is an Assistant Professor and Researcher with the Department of Measurement, FEE, CTU. He teaches courses concerning aircraft and space systems. His main research interests are in avionics, space technologies, inertial navigation systems, GNSS, AOCS, sensors and their modeling, and data processing methods.

Dr. Roháč is a member of the Czech Aeronautical Society and one of the representatives of the CTU in the PEGASUS Network.

Petr Nováček was born in 1983 in Prague, Czech Republic. He received an Ing. degree (M.Sc. equivalent) with a specialization in aeronautical instrumentation systems from the Department of Measurement, Faculty of Electrical Engineering (FEE) Czech Technical University (CTU), Prague, in January 2010. He is currently pursuing the Ph.D. degree under Prof. P. Ripka at the FEE, CTU.

His research interests include sensors (magnetometers and accelerometers), electronics of sensors, digital signal processing, and microcontroller design for low-cost precise navigation systems.

A Combined Angle of Attack and Angle of Sideslip Smart Probe with Twin Differential Sensor Modules and Doubled Output Signal

Pavel Pačes, Karel Draxler
Department of Measurement
Faculty of Electrical Engineering, CTU in Prague
Prague, Czech Republic
pacesp@feld.cvut.cz

Vítězslav Hanzal
Aeronautical Research and Test Institute,
Prague, Czech Republic
hanzal@vzlu.cz

Tomáš Čenský
Department of Aerospace Engineering,
Faculty of Mechanical Engineering, CTU in Prague
Prague, Czech Republic
tomas.censky@fs.cvut.cz

Ondřej Vaško
MEACONT Praha,
Prague, Czech Republic
ondrej.vasko@meacont.cz

***Abstract*— This article presents a combined system for an angle of attack (AOA) and an angle of sideslip (AOS) measurements that will be integrated into an existing air data computer system (ADC) due to an early warning against loss of air lift followed by uncontrolled fall of an airplane. We present a set of probes for AOA and AOS measurement whose parameters, advantages and disadvantages are compared. The results were acquired by direct measurement of sensors and through a newly developed smart probe that contains a microcontroller for basic signal processing and a sensor module for the probes connection. Within the project time span, some probe types were simulated in computational fluid dynamic (CFD) software and twelve probes were manufactured and tested. The most promising probe is described in details and compared with other types, its transfer characteristics depending on its orientation with respect to the airstream, velocity of the airstream and temperature. A unique sensor interconnection method resulting in double amplitude measurement that is based on asymmetric connection of differential pressure sensors is presented.**

I. INTRODUCTION *(HEADING 1)*

The safe flight of an airplane depends on lift F_y (1) which have to match to the weight of the airplane m in order to keep a flight level. In this case gravity forces and lift forces equals. The lift force F_y depends on speed of flight v, air density ρ and a lift coefficient c_y. The staling speed v_{stall} of an airplane is then dependent on all these parameters an especially on c_y coefficient (2), that depends on angle of attack (AOA) α, Reynolds number Re and other parameters. The basic way of speed measurement includes a Pitot-static system measuring a pressure difference between its total p_c and static input p_s. The dynamic pressure p_d (3) depends on speed of flight and as well on the angles of attack and angle sideslip β that influences precision of pressure measurement on a Pitot-static system.

$$F_y - m\,g = 0;\ F_y = \tfrac{1}{2}\,c_y\,\rho\,v^2;\ v^2_{stall} = (2\,m\,g)/(\,c_y\,\rho), \quad (1)$$

$$c_y = f(\,\alpha, Re, \ldots), \quad (2)$$

$$p_c - p_s = p_d. \quad (3)$$

Bernoulli's equation gives a basic tool for air speed computation that results in form:

$$v = sqrt\,(2\,p_d / \rho). \quad (4)$$

While the basic relationship between AOA and AOS with other data is described by Gollomp [1], some approaches prefer to compute AOA and AOS from redundant information available onboard [2]. Based on the experiences from real aircraft accidents (e.g. an Airbus A330 crash during its flight

This project was encapsulated and supported by the research program no. MSM 6840770015 "Research of Methods and Systems for Measurement of Physical Quantities and Measured Data Processing" of the Czech Technical University in Prague, sponsored by the Ministry of Education, Youth and Sports of the Czech Republic.

from Brazil on 1 June 2009), resulting in demand for a more precise measurement systems [3], we consider more precise and reliable to design the AOA and AOS measuring system and probes as combined with air data inputs. This article presents several results obtained during the AOA and AOS probes development and testing containing multiple probe layouts, electronics, testing devices and ways of data evaluation. While there are several ways of AOA and AOS measurement, this article aims at systems using two inputs exposed to moving air stream that lead generated pressure to a differential pressure senor.

II. Measurement System

An AOA and AOS measurement system is basically composed from two parts:

- A probe facing the incoming airstream, and;
- Electronics, including sensors.

A. Probe Design

The probe is a mechanical part mounted in free, undisturbed airstream at the wing entering edge of an airplane (Fig. 1, see [4]). Precision of measurement depends on amount of turbulences of air mass in close space around the airplane. The quality of airstream is also influenced by the movement of the airplane and its speed. To lover unwanted influences caused by flight and the difficulties connected to a flight test, wind tunnels are used for initial development, testing and calibration. Tunnels are also very useful to test suitability of different probe designs [5].

The basic 1D types of probes are depicted in Fig. 2 and the extended examples used for both AOA and AOS measurement are depicted in Fig. 3. The simplest variant is composed from two pipes depicted in Fig. 2a and d that allows angle of attack measurement with precision ±0.2° in scale ±30°. D size depicted in the figure can range from 1.5 cm to 3.2 cm for all types of probes used in wind tunnel measurements. Tests presented in this article were made to compare Cobra, Chisel's and a ball (Fig. 3c) probe with diameter of 3.2 cm, whose characteristics were measured for air speed ranging from 0.1 to 2.5 Mach. The completed list of tested probes is showed in Tab. 1 and related probes are depicted in Fig. 4. Literature [5] presents probes depicted in Fig. 2c with opening angle 90° and Fig. 3c as the most precise.

TABLE I. Total Numbers and Parameters of Tested Probes

Probe type (Fig. 4 area)	Total count	Opening angles	Input holes
Cobra probe (A)	1	30°	3 mm
Chisel's probe (A)	6	30, 40, 50, 55, 60, 60°	3 mm
Ball probe (B)	3	44°	1, 2, 4 mm
Ball probe, combined AOA and AOS (A, C)	1	100°	2 mm
	3	44°	1, 2, 4 mm

Figure 1. Placement of an AOA and AOS probe

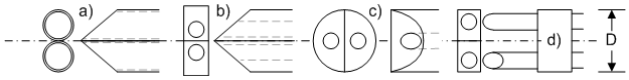

Figure 2. Precise AOA probes used for wind tunnel measurement a) double tube, b) Conrad probe, c) Chisel's probe and d) Reichardt's probe

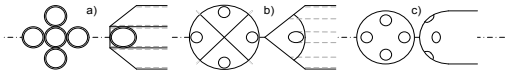

Figure 3. Modified probes for combined AOA and AOS measurement

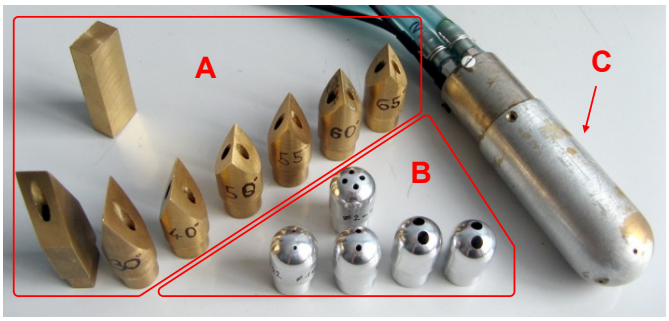

Figure 4. Set of probes prepared for testing

B. Electronics Sensing System

This system can be further divided on a sensor block and a smart probe that distributes measured data to other systems.

The sensor block consists of a unique interconnection (we are not aware about any rights regarding to this connection) of two differential pressure sensors depicted in Fig. 5. This system with pressure inputs P_1 and P_2 consists of first differential pressure sensors whose inputs A and B are connected directly to pressure inputs 1 and 2 and second differential sensor whose inputs are connected to system inputs 1 and 2 in an opposite order. In cases the output of one sensor moves in one direction and the second sensors output moves in opposite direction. This interconnection allows the user to obtain a double resolution output in comparison of a one sensor with advantage of zero offset value (otherwise the sensor usually provides zero reading in the middle of its output scale, see Tab. 2). The module output reading is measured through a differential amplifier as a positive or negative voltage related to orientation of applied input pressure.

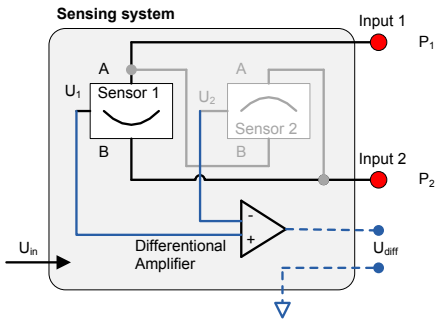

Figure 5. An interconnection diagram allowing double amplitude output by twin sensor arranment

TABLE II. MEASUREMENT MODULE SENSORS

Model	Range	Accuracy	Temp. comp.	Output
Freescale MPXV7002DP	±2 kPa	±2.5% FS	10 ÷ 60 °C	0.5 ÷ 4.5 VDC, center 2.5V
Honeywell DC001NDC41	± 1 inH2O (±250 Pa)	±2% FS	0 ÷ 50 °C	0.25 ÷ 4.25 VDC, center 2.25 V

Two different Measurement Modules (MM) were designed and manufactured with sensors mentioned in Tab. 2. Both sensors have unidirectional outputs with different offsets. When connected in doubled arrangement as was described the offset will not influence the measurement system. Even possible temperature influences, outside of the compensated range (see Tab. 2), will not affect the output because both sensors show the same reaction to the environmental effects. The maximal output value of the both sensor modules is ±4 V that matches doubled range showed in Tab. 2.

The smart probe is based on an embedded system called universal electronic module [6] that contains a micro controller with support electronics and input/output interfaces (RS232, USB, IIC, …). Two Serial Peripheral Interface (SPI) modules are used to communicate with AD converters and a CAN interface is used to send data to a Data Acquisition system (DAQ). All necessary module drivers are included in a basic C i/o library [7] that is available online and is used in a main-loop application performing a gate among sensors, MM's and DAQ system over the CAN bus. The DAQ system is running Mathworks Matlab extended by Matlab2CAN toolbox that was developed by us. The overall system structure containing probe, measurement module, embedded system and its interconnection to Matlab is depicted in Fig. 6.

An automatic positioning system was developed because of difficulties with measurement of a complete two dimensional (2D) characteristic of the probe, MM and influence of MM on measurement precision. This system is depicted in Fig. 7 that shows other measurement devices connected through GPIB bus to the DAQ system and especially Matlab, where Matlab Instruments toolbox was used. The automatic positioning was used mainly for determination of mutual dependence between AOA and AOS that represents exposition of the probe to the air stream in 2D, both in ranges from -30 to 30° with step 3° and for probe axial rotation from 0 to 90° with step 20°.

III. DATA EVALUATION

The presented measurement aims to determine differences between used probes and MM's.

The reference pressure values were measured by a mechanical differential water column system where water level change depends on gravity and relates to amplitude of applied input pressure.

Data evaluation i.e. reverse calculation of probe orientation (angles) can be done based on a set of measurement to determine system characteristics for different air speeds. These characteristics can be then interpolated and used for angles calculation with air speed as one input parameter. The easier way to determine orientation of the probe is to measure pressure difference (3) at Pitot-static system that relates to air speed (4). Then we can use total pressure p_c to normalize AOA or AOS outputs as follows:

$$f(\alpha) = \Delta p / p_c, \tag{5}$$

where $f(\alpha)$ is a dimensionless ratio independent on air speed, related to probe orientation and Δp is a pressure difference measured by MM on probe inputs.

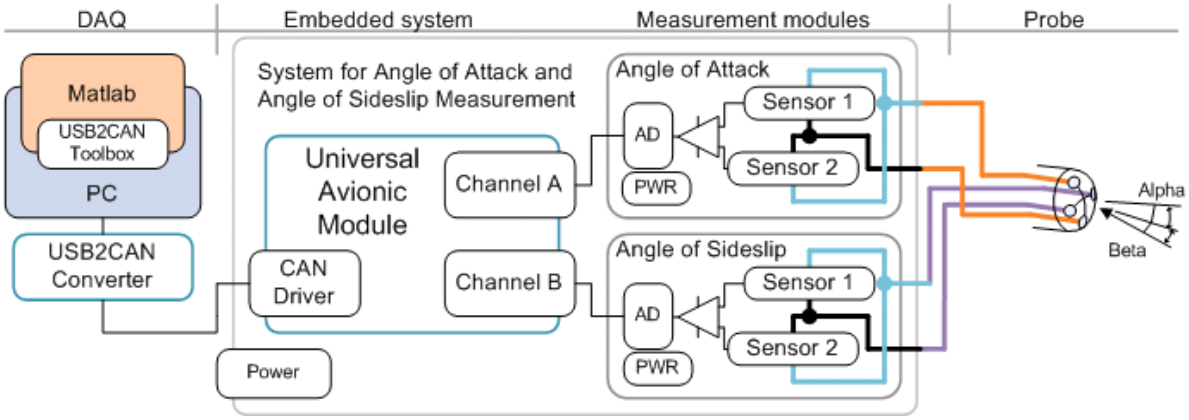

Figure 6. Measurement system and the probe interconnection with data acquisition software

Following tests were performed:

- Probe opening angle influence on output signal;
- Probe design (shape) influence on output signal;
- Entry holes size influence on output signal;
- Suitability of presented modules for AOA and AOS measurement;
- Mutual dependence between AOA and AOS.

A. Probe Opening Angle Influence on Output Signal

Figure 4A shows set of Chisel's probes with different opening angle. Fig. 8 and Fig. 9 shows output characteristics of probes with a different opening angle but measured at the same air speed. The curve related to sharpest opening angle (green one) shows strange, nonlinear behavior at angles ± 7° at both figures. The effect can be seen at Fig. 10 showing results from Computed Fluid Dynamics (CFD) simulation of a probe with 15° opening. Fig. 10a shows situation in the linear area near to the axes origin and Fig. 10b shows AOA 20° at which a wake area starts to appear due to AOA higher then opening angle of the probe. The wake area is characterized by pressure drop resulting in the nonlinearities depicted in Fig. 8 for MPXV module and Fig. 9 for DC001 module. The both figures show very similar pressure quantities but the measured voltages are significantly different which influences accuracy of the measurement.

Due to the presented nonlinearities the 30° probe can be used just in a limited range of angles. What we can see is the bigger opening angle the more linear curve appears. We can compare that the linear area of 30° probe corresponds to the 60° probe curve that imply usage of the higher opening angle probes.

B. Probe Design Influence on Output Signal

Fig. 11 shows characteristics comparing Cobra, Chisel's and ball probes that are evaluated in a similar way as the previously given example. The Cobra probe is even worse than a Chisel's probe with the same opening angle. The best possible characteristic is given by a ball probe with opening angle 44°. In this case the ratio (5) is used for comparison among the probes. The ball probe characteristic is almost ideally linear in the range ±20°and this probe type was selected for next designs.

C. Entry Holes Size Influence on Output Signal

The possible contamination of the probe entry point causes necessity of entry point size influence on output signal assessment. There were three ball probes measured at five different air speeds with following entry point diameters: 1, 2 and 4 mm. The final comparison showed just minor differences of dimensionless characteristic that can be easily corrected by software in the embedded system (Fig. 6). The final probe design can be driven by other parameters because even 4 mm size of the pressure entry point does not significantly influences the output characteristics.

D. Suitability of Presented Modules for AOA and AOS Measurement

Because the ball probe type provides very linear output (see Fig. 11) a set of characteristics with a different air speeds were measured by module DC001, the results are presented in Fig. 12, and module MPXV whose results are given in Fig. 13. First figure shows direct voltage readings with dependence on AOA and multiple characteristics under airspeed ranging from 63 to 150 km/h. The characteristics are approximated by linear curves whose gains and offsets are presented inside the figure. There is the desired, linear characteristic for low airspeeds but from 90 km/h the output is being saturated and that limits the range of measured angles. It is due to the sensor range limitation and the electronic power supply with range ± 5V. This is DC001 module case. If we use the ratio representation (5) the saturation will appear with similar shape in a graph.

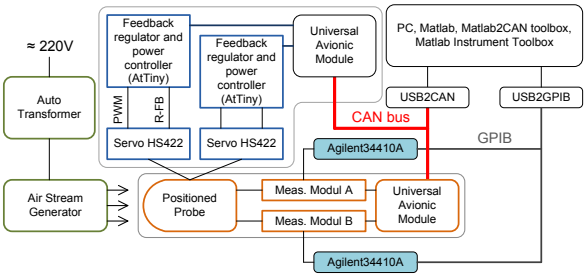

Figure 7. Measurement setup including remote controlled instruments and positioning system for probe orientation control

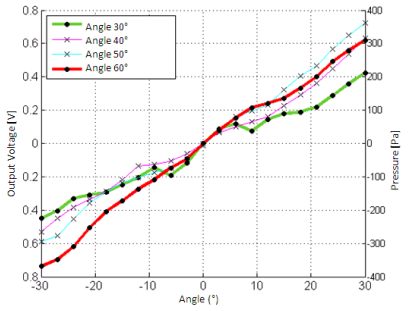

Figure 8. Outputs measured by MPXV module with different probe opening angles (v = 68 km/h)

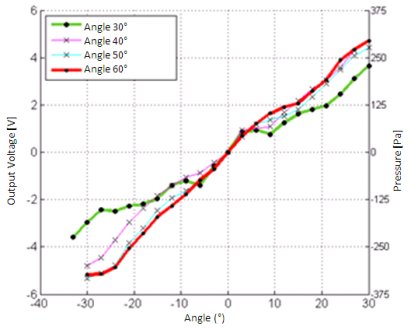

Figure 9. Outputs measured by DC001 module with different probe opening angles (v = 68 km/h)

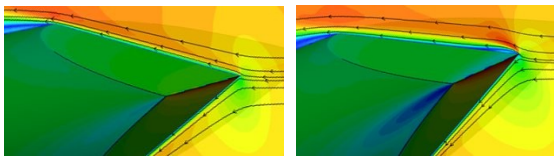

a) b)

Figure 10. CFD simulation of the airflow around the probe (a) with beginning of disturbances at Angle of Attack 20° (b)

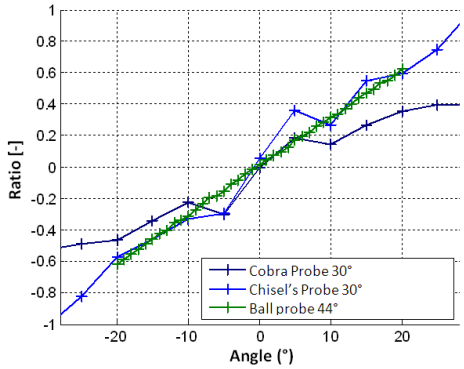

Figure 11. CFD simulation of the airflow around the probe (a) with beginning of disturbances at Angle of Attack 20° (b)

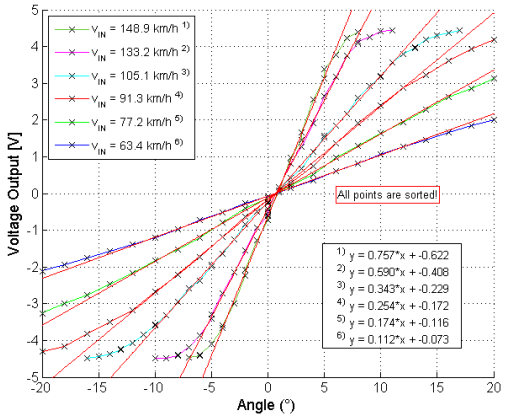

Figure 12. Pressure ratio measured at a ball probe ϕ 1 mm by DC001 module with different speeds

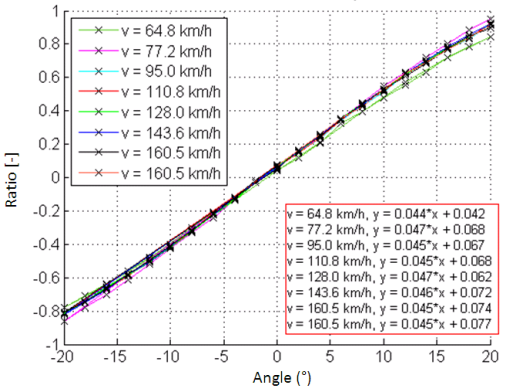

Figure 13. Pressure ratio measured at a ball probe ϕ 1 mm by MPXV module with different speeds

TABLE III. MEASUREMENT MODULE SENSORS

Speed [km/h]	Range of angles with no output signal saturation	
	Module MPXV	*Module DC001*
20	Low sensitivity	± 24°
40		± 24°
60	± 24°	± 24°
80		± 13°
120		± 6°
160		± 4°

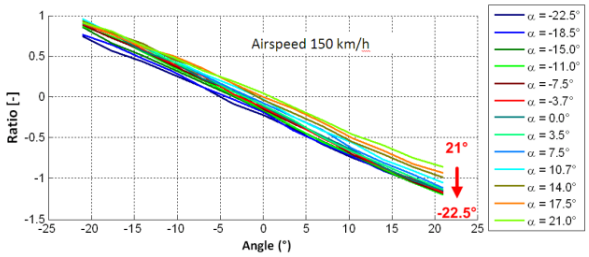

Figure 14. Shift of MPXV AOS output characteristics related to AOA

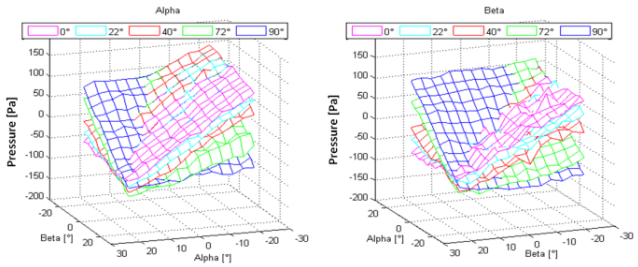

a) b)

Figure 15. Outputs measured by MPXV module with axial rotaion of the probe

Module based on Freescale MPXV sensors gives linear characteristics due to its higher range. The ratios (5) are calculated and drawn in graph depicted in Fig. 13. All the presented characteristics give very similar gains and offsets values that are shown in the Fig. 13 red box. Some variations can be seen in the graph that are caused by measurement errors of characteristics data points and air speed related to p_c.

E. Mutual dependence between AOA and AOS

All the presented graphs were measured in the AOA plane and the AOS angle was set to 0°. To investigate mutual dependence between AOA and AOS a 2D characteristic was measured for air speed 150 km/h. The results are given in Fig. 14 where AOS characteristics are presented. It can be seen that all the lines corresponding to different angles are parallel and shifts linearly from AOA -22.5° to 21°.

In case we turn the probe in axial rotation from 0 to 90° with 20° steps, we can see an effect depicted in Fig. 15 where the characteristic flips along an axe from point [20°, 20°] to point [-20°, -20°]. This is valid for initial AOA probe measurement depicted in Fig. 15a and the mirror line differs in Fig. 15b accordingly. The initial probe orientation was not precisely aligned that can be clearly seen from the both figures.

IV. Lessons Learnt

This block summarizes the most important findings we made during our work:

1) Probe size: Probe size did not cause any problem up to tested diameter D = 4 cm (Fig. 2). Possible fouling of entry points can imply that it is better to choose bigger entry point holes and shorter pipes guiding pressure to diff. sensor. Entry hole size in range from 1 to 3 mm does not significantly influence precision of measurement as is shown here.

2) Opening angle: The advantage of sharp opening angle is in steeper characteristics around its origin that can be used for precise but in range limited measurements. The ball probe gives linear output in range higher then ± 20° that makes it better for aerospace applications.

3) Combination with a Pitot-static system and iterative calculations: Due to simplification of all calculations while equation (5) is used it suggest to supplement AOA and AOS system by a Pitot-static pressure inputs, extend the electronics and combine all these equipment together in one smart probe. The Pitot-static system measurements are also influenced by AOA and AOS and so an iterative algorithm needs to be used.

4) Gravity influence: The gravity influence on MPXV and DC001 precise pressure sensors was measured. In case of double sensor module installation the gravity influences both sensors. When one sensor is mounted at the top of the PCB and the second one is on the other side the gravity influences both sensors in opposite direction. To keep the same orientation of both sensors and even during airplane maneuvers is a better arrangement because their influence will be compensated. The suitable area for the AOA-AOS probe is 1.5 times of fuselage diameter aside and 0.5 times of wing depth in front of its entering edge.

5) Module applicability: The results presented in Tab. 3 shows great sensitivity of DC001 module which is more suitable for slow movements of a small UAV airplanes and the MPXV sensor is more suitable for airspeeds up to 300 km/h where DC001 measures in a really limited range. The ideal solution is to combine both these modules to get higher precision at low speeds for precise stall warning system [8] and to keep AOA and AOS precision through the whole range of airspeeds.

6) Safety and redundancy: The double sensor arrangement brings a new possibility for built-in test functionality [9] especially by inclusion of a modern micro controller with multiple A/D converter inputs that can be used for a differential amplifier measurement (see Fig. 5) and also for single sensor output measurements that can be then mutually compared and evaluated.

V. Conclusion

This paper presents a combined AOA and AOS measurement system (see Fig. 6) that is composed from multiple modules. The most important part of the system is the couple of measurement modules (Fig. 5) that contains two differential sensors measuring the same quantity but with asymmetrically connected pressure inputs. This arrangement results in two times multiplied output value measured between the differential sensors outputs. Sensor dependency on the probe orientation in the airstream is presented here with multiple modifications of sensing probe. These results were acquired with a test bed presented in Fig. 7, where the cross dependency between AOA and AOS were measured (see Fig. 14). The measured results were compared with CFD simulation outputs that are depicted in Fig. 10a and b, that present simulation of airstream distortion at AOA 20°. The last part of the article summarizes experience gained during the probes development, measurement and the overall system realization.

Further work will be aimed on some unexplained phenomena like gravity influence on the measurement module with doubled differential sensor and investigation about fluid dynamic around the probe where turbulences appear.

Acknowledgment

Pavel offers special thanks to prof. Karel Draxler, who is the supervisor for his study, and to Ondrej Vasko and others, the co-authors of this article. We would like to thank to Faculty of Mechanical Engineering for possibility to use their circular wind tunnel and open wind generating device.

References

[1] Gollomp, B., "The angle of attack," Instrum. & Measurement Magazine, IEEE , vol.4, no.1, pp.57-58, Mar 2001

[2] Osterom, M.; Babuska, R.; "Virtual Sensor for the Angle-of-Attack Signal in Small Commercial Aircraft," Fuzzy Systems, 2006 IEEE International Conference on , vol., no., pp.1396-1403.

[3] Freisinet, S.; "Method and Device for Monitoring the Speed of an Aircraft," Pat. 20090299554, USA, 12 03, 2009.

[4] Chabera, T.; "Callibration of a direction probe." Prague: Aircraft Research and Test Institute, Inc., 2000. Z-3715/00.

[5] T, Arts; et al. Measurement techniques in fluid dynamics. Bern : Institut von Karman de Dynamique des Fluides, 2006. www.vki.ac.be.

[6] Pačes, P.; Universal Avionic Module - schematic [online]. 2009, available at: <www.pacespavel.net/Download/index.php?soubor=Paces_schUniversalModule>.

[7] Pačes, P. - Šipoš, M.; Sensors of Air Data Computers - Usability and Environmental Effects ICMT'09 - Proceedings of the International Conference on Military Technologies. Brno: Univerzity of Defence, 2009, p. 401-409. ISBN 978-80-7231-649-6.

[8] Pedro, J.O.; Mansfield, B.A.; "Nonlinear control of aircraft at high angles of attack," AFRICON, 2004. 7th AFRICON Conference in Africa , vol.1, no., pp.431-436 Vol.1, 17-17 Sept. 2004

[9] Jalovecký, R. Pařízek, J. The Technical Diagnostics Application in Aircraft Instruments, In Proceedings of the International Conference on Military Technologies 2009. May 5-6, 2009, Brno Czech Republic. Brno : University of Defence, 2009, p. 379-386. ISBN 978-80-7231-649-6.

JOURNAL OF AIRCRAFT
Vol. 47, No. 3, May–June 2010

Fusion of Smart-Sensor Standards and Sensors with Self-Validating Abilities

Pavel Pačes,* Michal Reinštein,† and Karel Draxler‡
Czech Technical University in Prague, 166 27 Prague, Czech Republic

DOI: 10.2514/1.43735

Airborne applications require a high degree of reliability, which is typically ensured by development guides, testing, quality checking, and overall certification processes. Although these processes provide a high level of product safety and reliability, the electronic devices can fail for various reasons. One of the main present-day problems is incompatibility of the communication interfaces of the smart sensors. This paper proposes a way of using a standardized IEEE 1451 interface with the information necessary for sensor self-validation ability. The necessary data are saved within the memory of the extended Transducer Electronics Data Sheet standard. This paper presents usage of the extended Transducer Electronics Data Sheet data on a servomechanism actuator with a feedback loop (servomechanism), designed for an unmanned aircraft.

I. Introduction

THE safe operation of sensors and actuators is primarily ensured by their redundancy together with a voter device that marks validity of the output signal. Technical development has made highly integrated electronics inexpensive and available for various applications; this is also true for the area of sensing devices. A smart sensor is usually a device consisting of a sensor element, analog data processing, analog-to-digital (AD) conversion, digital processing, and a digital output interface. Today, smart sensors are in use all around us, ready for measuring temperatures and for interconnection with testing devices, monitoring systems, systems of intelligent buildings, etc. All of these systems suffer from various digital output interfaces that differ in physical layers, logical levels, and communication algorithms. The group of IEEE 1451 standards proposes a way to standardize interfaces of smart sensors. First versions of the IEEE 1451 standard defined a new physical interface with its own logical levels and communication protocol. Because of the number of new emerging standards, the IEEE 1451 proposed interface was not widely spread. Despite of all changes, IEEE 1451 still divides the smart sensor at the transducer interface module (TIM) and network-capable application processor (NCAP), where TIM represents a sensing element and NCAP represents a gateway between a group of TIMs into a higher system. The important thing introduced by IEEE 1451 is electronic information about all details related to the sensor that is available in the nonvolatile memory. These data are collected in the Transducer Electronics Data Sheet (TEDS), which contains information about manufacturer, measured value, units, date of calibration, and calibration curve that can be saved in a number of ways (function and lookup table). A data format is predefined for sensors and referenced like a channel with assigned Channel TEDS. Calibration data related to a channel are saved in Calibration TEDS. The standard IEEE 1451.0 , the last issue from 2007, introduces a set of services for the TEDS and information manipulation. The physical layers are not being newly designed at all, but existing networks are used and included into the group of IEEE 1451 standards (e.g., wireless LAN and radio-frequency identification). More description about IEEE 1451 is presented in [2,3]. Controller–Area Network (CAN) is widely used in the automotive industry; its physical layer has no standard number yet in the group of IEEE 1451 standards.

Smart systems are used in aeronautics board instrumentation, but there is no IEEE 1451 standard. The standard is primarily suitable for measurements related to proving aircraft airworthiness [4], which includes a lot of sensors that need to be interconnected quickly.

The method proposed in this paper takes the existing idea of TEDS information and extends it in order to provide capability to self-validate measured values and also to provide information recognized from a measured signal. Common attributes were identified, and algorithms that can be used as an add-on safety feature for future sensing and actuating devices were developed. These common attributes are later used as building blocks for reusable software objects, in conjunction with the standards for smart-sensor interconnection. This paper proposes the use of extended smart devices on an unmanned aircraft (UA) (Fig. 1) as a standardized approach to simplify and improve their usage and maintenance through better data availability.

II. Device Under Development

The proposed methods were tested on a group of servomechanisms (SMs) (Fig. 2) that controls the Mamok UA that is being developed in the Czech Republic as a modernized replacement for the Sojka airplane. Each actuator converts an electric signal to a mechanical movement that controls such components as the engine power lever, the rudder, etc. The electric input signal is represented as a CAN-bus datagram, processed by the central module unit and converted into an angular movement. The distributed digital control simplifies the control, lowers the price, brings down the total weight, and improves reliability of the transferred commands. There are nine of these servomechanism modules on every UA (Fig. 3). SMs provide control of altitude (Fig. 3c), direction of flight (Figs. 3b and 3d), aircraft tilt (Figs. 3a and 3e), wheel braking (Fig. 3g), engine power lever (Fig. 3f), and ground turning (Fig. 3h).

The servomechanism can be divided into two parts: the electronic control system and the mechanical part containing the engine and gearbox (Fig. 4). The figure shows a simple design containing power conditioning, the main microprocessor (Philips LPC2129) with connected peripherals as memory for TEDS data, CAN driver, and engine drivers. The final assembly is shown in Fig. 5. The mechanical part of the servomechanism is based on the Hitec HS-5955TG

Presented at the 27th IEEE/AIAA Digital Avionics System Conference, St. Paul, MN, 26–30 October 2008; received 11 February 2009; revision received 12 September 2009; accepted for publication 20 January 2010.

*Ph.D. Student, Faculty of Electrical Engineering, Department of Measurement, Technicka 2, Praha 6; pacesp@feld.cvut.cz. Student Member AIAA.

†Ph.D. Student, Faculty of Electrical Engineering, Department of Measurement, Technicka 2, Praha 6; reinsm1@feld.cvut.cz. Student Member AIAA.

‡Associate Professor, Faculty of Electrical Engineering, Department of Measurement, Technicka 2, Praha 6; draxler@feld.cvut.cz.

Fig. 1 Mamok UAV.

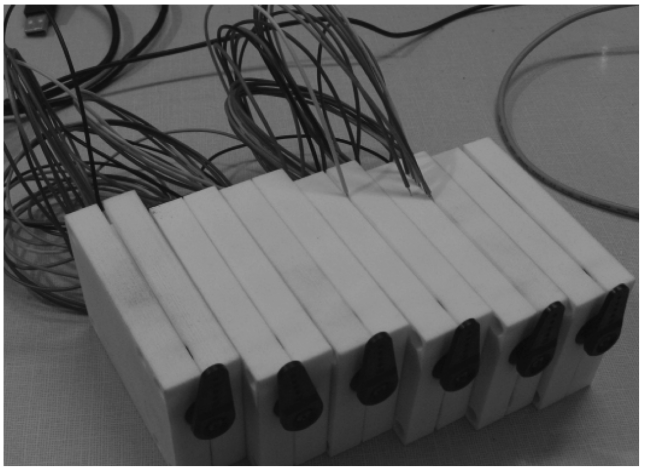

Fig. 2 Group of servomechanisms.

robotic servo, in which the original control system was removed and replaced by a new design that enables further software enhancement that could not be achieved with the original electronic interface. Software performs SM control algorithm and input–output control of the engine, read–write operation from external memory, communication sequences, and watchdog services.

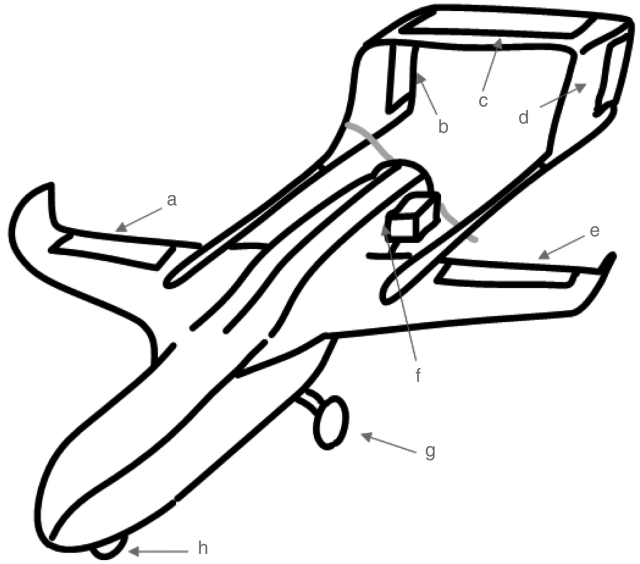

Fig. 3 Placement of servomechanisms.

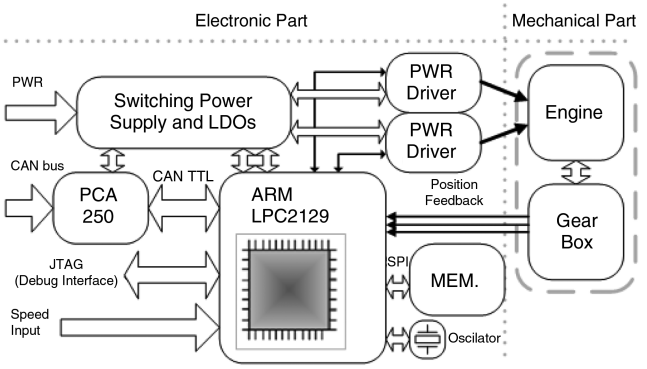

Fig. 4 Servomechanism block diagram.

Fig. 5 Final actuator assembly.

III. TEDS Extension

The main aim is to develop a feasible and easily maintained device in which different presumptions are placed together. These presumptions are coded as TEDS data included in the all devices within a network (Fig. 6). TEDS data ether need to be extended or they are composed from existing IEEE 1451 blocks or other standards are employed. The presented proposal takes advantage of the following items:

1) Existing description of SM feedback data representing the servomechanism position: channel TEDS.

2) The mechanism for calibrating the output value has already been defined: calibration TEDS.

3) A standardized command interface for the actuator exists: CANaerospace.

4) An application programming interface is provided for information access: IEEE 1451.0 [1].

5) An event generation mechanism is provided: IEEE 1451.0 [1].

Today's microprocessors have enough computing power to perform tasks such as sensor sensing, digital processing, and time measurement; they also can add calculations that allow catching important parts of the measured signal. Next, we will discuss two simple methods for direct signal output validation without external support. The following methods can be designated as IEEE 1451 user-defined TEDS structures: 1) range/limit check (Fig. 7a), 2) magnitude jump and rate of change (Fig. 7b), 3) magnitude model check (Fig. 7e), and 4) magnitude prediction (Fig. 7c).

The range signal validation is shown in Fig. 7a, which also shows signal-validation-block validity output. To describe the signal inside its defined range is complicated because of the unknown reference signal and its behavior. The most difficult method is magnitude prediction, which compares the actual measurement with the known point of the value on its transfer characteristic. Not all applications

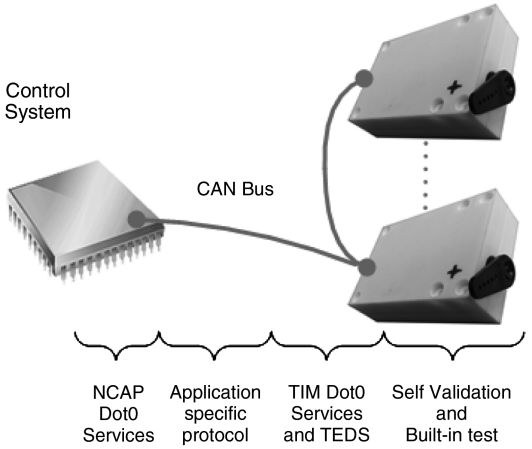

Fig. 6 Servo connection and services.

need to use all of these techniques; hence, unused TEDS proposals can be omitted.

IEEE 1451.0 [1] defines three devices: sensors, actuators, and event sensors. An event sensor is a simple block that generates an event when the analog input crosses a defined threshold. The IEEE 1451 standard consists of a short description of the sequence that leads to generation of an event. This paper describes simple input-signal-validation techniques that are applicable to all signals. We assume that the sensor knows exactly what it measures. It knows that the measured signal can reach only a defined range of values, and the rate of change of the signal is only within a defined range. All of these values were incorporated into the TEDS structures. The sensor also knows its actual position on the sensor's transfer characteristics and can compare its value with other sensors or with the model of an input signal.

The signal path from the sensing element, through signal conditioning and A/D conversion to the microprocessor, gives numerical values that are later processed by software, and into that we add another software block that contains a signal-validation gate, a fault-accommodation block, and fault-event generation. The data flow can be described as an input value that passes into the signal-validation (SV) block (see Fig. 8), which calculates requested data from the signal according to IEEE 1451.0 [1] TEDS (Channel, User-Defined TEDS, etc.) with the help of SV TEDS and system time services. The data processing results describe the validity or invalidity of the input signal.

Figure 9 shows the data flow of the software controller in the servomechanism. An analog value is read and then validated by the signal-validation block. Subsequent system behavior depends on the value that is returned by the SV block. This output value depends on whether or not an anomaly was detected and where we assume a logical output signal. In the case of an invalid return value, some other means of anomaly accommodation has to be performed by the system. For example, fault accommodation of a blocked gearbox results in an immediate stop of the engine driving signal. A blocked

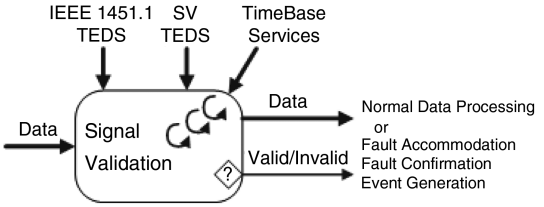

Fig. 8 SV block.

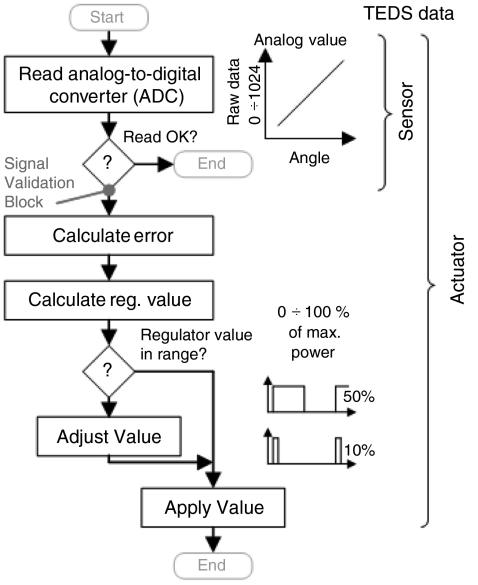

Fig. 9 SV-block placement (ADC is the analog-to-digital converter).

gearbox is detected when the engine is under full power, but the feedback value does not change for the specific amount of time. Generally, fault accommodation includes data measured by a group of the sensors measuring the same quantity, statistically calculated data, or model-based comparison. In the described application we use known attributes of the measured value and a model of the device that was generated from step responses. The model is used in a Kalman filter algorithm for prediction of the next measured value.

A. Range Check

The first and simplest signal-validation technique is a range test that determines whether or not the measured value is in a defined range of values. The range limitation can be caused by a physical quantity characteristic or by processing-path characteristics. Actually, the lower and upper signal limits are a part of the transducer channel TEDS [1]. Nevertheless, for the range-check purposes, the user-defined TEDS structure is depicted in Table 1, in which the group item indicates the TEDS borders. The second row

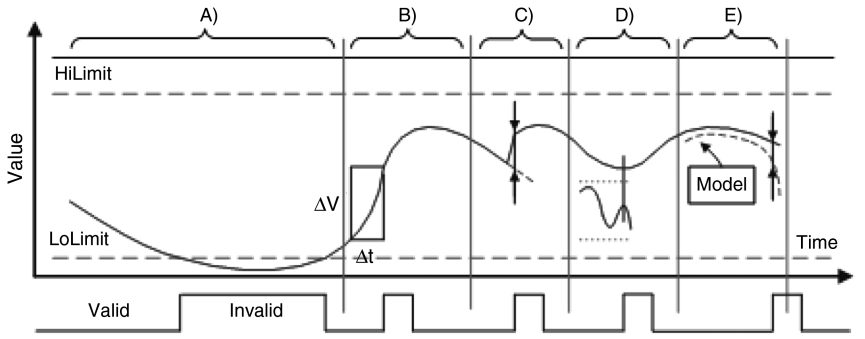

Fig. 7 Validation techniques.

Table 1 Limits TEDS structure

Field name	Description	Data type	No. octets
	Length	UInt32	4
TEDSID	TEDS identification header	UInt8	4
MaxLim	Number of records	UInt8	1
LimGrp	Limit group	——	——
ChID	Channel ID	Uint16	2
HiLim	High limit	Float32	4
LoLim	Low limit	Float32	4
	Checksum	UInt16	2

Table 2 Rate-of-change TEDS structure

Field name	Description	Data type	No. octets
	Length	UInt32	4
TEDSID	TEDS identification header	UInt8	4
MaxRate	Number of records	UInt8	1
RateGrp	Rate group	——	——
ChID	Channel ID	Uint16	2
MaxRate	Max signal rate change	Float32	4
	Checksum	UInt16	2

(TEDSID) defines the purpose of this TEDS, and the following line contains the number of range-check records. The limit group is a combination of limits and a channel ID item that connect the limit group with the transducer channel TEDS.

B. Rate of Change and Detection of Magnitude Jump

The input signal rate of change is described by extended TEDS values necessary for detection of the specified signal change in time. The technique requires hardware and software support for time-measurement services. A simple definition of rate-of-change TEDS is shown in Table 2. This TEDS consists of channel assignment (ChID) and maximal allowed change (MaxRate). The MaxRate field units are assumed to be in input signal units per second, and signal units are part of the transducer channel TEDS. This technique is suitable for magnitudes with slow changes, such as engine temperature measurements or altitude measurements. Current implementation uses moving-average filtering that cuts off peaks in signal. For future usage, where a different method of signal filtering could be used, the rate-of-change TEDS will require further development. The magnitude jump (Fig. 7c) is detected in a similar way, in which differences between specified samples are detected with no filtering algorithm. The simplest TEDS providing data for this purpose is also shown in Table 2.

C. Magnitude Prediction

Several approaches can be chosen to solve the general estimation problem. Given the appropriate vector of observations Z of size $(m \times 1)$, the vector of parameters to be determined X of size $(n \times 1)$ and assuming the model in the form of $Z = HX$, with H of size $(m \times n)$, the system is overdetermined for $m > n$ with enough information (equations) to specify all elements of X was chosen, but further methods have to be applied to guarantee a perfect data fit. One of the most common approaches in this case, which corresponds to our SM case, is to fit the data into the least-squares sense, as described by the equation

$$\hat{\mathbf{X}} = (\mathbf{H}^T\mathbf{H})^{-1}\mathbf{H}^T\mathbf{Z}; |\mathbf{H}^T\mathbf{H}| \neq 0 \quad (1)$$

There are, however, several drawbacks, as described by Grewal and Andrews [5], when using a simple least-squares estimation:

1) Results are predicated upon an assumed model, and miss-modeling can cause a serious flaw.

2) All data residuals, i.e., differences between predicted and measured values, are weighted equally; hence, there is no way to consider anomalous data.

3) There is no way to incorporate information regarding a priori knowledge of used parameters.

4) Batch processing is implied; all data need to be collected at first.

5) The criterion of the least-squares is data-fitting, not minimizing the estimation error.

To deal with all of the above concerns, a Kalman filter (KF) is the logical step to take. It brings into consideration points 2 to 5, so only the modeling still remains a problem. When compared with classical least-squares, the Kalman filter yields approximately the same results if the initial uncertainty in X is large, the system is overdetermined or exactly determined, and all observations are of equal quality, and this almost never happens.

D. Kalman Filtering

According to Grewal and Andrews [5], Kalman filtering is primarily a procedure for combining noisy sensor outputs to estimate the state of a general system with uncertain dynamics: dynamics that need to be precisely modeled. The system state vector includes any variables of the system, as well as inner variables for modeling time-correlated noise sources and random sensor parameters. The actual model determines the complexity and computational load of the KF. To determine the final uncertainty of the estimated system states provided by the KF, a covariance analysis was performed. Covariance analysis is a part of the KF algorithm and can be performed even without real data, based only on the sensor noise parameters given by the manufacturer. In the end, it shows how much the estimated system states vary from the optimal values in the means of variance, assuming the Gaussian distribution.

E. Servomechanism Model Creation

To create a suboptimal mathematical model of the servomechanism that would be mathematically stable and create a manageable computational load, a proper approximation method was sought. As Nassar [6] described, there are several simple random processes that can be used to approximate noises entering the KF, such as random constant, random walk or exponentially correlated random process (the Gauss–Markov process of first order). These processes exhibit a

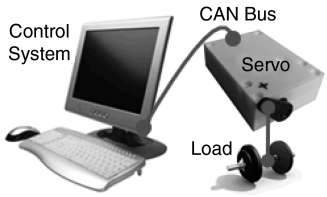

Fig. 10 Test setup.

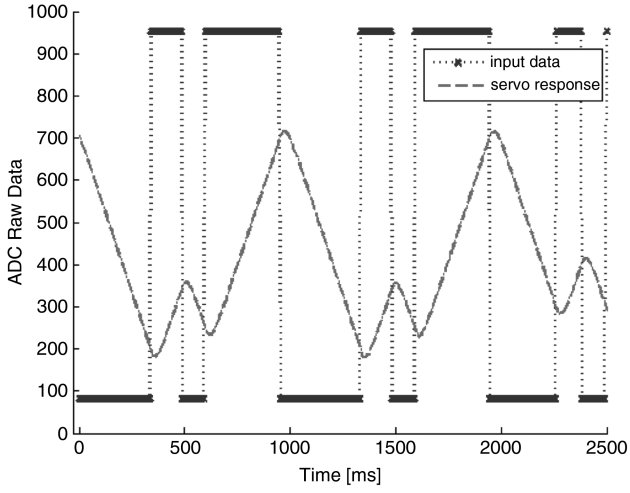

Fig. 11 Servo's pseudorandom input and its response.

Table 3 Model TEDS structure

Field name	Description	Data type	No. octets
	Length	UInt32	4
TEDSID	TEDS identification header	UInt8	4
ChID	Channel ID	Uint16	2
NumGrp	Numerator group	——	——
NumNu	Number of numerators	UInt8	1
NumItem	Numerator item no.	Float32	4
DenGrp	Denominator group	——	——
DenNu	Number of denominators	UInt8	1
DenItem	Denominator item no.	Float32	4
	Checksum	UInt16	2

simple power spectral density trend, which can be suitable for sensor bias or drift approximations; however, to approximate the servomechanism behavior, it is not suitable. One of the possible solutions can be found when using higher-order Gauss–Markov (GM) processes. Any GM process of any order can be represented using an autoregressive (AR) process of appropriate order [6]. The AR process of order p can be described using a pole-zero transfer function $H(z)$, where $X(z)$ is the z transform of the input $x(k)$, $Y(z)$ is the z transform of the output $y(k)$, and $\alpha_1, \alpha_2, \ldots, \alpha_p$ and β_0 are the AR process parameters in discrete time:

$$H(z) = \frac{Y(z)}{X(z)} = \frac{\beta_0}{1 + \sum_{n=1}^{p} \alpha_n z^{-n}} \tag{2}$$

$$y(k) = -\sum_{n=1}^{p} \alpha_n y(k-n) + \beta_0 x(k) \tag{3}$$

In the end, Burg's method was used for the creation of the servomechanism's AR model, which is described in [6]. Various data sets corresponding to servomechanism response to different loads were collected and used as input to the estimator implemented in MATLAB.

IV. Results

Data acquired during servomechanism development were measured using the measurement setup shown in Fig. 10. A personal computer with a Universal Serial Bus to CAN-bus converter was used for connection with the servomechanism, which is equipped with a CAN-bus interface. The SM is loaded with specific weight, which is moved by the servomechanism lever according to an input signal into regulator service. The servomechanism responses are sampled with a rate of about 170 Hz and transferred to the PC by the CAN bus with a speed of 1 MB (maximum for CAN bus). This method was chosen because the information collected in this way will be the only source available to the device in the final installation.

Figure 11 shows the pseudorandom signal for transfer characteristics determination (dotted line) with the servomechanism response (dashed line). Measured data were processed and modified in order to analyze the important details of the signal. The signal prediction is dependent on the system model, for which we use the data TEDS structure shown in Table 3. The model is assumed to be in polynomial form and calculated by SM's microcontroller. The numerator and denominator degrees are expressed by their count, followed by an array of coefficients. The KF algorithm was enhanced to detect the data outage. If data outage is detected, the calculation of residuals and state vector update step is omitted. Then a driving input to the system model is triggered using the precomputed Kalman gain in which KF works as a predictor. As the outage ends, the KF is switched back into filtering regime, calculating the residuals and updating the Kalman gain values. Variables necessary for algorithm calculation are not part of the tabled data.

The data acquired from the servomechanism are shown in Fig. 12. This figure shows response to the input signal that follows Fig. 11. To show important functions of the magnitude estimation, the input data were modified to simulate failure of the feedback input. In the case of the servomechanism, the failure of input signal leads to saturation of the analog-to-digital converter that will measure maximal input value. An example of the saturation is shown in Fig. 12b.

One of the important signal components is the beginning of the signal response, where the algorithm waits for its history (Fig. 12a). Figure 12c shows problem with a concave change of signal direction. It can be seen that the model-based estimation continues with the

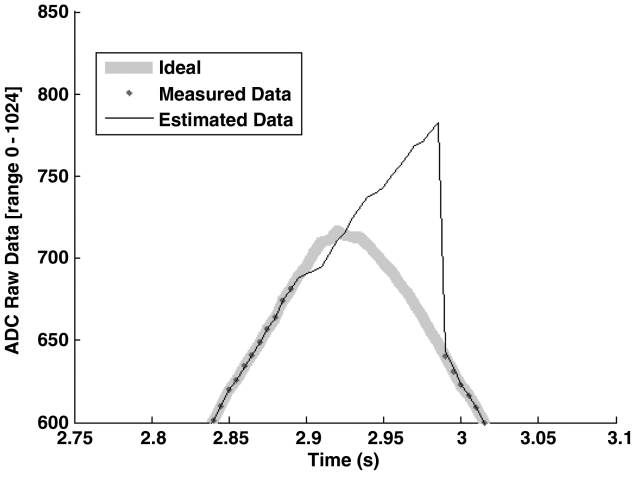

Fig. 13 Concave change: case C.

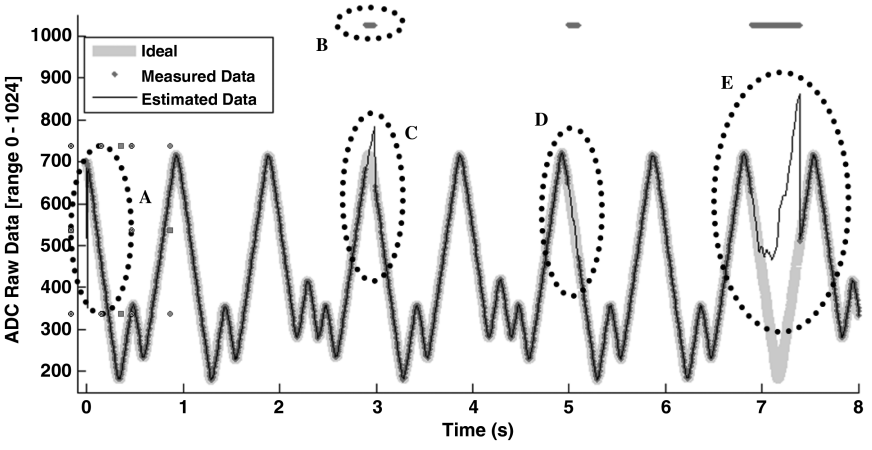

Fig. 12 Servomechanism response for random input sequence with data outage.

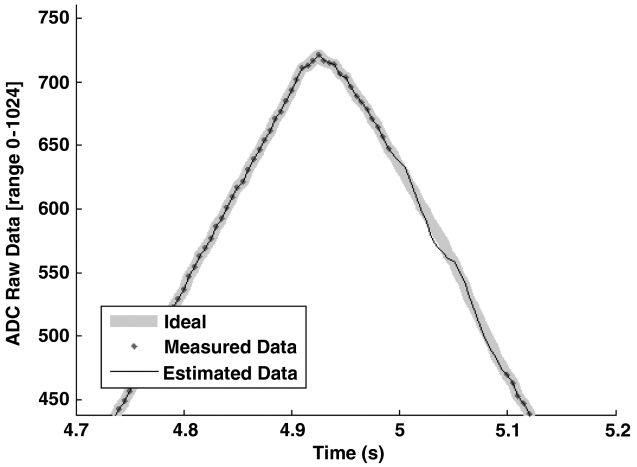

Fig. 14 Prediction: case D.

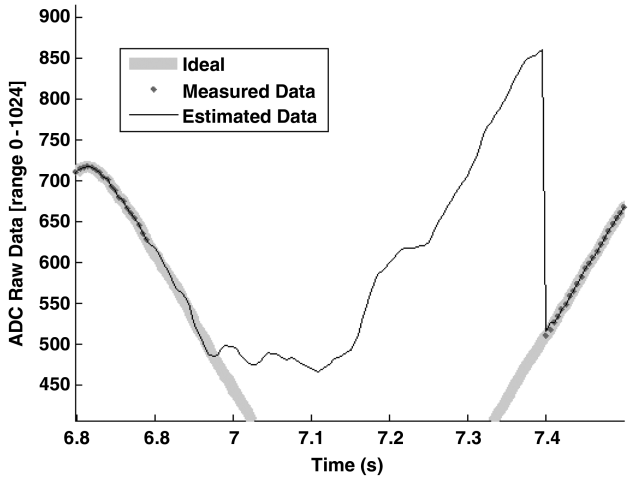

Fig. 15 Long-term nonstability: case E.

previous direction, which is incorrect, because the proper signal changed its direction. The prediction of the modeled signal can be improved by including the input command into the KF as an input data line (Fig. 11) and in detail (Fig. 12), but this is only applicable for feedback systems. The steep growth that returns estimated values back to the best line (Fig. 13) is caused by the return of proper feedback values.

The example in Fig. 12d (or details in Fig. 14) shows a situation in which the feedback signal is lost for a long time (0.12 s), which can be successfully covered by the data estimation. On the other hand, the longer data outage leads to unpredictable behavior, which is shown in Fig. 15.

V. Conclusions

A smart sensor, or a device called *intelligent* (see the definition of intelligence in [7]), should contain the following built-in features in a standardized form: 1) plug-and-play ability, 2) TEDS information availability in any form, 3) self-validation techniques, 4) fault-tolerance ability, and 5) sensor consciousness about measured value, as proposed in this paper.

The basic idea presented in this paper is to offer an existing solution (the TEDS data) and to extend it in order to be suitable for a new and reusable application. Already developed reusable algorithms are used in another application that allows suppressing bugs and picking up important parts of the measured signal. This paper proposes a new principle of using TEDS information [1] for signal validation that is used in a data processing algorithm of smart-sensor output. New TEDS structures are proposed as data storage for signal evaluation methods described in this paper. Described methods include signal limits (min, max) checking, signal rate-of-change calculation, and comparison of measured output with an estimated value. The third algorithm estimates a future output value with reference to previously measured data and compares this value with a value measured at the sensor input. In case of unacceptable differences, a time stamp is saved and a superior system is noted. A Kalman-filter-based algorithm is proposed and verified for servomechanism feedback output data filtering and estimation of a future value. The precision of prediction proves to be suitable for short-time-measurement outages. The algorithm's application is presented on an SM system for a new UAV project. The servomechanism combines a sensor and an actuator together with common and extended TEDS structures. Placement of the proposed algorithms is designed in the servomechanism control-loop feedback. The CAN-bus connection for data exchange with a master system is used in this paper.

Acknowledgments

This project was supported by the research program no. MSM6840770015, "Research of Methods and Systems for Measurement of Physical Quantities and Measured Data Processing," of the Czech Technical University in Prague, sponsored by the Ministry of Education, Youth and Sports of the Czech Republic. Pavel Pačes offers special thanks to Karel Draxler, who is the supervisor for this study, and to Michal Reinštein, the coauthor of this paper.

References

[1] "IEEE Standard for a Smart Transducer Interface for Sensors and Actuators—Common Functions, Communication Protocols, and Transducer Electronic Data Sheet (TEDS) Formats," Inst. of Electrical and Electronics Engineers, Piscataway, NJ, Sept. 2007.

[2] *How Can IEEE 1451 Be Applied?*, National Inst. of Standards and Technology, Gaithersburg, MD, http://ieee1451.nist.gov/, [retrieved 21 July 2008].

[3] Ramos, H. M., Ramos, P., and Pačes, P., "Development of a IEEE 1451 Standard Compliant Smart Transducer Network with Time Synchronization Protocol," *IMTC/2007 IEEE Instrumentation and Measurement Technology Conference Proceedings* [CD-ROM], Inst. of Electrical and Electronics Engineers, Piscataway, NJ, 2007.

[4] Eccles, Lee H., "The Need for Smart Transducers: An Aerospace Test and Evaluation Perspective," *IEEE Instrumentation & Measurement Magazine*, Vol. 11, No. 2, April 2008, pp. 23–28.

[5] Grewal, M. S., and Andrews, A. P., *Kalman Filtering—Theory and Practice Using MATLAB*, Wiley-Interscience, New York, 2001.

[6] Nassar, S., *Improving the Inertial Navigation System (INS) Error Model for INS and INS/DGPS Applications*, Univ. of Calgary, Dept. of Geomatics Engineering, Rept. 20183, Calgary, Canada, 2003.

[7] Gottfredson, L. S., "Foreword to 'Intelligence and Social Policy'," *Intelligence*, Vol. 24, No. 1, 1997, pp. 1–12. doi:10.1016/S0160-2896(97)90010-6

SMART SENSOR DATA PROCESSING FOR AEROSPACE APPLICATIONS IN EDUCATION ILLUSTRATED BY SMALL SATELLITE PLATFORM DEMONSTRATOR

Pavel Pačes, Jan Popelka, Emidio Marchitto, Tomas Levora,
Czech Technical University, Prague, Czech Republic

Abstract

This article describes a tasks for undergraduate students from the area of signal processing that is often used in aerospace for data fusion of different kinds of sensors onboard of an airplane or a spacecraft. It includes a Kalman filter merging angular rates, accelerations and vector of the magnetic field. These topics are illustrated on a remotely controlled educational platform and its internal Inertial Measurement Unit. The article describes a set of sequential topics that introduces students with Attitude Heading and Reference System data processing on a remotely controlled platform that contains all necessary sensors. The hands-on experiments with the remotely controlled platform presented in this article takes advantages of the existing technology and shifts the currently used educational approach to the more interactive level. We mainly describe an algorithm to calculate position angles from raw sensor data which is used within Attitude Heading and Reference Systems and we propose a new arrangement of the AHRS unit which uses self-calibrating magnetometer and the Pressure Reference System for pitch and roll angles measurements to remove influence of accelerations generated during the flight.

Introduction

Aviation industry developed from a manned flight, over remotely controlled airplanes, space probes and manned space flight, to the present stage by the effort of enormous amount of people who gained their knowledge through an educational system that was developed as a secondary product of the aviation advances. The complexity of the educational system rises with the complexity of the crafts nowadays used. Students are often educated in different subject areas and it is not rare the universities want to combine student's theoretical knowledge with hands-on projects such as building an unmanned airplane with a control station. In these projects, the team is supposed to design the airplane fuselage, to propose a power system, an avionic system, and a remote control station with intent to use low-cost components. The team struggles with money and time constraints, permission to fly, insurance for the craft, transportation and also with quality and the amount of data they are able to measure and transfer to the control station for evaluation [1]. To get a reliable data source (a reference unit) including attitude and navigation data of the craft is often too difficult [2]. The current educational approach is to introduce partial problems on an existing subsystem, e.g. AHRS unit, which is provided to the school as a free spare part by a local airliner. These gift units provide limited functionality and interaction with the device (because of missing schematics and internal microprocessor source code).

This article presents data processing algorithms used in an Attitude Heading and Reference Systems (AHRS) on a spacecraft model called Small Satellite Platform (SSP) which is used for university, different summer schools, and other classes. We also present a modified data processing algorithm which corrects for magnetic field changes and for accelerations that are generated within the flight time, e.g. in turns, by engine vibrations, etc.

Small Satellite Platform

The SSP platform serves as a laboratory tool which can illustrate principles of spacecraft stabilization. It is composed from components that are usually used on a spacecraft and it allows closing a control loop that stabilizes the platform heading. The platform is usually hanged to a holder with thin,

low friction, tether in a kind of zero gravity experiment. It provides various sensors for its position determination (Star Tracker, Magnetometer, and Angular Rate Sensors), an On-Board Computer (OBC), and actuators. A complete description of the platform is available in [3]. Figure 1 shows the main components of the platform and Figure 2 shows the interconnection of the electronics subsystems. The On-Board Computer of the platform can be directly programmed with a required controller setting or the platform can just provide data through its wireless interface into Matlab where it is processed and the actuator command is returned to the platform. This approach was used to measure the data presented in this article.

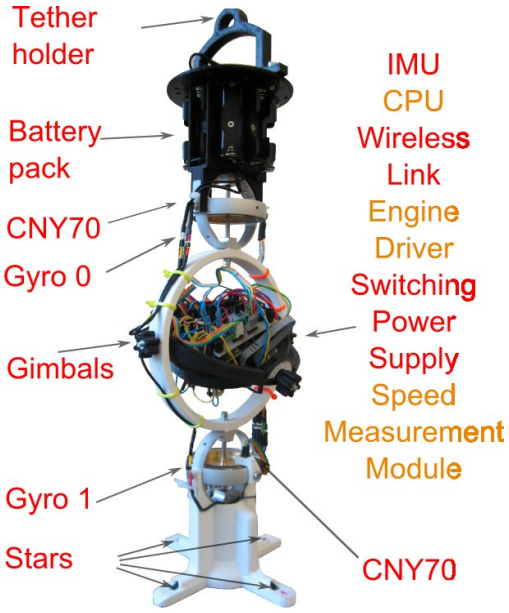

Figure 1. Main Components of the Small Satellite Platform

Navigation Systems

Inertial navigation systems (INS) periodically update information about airplane position (it includes orientation and geographical position) according to the information measured by inertial sensors [4]. The periodic update of a small measurement cumulates all the errors which require precise sensors to be used [5]. The market offers Micro-Electro-Mechanical Systems (MEMS) sensors and sensors working based on different principles, e.g. Ring Laser Gyroscope (RLG) [4]. To evaluate their performance we can use different methods but the most used is called Allan Variance. Article [6] illustrates performance of RLG gyroscope and a MEMS Angular Rate Sensor (ARS) by comparison of their Allan Variance plots. It shows the performance of the RLG gyroscope is five orders better than its MEMS counterpart. Though, the MEMS sensors are used mainly for airplanes orientation determination within Attitude Heading and Reference Systems [6] and not for INS implementation.

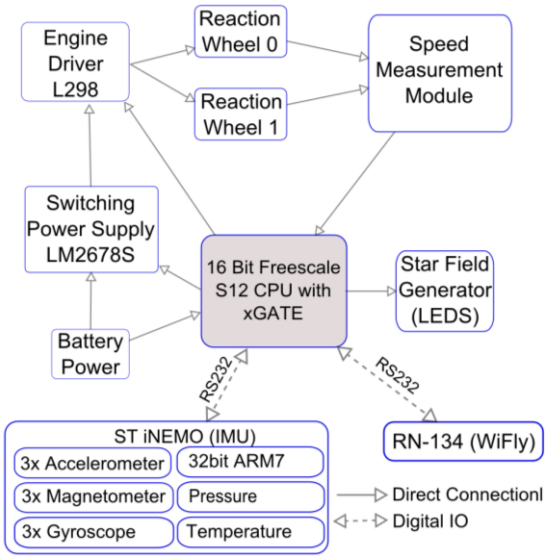

Figure 2. SSP Electronic Subsystem Block Diagram

Inertial Navigation Systems

The INS data processing follows the data flow diagram depicted in Figure 3. Angular rates are one time integrated to determine actual orientation of the airplane, e.g. they serve for pitch and roll angles determination. While integration is used there is a problem with initial alignment of the airplane. Initial position can be entered by the crew, determined by accelerometers or by gyro-compassing [5]. Pitch and roll angles are used to transform readings of the accelerometers from body frame of the measurement unit into the navigation frame where the position and velocity calculations take place. The basic data flow is depicted in Figure 3 with more detailed description matching description in this paragraph in Figure 4. There are other complications that depend on: gravitational field model used within the gravity correction block, what reference frame is used for

navigation solution computation (ECEF, LLH, etc.), Earth rotation, etc. [7][8].

The initial alignment, e.g. position angles determination, can be performed according to the modified data flow diagram which is depicted in Figure 5. In this case the platform is stationary and except of gravity no other forces act on the measurement unit. Though the signals measured by accelerometers allows us to determine position angles which can be also used for ARS or a vector magnetometer data transformations – compare Figure 5 and Figure 3. These transformations are used for SSP gimbal angles corrections [3] to control the platform in heading. The pure inertial system [1] heading alignment is performed through its very precise angular rate sensors that are able to measure Earth's rotation.

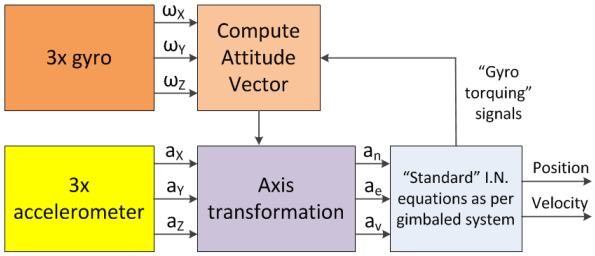

Figure 3. Data Transformation Used within Inertial Measurement Systems [4]

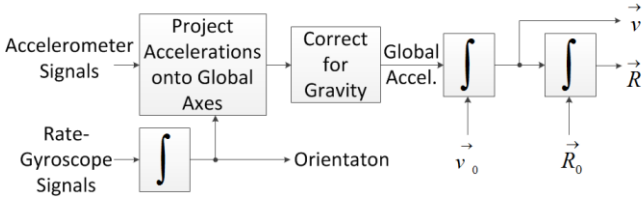

Figure 4. Flat Earth Navigator (based on [7], [8])

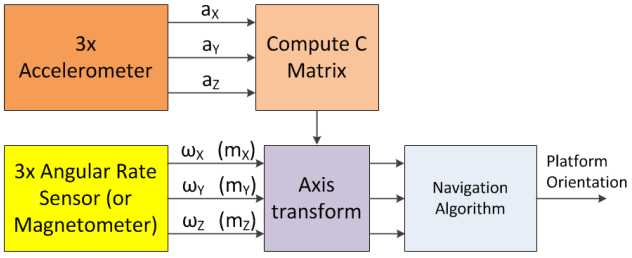

[1]This system uses just angular rate sensors and accelerometers.

Figure 5. Data Transformation Procedure Used within SSP for Gimballed Platform [3]

A measurement unit with precise RLG sensors costs around USD 75 000 while the low-cost MEMS sensors costs around USD 20. The [9] claims the long term precision of an ARS relates to the size of the sensor and so it will not be possible to design working pure INS based on MEMS sensors. On the other hand it summarizes: the precision of the orientation measurements (attitude) based on MEMS sensors is much better (within one degree error after 30 seconds) then position determination (50 meters error after 30 seconds) [9] and the required precision of the measurement system can be acquired by merging different sources of information as e.g. IMU, GPS, Air Speed, Altitude, etc.

Attitude Heading and Reference Systems

The AHRS block diagram, as it is depicted in [6], is similar to INS but it uses more sources of information. The information data flow within AHRS is depicted in Figure 6. With respect to an INS, the AHRS does not double integrate signal provided by accelerometers. It still integrates data provided by ARSs and uses an estimator to predict platform orientation. This estimation is used to get corrections for sensor errors. The accelerometer data are used to correct the integrated data from ARSs for pitch and roll angles and a vector magnetometer is used to correct for integration errors in yaw angle. The correction signals can be simple as a reset of the integration algorithm as presented in [11] for pitch and roll corrections or a continuous data processing as illustrated in [12] for the yaw angle correction. Both methods ([11] and [12]) provide exceptionally good results. Pitch and roll corrections are tricky because during a flight an airplane is exposed to variety of forces that influences accelerometers and cross axes sensitivity of ARS. To cope with this a new source of information about pitch and roll angles has to be found or an algorithm which is able to eliminate these problems will be used. Within this article we will provide both solutions: a new source of pitch and roll angles data and we describe the data processing algorithm depicted in brief in Figure 6 which uses Kalman filter for system orientation estimation and Euler angles computation.

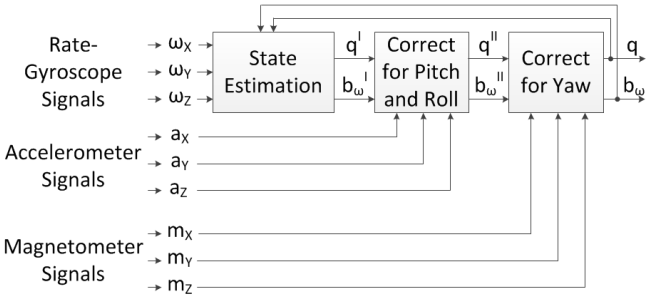

Figure 6. Data Flow within an AHRS System [10]

Data Representation

The mathematical process of raw sensor data transformation into velocity and position information into a useful coordinate frame is called mechanization. To represent orientation of a spacecraft or an airplane Euler angles (pitch, roll and yaw) are used. A transformation between a body and navigation frame is performed with help of Direction Cosine Matrix (DCM) as defined in [3]. This representation is easy to understand and used for artificial horizons or even for GRACE[2] inter-satellite pointing control [13]. But because Euler angles suffers by singularity problems called "gimbal lock", e.g. we lose one degree of freedom, another representation is often used: quaternions. They are extension of complex numbers used for calculations in three dimensional space and their use removes "gimbal lock" problem. They can be easily converted into Euler angles and opposite.

Data Processing

All the sensors need to be calibrated as it is described in [6]. Especially magnetometers change their characteristics with regard to amount of iron materials in the surroundings. While the calibration process can improve the measurement precision by order of magnitude [13], the MEMS sensors needs continuous estimation of their error models because it changes in time. The low-cost MEMS based AHRS units suffer with drift problems described in the following chapter even in case they have the described mechanisms to cope with sensor characteristics implemented. The solution for this issue is proposed at the end of the article.

[2] Gravity Recovery and Climate Experiment

Algorithm

A Kalman filter describes method how to estimate state of a discrete time controlled system which is described by linear differential equation (1).

$$x_k = Ax_{k-1} + Bu_k + w_{k-1} \tag{1}$$

Where k represent sample time, x_k is the state vector of the system, u_k is the input vector to the system, w_{k-1} is process white or Gaussian noise with normal distribution, zero mean value and covariance matrix Q. Measurement of the controlled system state can be described by equation (2).

$$z_k = Cx_k + v_k \tag{2}$$

Where z_k is the measured state of the system and v_k is the measurement normally distributed white noise with zero mean value and covariance matrix R. A, B, and C matrixes represents state, input and output matrix. All of them represent some transitions: between the consecutive states, between input and state, and between the measurement and state vectors respectively. Both white noises, represented by w and v, are anticipated to be independent on each other with time-invariant parameters.

For every k the algorithm updates the system state estimation x_k and error covariance matrix P_k. The errors between actual and estimated a priori (includes states from beginning to time $k-1$) and a posteriori (includes a priori states and state in time k) system states can be defined as (3) and (4).

$$e_k^- = x_k - \hat{x}_k^- \tag{3}$$

$$e_k = x_k - \hat{x}_k \tag{4}$$

Where e_k^- is a priori estimated state error and e_k is a posteriori state error estimation. From a priori and a posteriori state estimation errors the error covariance matrixes can be defined as (5) and (6).

$$P_k^- = E\left[e_k^- e_k^{-T}\right] \tag{5}$$

$$P_k = E\left[e_k e_k^{\,T}\right] \tag{6}$$

Where $E[\ ]$ is the correlation of error estimations and P_k represents uncertainty of the current state estimation.

The principle of discrete Kalman filter algorithm is based on two steps iteration – a time and a data step (see Figure 7). In the time step, a priori state of the system is estimated from the previous system state. In this step, the a priory error covariance matrix is estimated from its previous state together with state covariance matrix Q. In the data step, the actual state of the system is measured and the estimations of the system state and error covariance are corrected. The correction of the system state is performed through the difference between measured system state z_k and estimated state. This difference is weighted with Kalman gain K. The estimated a priori error covariance matrix is also corrected with Kalman gain. The Kalman gain is computed by minimizing the a posteriori error covariance. The K can be computed as (7).

$$K_k = P_k^- C^T \left(CP_k^- C^T + R\right)^{-1} \tag{7}$$

As depicted in Figure 7 the initial system state estimations $\hat{x}_0$ and initial error covariance matrix P_0, or P_{k-1}, has to be provided. The algorithm description is a derivate from [14-16].

Measurements

To evaluate the described algorithm the STmicroelectronics iNemo IMU mounted in the SSP platform was used and the Kalman filter was implemented according to the block diagram depicted in Figure 8 [17]. The sensor offsets were calibrated according to the parameters depicted in Table 1.

The test procedure performed with the AHRS unit was as follows: the unit was placed on a horizontally leveled support with Z axis oriented in the direction of the gravitational field. The initial alignment of the unit was not precise as it is depicted in Figure 10 – legend to this figure is part of the first graph in Figure 9. We can see the Z axis gyroscope gives zero reading but he horizontal acceleration sensors gives 25 mg in X direction and 10 mg in Y direction which causes the Kalman filter algorithm to compensate and calculate non existing pitch (-7°) and roll (10°) angles. During the time up to 5 seconds we can see how the filter gains his history and performs corrections. Figure 9 B shows behavior of quaternions and Figure 9 C provides outputs generated by the vector magnetometer which is almost ideally compensated for hard and soft iron distortions [6]. The test circle with the unit starts after approx. 10 seconds which is illustrated by red arrows.

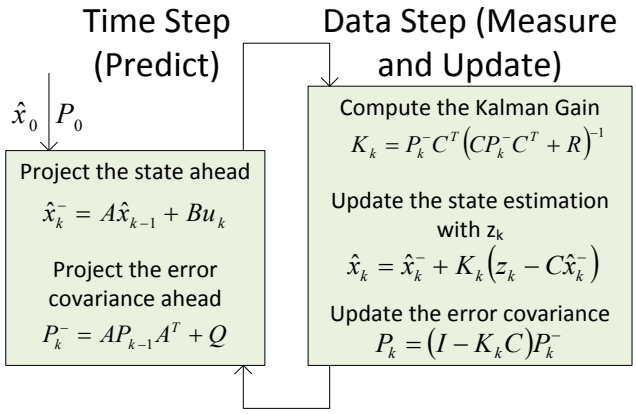

Figure 7. Kalman filter algorithm flow [14]

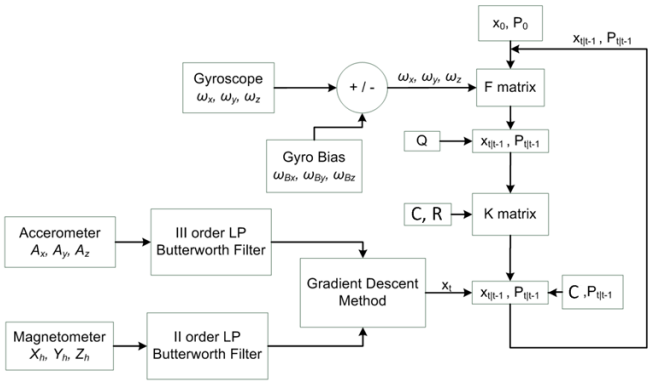

Figure 8. Block Daigram of the Quaternion Kalman filter [17]

Table 1. iNemo Calibration Parameters

	Sensor		
Axe	**ARS [°/s]**	**Acc. [mg]**	**Mag. [mGauss]**
X	-2	-6	-100
Y	0	-14	-200
Z	-6	-28	520

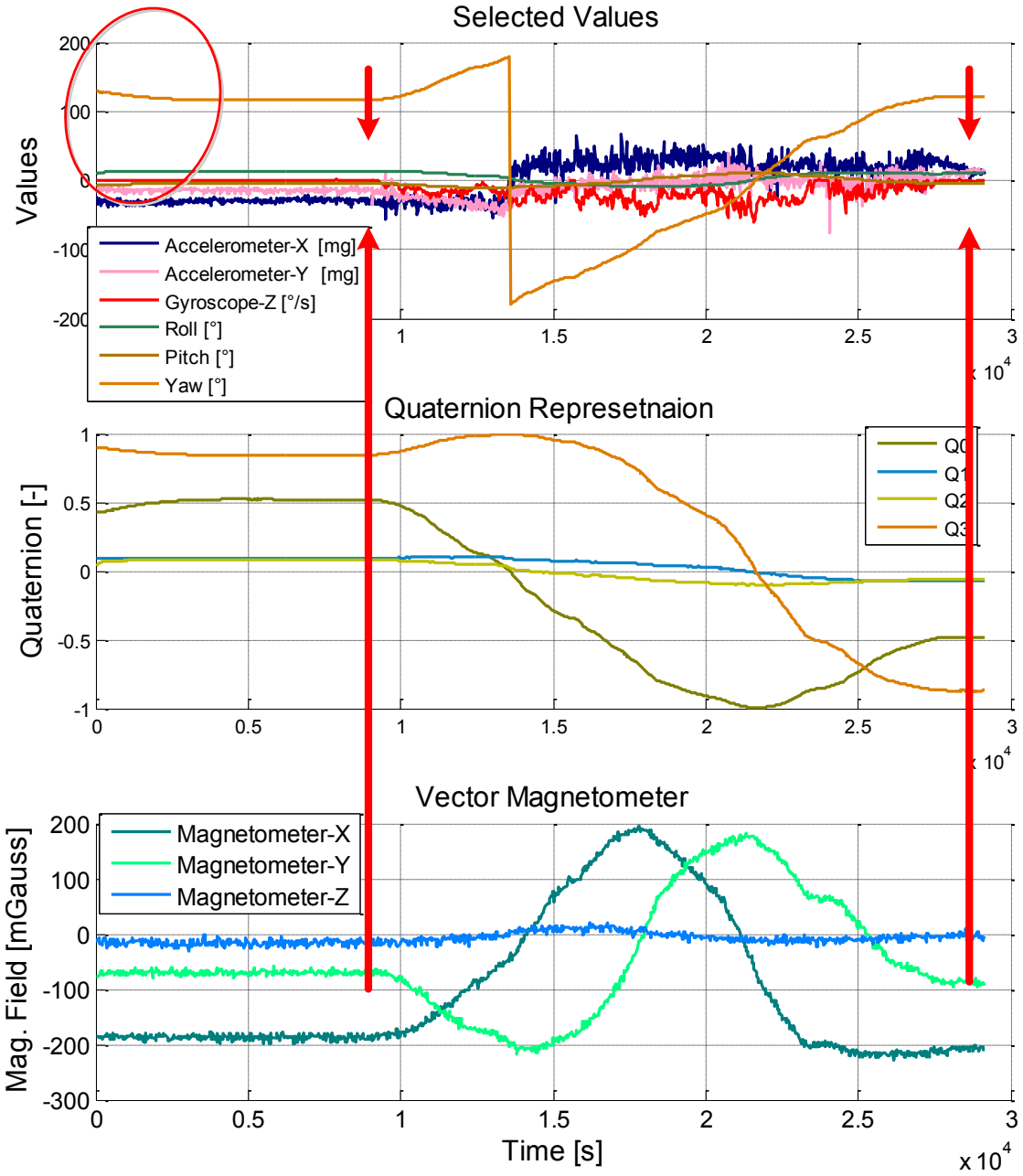

Figure 9. Outputs of the MEMS sensors and the data procesing algorithm

What is being mainly tested is the yaw movement of the unit which is sensed by the Z axe of ARS and merged with magnetometer. The resulting yaw movement matches the expectation as it is depicted in Figure 9 A. At the time of 14 seconds there is a change of sign of the yaw angle and also X and Y accelerations change sign due to the movement. Their change has immediate impact on the pitch and roll angles calculated from quaternions. The behavior of the Kalman filter output is smooth in comparison with outputs of the sensors due to the filtering (see Figure 8). All the presented results were measured just with the angular rotation effecting on the Z axe and there was no other acceleration.

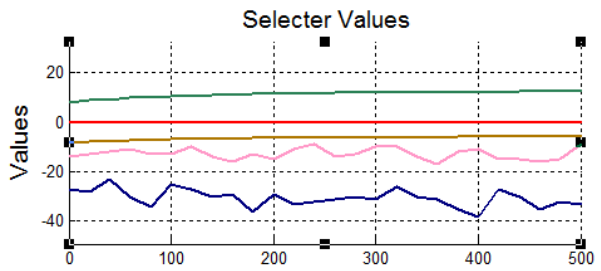

Figure 10. Initial Alignment of the AHRS Unit

Modified AHRS Proposal

The data presented in the previous paragraphs shows the small sensor imperfections can influence even sophisticated algorithms used within AHRS units under static conditions. This meant there are no other forces effecting on the unit which are usually generated during the flight, like turns, engine vibrations, etc. This means the correction algorithm requires certain level of sensor precision and it can be used just under no other forces condition. To detect the fact no other forces influences on the airplane we can use condition (8).

$$1 = |\vec{a}| = \sqrt{a_x^2 + a_z^2 + a_z^2} \qquad (8)$$

Where a_x, a_y, and a_z represent components of the acceleration measured by the vector accelerometer. While the magnitude of the vector is equal to 1 there is just the gravitational field being measured by the sensors. This condition can or cannot happen. To cope with this problem we propose a new arrangement of the data flow being used within AHRS system which is depicted in Figure 11. The presented data flow uses improved magnetometer sensor head which is able to recalibrate itself and whose concept is presented in [6] and [12]. Another improvement is by using the data provided by Pressure Reference System [6] that are merged with data conditionally provided by the vector accelerometer. The data fusion block can be e.g. weighting the both signals as described in [10] equation 1.9.

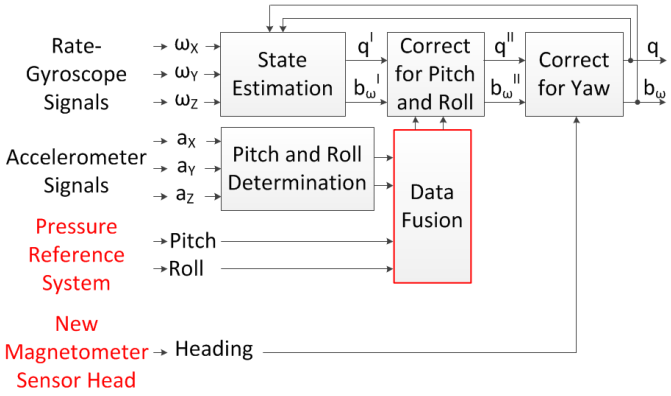

Figure 11. New Arrangement of the Data Flow within an Extended AHRS System

Conclusion

This article uses Inertial Measurement Unit used within Small Satellite Platform to illustrate implementation of a Kalman filter that provides Euler angles and quaternions. The data processing algorithm is described here and implemented within the unit. This implementation is usual in the area of cheap AHRS units used for Light Sport Aircrafts. The pilots often complain about drift of the artificial horizon which is caused by imperfection of the sensors. While the sensors were miscalibrated here the orientation angles are also influenced.

This article proposes a new modified arrangement of the AHRS data processing which is based on two new sensors. First is a new magnetometer head which provides information about platform heading and it is able to calibrate itself with regards to hard and soft iron distortions. The second is utilization of the new system for position angles measurement that provides pitch and roll angles based on measurement of small differences in the atmospheric pressure. These redundant pitch and roll angles can be used instead of those calculated based on accelerometers.

References

[1] Petr, Novacek, Sipos, Martin, Paces, Pavel, 2011, Modular System for Attitude and Position Determination. In POSTER 2011 - 15th International Student Conference on Electrical Engineering [CD-ROM]. Prague: CTU, Faculty of Electrical Engineering, p. 1-5. ISBN 978-80-01-04806-1.

[2] Martin, Sipos, Novacek, Petr, Paces, Pavel, 2011, Development of Platform for Measurement and Signal Processing of Navigation and Aerometric Data. In POSTER 2011 - 15th International Student Conference on Electrical Engineering [CD-ROM]. Prague: CTU, Faculty of Electrical Engineering, 2011, p. 1-5. ISBN 978-80-01-04806-1.

[3] Pavel Paces, Sipos, Martin, Laifr, Jaroslav, Batek, Miroslav, 2011, Small Satellite Systems Control for University Curriculum. In 62nd International Astronautical Congress [CD-ROM]. Cape Town: South African National Space Agency (SANSA), p. E1.2.5.1-E1.2.5.9. ISSN 1995-6258.

[4] King A.D. Inertial Navigation - Forty Years of Evolution. GEC REVIEW. Vol. 13, 1998

[5] Weed D, Broderic J, Love J, Ryno T, GPS Align In Motion of Civilian Strapdown INS. Honeywell Commercial Aviation Products, Honeywell International. Development, Picastaway. IEEE, 2004. p. 184- 192. ISBN 0-7803-8416-4/04.

[6] Pavel, Paces, Popelka, Jan, Levora, Tomas, 2012, Advanced Display and Position Angles Measurement Systems, 28th International Congress of the Aeronautical Sciences, accepted for publication.

[7] Sherryl H., Stovall, 1997, Basic Inertial Navigation, Naval Air Warfare Center Weapons Division, fas.org/spp/military/program/nav/basicnav.pdf.

[8] Oliver J., Woodman, 2007, An introduction to inertial navigation, University of Cambridge, Computer Laboratory, UCAM-CL-TR-696, ISSN 1476-2986

[9] Naser, El-Sheimy, Xiaoji, Niu, 2007, The Promise of MEMS to the Navigation community, Inside GNSS.

[10] Daniele Comotti, Michele Ermidoro, 2011, Efficient Orientation Estimation Algorithms using Inertial Measurement Unit Measurements, Final Report, Università degli studi di Bergamo.

[11] Pavel, Paces, Popelka, Jan, 2012, IMU AIDING USING TWO AHRS UNITS, 31th Digital Avionics System Conference, accepted for publication.

[12] Popelka, Jan, Pavel Paces, 2012, Miniaturization and Sensor Fusion of a Measurement Unit for a Trailing Bomb, 31st Digital Avionics System Conference, accepted for publication.

[13] Tamara, Bandikova, Fury, Jakob, Ko, Ung-Dai, 2012, Characteristics and accuracies of the GRACE inter-satellite pointing, Advances in Space Research, Elsevier, http://dx.doi.org/10.1016/j.asr.2012.03.011.

[14] D. Simon, 2001, "Kalman Filtering," Embedded Systems Programming, vol. 14, no. 6, pp. 72-79, June 2001, academic.csuohio.edu/simond/courses/eec644/kalman.pdf.

[15] Greg Welch, Gary Bishop, 2001, An Introduction to the Kalman Filter, SIGGRAPH.

[16] Vladimir Havlena, Jan Stecha, 1999, Moderni teorie rizeni, Modern Control Theory, Text book, CTU in Prague (in Czech).

[17] Daniele Comotti, 2011, ORIENTATION ESTIMATION BASED ON GAUSS-NEWTON METHOD AND IMPLEMENTATION OF A QUATERNION COMPLEMENTARY FILTER.

Acknowledgements

This work was supported by the research project no. SGS12/193/OHK3/3T/13 "Safe and Safety Elements in Aerospace and Space Technology" of the CTU in Prague, sponsored by the Ministry of Education, Youth and Sports of the Czech Republic.

Email Addresses

Authors can be contacted via an email at:

Pavel Pačes: pacesp@fel.cvut.cz

Jan Popelka: popelja3@fel.cvut.cz

Emidio Marchitto: emidio.marchitto@gmail.com

Tomáš Levora: levortom@fel.cvut.cz

IMU AIDING USING TWO AHRS UNITS

Pavel Pačes, Jan Popelka, Czech Technical University, Prague, Czech Republic

Abstract

This paper describes usage of two modified attitude heading and reference systems whose two pressure sensors are used to provide a new source of altimetry information that allows determination of position angles and inertial measurement unit sensor error models. The system is called Pressure Reference System. The two collaborating units use MEMS based triads of gyroscopes, accelerometers, magnetometers and multiple pressure sensors each. The two modules with their pressure sensors allow us to perform altitude measurements at two places from which a position angle can be determined. The altimetry data are recalculated to the position angle that is stable in time and does not suffer by drift errors amplified by the numerical integration algorithm used in inertial measurement units. This new information is fed back to the module as a correction signal for MEMS sensors and it is used to remove their drift errors. The method used for data fusion is described in this paper together with error model identification method, a testing system, laboratory test procedure and its results.

Introduction

There is enormous innovation effort in area of avionic systems [1-7]. Especially the precise sensors [1-3], networks [4-5], systems [6-8], navigation systems [9], guidance algorithms [10-11], and procedures [12] are often being presented at conferences. Airplanes use Global Positioning System (GPS) [13] for position determination and Attitude Heading and Reference Systems (AHRS) [14] for airplane orientation (or position) determination [15]. AHRS usually measures [16] also airspeed and altitude through atmospheric pressure [17]. All the sensors used in these systems need to be calibrated to provide precise information [18]. A top line of commercial-of-the-shelf sensors are usually used for position angles determination and even more precise and even more expensive sensors are used for position angles determination and also for navigation purposes [19] in Inertial Navigation Systems (INS) [20]. The cost of these INS systems is related to their precision. In the area of ultra light and small airplanes the price of a precise INS system (~$75000) overcomes the price of the airplane.

Nowadays all the airplanes fly according to the atmospheric pressure at Flight Levels (FL). The measured pressure is recalculated according to the International Standard Atmosphere (ISA) behavior [21] to airspeed and altitude. As used in [22] we propose a new idea of a new system for position angles measurement which is called Pressure Reference System (PRS). This system is going to be used with existing measurement systems, like GPS, AHRS, or AoA and AoS [23], as a new source of information which can be used in data fusion algorithms [24]. The new measurement system, whose concept and first realization was presented in [22], measures small vertical pressure differences which are then converted to vertical difference as illustrated in Figure 1. While the measurements presented in [22] had not provided proof of the system functionality a new arrangements of the new measurement system were proposed, evaluated, described and the results are presented in this article.

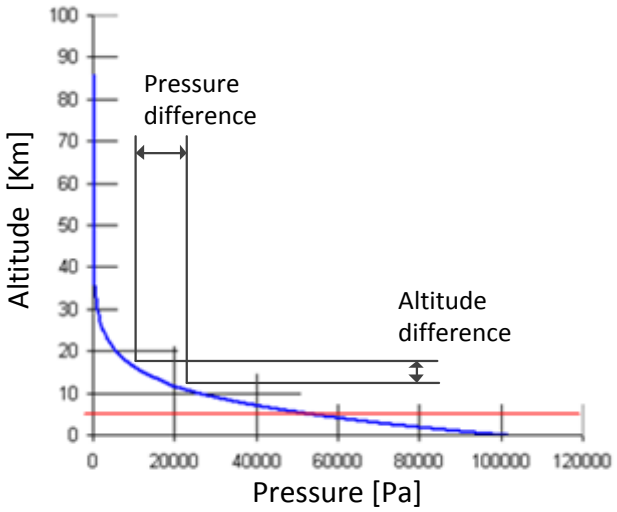

Figure 1. Behavior of Pressure in International Standard Atmosphere and Principle of Pressure Reference System [22]

Installation of precise (and expensive) AHRS systems is not efficient in the area of small airplanes and a new, precise, and low-cost source of information about airplane orientation is needed. This article presents results measured with a new system for position angles measurement, called Pressure Reference System, which uses two modified AHRS units connected by the reference pressure volume. The data fusion algorithm that integrates the new data into existing inertial measurement systems is also described here and its performance was evaluated.

Pressure Reference System

The new system for position angles measurement was patented in [25] and [26]. First results of a system with one sensing unit [25] are published in [22] with promising but not convincing results. It was necessary to define assumptions under which the system will operate and redefine the composition of the measurement system, e.g. use two modified AHRS units [26].

Assumptions

In case it is possible to measure position angles through small pressure differences at such places of airplane that asymmetrically change their position with regards to each other when the airplane changes its orientation we need to define following assumptions:

- The atmospheric pressure does not significantly change in space defined by the airplane dimensions
- The change of atmospheric pressure is smooth following the standard [21] and does not perform step changes

With these assumptions, the PRS measurement system using entry points distributed as depicted in Figure 2, will perform according to the expectations where the vertical difference $dZ = f(2*\Delta P)$. The measurement system implementation can be performed in multiple ways as described in the next chapter.

Measurement System Arrangement

While the PRS position angles measurement system is a new concept there were multiple attempts to gain results reflecting the theoretical expectations. All these attempts were implemented and tested in multiple iterations. The arrangements are presented in the following bullet list:

- Central sensor/sensors

This way of the PRS implementation is described in [22]. There is a data acquisition unit (DAU) placed in the axe of system rotation and the pressure is fed by pipes to the DAU. The system is patented in [25] and the measurement results are described in [22].

- Distributed sensors with a reference volume

To cope with high measurement uncertainty of the previous PRS implementation there were three DAUs used and equipped with differential sensors whose one entry point is connected to a reference volume. This volume creates the same pressure reference level for all the sensors as depicted in Figure 3 in principle. This means the all sensors measure just a small pressure difference between the outside environment and the pressure within the reference volume. This system is described in [26].

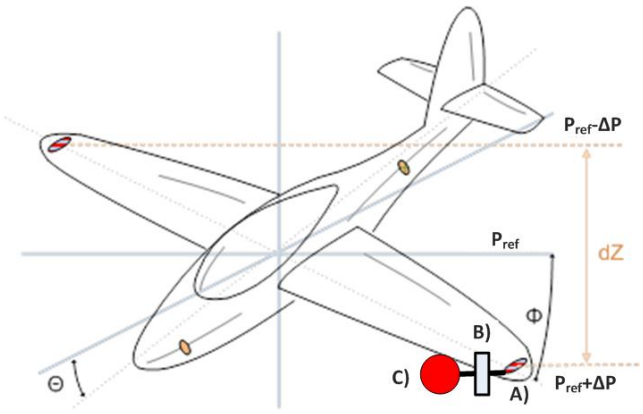

Figure 2. Proposed Placement of Entry Points of the Pressure Reference System (based on [22] and extended)

- Distributed sensors with separate volumes

The last arrangement uses system implementation defined in the previous paragraph but it allows dividing the reference volume into multiple smaller compartments (see one compartment in Figure 2). The compartments carry sample of the pressure which serves as a reference pressure for the

all measurements. The sampling unit carrying pressure samples is described in [27] and here, it is being extended to perform position angles measurement with help of the reference pressure level which is distributed among the separated compartments. This arrangement brings problems with pressure leveling among the compartments.

The PRS system final implementation will combine all of the described methods and all the DAUs use the double sensor arrangement that doubles the unit output magnitude as it was published in [23].

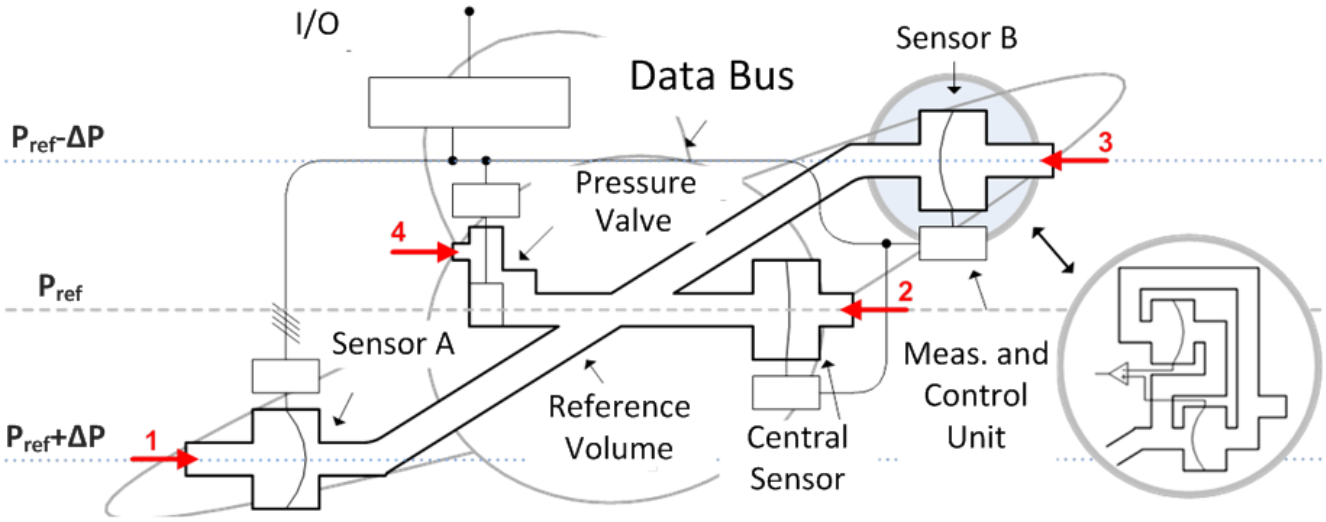

Figure 3. Composition of Pressure Reference System using Reference Volume and Three Data Acquisition Units using the Double Sensor Arrangment that Doubles the Output Signal

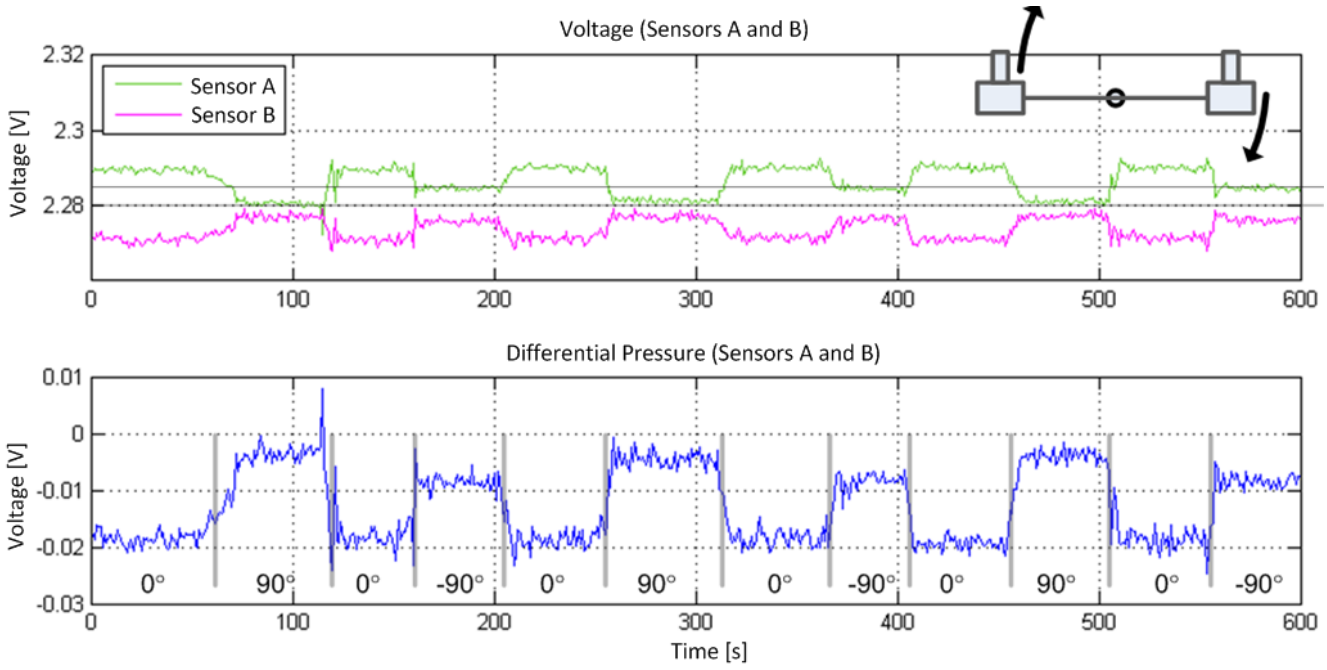

Figure 4. Measurement Results of a Data Acquisition Unit Components Used for Vertical Difference Measurement within the Pressure Reference System for Position Angles Determination

System Evaluation

This chapter introduces measurement results performed with the PRS implemented according to the arrangement depicted in Figure 3. It is composed of a reference pressure volume that provides the same pressure level for three DAUs. Two entry points match the placement depicted in Figure 2 (entry 1 and 3) and the third (entry 2) is placed in the center of the reference volume to correct small atmospheric pressure changes and to detect sensor maximum scale problems in case of precise sensors with small full scale. When the system changes its altitude the atmospheric pressure also changes according to [21] and while we use precise differential pressure sensors with range ± 250 Pa the sensors gets easily saturated. This problem is solved by the pressure valve in the middle that allows opening the reference volume and balances the pressure difference through the entry 4. The system sends the data measured by the DAUs out through a digital CAN bus interface.

Figure 4 shows data measured by the system depicted in Figure 3. The top part of the figure shows outputs of two sensors placed on a holder with 1 m length. The system was being placed into three positions: 0 degrees – horizontal position, +90 degrees rotation, back to zero, and -90 degrees rotation. The difference between the sensor A and B outputs is depicted in the bottom part of Figure 4. The figure clearly shows significant voltage changes on the output for different positions of the system. Please note the repeating difference in magnitude of the signals for rotations +90 and -90 degrees.

Data Fusion

Previous chapter describes three methods of the Pressure Reference System arrangement and depicts data evaluating performance of the second arrangement (the system is depicted in Figure 3 and the data in Figure 4). These data shows better system performance than data provided by the first arrangement published in [22]. The best results and system precision are achieved with the third arrangement of the system and they will be published soon. While this article deals with data fusion of the data provided by the new PRS measurement unit this chapter proposes multiple ways of PRS data integration with data provided by an IMU. This concept follows the trend to improve data provided by an IMU by other independent sources of information. The next chapter proposes a test system based on a flight simulator and its flight model that provides IMU data and evaluates two methods of data fusion between PRS and IMU units.

Test System

To test usability of the data fusion algorithm a Flight Gear (FG) flight simulator was used [28]. The simulator provides access to its internal flight model data through an Ethernet TCP/IP interface. The simulator was configured to send data periodically through a preset port and IP address to special software [29], called Flight Gear Connector, which translates data from the representation used by FG to CAN aerospace frames that are available on request from Mathworks Matlab environment.

The algorithms presented here were tested with an ultra-light airplane Moyes DragonFly flight model. The test script in Matlab periodically asked for data from flight model and saved them into Matlab workspace. After each sample acquisition the script performs integration of angular rate data to gain position angles and performs PRS data fusion. While the FG provides ideal data without any sensor noise, the angular rate sensor (ARS) error model was used as depicted in Figure 5. It shows the data flow from the simulator flight model whose data are merged with sensor error models and other data, e.g. data provided by PRS.

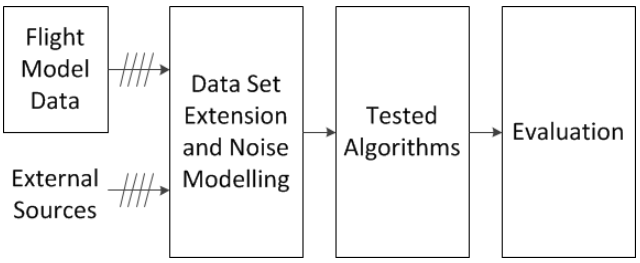

Figure 5. The Data Flow Used for Data Fusion Algorithms, Sensor Error Model Implementation and Performance Evaluation

Methods

The approach for data fusion implementation was divided on simple tasks based on identification

of flight states that can be determined by the commonly available measurement systems. In these states the behavior of measured quantities has characteristics that are suitable for different data integration with other systems, or identification of error models of other systems. These flight states can be used for following integration algorithms:

1. Stable flight with pitch and roll angles equal to zero, e.g. $\Phi = \Theta = 0$

2. Stable flight with constant pitch and roll angles, e.g. $\Phi = k1$ and $\Theta = k2$

3. Stable turn with constant altitude *h*, known radius *r* and constant pitch and roll angles, e.g. $\Phi = k1$, $\Theta = k2$, $r = k3$ a $h = k4$

To implement data fusion algorithms following assumptions were made:

1. PRS unit allows:

    a. to determine orientation of it inputs with regard to the reference horizontal plane

    b. proportional measurement of pitch and roll angles

2. The angular rate sensors of the Inertial Measurement Module provide stable data for at least 3 seconds. This means the sensor output is influenced just by the variable error which depends on the ambient environment effecting on the sensor.

3. The data provided by PRS are not influenced by accelerations effecting on the airplane. It means the measurement signal is not cross-dependent on other physical behavior like linear acceleration in case of accelerometers or electronic tilt sensors [30].

4. Based on GPS data it is possible to get parameters describing the turn of an airplane and the ADC system provides information about constant altitude, e.g. zero vertical speed.

Zero Crossing Detection

The first assumption claims the PRS is able to perform detection of its sensing points crossing the horizontal plane. The transition is detected when the output of the module is zero or the output change sign from positive to negative or opposite. We can use this binary information to reset the position angle computation. The angular speed sensor integration depends on its output signal characteristics and the previously calculated values. In case the ARS output provides data which are acceptable to use for short times (e.g. at least 3 seconds) the reset will significantly improve precision of angle determination. The reset can be implemented by a condition in code.

The integration is performed according to a classic approach using an ideal time integration algorithm that does not perform any other corrections used in INS [31]:

$$\Delta\varphi = \varpi_T (T_2 - T_1) + \delta \qquad (1)$$

Where $\Delta\varphi$ is change of the angle [°], ϖ_T represents actual angular speed [°/s], T_2, T_1 represents sampling rate [s] and δ is an error [°] caused by sensor properties and ambient environment, where $\delta = f(t, \vartheta, ...)$. The biggest problem with integration is caused by the previous sample φ_{T-1} which is added to the present value calculated by (2) and which carries all the previous errors. The integration is written as:

$$\varphi_T = \varphi_{T-1} + \Delta\varphi \qquad (2)$$

Where φ_T is the actual value of the position angle [°], φ_{T-1} represents the previous sample [°] and $\Delta\varphi$ is calculated according to the equation (1).

In the present time a magnetometer together with GPS and ADC are usually used for IMU sensor error compensation. All these systems suffer with different errors [22] that are difficult to compensate. The operators manual prescribes to pilot periodically keep the airplane in stable orientation which allows the system to measure actual sensor errors [32]. The PRS unit with zero detection removes this requirement and pilot is not required to take care about electronic system which lowers his workload.

Stable Orientation Detection

Based on assumption 1b, the PRS unit is able to measure position angles through the whole flight time. Position angle will be calculated like:

$$\theta = U_{Pitch} \cdot a \quad (3)$$

$$\phi = U_{Roll} \cdot b \quad (4)$$

Where θ is pitch, ϕ is roll, U_{Pitch} and U_{Roll} represent voltages provided by PRS, and a and b represents transformation constants between voltage and angle. The constants depend on the sensors precision and their geometrical arrangement. The stable orientation is evaluated by a condition that θ and ϕ do not change more than a preset limit.

In this case of the absolute orientation measurement we can online calculate a correction variable that compensates for actual sensor errors. It is determined during stable turns, stable inclinations, etc. The equation implementing the correction variable will look as follows:

$$\varphi_T = \varphi_{T-1} + \Delta\varphi - \delta_C \quad (5)$$

Where all the parameters are the same like in (1) except for δ_C which represents difference calculated from PRS and IMU outputs. The algorithm is illustrate in Figure 6 where PRS unit measures steady angle, e.g. during a turn, during which there is no other angular rate that could be measured by angular speed sensors. The difference is evaluated as an error and the correction variable is calculated. Figure 6 shows changes of a position angle (full line) with PRS sampling moments. The lower part of the figure shows output voltage of the ADRX610 angular rate sensor which shifts in time because of temperature influences, aging, etc.

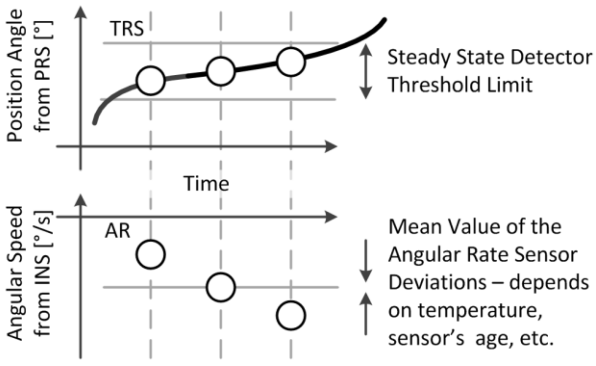

Figure 6. Function of Steady State detection Algorithm used for IMU Sensor Drift Error Determination

Sensor Error Model

The ADRX610 angular rate sensor is manufactured in range ±300 °/s, with sensitivity 6 mV/°/s. The output signal is converted into voltage in range from 0.25 to 4.75 V with zero level at 2.5 V The datasheet claims the sensor suffer by output changes caused due to linear accelerations up to 0.1 V. In case of a change 100 times smaller, 0.001V, we can calculate that the sensor will provide angular rate readings 0.133 °/s. Similar value is also generated by ambient temperature changes effecting on the sensor. This value is used to model sensor behavior (see Figure 5) in the following chapters.

Results

The algorithms evaluation was performed with help of the test system presented before on the described airplane. In four minutes, the pilot performed take off, one turn and landing with hard breaking which can be seen in the following figures at time 250 s. There was a complete data set acquired with sampling frequency 10 Hz during the test but the results here reflect only the pitch angle. Pitch angle behavior during the flight is depicted in Figure 7. This signal is used as a reference for all the other simulations and algorithms. The step change at time 25 s (see Figure 7) is caused by airplane placement on the runway after flight model initialization. Figure 8 shows pitch angle calculated by equations (1) and (2) from an ideal angular rate sensor (see Figure 15 red line).

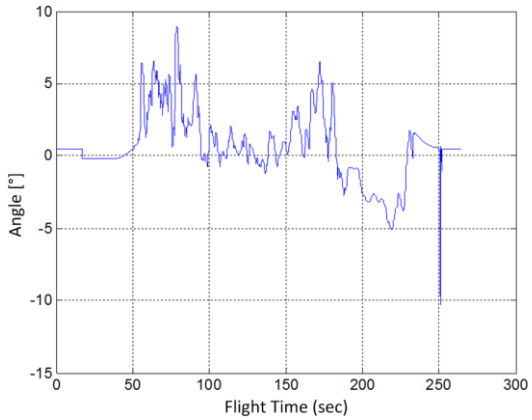

Figure 7. True Value of Pitch Angle through the Test Flight

Figure 9 shows difference between the true pitch angle (Figure 7) and the calculated pitch angle (Figure 8) where we can see deviations in range ±1°. The cumulative Root Mean Square Error (RMSE) of these graphs is depicted in Figure 10. While all these data are almost ideal the error is under 0.5°.

If we use the zero crossing detection and correction algorithm the resulting error is much smaller as we can see in Figure 11 where we can recognize that the vertical deviation was removed in range from 50 to 225 seconds. It is clearly visible in RMSE graph in Figure 12 which can be compared with data depicted in Figure 10.

The result of the stable states detection implementation is depicted in Figure 13 as deviations from data in Figure 7. Its RMSE is depicted in Figure 14 where we can see the rising cumulative error. The advantage of the algorithm lays in the fact it removes offset in range from 175 to 230 seconds that we can see in Figure 9.

In case we will combine the zero crossing detection and correction algorithm and also steady state detection we will get the deviations depicted in Figure 11 and RMSE depicted in Figure 12. The results here show that the zero crossing algorithm has much higher impact on the overall precision of the combined systems. Therefore it would be valuable to develop a system that recognizes crossing through the horizontal reference plane.

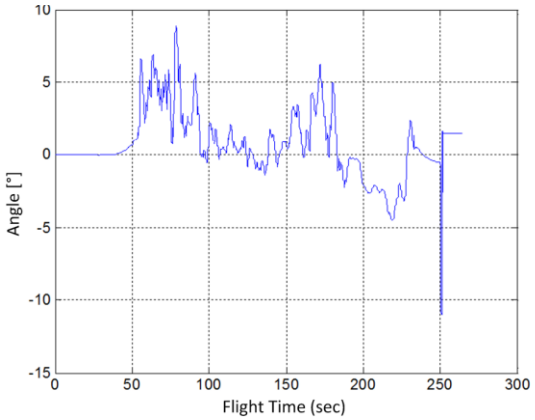

Figure 8. Pitch Angle Calculated from an Ideal Angular Rate Sensor

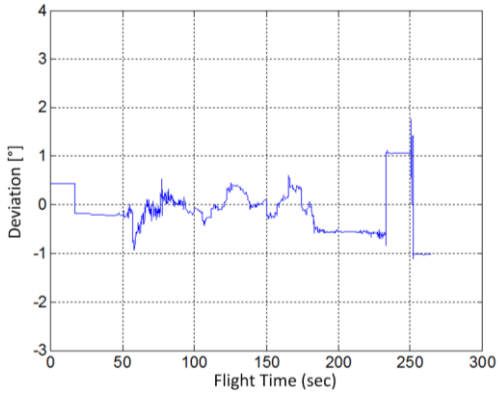

Figure 9. Deviations between True and Calculated Pitch Angles

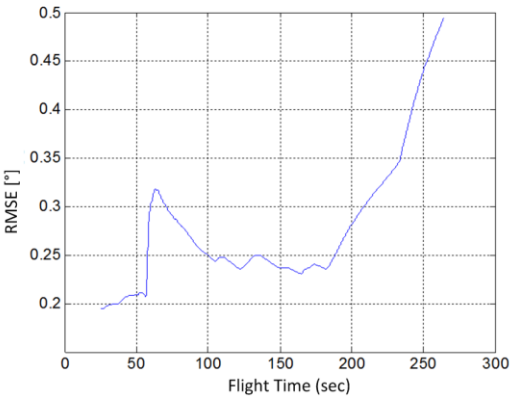

Figure 10. RMSE between True and Calculated Pitch Angle

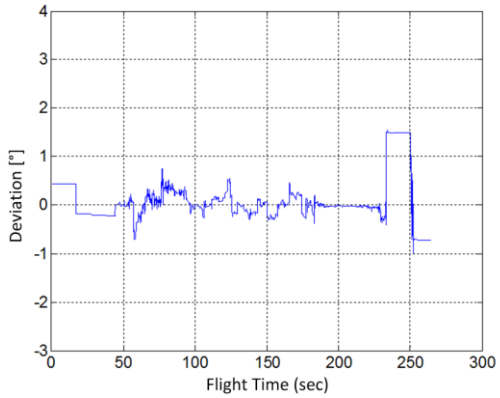

Figure 11. Deviations between True and Calculated Pitch Angle after Using Zero Crossing Detection Algorithm

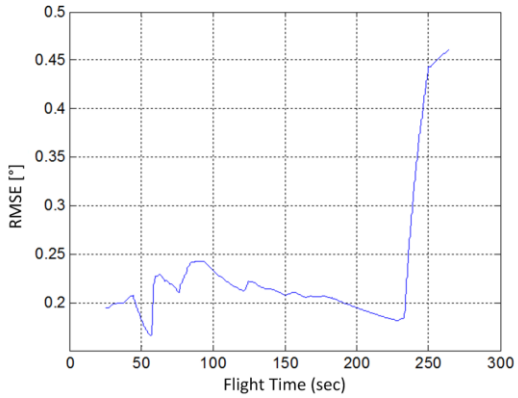

Figure 12. RMSE between True and Calculated Pitch Angle after Using Zero Crossing Detection Algorithm

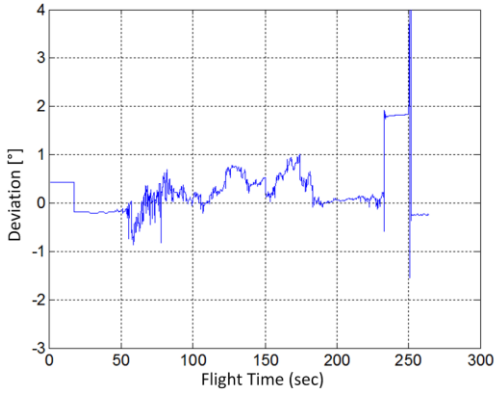

Figure 13. Deviations between True and Calculated Pitch Angle after Steady State Detection Algorithm Application

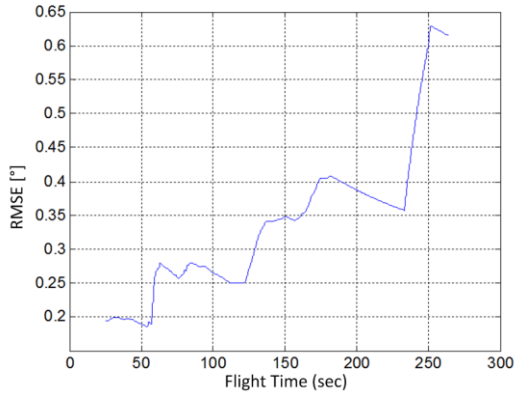

Figure 14. RMSE between True and Calculated Pitch Angle after Steady State Detection Algorithm Application

All the data illustrated before were ideal data (no sensor errors) from the flight model without any sensor model connected into the data flow (see Figure 5). Following images and results includes sensor error model characteristics with following influences:

- The signal used for steady state detection was loaded with rand (Matlab function) noise with amplitude 1% FS
- The detector illustrated in Figure 6 was set to 0.8% FS
- The angular rate sensor was loaded with offset error 0.133 °/s (according to the ADRX610 sensor) and random noise with amplitude of 0.5 °/s
- A moving average with length of 30 seconds was used for the correction variable δ_C (5) calculation

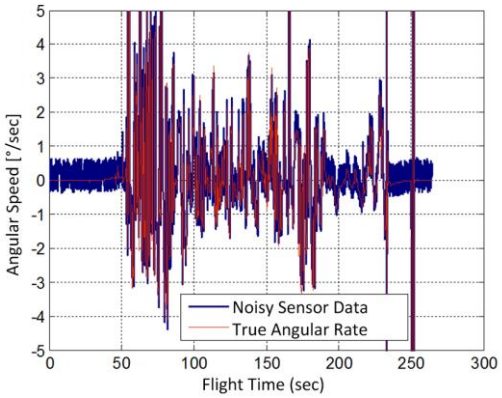

Figure 15. Reference Angular Rate Data and Sensor Data with Noise

Figure 15 shows the ideal angular rate sensor (red line) together with sensor output loaded with the previously described noise parameters (blue line). The blue line represents angular rate data provided by a low-cost sensor. We can use equations (1) and (2) to integrate its output but the result of the integration – the angle – will drift away from the true value very fast. Similar output value drift is depicted in Figure 16 [33]. This image shows the error introduced by the double integration algorithm of a three axial accelerometer data. The drift has exponential shape and after two seconds the error reaches five meters. Because we use only one integration of angular rate

sensors, the drift of the output would not be so aggressive (it will be a ramp) and we can claim the expectation of the ARS sensor output stability for at least three seconds is reasonable.

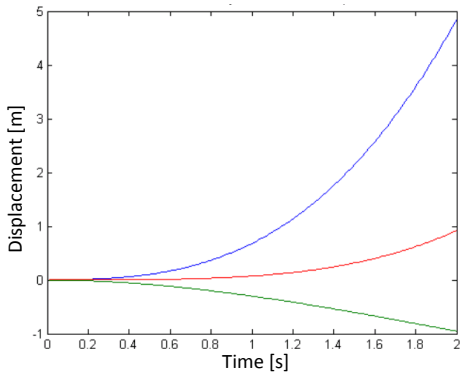

Figure 16. Typical Output of a Flat Earth Navigator – Stable Sensor Drift Errors [33]

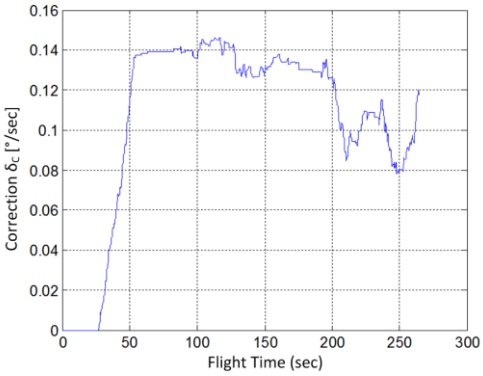

Figure 17. Time Domain Evolution of the Angular Rate Sensor Correction Parameter

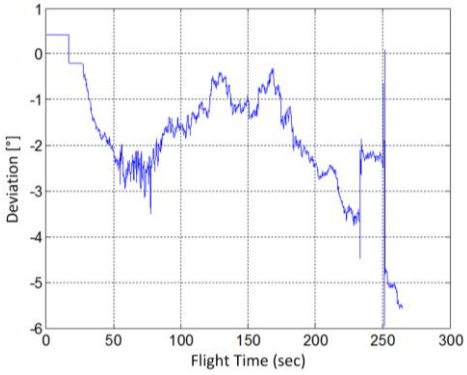

Figure 18. Deviations between True Pitch Angle and Pitch Angle Calculated from Noisy Data using Steady State Detection Algorithm

In case we will use just equation (1) and (2) on the real sensor signal (Figure 15) there will be an error of 13 degrees after 90 seconds (about 4% FS), which is not usable for a pilot to fly an airplane.

Figure 17 shows time behavior of the correction variable δ_C (see equation (5)) which is calculated according to the presented algorithm. Figure clearly shows the length of the moving average filter in range from 25 to 55 seconds, where it cumulates the measurement history.

In case we use the steady state detection algorithm on the noisy data depicted in Figure 15 (blue line) according to the equation (5) we will get deviations as depicted in Figure 18 and related RMSE depicted in Figure 19.

Figure 19 clearly shows standard deviation of 2.2° which is better than 39° in case no correction algorithm used. The 2.2° value in Figure 19 is gained mainly through the time of moving average filter filling and δ_C initialization (see Figure 17).

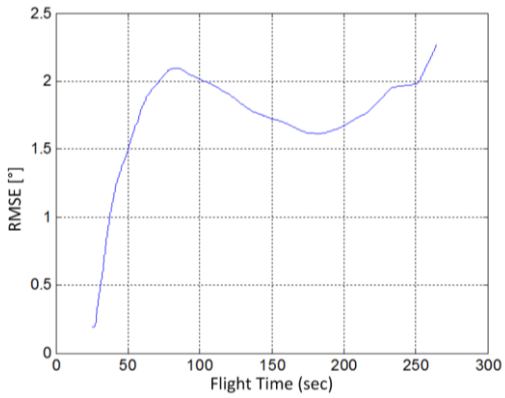

Figure 19. RMSE between True Pitch Angle and Pitch Angle Calculated from Noisy Data using Steady State Detection Algorithm

Figure 20 shows situation where we applied also zero crossing detection algorithm and integration reset next to the steady state detection. We can recognize similar behavior as it is depicted in Figure 18 but the signal is often returned back to zero deviation (see the steep change at 45 s) and the errors caused by sensors and integration algorithm are all the time being removed. Figure 21 shows the maximal standard deviation of this composition of algorithms about 1.2° and it is caused through the

time of the correction variable δ_C initialization. Then the error rapidly descends and the rise at the end is not such steep as depicted in Figure 19.

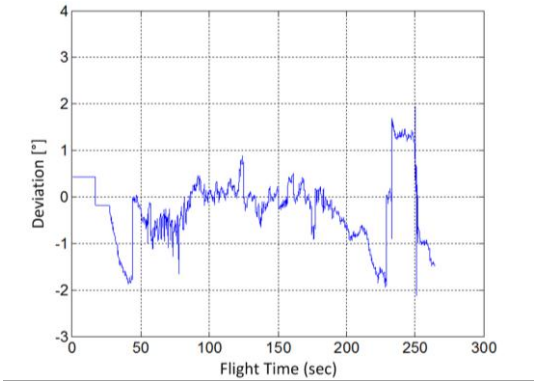

Figure 20. Deviations between True Pitch Angle and Pitch Angle Calculated from Noisy Data using Steady State Detection and Zero Crossing Algorithms

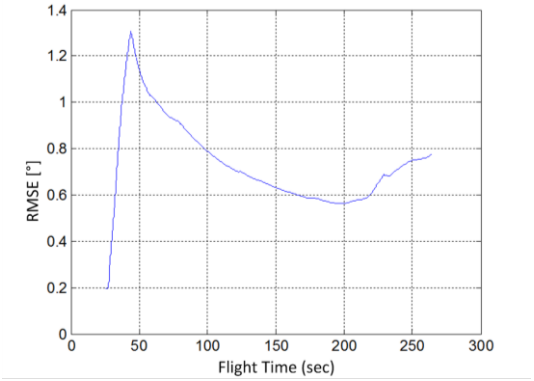

Figure 21. RMSE between True Pitch Angle and Pitch Angle Calculated from Noisy Data using Steady State Detection and Zero Crossing Algorithms

Conclusion

While the atmospheric pressure measurement systems are all the time used in aerospace for safety-critical air speed and altitude measurements this article presents results provided by a system that is designed to measure position angles based on small pressure differences. The results show improved performance against to the previously published data which means they show clear output signal changes related to the change of the system orientation.

This measurement system, called Pressure Reference System, can extend the range of measurement devices used within the Attitude, Heading and Reference Systems. It provides another source of information which is stable in time and no numerical integration is required. It is designed to measure position angles and its output can improve precision of commonly used low-cost triads of accelerometers and angular rate sensors. This article describes one possible solution of the system integration with data provided by angular rate sensors within inertial measurement module. The system allows detection of transition from positive to negative angles with regard to the reference level (isobar). This detection algorithm provides logical signal which triggers reset of the numerical integrator history. The integrator integrated data provided by angular rate sensors which are after one numerical integration transformed to positional angles. The reset significantly improves long-term precision of angle determination.

The article also describes a method of adaptive filtration which online evaluates behavior of angular rate sensors and compares them with PRS output. This method allows us to remove the sensor output offset which is caused by temperature shifts or acceleration changes. The result shows the zero crossing detection algorithm has the biggest effect on the angle determination precision with comparison to other presented algorithms. It means a device that is able to detect the zero position angle will significantly improve aviation safety. The error was lowered from 39 degrees deviation in case no correction algorithm used to 1.2 degree after zero crossing detection and steady state detection algorithm usage.

The future work will be focused on improvement of the PRS measurement modules and its integration with other systems and intelligent sensors.

References

[1] Jan, Cizmar, Jalovecky, Rudolf, 2010, Design of an Inertial Reference Unit with the mixed gravitational and magnetic correction of gyroscopic drift. Transport Means - Proceedings of the International Conference, Kaunas; 21 October 2010, ISSN: 1822296X.

[2] Mahapatra P.R, Zrnic D.S. Sensors and systems to enhance aviation safety against weather hazards. Proceedings of the IEEE , vol.79, no.9, pp.1234-1267, Sep 1991, doi: 10.1109/5.97295.

[3] WenwenWang, Chunzhi Li, Junying Zhang, Xungang Diao, 2010, Effects of atomic oxygen treatment on structures, morphologies and electrical properties of ZnO:Al films, Journal of Applied Surface Science, 2010, Elsevier, ISSN: 0169-4332.

[4] Jalovecky, Rudolf, Jan Bajer, Petr Janu, 2010, Controller Area Network based On-board Data Acquisition System on Military Aircraft. In Concepts and Implementation for Innovative Military Communications nad Information Technologies. Warsaw, Poland: Military University of Technology, pp. 589-598. ISBN 978-83-61486-70-1.

[5] Makula, Petr; Andrle, Milos. 2009, Conception of the Digital Communication System for Small UAVs, Proceedings of the International Conference on Military Technologies, ICMT 2009, May 5-6, Brno, Czech Republic, University of Defence, pp. 235-239, ISBN 978-80-7231-649-6.

[6] Leuchter, Jan, Pavel, Bauer, 2011, High-speed Generator – Converter Set for Auxiliary Power Units. In 30th Digital Avionics Systems Conference (DASC.). Seattle, WA, USA, 2011. ISBN 978-1-61284-796-2.

[7] Petr Bojda, Frantis, Petr, 2009, Multipurpose visualization system, Aerospace and Electronic Systems Magazine, IEEE , vol.24, no.4, pp.4-8, April 2009, doi: 10.1109/MAES.2009.4839270.

[8] Petr, Chudý, Rzucidlo, Peter, 2009, TECS/ THCS Based Flight Control System for General Aviation. In Conference Proceeding Series (GNC/AFM/MST). 2009 AIAA Meeting Papers on Disc, Vol. 14, No. 9 (GNC/AFM/MST). Chicago: American Institute of Aeronautics and Astronautics, 2009. s. 1-13. ISBN: 978-1-56347-978- 6.

[9] Sheffels M.L. 1993, A fault-tolerant air data/inertial reference unit. Aerospace and Electronic Systems Magazine, IEEE. vol.8, no.3, pp.48-52, March 1993, doi: 10.1109/62.199822.

[10] Petr, Frantis, 2011, Emergency and precautionary Landign Assistant. In: 30th Digital Avionics Systems Conference. IEEE, 2011, p. 1-6. ISBN 978-1-61284-796-2.

[11] Bruna, Ondrej, 2012, Usability Testing of Interface for Emergency Landing Navigation Assistant. In POSTER 2012 - 16th International Student Conference on Electrical Engineering [CD-ROM]. Praha: Czech Technical University in Prague, 2012, p. 1-4. ISBN 978-80-01-05043-9.

[12] Rierson L.K., 2010, Best practices for certifying IMA systems in civil aircraft. Aerospace and Electronic Systems Magazine, IEEE , vol.25, no.1, pp.4-8, Jan. 2010, doi: 10.1109/MAES.2010.5442147.

[13] Petr, Dittrich, Chudy, Petr, 2011, Application of Kalman Filter to oversampled data from Global Position System. ElectroScope - http://www.electroscope.zcu. cz, 2011, roč. 2011, č. 2, s. 0-0. ISSN: 1802- 4564.

[14] Sherry, L., Brown, C., Motazed, B., Vos, D., 2003, Performance of automotive-grade MEMS sensors in low cost AHRS for general aviation, Digital Avionics Systems Conference, 2003. DASC '03. The 22nd , vol.2, no., pp.12.C.2-12.1-5 vol.2, doi: 10.1109/DASC.2003.1245952.

[15] Martin, Sipos, Paces, Pavel, Reinstein, Michal, et all, 2009, Flight Attitude Track Reconstruction Using Two AHRS Units under Laboratory Conditions. In IEEE SENSORS 2009 - The Eighth IEEE Conference on Sensors [CD-ROM]. Christchurch: IEEE, 2009, p. 675-678. ISBN 978-1-4244-5335-1.

[16] Svatos, Jakub, Pavel, Fexa, Josef, Vedral, 2009, Methods of Education Electronic Measurement Circuits and Systems at FEE CTU In: Applied Electronic 2009. Pilsen: University of West Bohemia, 2009, pp. 9. 12. ISBN 978-80-7043-781-0.

[17] Pavel, Hospodar, Proks, Martin, Golda, M., 2009, LowCost Sensors for Aero-dynamics Identification, Czech Aerospace Proceedings, Aircraft Research and Test Institute of the Czech Republic, Aerospace.

[18] Martin, Sipos, Paces, Pavel, Rohac, Jan, Novavek, Petr, 2012, Analyses of Triaxial Accelerometer Calibration Algorithms. IEEE Sensors

Journal. 2012, vol. 12, no. 5, p. 1157-1165. ISSN 1530-437X.

[19] King A.D., 1998, Inertial Navigation - Forty Years of Evolution. GEC REVIEW. Vol. 13, 1998.

[20] Weed D, Broderic J, Love J, Ryno T, 2004, GPS Align In Motion of Civilian Strapdown INS. Honeywell Commercial Aviation Products, Honeywell International. Development, Picastaway. IEEE. p. 184- 192. ISBN 0-7803-8416-4/04.

[21] International Organization for Standardization, 1975, Standard Atmosphere. Geneva, ISO, 1975. ISO 2533:1975.

[22] Paces Pavel, Jan Popelka, Tomáš Levora, 2012, Advanced Display and Position Angles Measurement Systems, 28th International Congress of the Aeronautical Sciences, accepted for publication.

[23] Pavel, Paces, Censky, Tomas, Hanzal, Vitezslav, Draxler, Karel, Vaško, Ondrej, 2010, A Combined Angle of Attack and Angle of Sideslip Smart Probe with Twin Differential Sensor Modules and Doubled Output Signal. In IEEE Sensors 2010 - Proceedings [CD-ROM]. Stoughton, Wisconsin: IEEE Sensors Council, p. 284-289. ISBN 978-1-4244-8168-2.

[24] Pavel, Paces, Reinstein, Michal, Draxler, Karel, 2010, Fusion of Smart Sensor Standards and Sensors with Self-Validating Abilities. Journal of Aircraft, vol. 47, no. 3, p. 1041-1046. ISSN 0021-8669.

[25] Paces, Pavel.: System for inaccuracy correction of inertial measurement systems. Patent, Industrial Property Office, #302336. 2011-02-02. (in Czech).

[26] Paces, Pavel.: System for Position Angles Measurement, especially for airplanes. Patent, Industrial Property Office, #302731. 2012-01-09. (in Czech).

[27] Kuno, Akira, Shinoda, Yoshio, Yoshino, Yasuhisa, 1980, Altitude difference measuring apparatus, US Patent No: 4,302,973.

[28] The FlightGear flight simulator project. [Online] http://www.flightgear.org/.

[29] Pavel, Paces, Levora, Tomas, 2012, Flight Gear Connector, online: sourceforge.net/projects/flightgear conne/ .

[30] Martin, Sipos, Rohac, J., Novacek, P., 2012, Analyses of Electronic Inclinometer Data for Tri-axial Accelerometer's Initial Alignment In: Przeglad Elektrotechniczny. 2012, vol. 88, no. 01a, p. 286-290. ISSN 0033-2097.

[31] Stovall, Sherryl H., 1997, Basic Inertial Navigation. California : Naval Air Warfare Center, Weapons Division, 1997. NAWCWPNS TM 8128.

[32] MGL Avionics. 2010, SP-2 Magnetometer, SP-4 AHRS User and installation manual. [Document] Somerset West: MGL Avionics, 2010. SP2-SP4.

[33] Crittenden J, Evans P. MEMS Inertial Navigation System. 2008.

Acknowledgements

This work was supported by the research program no. TA01030651 "Safety Improvement of Flight, Crew and Other Participants of Flight Transport in Normal and Emergency Situations by Assistive Technologies" of the Czech Technical University in Prague, sponsored by the Technological Agency of the Czech Republic and partially by the project no. SGS12/193/OHK3/3T/13 “Safe and Safety Elements in Aerospace and Space Technology” of the CTU in Prague, sponsored by the Ministry of Education, Youth and Sports of the Czech Republic.

Email Addresses

Authors can be contacted via email at:

Pavel Pačes: pacesp@fel.cvut.cz

Jan Popelka: popelja3@fel.cvut.cz

STANDALONE TRAILING PROBE FOR AERO METRICAL MEASUREMENTS

Pavel Paces, Jan Popelka, Jan Auersvald
Czech Technical University in Prague, Prague, Czech Republic

Abstract

This article describes a design of a probe intended for aero metrical instrument testing which is being hanged under an airplane. The probe collects data in an undisturbed airfield and compares them with data provided by dashboard instruments. The differences reveal quality of an airplane prototype design during maiden flights. The most important flight instruments are an altimeter and an air speed indicator. These instruments can be tested by comparison with data from a trailing bomb probe. While commonly used probes fed pressure from the probe entry points up to the airplane cabin by pipes, the prototype described in this paper uses wireless data link to transfer data to a data acquisition unit. Beside the altitude and speed the probe also measures its angle of attack and angle of sideslip which are used onboard to compensate for errors caused by probe alignment within the airfield. The designed system consists of two parts: the probe itself and a winch mechanism. Because the probe sensors are standalone the measured data reflects exactly the situation at the probe entry points. It means the probe measurements have to be corrected with regards to the length of the wire released from the winch and also for the speed of flight that influences the angle between the horizontal axe of an airplane and the wire connecting the airplane and the probe. Because the winch mechanism introduces problems with mounting and data correction the probe is designed to allow direct mounting on the airplane wing after removing its tail stabilization part. This design feature prepares the probe to be used also as an entry point for the new system for position angles measurement. Precision of the probe, pros and cons of both methods are discussed in the article.

Figure 1. Trailing Probe, Winch and Test Equipment

Introduction

Trailing probe is a specialized calibration device that is used to measure speed of flight and altitude which is compared with data provided by dashboard instruments. This probe is used mainly for airplane prototypes but also for calibration of the instruments after any change at the airplane surface, e.g. new wing shape or a new antenna arrangement. The probe serves just as a pressure entry point and in case a sensor is used it is connected by a digital bus [1].

Shape of the probe resembles a missile with long cylindrical body, rounded head and tail stabilization wings (see Figure 1). The probe can be directly attached to the airplane after removing its tail section and also by a winch which is depicted in Figure 1. To test precision of the probe GE Druck Pace6000 pressure automated calibration equipment was used.

Trailing probe is usually hanged under the tested airplane where the probe measures pressure in an undisturbed environment. The trailing probe is usually a dumb device which is used just to provide inputs for static and total pressure that are then guided by pipes into the airplane fuselage where the measured pressures are converted into electrical signals [2] by a data acquisition system. Following quantities are usually measured:

- Total pressure (Pc) at the head of the probe
- Static pressure (Ps) at the one third of the probe length from its beginning
- Temperature

Besides these basic quantities which reflects the standard atmosphere [3] the proposed probe design allows measurement of other values and brings in some advantages which are introduced in the following chapter.

Advantages of the Proposed Design

The on-the-shelf trailing probes are usually just an entry points for the measured pressures. To increase usability of the probe following improvements were introduced:

- The probe is completely stand-alone

  All the required sensors and electronics are present within the probe. The electronics performs all the necessary computations onboard. Next to the sensors and measurement electronics the probe also contains following components:
  - Onboard power (battery)
  - Wireless interface
- There are two ways of probe mounting on the airplane under test

  Usage of the trailing probe usually required to prepare an opening in the fuselage to allow the probe tether and pressure tubes to go out of the plane because there is a winch onboard. Because we have designed a stand-alone probe these methods can be used to attach the probe to the airplane:
  - Remotely controlled winch mechanism outside of the airplane
  - Direct mounting on the wing or other suitable place on the airplane
- Angle-of-attack and angle-of-sideslip are measured

  To detect and compensate for small misalignments of the probe centerline with the vector of the airflow, angle-of-attack and angle-of-sideslip has to be measured for total and static pressure entry points misalignments corrections.
- Possibility to attach another sensors

  The probe still provides a space available to attach another sensor like a magnetometer [4] or an inertial measurement unit [5].

Probe Design

Because all the components are placed within the probe, size of internal space is the first requirement for the probe design. Probe diameter reflects size of the electronics and sensors used within the probe. The initial design uses COTS components which are not optimized for space and weight but it can be solved by replacing the COTS components by small and custom made sensors [6].

Table 1. Probe Parameters

Probe Parameter	Value
Diameter	70 mm
Length with trailing cone	1320 mm
Length without trailing cone	924 mm
Length without tail	745 mm
Static pressure input position (length from head)	253,15 mm
Weight (including tail and cone)	5,1990 Kg
Weight (without tail)	3,2885 Kg

The probe mechanical design comes from [7]. Based on [8], the diameter of the probe was chosen 70 mm. Other mechanical characteristics are depicted in Table 1. The probe uses two complementary frames: internal and coating. The internal frame is composed by two bars and it is used to hold position of all the internal components which are depicted in Figure 2. Figure shows sensors (red areas), electronics (white oblongs), battery (blue box) and spare space (gray boxes) intended for other sensors. The coating provides stiffness of the frame during flight and also protects the internal electronics. The length of the probe is divided into three partitions. AOA, AOS and air-speed sensors are placed just behind the head of the probe with a control CPU and power distribution unit. Mechanical drawing of the probe head is depicted in Figure 3.

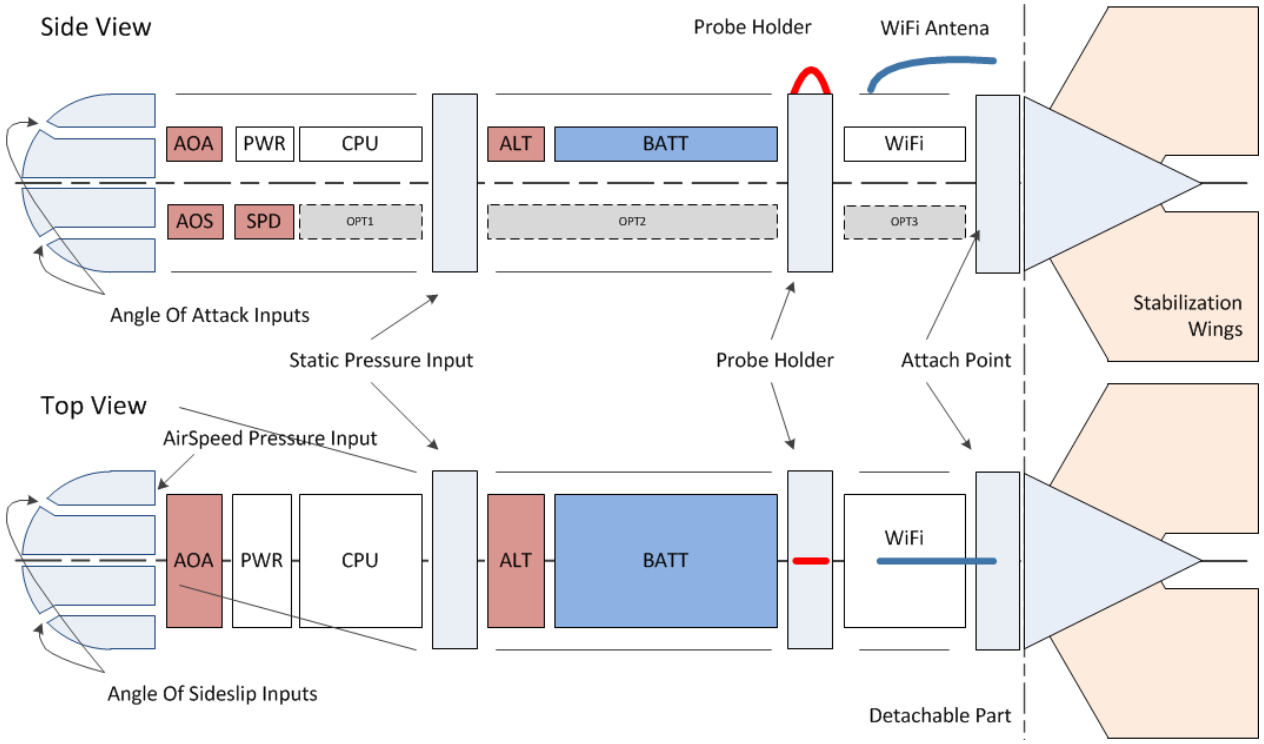

Figure 2. Schematic Diagram of Component Arrangement Withinn the Probe

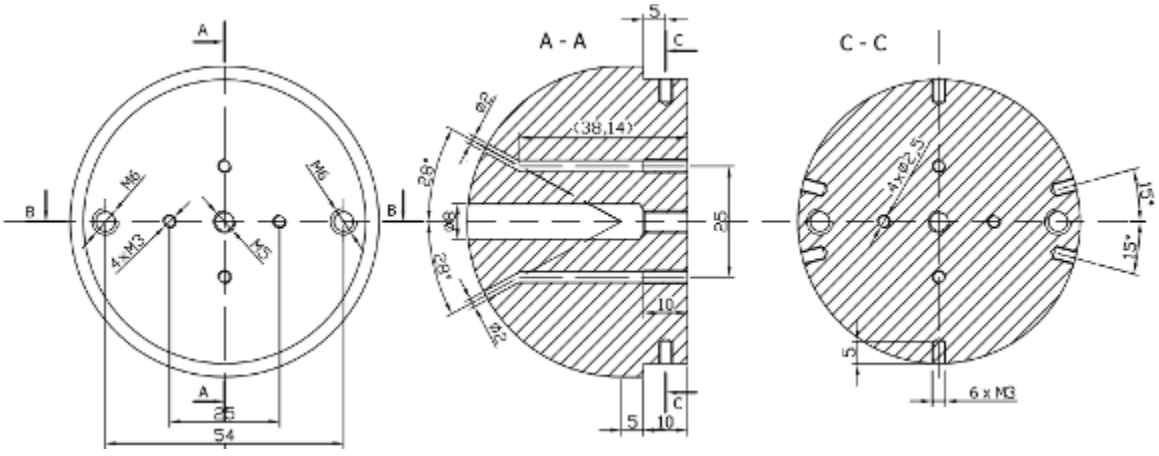

Figure 3. Mechanical Drawing of the Probe Measurement Head with Speed Pressure Inputs and Angle of Attack and Angle of Sideslip Inputs

The measurement head provides input for air-speed measurement and also inputs for angle-of-attack (AOA) and angle-of-sideslip (AOS) measurements. The probe diameter of 70 mm and position of AOA and AOS inputs were chosen according to the results provided in [8] where probes with different diameters were evaluated. First compartment of the probe contains AOS, AOS, air-speed sensors, power conditioning circuit and central processing unit (CPU) which is used for data acquisition and to manage communication. The first compartment ends by a block that serves as the static pressure input. Its mechanical drawing is depicted in Figure 4. Third component which separates compartment two ends by a mechanical block used to hang the probe to the airplane by a hinge. Compartment two carries Memscap SP82 absolute pressure sensor and Li-Pol battery. Last compartment is used for a wireless modem. The internal frame is finished by a last wall (see Figure 7) which is used to attach tail part and stabilization wings or for direct probe mounting to the airplane.

Real composition of all components is depicted in Figure 5 where we can see probe head, static pressure inputs, hanging wall and WiFi antenna. All of the walls are mechanically connected by two bars which hold all the components together. Electronic circuits are mounted on holders which are made from plastic on a 3D printer. A sensor, CPU and battery holder models are depicted in Figure 6 and the used printed component are displayed in Figure 5.

Figure 5 also shows probe coating which is designed as six halves of aluminum cylinders, two for every compartment. Each part of the six coating elements holds on six screws and provides rigidity to the probe body. The figure shows the probe with first and second top coating disassembled. The coating components fit into grooves depicted in Figure 3, Figure 4, and Figure 7. We can see the internal electronics, wiring, guidance pipes and total and static pressure inputs used for probe calibration (Figure 5 red arrows).

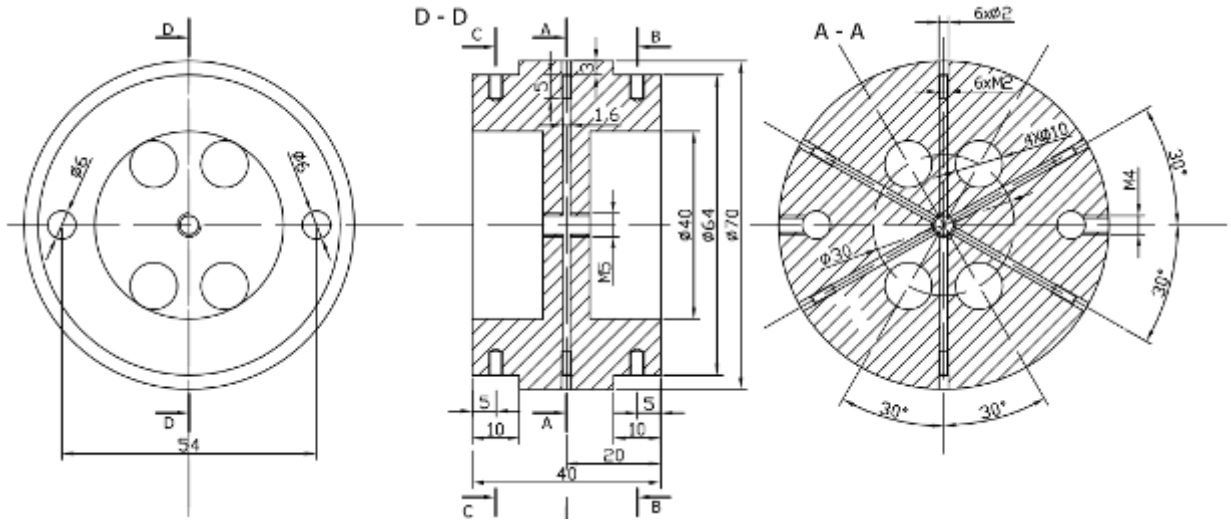

Figure 4. Mechanical Drawing of the Static Pressure Inputs

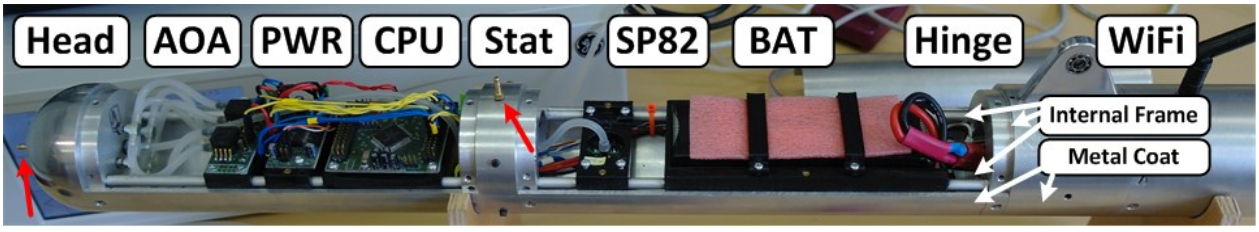

Figure 5. Component Arrangement Withinn the Probe

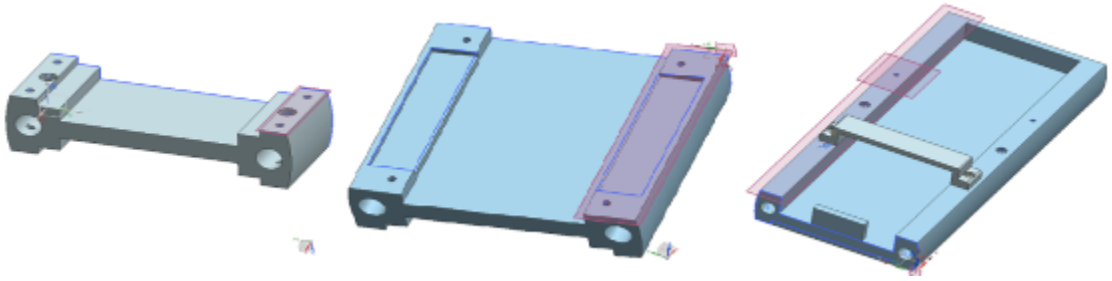

Figure 6. 3D Models of Electronic Circuits Holders which were 3D Printed and Used Inside of the Probe

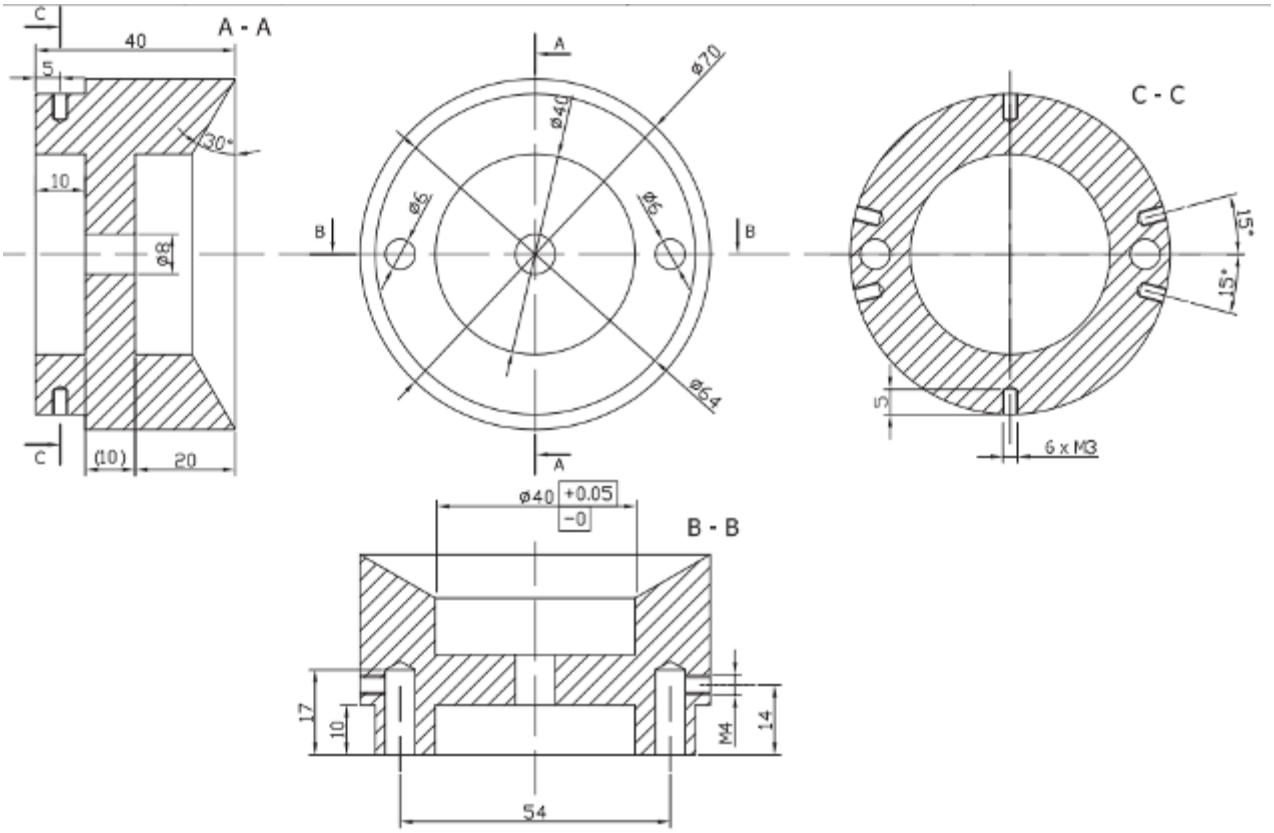

Figure 7. Tail Area Mounting Wall

Probe Mounting – Winch and Tail Mounting Area

The probe is intended to be attached to an airplane by two means:

- Hanged under the airplane on a winch
- Directly mounted on an airplane fuselage

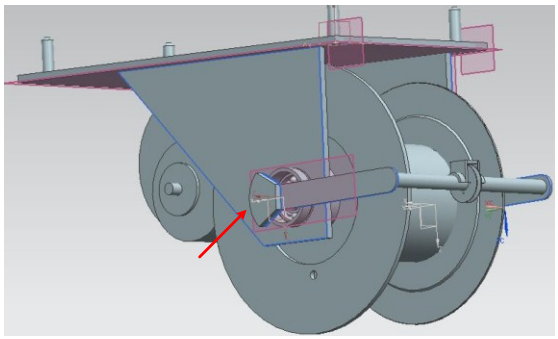

Figure 8. 3D Model of a Winch Mechanism

Figure 9. Final Winch Mechanism

Figure 8 shows composition of winch components as a 3D model and Figure 9 shows the final product ready for control electronics assembly. While the probe is completely independent its measurements have to be compensated for the altitude between the airplane and probe flight level according to the equation (1).

$$H = l \cdot \cos\alpha \qquad (1)$$

Where H is altitude between the airplane and probe flight level, l is length of the tether between airplane and probe, and α is angle between vertical axe aligned with g-force vector and vector of the probe tether. The angle is created by inertial forces and air pressure acting on the probe. It is measured by a position sensor (Figure 8 red arrow) and the lever with an eye through which the tether connects the winch and the airplane.

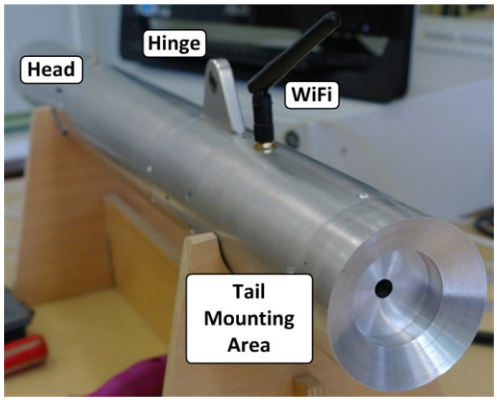

Figure 10. Probe Tail Mounting Area Used for Stabilisation Wings Attachement or Direct Mounting to the Plane

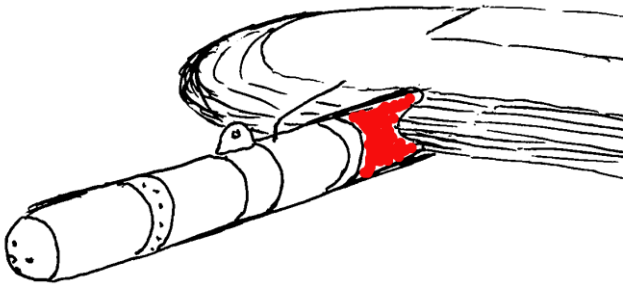

Figure 11. Probe Mounting On the Edge of an Airplane Wing

Figure 10 shows the last mounting wall, whose drawing is depicted in Figure 7, which is intended for the probe stabilization wing. Besides stabilization wings, it can also be used for direct mounting to a wing, or other part, of an airplane as it is depicted in Figure 11.

Probe Sensing and Electronic System

A block diagram of internal mechanical and electronic component interconnection is depicted in Figure 13. This figure shows probe head (drawing in Figure 3) and static pressure inputs (drawing in Figure 4) that are connected by pipes with pressure sensor boards (also visible in Figure 5). There are two types of sensor boards present in the probe. First type is used for Freescale MPXV sensors which are used for AOA, AOS and air-speed measurements. There are three PCBs with six sensors. Four MPXV7002DP sensors are used for AOA and AOS measurements and two MPXV7007DP sensors are used for air-speed measurement. There are three boards with two sensors each which are connected to the pressure inlets by pipes in style which doubles amplitude of the output signal [8]. Static pressure is measured with a Memscap SP82 sensor [9] and for this application a Memscap TP3100 Pressure Measurement Module was used. The sensor provides a digital interface for measured data which are transferred to the CPU that collects also data from analogue Freescale MPXV sensors. The CPU controls a wireless modem through which all the data and probe setting can be controlled. The probe uses Roving Networks RN-134 WiFi module. Embedded CPU allows direct connection of other sensors like uBlox LEA-6 GPS receiver and ST microelectronics iNemo IMU for which all the firmware drivers are already available. Other sensors like a customized

magnetometer head [4][14] can be connected to the system and placed in OPT1, 2, 3 areas (see Figure 2 and Figure 13). The CPU is Freescale HC9S12XET512 16-bit communication processor. While some of the components require 5V0 DC voltage and other 3V3 DC voltage, different voltage stabilizers are used on the power distribution PCB. This PCB also employs Texas Instruments TXS0104E voltage level converters to interconnect digital busses running at different voltages. The probe is now designer to use 7,4V Raytronic G3 2S1P 26/50C 3250 mAh Li-Pol battery. While this battery requires a special treatment and charger a standard AA batteries are considered as an alternative power source. The Li-Pol battery can be damaged by excessive discharge. To protect the battery a special circuit was designed to check battery voltage level and prevent their damage. The battery is able to power the probe for more than 12 hours. For future use and because of the described problems a new battery type [10] of high capacity and less demanding maintenance would be preferred.

Probe Data Interface

To download data from the probe a custom interface was developed as it is depicted in Figure 12. The figure shows data acquisition chain supported by Mathworks Matlab suite. It provides runtime environment for a DLL, which encapsulates and hides communication protocol and takes care about initialization of the communication, hand shaking, and start and stop bytes. The data purified from the protocol characters are used within Probe Input/Output Interface (PIO) which defines one script file (Matlab function) for every quantity measured by the probe. The user can prepare own control script which can use the functions available in PIO interface. While Figure 12 shows one possible usage of the DLL library other software suites (Lab View, Lab Windows, custom SW …) can use the same library to access the probe. The Matlab2CAN exchanges data with code in the CPU. The exchange protocol access different data register which are filled by data acquired by the hardware of the CPU [11] with help of Hardware Abstraction Layer available at [12].

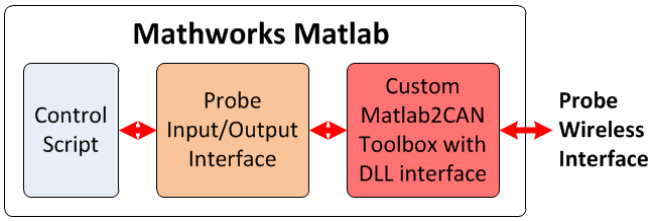

Figure 12. Probe Data Interface used in Mathworks Matlab

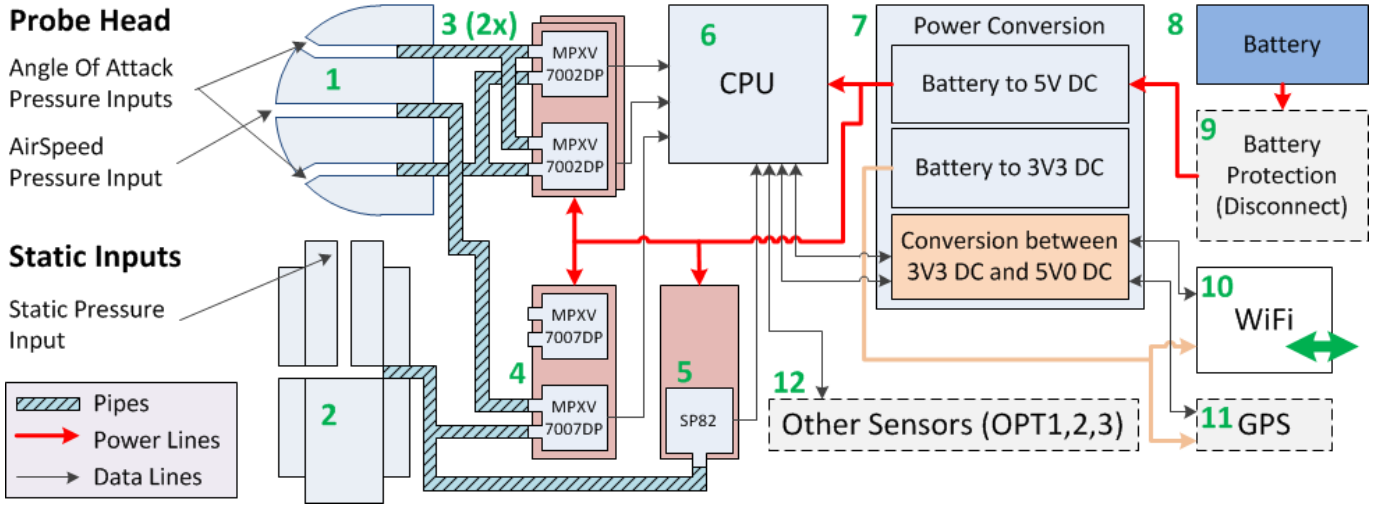

Figure 13. Trailing Probe Electronics and Sensing System

Probe Calibration

To evaluate precision of the probe sensing system, three test procedures were performed. First task was to determine dependence of the total pressure input on the probe angle of attack and angle of sideslip. The second task required testing the angle of attack and angle of sideslip inlets. And the third task tests the probe static pressure measurement system precision.

Total Pressure Port Dependency on AOA

Dependency of the total pressure port inlet on the angle of attack is crucial for the precision of air speed calculation. The dependency was tested in a wind tunnel, Eiffel type, with 1.8 m diameter as depicted in Figure 14. Just the probe head and the first compartment (see Figure 2) of the probe were placed in the tunnel. The results of multiple measurements taken on multiple probes during the wind tunnel test are available in [13] but here we describe just the trailing probe total port behavior.

The result of the total port dependence on the angle of attack is depicted in Figure 15. It is obvious that the designed diameter of the total pressure input is large enough to compensate for angle of attack influences because the total error caused by the angle of attack is less than 0.5% for speed up to 40 m/s (144 km/h). It is obvious the error will rise with speed. The graph clearly shows the rising error at AOA angle of 17 degrees, which is caused by the shape of the probe head (see Figure 3). Up to about 20 degrees of AOA the air pressure concentrates at the air-speed input as depicted in Figure 16. For AOA angle greater than 19 degrees the shape of the probe head, the spherical surface begins to lean apart from the air flow and the pressure begins sharply drop down (compare Figure 3, Figure 15, and Figure 16).

Angle of Attack Inlets Performance

Angle of Attack inlets allow detecting probe displacement with regards to the airflow. The measurement principle uses pressure difference between two inlets on a spherical surface that changes their position, or alignment, within the airflow (see Figure 3). In case of the airflow parallel with the probe longer axis there is the same pressure on the both inlets and the differential pressure sensor reads zero difference. The another extreme example is alignment of one inlet axe with the airflow then the second input gets into shadow of the head spherical shape and the pressure sensor provides the maximal amplitude of the output signal.

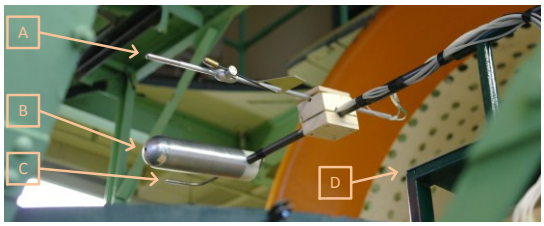

Figure 14. Probe Placement during Wind Tunnel Measurement [13]

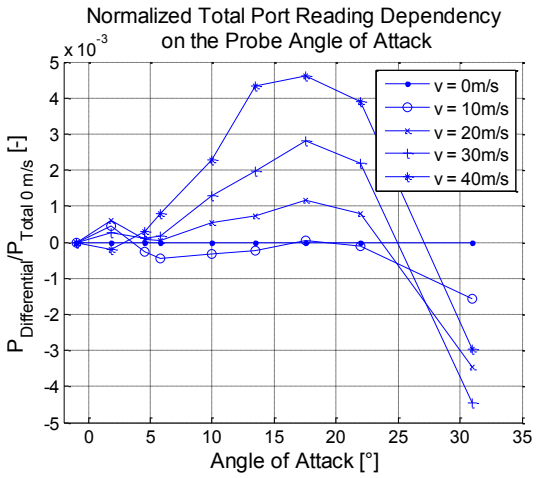

Figure 15. Normalized Total Port Dependency on Angle Of Attack and Variable Air Speed

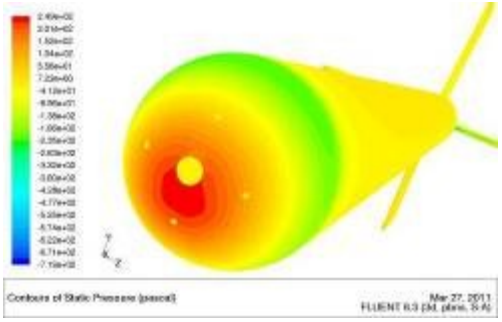

Figure 16. Pressure Distribution on the Probe Head for AOA 10 Degrees

The amplitude of the signal provided by the differential sensor depends on the airspeed, the higher airspeed the bigger pressure difference as depicted in Figure 17. The figure compares readings provided by the probe electronic system described in the previous chapter (data designated by letter P in Figure 17) and a laboratory data acquisition system HewletPackard 34970A (designated by letter C in Figure 17). The ratio of pressure difference to total pressure ($\Delta p/p_c$) is depicted in Figure 18. While the total port is used for calculation, its behavior depicted in Figure 15 influences also this data. Figure 18 shows the gain ratio of the probe head which is independent on the actual air speed (air pressure).

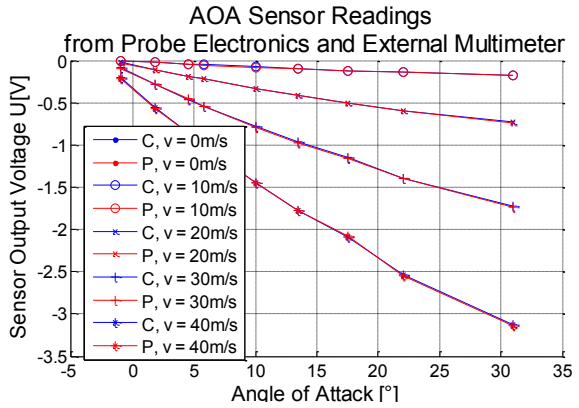

Figure 17. Comparison of the Probe Measurement System with External DAQ Board Measuring Angle of Attack Sensors

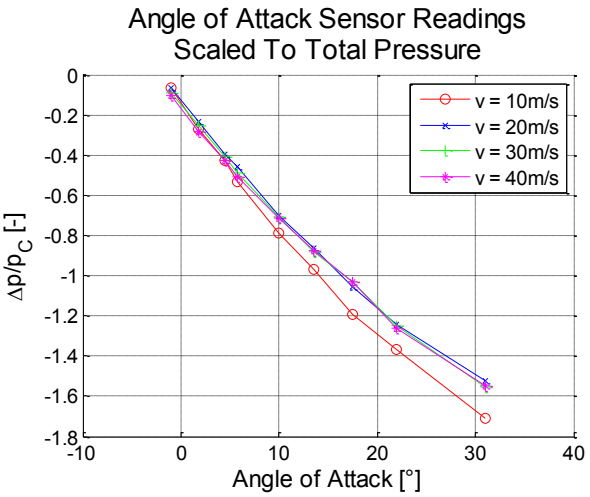

Figure 18. Differential Pressure to Total Pressure Ratio Generated by the Probe Head

The figure (Figure 18) shows slight difference of the characteristic for speed of 10 m/s. It is caused by the bigger measurement errors for the small changes of the both differential sensor (AOA and air-speed sensors). The biggest ratio between both pressures reaches value of 1.5 which is in relation with results presented in [8] where a bigger diameter of the probe means bigger precision of the angle of attack measurement system.

Using the ratio, the calibration of the sensor can be performed by one constant value because the characteristics are independent on the actual air-speed. For our case the calibration constant is 12.5 degrees in the linear range up to about 15 degrees AOA. The total precision of the AOA and AOS system will be ±1 degree in range of ±10 degrees which is in relation to the results published in [8].

Static Port Precision

To evaluate the probe static pressure measurement system precision a test setup was created as depicted in Figure 1 and in a block diagram in Figure 19. The setup is based on a vacuum pump which provides input to an Automatic Test Equipment which is able to control and measure pressure with outstanding precision. In our case GE Druck Pace6000 Automated pressure regulator was used. The regulator was controlled from a personal computer through an Agilent USB2GPIB interface. Software layer was provided by Mathworks Matlab and its Matlab Instrument Toolbox. Pace6000 provides absolute pressure measurement precision of 0.05 mbar (5Pa) + 0.005% Rdg + 0.005% FS. In our case the probe with 200 kPa FS and measurement around 100 kPa were used that means precision of the measurement ± 1.5 kPa with fully automatic pressure setting. Pressure is fed into the probe entry points through mechanical converters depicted in Figure 20.

The calibration procedure was performed as follows: the script requires the controller to set-up a prescribed pressure, then it wait for the controller to finish the pressure setting and when the pressure controller reached the required pressure level the script ask the probe through its wireless data interface for an array of measurements.

While the measurement setup is fully automatic it was required to evaluate the probe measurement

system in range from atmospheric pressure (around 100 kPa) to 50 kPa, which matches altitude of 5.5 km, with step of 500 Pa. In every step the control scrip took 30 samples from all of the probe sensors.

The result of static measurement subsystem calibration is depicted in Figure 21 which shows difference between preset pressure and pressure measured by the probe subsystem. There is difference of 150 Pa at the ground level (which means altitude of about 12 meters). The difference descends with increasing altitude (e.g. decreasing pressure). To calibrate the data a linear calibration was implemented. The calibrated value is being calculated as $y = a*x + b$ where x represents data provided by the probe, $a = 0.9988$ and $b = 30$. The pressure difference of the calibrated data and preset pressure after calibration is depicted in Figure 22. The figure shows variations of ± 6 Pa which can be recalculated as ± 0.5 m at zero altitude above ground level.

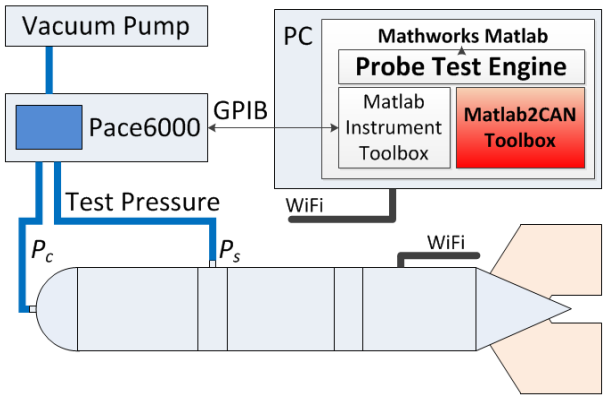

Figure 19. Probe Calibration Test Setup

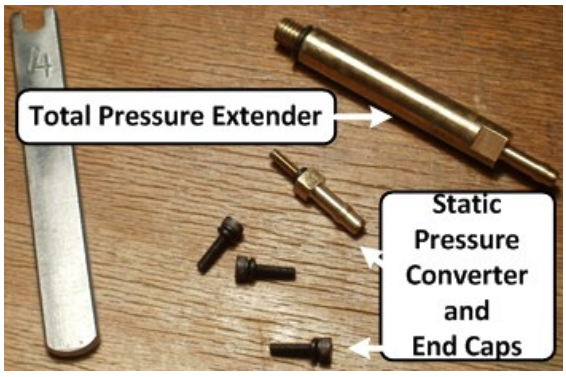

Figure 20. Mechanical Converters Used to Connect the Probe with Test System

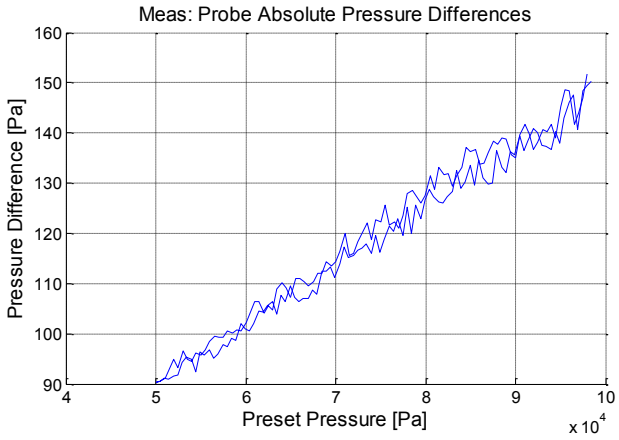

Figure 21. Static Sensor Differences from Required Value – No Calibration

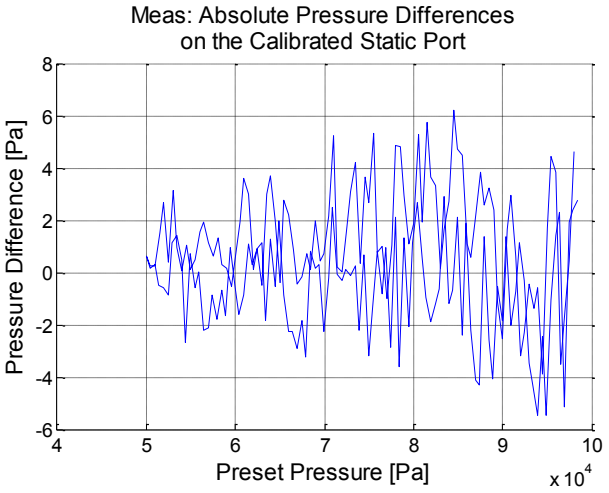

Figure 22. Static Sensor Differences from Required Value After Calibration

The results presented in this chapter show the probe still needs calibration which is necessary periodically repeat. The data provides overview about necessary computing power needed to be used for onboard calibration. While the measurements were made with just parts of the probe the complete wind tunnel test needs to be performed. The test should reveal behavior of the sensors of the completely assembled probe and also its stability in the airflow. Also the behavior of the static pressure inlets with regards to the actual angle of attack needs to be evaluated.

Conclusion

This article describes mechanical and electrical design of a probe that can be hanged under an airplane or directly attached to a suitable place on an airplane, e.g. an airplane wing. We discussed the probe sensors and electronic measurement system properties. The probe provides the measurement results by a wireless data interface with specially designed software layer consisting from a microcontroller firmware and a custom DLL library. The interface was used to acquire first datasets from the probe to prepare calibration constants for all the used sensors.

The probe can be used by two different means and it is prepared to be used as a part of the new system for airplane position angles measurement [14].

The calibration revealed that the total pressure input of the probe is independent on angle of attack up to ±10 degrees. The angle of attack and angle of sideslip measurement inlets provides linear output in range up to about ±10 degrees with precision of ±1 degree and proves presumptions published in [8]. The probe static pressure input uses Memscap SP82 sensor which is used in civil aviation and it holds hardware certification from Civil Aviation Authorities. Our measurement showed the output of the sensor has no hysteresis and small calibration is still necessary. The sensor is able to provide precision of ±0.5 m after calibration. The measurement described here proves the concept of the communication with the probe is working and can be used for further measurements.

References

[1] Jalovecky, Rudolf, Jan Bajer, Petr Janu, 2010, Controller Area Network based On-board Data Acquisition System on Military Aircraft. In Concepts and Implementation for Innovative Military Communications nad Information Technologies. Warsaw, Poland: Military University of Technology, pp. 589-598. ISBN 978-83-61486-70-1.

[2] Svatos, Jakub, Pavel, Fexa, Josef, Vedral, 2009, Methods of Education Electronic Measurement Circuits and Systems at FEE CTU In: Applied Electronic 2009. Pilsen: University of West Bohemia, 2009, pp. 9. 12. ISBN 978-80-7043-781-0.

[3] International Organization for Standardization, 1975, Standard Atmosphere. Geneva, ISO, 1975. ISO 2533:1975.

[4] Popelka, Jan, Pavel Paces, 2012, Miniaturization and Sensor Fusion of a Measurement Unit for a Trailing Bomb, 31st Digital Avionics System Conference, accepted for publication.

[5] Cizmar, Jan, Jalovecký R. Design of an Inertial Reference Unit with the mixed gravitational and magnetic correction of gyroscopic drift, Transport Means - Proceedings of the International Conference, Kaunas;21 October 2010, ISSN: 1822296X.

[6] Beutel T., N. Ferreira, A. Balck, M. Leester-Schädel, S. Büttgenbach, Nov. 2010, Cell manipulation system based on a silicon micro force sensor with self-calibration from backside, IEEE Sensors, pp.1419-1423, doi: 10.1109/ICSENS.2010.5690506, available online at: http://ieeexplore.ieee.org/stamp/stamp.jsp?tp=&arnumber=5690506&isnumber=5689839

[7] Auersvald, Jan, 2010, Probe for Airplane Aerometrical System Testing [Available Online], 2010. 71 pages. Bachelor Thesis. Czech Technical University in Prague.

[8] Paces, Pavel, Tomas Censky, Vitezslav, Hanzal, Karel, Draxler, Ondrej, Vaško, 2010, A Combined Angle of Attack and Angle of Sideslip Smart Probe with Twin Differential Sensor Modules and Doubled Output Signal. In IEEE Sensors 2010 Proceedings [CD-ROM]. Stoughton, Wisconsin: IEEE Sensors Council, pp. 284-289. ISBN 978-1-4244-8168-2.

[9] Nedved, Jan, 2009, Aerometrical System for Small Airplanes [Available Online], Master Thesis, Czech Technical University in Prague.

[10] Shuangze Ji, Junying Zhang, WenwenWang, Yan Huang, Zerong Feng, Zhongtai Zhang, Zilong Tang, 2010, Preparation and effects of Mg-doping on the electrochemical properties of spinel Li4Ti5O12 as anode material for lithium ion battery, Journal of Materials Chemistry and Physics, Elsevier, ISSN: 0254-0584.

[11] Paces, Pavel, 2009, Freescale HC12 demo board [Available Online].

[12] Paces, Pavel, 2012: Freescale HC12 Hardware Abstraction Layer [Available Online]. sourceforge.net/projects/hcs12hallibrary.

[13] Popelka, Jan, Pavel, Paces, Jan, Auersvald, Pavel, Hospodář, 2011, Evaluation of Pressure Distribution around a Pitot-static Probe and a Trailing-bomb with Position Angles Measurement Ability in a Wind Tunnel. In MDS 2011, Brno, Czech Republic, pp. 189-205. ISBN 978-80-7231-828-5. (in Czech).

[14] Paces Pavel, Jan Popelka, Tomáš Levora, 2012, Advanced Display and Position Angles Measurement Systems, 28TH International Congress of the Aeronautical Sciences, accepted for publication.

Acknowledgements

This work was supported by the research program no. TA01030651 "Safety Improvement of Flight, Crew and Other Participants of Flight Transport in Normal and Emergency Situations by Assistive Technologies" of the Czech Technical University in Prague, sponsored by the Technological Agency of the Czech Republic and partially by the project no. SGS12/193/OHK3/3T/13 “Safe and Safety Elements in Aerospace and Space Technology” of the CTU in Prague, sponsored by the Ministry of Education, Youth and Sports of the Czech Republic.

Email Addresses

Authors can be contacted at these emails

Paces Pavel: pacesp@feld.cvut.cz,

Jan Popelka: popelj3@fel.cvut.cz, and

Jan Auersvald: jan.auersvald@fel.cvut.cz.